Signalling and Crosstalk in Cytokine Pathways: Mathematical Modelling and Quantitative Analysis

Shabnam Khatibi

Submitted in total fulfilment of the requirements
of the degree of Doctor of Philosophy

Department of Electrical and Electronic Engineering
The University of Melbourne
April 2016

Produced on archival quality paper

ABSTRACT

Cancer is a leading cause of death all over the world. Focusing at the intracellular level, there are several cytokine signalling networks involved in inflammation and tumorigenesis. These pathways regulate the cell biological responses to the environment, both directly and via crosstalk. Recently, there have been several reports which have confirmed the strong relationship between inflammatory diseases and tumor development ([82,110,163], see [294] for a review). Two cytokines, in particular, have significant roles in wound healing, inflammation and cancer Transforming growth factor β ($\mathrm{TGF}-\beta$) and Interleukin-6 ($\mathrm{IL}-6$). Cytokine signalling pathways are an interconnected complex system of biochemical reactions which can be represented by kinetic equations. These signalling pathways can share proteins and genes which make the intracellular signalling networks extremely complex.

Systems biology and mathematical modelling are new approaches for the study of complex systems such as intracellular signalling networks. The focus of this research is to model mathematically new descriptions of the $\mathrm{TGF}-\beta$ and $\mathrm{IL}-6$ pathways based on new logistics and then integrate them into a single, robust, self-regulated model which can be used to investigate tumor development in the stomach and colon. At each level, experimental data sets were used iteratively in order to both parameterize and examine the models (e.g. the model and experimental data of Zi et al. (2011) and further model simulations have been used in Chapter 4 to parameterize our $\mathrm{TGF}-\beta$ model.).

Different approaches in Systems biology and their applications in cell signalling research are studied. $\mathrm{TGF}-\beta$ and $\mathrm{IL}-6$ signalling pathways and their components are reviewed next. The previous mathematical models of $\mathrm{TGF}-\beta$ and $\mathrm{IL}-6$ signalling are briefly discussed. Additionally, the role of individual signalling in cancer progression and inflammation is studied.

We developed a mathematical model which captures the details of $\mathrm{TGF}-\beta$ signalling. The detailed model consists of over 40 differential equations and highlights the necessity for the reduction and simplification methods. The $\mathrm{TGF}-\beta$ signalling model is simplified and reduced via analytical reduction methods to 6 differential equations and is further validated with experiment. For the first time an explicit negative feedback loop has been included in the model. Another contribution of the $\mathrm{TGF}-\beta$ model is that the inherent time-delays in signalling networks are incorporated in detail. In the final chapter different input patterns are studied for $\mathrm{TGF}-\beta$ signalling. Our model of $\mathrm{TGF}-\beta$ signalling

indicates that the positive feedback loop is one mechanism by which stability could be achieved. The thesis reports for the first time the coupling of the positive and negative feedback loops for $\mathrm{TGF}-\beta$ signal transduction. Furthermore, our $\mathrm{TGF}-\beta$ signalling model proposes predictions for the responses of cancer cells to $\mathrm{TGF}-\beta$ stimulation, which suggest new experimental protocols for future work.

We also developed a mathematical model that describes the $\mathrm{IL}-6$ signalling system thoroughly. The large number of equations involved in this model highlights the need for simplification. Similar to $\mathrm{TGF}-\beta$ signalling model, $\mathrm{IL}-6$ signalling model is simplified and reduced using mathematical methods. In order to develop a realistic model specific kinetics are used for the different reactions. Time-delays are incorporated in the $\mathrm{IL}-6$ transduction mathematical model for the first time. After being validated with different experimental data, the reduced $\mathrm{IL}-6$ signalling model predicts the behaviour of cancer cells in response to $\mathrm{IL}-6$ stimulation. Different pulsatile ligand inputs are studied using $\mathrm{IL}-6$ model and new hypotheses for the $\mathrm{TGF}-\beta$ and $\mathrm{IL}-6$ signalling crosstalk are raised.

Our initial hypothesis that $\mathrm{IL}-6$ signalling regulates $\mathrm{TGF}-\beta$ signalling via SMAD7, is examined using our integrated $\mathrm{IL}-6$:$\mathrm{TGF}-\beta$ model. The simulations produced by the integrated model confirm the importance of the negative feedback loop of $\mathrm{TGF}-\beta$ signalling (SMAD7) via $\mathrm{IL}-6$ downstream signalling, previously suggested by Jenkins et al. (2005). Various kinetic models are examined for the link between the two signalling pathways and several predictions are proposed for the pulsatile inputs and different stimulation patterns. The results of the integrated model are compared with the individual $\mathrm{TGF}-\beta$ and $\mathrm{IL}-6$ models. $\mathrm{IL}-6$-induced activation of SMAD7 leads to suppression of $\mathrm{TGF}-\beta$ signalling and causes double peak responses of PSMAD2 in the short-term, however, the long-term responses of the cells to $\mathrm{TGF}-\beta$ stimulation remain unchanged by $\mathrm{IL}-6$ signalling. The integrated model is also validated experimentally. Conclusively, we found that the regulation of $\mathrm{TGF}-\beta$ signal transduction by $\mathrm{IL}-6$ signalling occurs within the first 300 minutes after stimulation, i.e. within the transient phase of the response.

This thesis includes both theoretical and experimental work, performed by the applicant. Theoretical part of the thesis consists of designing and developing models, analytical analysis of the models and conducting numerical simulations with the numerical simulation of the models. In the experimental part, various experimental protocols were developed and examined in order to parameterize, test and validate the proposed models.

Declaration

This is to certify that:

(i) the thesis comprises only my original work towards the PhD except where indicated,

(ii) due acknowledgement has been made in the text to all other material used,

(iii) the thesis is less 100,000 words in length, exclusive of tables, maps, bibliographies and appendices.

Signed,

Shabnam Khatibi
8 April 2016

Acknowledgements

I would like to express my sincere gratitude to my supervisors Professor Tony Burgess, without whom this dissertation would not have been possible, Dr. John Wagner for his wonderful guidance throughout my Ph.D. and Professor Jonathan Manton for his supports.

I also want to thank Dr. Hong-Jian Zhu for his continues assistance and invaluable advices during last four years. Additionally, I wish to acknowledge the help provided by Burgess lab members from whom I have learnt many laboratory techniques.

I take this opportunity to express gratitude to all of my friends and colleagues who have put smile on my face with their love, kindness and support.

A special thanks to my family who have always stood by me and encouraged me to pursue my dreams.

Contents

List of Figures

List of Tables

Chapter 1

Introduction

1.1 Motivation

Statistics document an increasing rate of cancer incidence worldwide [368,399]. According to cancer council Australia, 1 in 3 women and 1 in 2 men are diagnosed with cancer before the age of 85 [368]. This makes cancer a major health problem for the majority of countries. The most common types of cancer in Australia are prostate, bowel, breast, melanoma and lung cancer respectively (cancer council NSW annual report). As a result, research has focussed on understanding cancer and developing specific treatments.

Inflammation is reported as one of the conditions that is closely related to different cancer types (see [56, 341, 371] for reviews). Although it is not clear whether inflammation results from cancer or is a cancer initiator, considerable evidence confirms the links between chronic inflammation and tumor development [22, 23, 33, 377, 391]. As a result, it is essential to consider inflammatory components when investigating cancer initiators, promotor and progression.

In attempting to understand cancer, the key issue is its emerging complexity [188]. Cancer is a multi-scale, multi-variable and complicated disease that involves deregulation of distinct, connecting pathways which control fundamental cell responses [259]. One way to tackle this problem is by applying quantitative methods of Systems biology and engineering analysis to cancer research. Furthermore, quantitative modelling creates the power of prediction in this area of research.

Focusing on the intracellular level, there are several distinct signalling networks involved in cancer and inflammation that connect directly and/or indirectly [394, 403]. Connections among the signalling pathways lead to a broader range of genes which are affected by mutations of the contributing components within the pathways.

$\mathrm{TGF}-\beta$ and $\mathrm{IL}-6$ signalling pathways are two pleiotropic signalling systems which become deregulated in tumor development and chronic inflammation, respectively. Recent studies have proposed an indirect crosstalk between

these two signalling networks [207]. Jenkins et al. [207] have tested their proposed system experimentally and qualitatively. Particularly, $\mathrm{IL}-6$ affects the $\mathrm{TGF}-\beta$ signalling negative feedback and eventually regulates its anti-proliferative pathway. This points to the need for understanding the vital role of feedback loops in designing of the regulatory networks.

The current research investigates the signalling crosstalk between $\mathrm{TGF}-\beta$ and $\mathrm{IL}-6$ transduction using mathematical modelling and precise analytical analysis. We have focused on the feedback loops involved in each signalling pathway and their effects on the stability and robustness of the individual systems as well as the integrated $\mathrm{IL}-6$:$\mathrm{TGF}-\beta$ network. Each model is validated using experimental data from literature and/or data derived in our lab. Furthermore, several predictions are presented which pave the way for future studies in this field.

1.2 Research Objectives

The overall goal of this research is to develop a quantitative model which describes the crosstalk between the $\mathrm{TGF}-\beta$ and $\mathrm{IL}-6$ signalling pathways and demonstrates a better understanding of the role of feedback loops in regulating signalling networks. In order to achieve this, the following steps have been taken:

1. To develop a mathematical model for $\mathrm{TGF}-\beta$ signalling

   A biological model is designed in order to capture the interactions of $\mathrm{TGF}-\beta$ signalling. This model then is translated to a mathematical model. In this step every biochemical reaction maps to its corresponding equation.

2. To simplify and reduce the components of $\mathrm{TGF}-\beta$ signalling model based on analytical methods

   After development of a mathematical model for $\mathrm{TGF}-\beta$ signalling, the model is reduced and simplified to its key components. This was done by using rigorous mathematical methods and assumptions. Steady-state and equilibrium analysis help us to acquire an insight to the mechanism of the signalling system.

3. To experimentally validate our proposed $\mathrm{TGF}-\beta$ signalling model

   Experimental data sets are used to validate the model predictions at this stage. The output of the model is the time course of a protein concentration which is specific to the signalling pathway. For $\mathrm{TGF}-\beta$ signal transduction, we used Phospho-SMAD2/3 concentration level as the marker for $\mathrm{TGF}-\beta$ stimulation.

4. To develop a mathematical model for $\mathrm{IL}-6$ signalling

We repeated similar steps in design and development of $\mathrm{IL}-6$ signalling network. By the end of this step, we have two sets of mathematical equations corresponding to $\mathrm{TGF}-\beta$ and $\mathrm{IL}-6$ signalling respectively. Each system of equations is solved in order to produce predictions from the model.

5. To simplify and reduce the components of $\mathrm{IL}-6$ signalling model based on analytical methods

   Similar to $\mathrm{TGF}-\beta$ signalling model, we benefit from a series of mathematical and system analysis which leads to a simpler and more understandable model of $\mathrm{IL}-6$ signalling. The key idea here is to maintain the critical information of the system while reducing the extra details. The final output of the reduced and simplified model should be as rigorous as the full system.

6. To experimentally validate our proposed $\mathrm{IL}-6$ signalling model

   The Phospho-STAT3 time course is used to experimentally validate the $\mathrm{IL}-6$ signalling model in this step. It is also important to keep the consistency in the validation steps of the two pathways.

7. To integrate the models of $\mathrm{TGF}-\beta$ and $\mathrm{IL}-6$ signalling and predict the output level, in addition to experimental validation of the integrated model

   The final step is to join the two signalling models to design an integrated $\mathrm{TGF}-\beta$ and $\mathrm{IL}-6$ model. This model predictions can be tested with more experiment.

1.3 Thesis Outline

In this chapter a high-level introduction that motivates this research has been provided, following by an explicit statement of the thesis objectives. The outline of the remaining chapters is as follows.

In Chapter 2, Systems biology principles and its contribution in cytokine signalling are reviewed. The importance of mathematical modelling in studying the biological systems is explained. $\mathrm{TGF}-\beta$ and $\mathrm{IL}-6$ signalling pathways and their provided mathematical models in the literature are studied specifically, in detail. This chapter will discuss about the crosstalk between $\mathrm{TGF}-\beta$ and $\mathrm{IL}-6$ signalling pathways and their critical role in tumor progression.

In Chapter 3, the methods which are developed and used in this project are reviewed. Both experimental and theoretical methods are included in this chapter. A stepwise experimental data extraction procedure is indicated. Furthermore, the materials used in this project, including the laboratory reagents and machines, programming platforms and quantitative computer programs are described in Chapter 3.

Chapter 4 presents a framework for the design, analysis and validation of $\mathrm{TGF}-\beta$ signalling network from a Systems biology point of view. Simplification and reduction methods emphasising on the feedback loops of the signalling system are highlighted. The simulations of the final $\mathrm{TGF}-\beta$ signalling model are compared with the experimental results of the previous models in the literature. Model predictions are proposed and experimentally validated, explaining the deregulated $\mathrm{TGF}-\beta$ signal transduction in tumors.

In Chapter 5, we have repeated the design and analysis steps for $\mathrm{IL}-6$ signalling pathway which lead to a simplified $\mathrm{IL}-6$ mathematical model. The $\mathrm{IL}-6$ signalling model explains the experimental data provided in the literature. This model is further validated with our new sets of experimental data on normal and immortal cells. Similar to the previous chapter, predictions are proposed which interpret how the components of $\mathrm{IL}-6$ signalling alter in tumors.

Chapter 6 is dedicated to the integrated model of $\mathrm{IL}-6$:$\mathrm{TGF}-\beta$ and investigates how $\mathrm{IL}-6$ down-regulates $\mathrm{TGF}-\beta$ signalling, causing uncontrolled proliferation of the cells. The integrated model provides various simulations to predict and analyse different stimulation conditions. This chapter ultimately proposes evidence to confirm our hypothesis on the interaction between the $\mathrm{TGF}-\beta$ and $\mathrm{IL}-6$ signalling systems. The contributions of the currant thesis briefly recapitulate in Chapter 6 focusing on the future areas of research.

Chapter 2

Literature Review and Background

2.0 Summary of the information included in Chapter 2

Systems biology provides a unique, comprehensive approach in solving the current issues of Biology. Researchers have been attempting to apply Systems biology principles in order to understand cancer and develop treatments. Using mathematical models to capture the details of intracellular signalling pathways quantitatively, is a starting step of identifying the cancer initiators. Focusing on the close connection between tumor development and chronic inflammation, we have studied two specific signalling pathways which are often deregulated in cancer and inflammation($\mathrm{TGF}-\beta$ and $\mathrm{IL}-6$ signalling). Each signalling pathway is reviewed precisely in this chapter. The previous mathematical models, their strength and their weaknesses are analysed for individual signalling system. Finally the advantages of crosstalk studies are specified.

2.1 Systems Biology

Systems biology is a system-level understanding of living systems which often involves computational modelling and analysis of biological data [25, 240, 241, 245]. Although the study of biological systems commenced in the middle of 20th century [55,245,455,470], it is only during the last decades that the developments in science and engineering have enabled us to progress the affectiveness of the systems approach to biology. What do we mean by "Systems biology": if we substitute the ambiguous "systems" word by a "network of components" and add the important "dynamic" concept, we are starting to approach the power of Systems biology [25, 250].

In general, four steps are required to gain a systems-level understanding of a biological process. The first and the most vital one is identification of the system's structure (a topology). The structure of the system includes both the

physical structures (the actual location of implied components of the system) and the interactions between the components (the network that confines the system's components). The interactions among the components determine the final state of the physical structure of the system and hence, must be studied in detail. However, determination of the system's structure does not define the status of the system completely. Dynamic changes to the components of the system is an intrinsic characteristic of biological systems [245,250,283]. The second step is to understand exactly how the components vary with time. This step requires integration of both scientific and engineering principles, such as computational model development, new experimental information which is relevant to the structure and dynamics of the system. The third step: the controllers of the system and methods of control need to be determined. This step allows us to predict and simulate the output of the system. The forth step in a system-level understanding is to find a suitable method to simulate the biological system as a comprehensive, robust model which can be interrogated, perturbed and analysed over a time-frame relevant to the biology [241,245].

In the Systems biology world, the fundamental principle is to be robust [245, 443, 457]. Robustness is the insensitivity of biological functions to various disturbances [245]. Robustness is a characteristic of biological systems [243, 245, 276]. There is a close relationship between the evolution of a biological system and robustness [245, 457]. If a biological system lacks the sufficient robustness, it will not survive environmental and genetic perturbations [245, 372, 452, 458]. Only individuals with more robust properties survive sudden significant change. Robustness of a biological system cannot be identified from the components of the system only, however, robust systems have a few common characteristics by which they can be controlled e.g. possession of regulatory feedback loops [245,443]. Common mechanisms across engineering and biology which give a system robustness to different perturbations are [245]:

- Extensive system control

  Extensive system control refers to negative feedback loops which provide dynamic regulation of the system and maintain the system around a stability point. Feedback loops occur when the input(s) of a system is regulated by the output continuously [126]. The feedback loop can be positive or negative depending on whether the loop enhances or dampen, respectively, the perturbations from the equilibrium point [210]. Self-regulation has been observed in bacterial chemotaxis [7, 26, 496]. Controlling biological systems can happen through positive feedbacks as well. Positive feedbacks create bi-stability in signal transduction and cell cycle processes which resist minor perturbations and facilitate robustness in response to environmental changes [63, 122, 439].

- Redundancy and phenotypic plasticity or diversity

A system can tolerate environmental change if it has alternative components and methods [245]. Phenotypic plasticity [2, 383] is the process by which a biological system changes its phenotype when reacting to perturbations caused by environmental or genetic change. Redundancy occurs when a critical component(s) of a system is duplicated in order to increase the reliability of the system [243, 245]. Reliability of a system defines the probability that the system achieves its expected function [141, 475]. In both cases systems with alternative mechanisms can overcome perturbations and are more robust [243, 245].

- Modularity

  Systems with different modules consist of a number of isolated parts. Perturbations occur in one module is isolated to the same module and do not affect the rest of the system. Several functions in biological evolution can increase modularity, e.g differentiation and gene mutation [125, 128, 410]. Modularity is important during the development of a biological system, as it helps to provide a more robust and more reliable topology by, for example, providing the accommodation of a foreign DNA [363] and/or limiting the developmental constrains [106, 245, 306, 446, 456].

- Decoupling

  By decoupling minor perturbations in the low levels of a system, the higher levels of the system can be protected. For example, Hsp90 limits the misfolding of proteins as a result of environmental stress and consequently reduces the perturbation of the gene regulation [245, 361, 372, 373].

- Bow-tie architecture networks

  Biological systems often have a special architecture (i.e. bow-tie organization in bacterial metabolic networks [84]) which implies intrinsic robustness [245]. What makes bow-tie networks powerful is that there is a large range of inputs and outputs connecting via a much smaller range of processes and protocols in the "core" [84, 243, 245]. In a bow-tie system, the inputs transfer to the core via a funnel and become suitably organized and processed. Hence, these systems are more flexible against the environmental changes [84]. Bow-tie systems are complex (multiple interacting components and linkages) and self-organized (systems which exhibit an overall order via their local interactions between their components i.e. biomacromolecules [54]) and are observed in metabolic pathways [288] and signal transduction [335, 336].

Cells Mostly control their functions via the environmental cues produced by other cells [127]. Cell functions are the results of intracellular signalling many of which are identified in the last few decades [127]. Intracellular signallings networks must be precisely regulated to avoid improper responses [127]. Precision,

robustness and versatility of the cell signalling pathways originate from the crucial influences they cause [51,127]. It has been suggested that extensive control of signalling networks can be done by using feedback loops [51,127]. Similarly, redundancy, modularity and decoupling are often seen in different signalling systems causing high robustness [51,380,436,473].

Although robustness is an essential feature of a biological system, robustness often needs to be balanced against, fragility and resource demands [243,245]. Often, when robustness develops against a group of environmental changes, the system becomes more fragile in response to other specific perturbations. Diseases can be the direct result of the fragility of a biological system against changes from the outside. In some cases, the biological system shows resistance against therapies too [243,245]. This can be caused by the same processes that enhance the robustness of that system against harmful perturbations [243,245]. One example of robustness "hijacking" is cancer [244–246](and autoimmune diseases) [242,244,247]. It is evident that many signalling systems are deregulated in cancer [145]. In fact, changes in the intracellular signalling networks transfer a normal cell to cancerous conditions which then acquires new robustness. Tumors are highly robust, these cells resist a wide range of therapies. Tumor cells become robust via the same ways that were mentioned earlier [242,247]. Having clarified the role of robustness in autoimmune diseases, it is important to build treatment strategies based on this robustness.

Since biological systems are complex combination of networks of components [240], crosstalk study between individual signalling systems (which arise to a cellular function) is essential. This research is focused on how two specific signalling pathways, TGF$-\beta$ and IL $-$ 6, interact in order to regulate cell characteristics. Additionally, we want to study disruptions of these signalling systems in cancer. In order to achieve this, individual computational models are designed and used to predict the cellular responses in normal and tumor cells. In the final chapter, the two separate models are integrated to provide crosstalk predictions.

2.2 TGF$-\beta$ Signalling Pathway

Transforming growth factor, TGF$-\beta$, is a member of a transforming growth factor superfamily which also includes bone morphogenic proteins signalling (BMP) , Mullerian inhibitory substance, activin, inhibin, and Nodal [75,296,396]. Each family member controls a broad range of a cell's biological characteristics such as: differentiation, proliferation, migration, life time and apoptosis [118, 290, 296]. Signal transduction from the TGF$-\beta$ superfamily receptors is initiated at the membrane of a cell by ligand binding and a range of intracellular signalling reactions which cause gene responses in the nucleus [300, 433]. Recent studies revealed that ligand concentration, stimulation time, cell type

and even the percentage of active signalling components can affect the gene responses to TGF$-\beta$ stimulation [75, 297]. Changes in $TGF-\beta/SMAD$ signalling can affect the transition of normal epithelial cells to cancerous cells in the colon [168, 206, 297, 299, 330, 396]. In spite of the many studies on TGF$-\beta$ signalling, there are still unanswered questions concerning the impact of signalling from this pathway on cancer cell progression. In particular, there are two essentially opposite reactions of cancer cells to TGF$-\beta$ [149, 357, 503]. When cancer cells are in an early phase of malignancy, TGF$-\beta$ acts as an inhibitor of proliferation and slows down cancer progression [265]. Surprisingly, when cancer cells are at a more advanced stage of malignancy, TGF$-\beta$ stimulates proliferation (For review see [357, 376, 503]). Thus the TGF$-\beta$ signalling has a dual behaviour towards cancer cells. In order to clarify such paradoxical behaviours, TGF$-\beta$ transduction and its components need to be studied in detail. The focus of this review is to identify the key parameters in TGF$-\beta$ /SMAD signalling including: the ligand TGF$-\beta$, the receptor proteins TGF$-\beta$ R1 and TGF$-\beta$ R2, the mediator proteins SMADs (SMAD1, 2, 3, 4, 5, 6, 7 and 8) and finally nuclear target genes such as JUN, MYC and COL4A1 (the key components of TGF$-\beta$ signalling are shown in Figure 2.1).

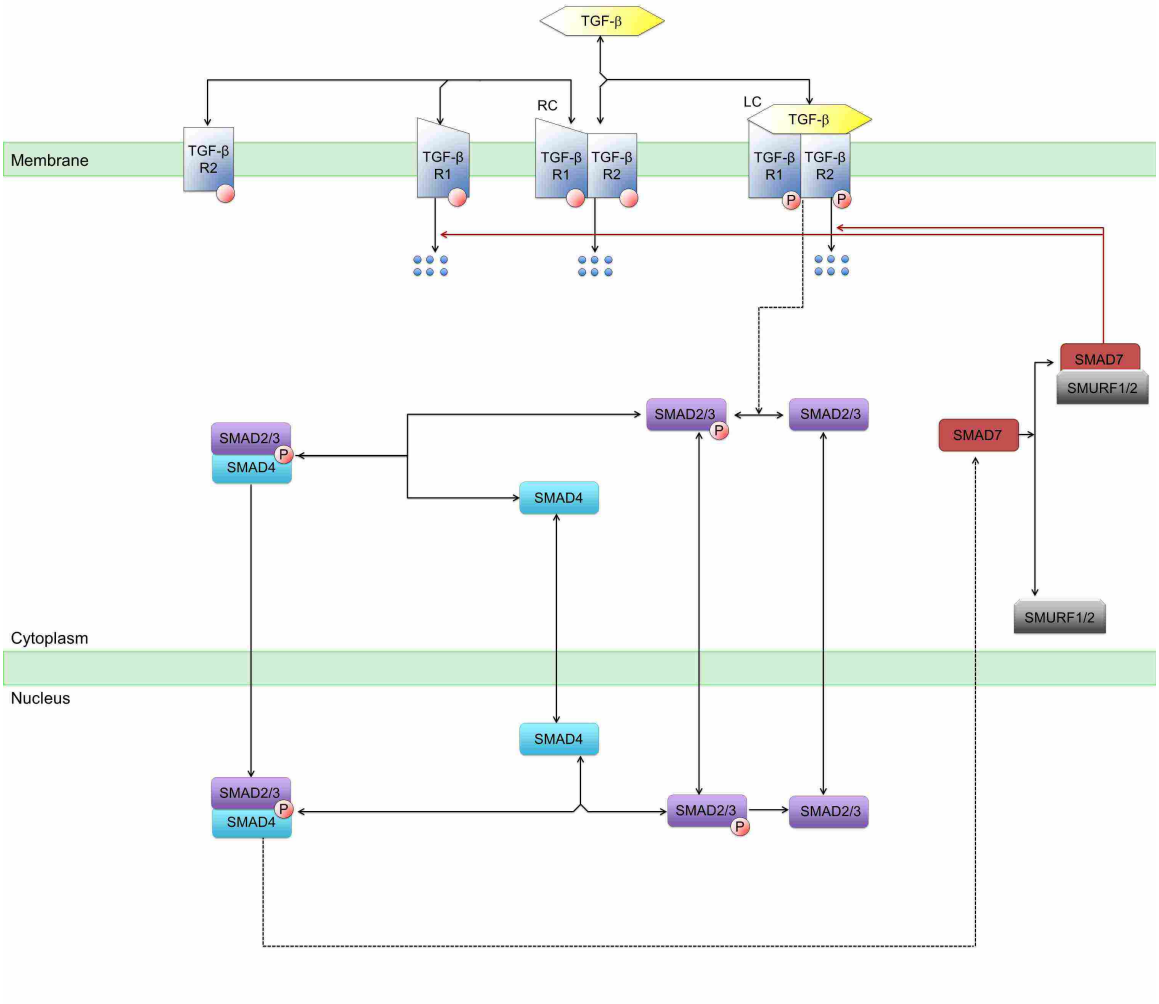

Figure 2.1: *The sketch of* TGF−β *signalling network. Potential phosphorylation sites of the receptors are specified with empty circles attached to membrane receptor components. Arrows pointing to 6 blue dots represent degradation process. The red solid arrows originating from SMAD7:Smurf1/2 apply negative feedback on the receptor components. The dot arrows represent the transcription and translation reactions. Note that the logistics of the signalling are expanded in Figure 4.1.*

2.2.1 Key Components of TGF−β Signalling

- TGF−β receptors: TGF−β R1 and TGF−β R2

  Defects in TGF−β signal transduction can lead to a range of diseases, including cancer [18,112,290,299,344]. Lack of sufficient levels of a functional TGF−β R2 in the cell membrane is reported as one of the main reasons of abnormal signalling in cancer cells [18, 297]. There are two ways the ligand receptor complex can form. Firstly, TGF−β binds to TGF−β R2 [297], the TGF−β: TGF−β R2 complex then recruits TGF−β R1 and leads the TGF−β R2 : TGF−β and TGF−βR1 : TGF−βR2 complexes to combine. The second model requires the two receptor types (TGF−β R1 and

TGF$-\beta$ R2) to bind the ligand, but in no particular order. The latter model occurs in BMP signal transduction [297]. Interestingly, even in the absence of TGF$-\beta$ ligand, TGF$-\beta$ R1 and TGF$-\beta$ R2 can form an active complex when over-expressed [62, 297, 313, 447]. Though TGF$-\beta$R2 can bind independently with TGF$-\beta$R1 and consequently, phosphorylate other components in the pathway to bring about downstream signalling, no data on TGF$-\beta$ responses have been reported for this particular pathway [297, 311,396]. Two different mechanisms have been suggested for TGF$-\beta$R internalization in the presence of TGF$-\beta$. The TGF$-\beta$ R:ligand complex can be internalized through a lipid raft-caveolar degradation pathway, without participating in signalling [93, 449] or, it can activate mediator proteins in the standard manner (through phosphorylation processes) and degrade after recycling to the membrane [449]. These different internalization paths will result in different TGF$-\beta$R signalling responses [194, 348]. If we are to understand the tumor-suppressive effect of TGF$-\beta$ signalling verses its tumor-promoter effects, it is essential that we understand the kinetics of TGF$-\beta$R internalization and recycling [265, 449].

- TGF$-\beta$ mediators: SMAD proteins

  The first downstream proteins activated by the TGF$-\beta$ R1 are from the SMAD family [224, 290, 297]. SMADs (Sma/mad referring to Small body sized homologues of MAD gene [297]) play a major role in TGF$-\beta$ signalling transduction and its nuclear relocation. There are three categories of SMADs (a total of 8 types of SMAD proteins) activated in TGF$-\beta$ signalling [178, 224, 290, 297, 330, 396]; receptor-regulated SMADs (R-SMADs) that interact directly with TGF$-\beta$ family receptor kinases [290, 297], common SMADs (Co-SMADs) that bind with R-SMADs and regulate TGF$-\beta$ transduction [290, 297] and inhibitory SMADs (I-SMADs) that inhibit - TGF$-\beta$ signalling by controlling the function of the other two groups of SMAD family proteins (R-SMADs and Co-SMADs function) [178, 224, 290, 297, 330, 396]. SMADs are regulated not only by TGF$-\beta$ signalling but also by the mitogen-activated protein kinases (MAPK) signalling pathway [131, 260, 297]. SMADs appear to mediate some aspects of MAPK signalling [14,297,506]. SMADs are continuously shuttled between cytoplasm and nucleus independently from TGF$-\beta$ induced activation [200, 386]. The cytoplasm-nucleus interchange of the SMADs is initiated through phosphorylation of the SMAD complex in the cytoplasm [30, 200, 386] and exit from the nucleus is controlled by dephosphorylation [200, 290, 386]. Activation of nuclear import receptors (importin7 and importin8) on the surface of the nucleus facilitates the phosphorylated R-SMADs to enter into the nucleus [200, 386]. It is also postulated that the dephosphorylation of R-SMADs mainly occur within the nucleus [30, 200, 386]. The TGF$-\beta$ signalling system is robust, with the ability to filter rapid input and noise

fluctuations [200, 386]. The robustness of the TGF$-\beta$ signalling system is due to the inherent delay between the input from TGF$-\beta$ binding and the nuclear internalization of the SMAD complex [200,386]. Inhibitory SMADs (SMAD6 and SMAD7) control the intensity and/or duration of cellular responses to TGF$-\beta$ stimulation [1, 297]. One of the proposed ways that I-SMADs regulate TGF$-\beta$ signalling is by binding to TGF$-\beta$ family receptors in competition with R-SMADs and hence, decreasing the rate of activation of the R-SMADs [74, 225, 297, 297, 396].

- TGF$-\beta$ effectors and nuclear re-localization

  TGF$-\beta$ superfamily signalling pathways start from ligand binding to the membrane receptors and leading to interactions in the nucleus and specific gene responses. The key parameter for measuring TGF$-\beta$ signalling is the level of SMAD2/3 nuclear accumulation [18, 75, 511] . It has been shown that SMAD accumulation in the nucleus is directly proportional to TGF$-\beta$ receptor activity [73, 75, 199, 329]. As mentioned previously, there are eight types of SMADs in mammals. These eight genes map to four chromosomes [12]. The SMAD2, SMAD4 and SMAD7 genes which are mutated in broad range of cancers [12, 143], are found on chromosome 18 (mostly around 18q21.1), while the SMAD3, SMAD5 and SMAD6 genes map to chromosome 15 [12, 143]. Finally, the SMAD1 and SMAD8 genes are located on chromosome 4 and 13 [12].

  Most of the SMAD family members proteins are 400-500 amino acids in length and all SMADs share two homology domains: MH1 (Mad homology 1) and MH2 (Mad homology 2) [27, 290]. The SMADs have a nuclear localization signal (NLS) in the MH1 domain of the R-SMADs and this appears to be the reason that the R-SMADs enter the nucleus without necessarily binding to a Co-SMAD [12, 143, 262, 483]; this is one of the important distinctions between R-SMADs and Co-SMADs [12, 262, 483]. Additionally, the MH1 domain of R-SMADs interacts with several transcription factors in the nucleus [290, 486]. The MH2 domain doesn't participate in DNA binding but also plays a role in protein association processes [12, 27, 290]. The SMAD linker region, which connects the MH1 and MH2 domains, is required for interactions with other signalling pathways such as, MAPK [12, 297]. It is through this linker that SMAD7 binds with Smurf1/2 and exerts its TGF$-\beta$ signal inhibitory role [12, 35, 510]. Interestingly the SMADs can bind directly to DNA with low affinity [91, 319]. However, they appear to have higher binding to the transcription factors associated with specific target genes [12, 14, 318].

- Phospho R-SMAD/SMAD4 complex; a closer look

  Co-SMADs also have the MH1 and MH2 domains connected by a linker region [179, 297, 397]. R-SMADs (except SMAD2) and Co-SMADs bind

DNA through the MH1 domain [179,397], while binding of the SMADs to the TGF$-\beta$ receptor occurs via the MH2 domain [93,179]. Two common R-SMADs which participating in TGF$-\beta$ signal transduction are SMAD2 and SMAD3 [297,323,396]; both are phosphorylated in their C-terminus via TGF$-\beta$-R1 [91,93,179,318,323]. The phosphorylated R-SMADs bind with SMAD4 (a Co-SMAD) through the MH2 domains [200,465]. The details of the formation of the R-SMAD/Co-SMAD complex are still being debated [116,179,323]. It is unclear whether the structure of this complex is trimeric or dimeric [57,116,179,205,227,290,481]. There is evidence for formation of SMAD trimers: SMAD2/SMAD2/SMAD4, SMAD3/SMAD3/SMAD4 and SMAD2/SMAD3/SMAD4 complexes [179,385]. One important observation is the obligatory presence of SMAD4 in the signalling complex. Phosphorylation of the R-SMADs changes the protein structure [133,481]. This is more than supplying a phosphate group that normally occurs during SMAD4 activation. The difference in the responses of R-SMADs and Co-SMADs to phosphorylation processes explains why one SMAD4 can bind to several R-SMADs [397,413,481].

The affinity of the R-SMAD/Co-SMAD binding influences the time that the complex spends in the nucleus [179,386]. Recent studies show that nuclear translocation of the complex is associated with the interactions between phosphorylated SMAD3 and importin-β1 [262,483]. The MH1 domain of SMAD2 is unable to interact with importin-β1 [71,360]. Instead, the MH2 domain of SMAD2 participates in nuclear translocation [179,262]. SMAD4 is imported into the nucleus either via the interaction of its MH1 domain with importin-α [351,482] or through the interaction via its MH2 domain with nucleoproteins CAN/Nup214 [71,482,487]. Also, there is also evidence claiming an important role for transcription regulators such as TAZ in binding with SMAD complexes [182,445] and forcing them to be retained in the nucleus [179,445]. Nuclear SMAD3 uses exportin4 and GTPase Ran which allows it to recycle from the nucleus to the cytoplasm [351,465]. SMAD4 also uses its nuclear export sequence, in the linker region, to interact with exportin1/CRM1 and exit the nucleus [351,465]. The export mechanisms of SMAD2 are not yet clear [262], however, there are evidences which nominate different nuclear proteins which initiate nuclear export of SMAD2/3 and terminate TGF$-\beta$ signalling [61].

- SMAD6 and SMAD7, negative regulators:

  Over the last decade SMAD7 has emerged as one of the main antagonists for TGF$-\beta$ and BMP signalling [396]. SMAD6 and SMAD7 negatively regulate signalling by TGF$-\beta$ family ligands [200,396]. SMAD7 acts as an inhibitory factor for both TGF$-\beta$ and BMP signalling while SMAD6 only inhibits the BMP signalling pathway [485]. Moreover, SMAD7 is a candidate element for mediating the crosstalk between TGF$-\beta$ and other sig-

nalling pathways (such as BMP and Wnt) [69,324,343,492]. The inhibitory feedback for the TGF$-\beta$ pathway is initiated in the nucleus by stimulation of smad7 mRNA [153, 162]. The inhibitory regulator SMAD7 recruits Smurf1 (SMAD ubiquitin regulatory factor 1) and Smurf2 to increase the TGF$-\beta$ receptor complex degradation [74, 225]. Smurfs are ubiquitin ligases [69]. Both SMAD7 and Smurf2 can decrease the half-life of the TGF$-\beta$ R1 [225]. There are two other mechanisms by which I-SMADs inhibi TGF$-\beta$ signalling: SMAD7 competes with R-SMADs for binding to the TGF$-\beta$ receptor and SMAD7 competes with R-SMADs for binding to Co-SMADs [216, 396]. SMAD6 and SMAD7 also contain the MH2 domain, however, there is no C-terminal SXS phosphorylation site as in the R-SMADs [216]. SMAD7 binds to TGF$-\beta$ receptor type1 with higher affinity than the R-SMADs [216]. The competition between R-SMADs and SMAD7 causes modulation of TGF$-\beta$ signal transduction. Interaction of the N-terminus of SMAD7 with its MH2 domain leads to the most efficient inhibitory effect of SMAD7 on TGF$-\beta$ R1 [166, 325, 492]. As mentioned before, in order to induce the receptor type1 degradation SMAD7 recruits a group of E3 ubiquitin ligases such as Smurf1/2. During this process, SMAD7 is also ubiquitinated and degraded [100, 225, 423]. In the absence of TGF$-\beta$, SMAD7 tends to reside in to the nucleus as it has NLS in its N-terminal [225]. TGF$-\beta$ stimulation causes the SMAD7/Smurf complex to translocate to the cytoplasm [100, 225, 423, 492]. Smurfs have a nuclear export sequence which interacts with exportin1/CRM1 [179, 427]. It has been proposed that SMAD7 induces dephosphorylation of TGF$-\beta$ receptor type1 via the GADD34-PP1c phosphatase [395]. Additionally, SMAD7 interferes with the action of R-SMADs on the target genes in the nucleus [504] by interfering with the binding of R-SMAD/SMAD4 to DNA [504]. There is evidence that SMAD7 may also affect the transcription of target genes directly [155, 179, 261, 315, 400, 492]. SMAD7 is phosphorylated in the linker region (Ser-249 as phosphorylation site) via kinase(s), independent of TGF$-\beta$ receptor [358]. Whilst this phosphorylation doesn't influence SMAD7's inhibitory function, it does affect the transcription processes stimulated by SMAD7 [179, 358].

- TGF$-\beta$ signalling target genes:

  Microarray analysis has facilitated the acquisition of information on TGF$-\beta$ receptor dependent gene expression [48, 49, 96, 280, 281]. Microarray analysis has led to a number of new hypotheses on potential functions for TGF$-\beta$ signalling [49, 96]. It is well-known that the TGF$-\beta$ superfamily signalling pathways stimulate genes related to cell-cell interactions [49], however, as the following table (derived from chapter 17 of "SMAD signal transduction" by Dijke et. al. 2006 [49]) shows the microarray expression analysis reveals other epithelial gene expression signatures in response to

TGF$-\beta$ stimulation.

Gene	Score	Cell Type	Biological Process associated with gene product	Source Reference
JUN	0.75	epithelial	transcription	V,X,C,K,L,D
FOS	0.5	epithelial	transcription	Z,V,C,W
JUNB	0.5	epithelial, fibroblast	transcription	C,K,L,D
MYC	0.75	epithelial, fibroblast	cell cycle arrest	Z,V,C,K
SMAD7	0.38	epithelial, fibroblast, C2C12	signal transduction	Z,C,K
CTGF	0.38	epithelial, fibroblast, C2C12	cell-cell signalling	Z,C,K
TIMP3	0.38	epithelial, C2C12	apoptosis	Z,V,L
COL4A1	0.63	epithelial, fibroblast	cell-matrix adhesion	Z,X,C,K,L
ID1	0.5	epithelial, fibroblast	transcription	X,C,K,W
ID2	0.5	epithelial	transcription	Z,V,K,L
ID3	0.63	epithelial, fibroblast, C2C12	transcription	Z,V,X,K,L

Table 2.1: TGF$-\beta$/SMAD gene expression signatures in cells of epithelial origins. *V = Valcourt et al., Mol.Biol.Cell, 2005 [441]; X = Xie et al., Breast Cancer Res., 2003 [484]; C = Chen et al., Proc.Natl.Acad.Sci.U.S.A, 2001 [60]; K = Kang et al., Mol.Cell, 2003 [220]; Levy et al., Mol.Cell Biol., 2005 [266]; Deacu et al., Cancer Res., 2004 [89]; Z = Zavadil et al., Proc.Natl.Acad.Sci.U.S.A, 2001 [499].*

1458 target genes have been reported to be TGF$-\beta$ target genes in total 8 quality-verified studies [49]. To determine the level of robustness, Böttinger et. al. [49] scored each TGF$-\beta$ target gene in Table 2.2.1 by a number between 0.25 (lowest) and 1 (highest). Score 1 means that the target gene was listed in all 8 of the cross-referenced studies and score 0.25 means the gene was named in only 2 out of 8 studies. 11 of the highly robust signatures and genes which are reported frequently are listed in Table 2.2.1. These genes include well-known TGF$-\beta$ regulated proteins including the

Jun oncogene (JUN), FBJ osteosarcoma viral (v-fos) oncogene homolog (FOS), Jun-B proto-oncogene (JUNB), c Myc proto-oncogene (MYC), MAD homolog 7 (SMAD7), connective tissue growth factor (CTGF), TIMP metallopeptidase inhibitor 3 (TIMP3), procollagen, type IV, alpha 1 (COL4A1), and Inhibitor of DNA binding proteins (ID1, ID2, ID3). Using Gene Ontology tables, most of the known biological functions of the TGF$-\beta$ signalling pathway (such as; cell cycle control, cell adhesion and cell apoptosis) are associated with $\sim$ 160 target genes [49].

2.2.2 The Role of TGF$-\beta$ Signalling in Cancer

As mentioned earlier, TGF$-\beta$ signalling transduction has been associated with several disorders, especially several cancers [95, 161, 430]. TGF$-\beta$R2 is inactivated in many gastrointestinal cancers [197,234,297]. The disruption in TGF$-\beta$ signalling also occurs in response to mutations in SMAD2 and SMAD4 [18, 75, 297, 330]. These mutations occur in different SMAD exons [297].

The role of TGF$-\beta$ signalling in cancer cells (tumor-promoter or tumor-suppressor) depends on both the micro-environment and the set of cancer gene mutations in the signalling pathways [449]. For example, *in vivo* cancer cells compete with neighboring cells [449]. There is evidence that the duration of exposure to TGF$-\beta$ might explain the dual-behaviour of cells to this signalling protein [135]. Chronic TGF$-\beta$ stimulation (2-3 weeks) can induce cells to become resistant to the anti-proliferative, apoptotic effects of TGF$-\beta$ signalling [135]. In other words, TGF$-\beta$ may down modulate its own signalling [135]. In addition to all the other mutations that cause cancer, the duration of TGF$-\beta$/SMAD signalling appears to be a critical element that changes during the transition of normal cells to cancerous cells [511]. It has been postulated that cells respond differently to sustained and transient TGF$-\beta$ stimulation [330]. Sustained exposure to TGF$-\beta$ may be responsible for the growth inhibition and transient TGF$-\beta$ stimulation may be required for the anti-proliferation in a certain group of tumors [330, 511].

Another detectable change that often occurs when normal cells transform to cancer cells is the loss of E-cadherin [330]. This loss is a characteristic of an epithelial to mesenchymal transition (EMT) [297, 330]. As a result of the complexities occur in cell responses to different TGF$-\beta$ simulation and the leading role of TGF$-\beta$ signal transduction in cancer development, it is essential that powerful methods, such as mathematical modelling be used to explain the role of TGF$-\beta$ in the establishment of the robustness of the biochemical models proposed for signalling during the cancer suppression, promotion and progression phases [19, 73].

2.2.3 Mathematical Approach to Modelling TGF$-\beta$ Signalling

Although TGF$-\beta$ signalling components were discovered decades ago [13,414], the interactions which occur after activation have been difficult to understand. The signalling components change dynamically with respect to time: both the concentration and location of signalling components change within a few hours of ligand stimulation [511]. The TGF$-\beta$ signalling system will be best understood by a reliable, robust model using well-designed mathematical simulations of the processes [19, 511].

Even today most biological and even biochemical studies on growth factor/cytokine signalling are qualitative (for example see [28, 85, 314]). The intrinsic complexity of biological systems gives rise to the need for computational simulation [123, 164]. Mathematical modelling is ideal for studying inherent, complex processes (such as signalling systems) [123, 164]. This is because mathematical models are amenable to computer simulations and can be systematically analyzed [123, 164]. Using mathematical modelling of the biological systems provides prediction capabilities of system's behaviour which is otherwise difficult to obtain due to the simultaneous involvement of numerous components [123, 164].

Several methods for the mathematical modelling of cell signal transduction have been developed [75, 402]. As the concentrations and locations of signal transduction components are time variant, dynamical study of cell's behaviour and the signalling components is required. Generally, there are two main directions in signalling pathways system biology studies (the study of interactions among components of a signalling pathway that control to the function and behaviour of the system): 1. a'top-down' approach which gathers as much experimental information as is possible from the key biological parameters and outputs and simulates the signalling network bioinformatically [19, 392]; or 2. a 'bottom-up' approach which uses a small-scale model with quantitative data for each of the signalling components which are integrated to make a highly predictive simulation system. In short, the top-down method deals with more qualitative and static data and the bottom-up method is supported by more quantitative and dynamic data [19, 291]. The current challenge is how to bring both of these methods together [19].

The most computer representations of the cytokine signalling pathways use a set of ordinary differential equations (ODE) [230, 512]. In the ODE method, the reaction rates are representations of the mass action kinetics, and are proportional to the reactant concentrations. Generally, a system of a small number of ODE equations can be solved either precisely or via analytical approximations [90, 172]. As the number of equations increase, providing an analytical or graphical solution for the system becomes difficult. When all of the parameters for all the components are known, a reliable interpretation of dynamic behaviour of the system components can be expected [230]. The parameters for

this model need to be estimated quantitatively using mass spectrometry [472], immunoblotting [86] or protein antibody microarrays [268]. However, for complex dynamic system with so many equations, such as the cell signalling pathways, it is not possible to solve the ODEs analytically [123]. Consequently, numerical integration solutions are used and hence, sensitivity analysis is vitally important to identify the critical signalling components regulating the output of the system [293]. Numerical integration can result in large changes even in outputs from small changes in parameter values; therefore, by identifying the components to which the system is more sensitive, a more robust and reliable model of the system can be developed [177].

Alternative modelling methods such as Boolean, stochastic and spatially resolved models (e.g. PDE-based models) have been used to model cytokine signalling networks [192]. PDEs are used when attempting to model the spatial and temporal dynamics of the biochemical species. In many intracellular signalling networks the important spatial information is often incorporated in ODEs via compartmentalization [192, 289]. This approach is often used in order to simplify PDEs to ODEs [192, 289]. Stochastic modelling assists in the robustness analysis of a system [192, 289]. One way to incorporate stochastic analysis in an ODE-based model is to consider that the noise can be represented by a Gaussian distribution. The other way is to perform sensitivity analysis on the system, thus identifying which parameters influence the output of the model [192,289]. When there is lack of kinetic information and transcription details, Boolean networks are often used in gene activation and transcription models [289]. However for larger systems, Boolean modelling becomes impractical, due to a large number of possibilities [289].

The signalling systems studied in this thesis have numerous components and involve all three spatial components: membrane, cytoplasm and nucleus. Because of the complexity of the system and number of possibilities for the reactions, it is not sensible to use a Boolean modelling. Also we have considered the most probable possibility for each reaction based on the experimental data and hence, deterministic modelling is chosen over stochastic modelling. Conceptually all the cytokine signalling models should consider spatial information of the components and thus should be modelled by PDEs. However, mathematical analyses of PDEs are not straight forward and it is more convenient to simplify PDEs to ODEs where possible. We have used spatial compartmentalization and sensitivity analysis to develop our signal transduction models in this thesis. Consequently, our systems meet the conditions of using ODE-based modelling.

We have chosen to follow an ODE modelling approach. This allows us to use experimental data (e.g. time course of protein expression) to parameterize our models, at the same time it is possible to investigate the mechanism, robustness and behaviour of the networks. The results of Chapter 4, 5 and 6, in which the proposed ODE-based models are analysed and tested experimentally, confirm

the validity of our modelling approach.

Approaches to modelling:

There have been at least 7 independent mathematical models of the TGF$-\beta$ signalling pathway (the whole pathway or only part of it), see table 7.1 in the Appendices. Most literature models of cell signalling use differential equations to model the networks of biochemical reactions. In the current research, we have built on the most recent ODE model of TGF$-\beta$ signalling provided by Zi et al. [511]. We have focused on the models with inhibitory feedback of the signalling pathway, this essential topological component seems to be missing in most of the existing models [72, 74, 308, 449, 511, 513]. The I-SMAD role as the inhibitory feedback component in TGF$-\beta$ signal transduction assures the stability and robustness of the system. It raises hypothesis that the signalling system is regulated by a balance between the feed-forward and feed-back reactions, therefore to achieve more accurate simulations it is essential to simulate both the inhibitory feedback as well as the feed-forward effects (signal transduction).

SMAD7 is assumed to be a key component for the crosstalk of TGF$-\beta$ signal transduction with other signalling pathways (see section 2.2.1 "SMAD6 and SMAD7, negative regulators"). A more complete description of the topology of the TGF$-\beta$ signalling models, the parameter and values outputs is given in Appendices.

2.3 IL − 6 Signalling Pathway

The interleukin-6 (IL − 6) family of cytokines all signal from the plasma membrane to the nucleus [186,254,389,514]. These cytokines act principally by changing the function of target cells, whether it happens in a paracrine or autocrine manner [239,251]. Cytokines of the four helix bundle family, such as IL − 6, participate in the differentiation, growth and regulation of the cells of the immune and hematopoietic systems [285]. However, it should be noted that members of the IL − 6 family signal in a wide range of cell types [83, 138, 444, 476]. Signalling happens when the IL − 6 cytokine binds with its specific receptor, such as $IL-6R$ (also called Gp80 [448]) and then to a common signal transduction co-receptor, 130 kDa glycoprotein (Gp130) [253]. Equilibrium binding studies have documented that Gp130 increases the affinity of the interactions between the IL − 6 and $IL-6R$ [189].

All members of IL−6 family, IL−6, $IL-11$, leukaemia inhibitory factor (LIF) , oncostatin M (OSM) , ciliary neurotrophic factor ($CNTF$) and cardiotrophin-1 (CT-1) use Gp130 to transfer the signalling to the cytosol. It is also known that Gp130 induces the cytoplasm signalling by activating the Janus kinases (JAK) [187,346]. The target genes activated by IL − 6 signalling participate in differentiation, apoptosis, proliferation, inflammation and the immune responses [175].

$\mathrm{IL}-6$ target genes have been studied carefully both structurally and functionally [175].

$\mathrm{IL}-6$ family members play a significant role in the response of the body to injury and inflammation [175,431,454]. Deregulation of the signalling pathways of $\mathrm{IL}-6$ member cytokines is associated with human hematological and epithelial malignancies [109]. $\mathrm{IL}-6$ is known to both promote and inhibit tumors [251]. It has been reported that $\mathrm{IL}-6$ is secreted via tumor cell lines together with many other cell types (such as fibroblasts, endothelial cells, monocytes, keratinocytes, lymphocytes, macrophages and mast cells) [83, 170, 193, 370, 444].

$\mathrm{IL}-6$ is responsible for the regulation of many inflammatory processes [24, 175, 431, 454]. Examples for inflammatory processes are: B cell development, macrophage activation, initiation of organ repair and the production of hepatic acute-phase protein [29, 83, 183, 255, 364]. An inflammatory disease occurs when the natural inflammation processes get deregulated [209]. One clinical treatment for inflammatory diseases is to block cytokine activities that have caused an exaggerated inflammatory response [209]. Drugs using this method have brought many clinical benefits to the treatment process for inflammatory diseases [209], however, it is essential to understand completely how/why this cytokine signalling system is distorted chronically and how this might be prevented or reversed [209].

$\mathrm{IL}-6$ signal transduction is likely to vary with respect to the strength of the initial signal i.e. the cytokine and receptor levels. In the remainder of this section, the Gp130 co-receptor and its role in $\mathrm{IL}-6$ signalling via the JAK/STAT [421] and MAPK pathways [98, 401] and the negative auto-feedback via SOCS3 [15, 138]will be discussed. The importance of $\mathrm{IL}-6$ transduction during the cancer progression and its effects on other signalling pathways is considered in the following sections (2.3.6 and 2.3.6). Finally, quantitation and mathematical modelling of $\mathrm{IL}-6$ signalling are introduced in a Systems biology context as the best approach to achieve an understanding of the signalling networks and their role in cancer studies.

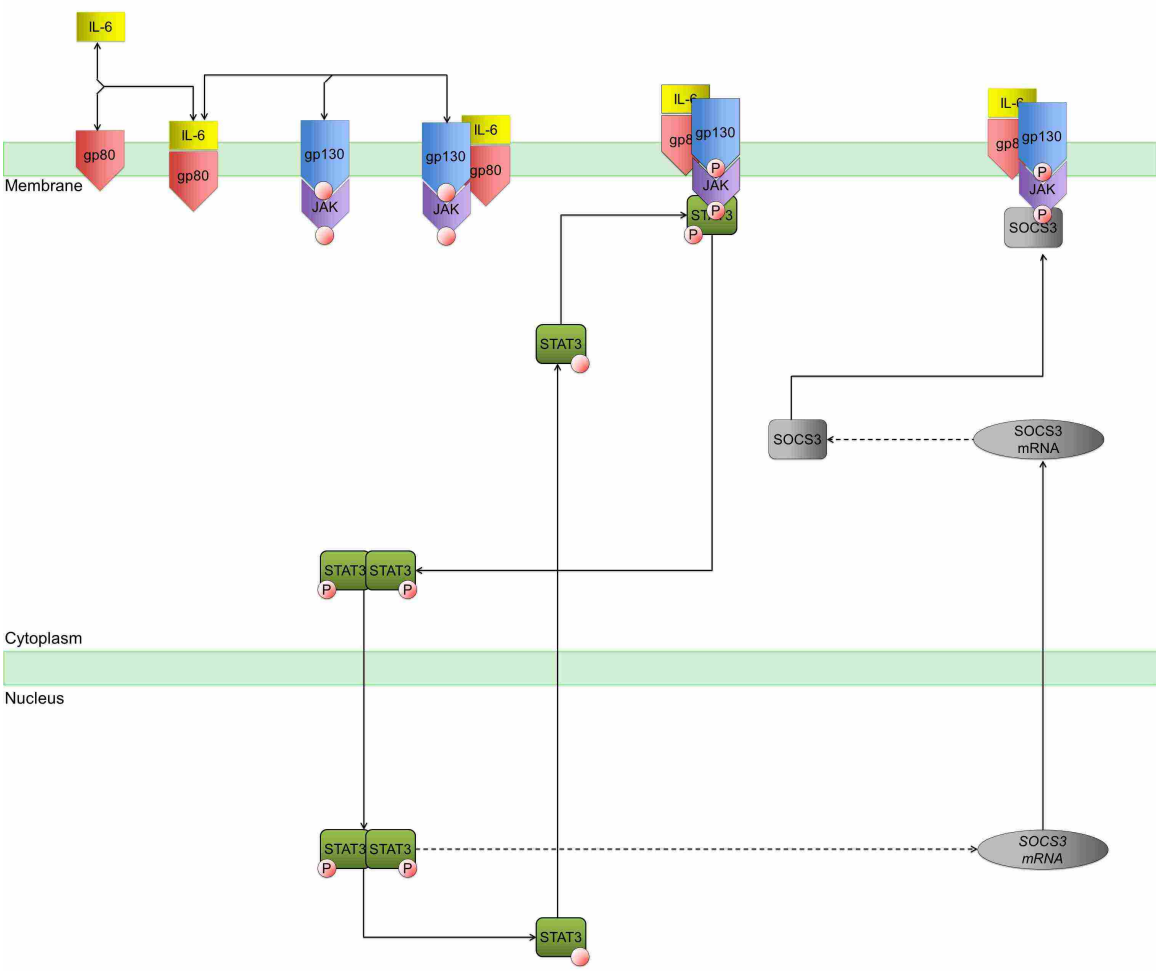

Figure 2.2: *The sketch of* IL − 6*:Gp130:JAK:STAT signalling. Potential phosphorylation sites of the receptors are specified with empty circles attached to membrane receptor components. The dot arrows represent the transcription and translation reactions. Note that the logistics of the signalling are expanded in Figure 5.1.*

2.3.1 Gp130 Membrane Co-receptor

Gp130 is found on almost all cell membranes (e.g. see [34, 160, 278, 310]). For example, cells from heart, lung, brain, kidney, spleen, colon and placenta all express Gp130 on their plasma membrane [209, 497]. Gp130 is essential for development [491], hematopoiesis [67], cell growth [81] and survival [113,209,497]. Gp130 regulates the binding sites for a broad range of cytokines [36, 38, 285]. In conjunction with the cytokine specific receptors, Gp130 transmits signalling for all of the IL − 6 family members (LIF, OSM, IL-6, IL-11, CNTF, CT-1, CLC, LIFR, OSMR and TCCR) [15]. Gp130 contains 6 tyrosine residues in its cytoplasmic domain, each prepares a different binding site for signalling proteins in the cytosol.

Gp130 is important for participating in a complex together with IL − 6 or IL-11 specific receptors (the $IL-6R$ is also known as Gp80 [181,309]). Ligand acti-

vation of the $\mathrm{IL}-6$:Gp130 complex leads to the activation of Src [432], JAK/Tyk tyrosine kinases [285] and STAT family transcriptional regulators [37, 176, 196]. Activation of JAK consequentially leads to phosphorylation of proximal tyrosine residues on Gp130 receptor [109, 209, 402]. The phosphorylated Y residues lead to binding of STAT3 and STAT1 [109, 144, 209]. Shp2 is also regulated through Y phosphorylation on Gp130 [109, 328, 402]. Shp2 contains a SH2 (Src Homology 2) domain in the N-terminal region and a Grb2 binding motif in its C-terminal region [117, 214, 453]. The activation of Shp2 is necessary for mitogen-activated protein kinase (MAPK) signal transduction to occur. MAPK activation involves the successive activation of Ras, RAF, MAPK MEK and ERK [109,402,428]. It is reported that Shp2 can act as an inhibitor for $\mathrm{IL}-6$ transduction via dephosphorylation of Gp130 receptors (this fact will be discussed later in this document). $\mathrm{IL}-6$ signalling activates two distinct pathways for transferring the incoming receptor-initiated signals to the nucleus: JAK/STAT and MAPK pathways [175, 176, 402]. In the following subsections these two pathways and their components are described in more detail.

2.3.2 JAK/STAT Pathway

As discussed earlier, the two of the receptors that take part in the JAK/STAT signalling pathways are Gp130 and Gp80 (also called IL-6Rβ and IL-6Rα, respectively [309]). Although Gp80 is essential for the $\mathrm{IL}-6$ transduction, it is Gp130 that activates the cytoplasmic signalling through its cytoplasmic domain [309]. This can be seen from the size of the cytoplasmic domains for each receptor. Gp80 contains only 82 amino acids in the cytoplasmic domain [309], compared to 277amino acids in the cytoplasmic domain of Gp130 [94, 309]. Most of the intracellular signalling is through Gp130 motifs (such as the $YSTV$ sequence for signalling through Shp2, MAPK signalling [114, 309], and the $YXXQ$ motif for STAT signalling [114, 309]).

Research on the crystallography of the cytokine/receptor complex of $\mathrm{IL}-6$ signalling pathway suggests a sequential sequence of binding [37]. First, $\mathrm{IL}-6$ binds to the extracellular domain of IL-6Rα. Next, the IL-6/IL-6Rα complex interacts with Gp130 and finally, the resulting complex is dimerised [37,138,411]. This hexameric complex is ready to initiate JAK/STAT signalling.

The cytoplasmic domain of the hexameric receptor complex has the ability to interact with an intracellular tyrosine kinase (JAK). In this pathway, JAK is the key protein through which the downstream signalling is propagated [109, 181, 309]. Four members of JAK family are found in mammals: JAK1, JAK2, JAK3 and TYK2 [214, 286, 326, 415]. All, except JAK3, are constitutively associated with cytoplasmic domain of Gp130 monomers [109, 478]. Binding of $\mathrm{IL}-6$ initiates the activation of JAKs. JAK activation happens via an autophosphorylation process after the octamer (2IL-6/2IL-6Rα/2Gp130/2JAK) is formed [109, 175, 181, 478]. The phosphorylation of JAK triggers the phospho-

rylation of the tyrosine residues of the two Gp130s in the complex and hence, creates binding sites for proteins containing phosphotyrosine binding domain (such as STAT transcription factors) [478]. It has been suggested that JAK1, among all the family members, is the most common kinase associated with Gp130 that triggers the STAT3 nucleocytoplasmic shuttling (reviewed by [214]). Immediately after the phosphorylation of the Gp130s, the receptor complex is ready to phosphorylate STAT3 [196,425]. Phosphorylated STAT3 separates from the receptor complex in the form of a dimer [196, 425, 478]. Phospho-STAT3 dimer is imported to the nucleus, acts as a transcription factor and loses its phosphatase there (dephosphorylation of STAT3) [232,490].

Mammalian STAT proteins are normally categorised into 7 major groups (STAT1, 2, 3, 4, 5a, 5b and 6) [176,195,196,346,426]. There are no identified STAT-like gene in unicellular organisms [176] so STATs are assumed to be the result of the multicellular organism evolution. Reports show that STATs can be activated via different receptor tyrosine kinases such as: epidermal growth factor(EGF) receptor [137,139,509], fibroblast growth factor(FGF) receptor [339,440], platelet-derived growth factor(PDGF) receptor [40, 338] and etc [46, 176, 332, 342]. All $\mathrm{IL}-6$ family members activate STAT3 and STAT1.

STATs are relatively large proteins with 750 to 850 amino acids [176]. This property let the STAT family members interact with many different proteins through their various domains [176]. The Src homology 2 ($SH2$) is the domain responsible for STAT binding to the tyrosine-phosphorylated receptor motifs and also homo- and hetro- dimerization among the family members [152, 176, 398]. This variety in binding sites of STATs gives them the capability to be the common transcription factors for multiple transcription factors [176,468,488].

The dimerization of STATs is essential for the DNA binding. The DNA binding domain is located in the middle of the STAT molecule [176, 398]. Nuclear translocation of the STAT dimer can be followed by indirect immunofluorescence [176,342]. STAT translocation to the nucleus is transient, i.e. the STAT concentration returns to its pre-stimulus levels within 2 hours [176,342]. A nuclear localization sequence (NLS) has not been identified for the STATs [176,307,390].

There are number of $\mathrm{IL}-6$ target genes activated by STATs:

1. APP genes [31,500]: C-reactive proteins, α_1-antichymotrypsin [66,256], α_2-macroglobulin [349, 466], lipopolysaccharide-binding protein [8, 387]and tissue inhibitor of metalloproteinases ($TIMP$) [50,231]

2. transcription factors: $JunB$ [78], $c-Fos$ [184, 480], interferon regulatory factor (IRF)-1 [167, 418] and CCAAT enhancer binding protein (C/EBP) [252, 489]

3. Other genes: interstitial collagenase [105, 257], vasoactive intestinal peptide [77, 424], pro-opiomelanocortin [366, 442], heat-shock protein hsp90

[8,419], bcl-x [129,435] and IL − 6 signal transducer Gp130 [334]

2.3.3 MAPK Pathway

IL − 6 stimulation activates the MAPK pathway. Mitogen-activated protein kinase (MAPK) [190, 337] is a highly conserved mechanism associated with the regulation of cell proliferation [263]. MAPK signalling can be initiated by different types of cytokine stimulation, including TGF−β [87, 420] and IL − 6 family stimulations [185, 263]. MAPK activation plays a role in gene transcription, cell cycle regulation, apoptosis, protein biosynthesis and cell differentiation [229, 263].

Sh2-domain of Shp2 is used to help the phosphorylation of Tyr^{759} residue of activated Gp130 [39, 331, 416]. Sh2-containing tyrosine phosphatase (SHP2) is then phosphorylated by the activated JAKs [144, 185, 381, 416]. Phosphorylated Shp2 interacts with growth factor receptor bound protein 2 (Grb2) [505] that associates with son of sevenless (Sos). Sos [142]is a GDP/GTP exchanger for Ras [58]. Activation of ERK/MAPK cascade happens through the GTP form of Ras [180]. The activated ERK/MAPK signal is transferred to in the nucleus, targeting the transcription factors i.e. NF-IL-6 [185, 309].

The ERK/MAPK [233] signalling pathway has been investigated in detail [214]. In this document, we focus on the IL-6/JAK/STAT signal transduction in order to emphasize on the STAT3 key role in inflammation and cancer [171]

2.3.4 Inhibitory Feedback of SOCS3

The mechanism for down-regulation of JAK/STAT signal transduction is caused by the suppressor of cytokine signalling (SOCS) proteins [176]. This family of proteins is also known as "JAK-binding proteins (JAB)" and/or "STAT-induced STAT inhibitors (SSIs)" [15, 108, 176, 322, 417]. SOCS transcription is induced by the IL − 6 and LIF [303] cytokines. SOCS function as inhibitors of tyrosine phosphorylated Gp130, STAT1 and STAT3 [108, 176, 322].

The SOCS family contains 8 members: SOCS1-SOCS7 and CIS [83]. Due to their SH2 domain, SOCS are able to directly interact with the kinase domain of JAK family members [108, 176, 328], reducing their tyrosine kinase activity. Thus SOCS proteins are JAK inhibitor and provide negative feedback on the JAK/STAT signalling system [176]. The ability of SOCS to inhibit the JAKs comes from a short motif in the SH2 domain, known as the KIR (kinase inhibitory region) [16,42]. JAK inhibition via KIR is the dominant mode of action of SOCS1 and SOCS3 *in vivo* [16,42,502].

Through the carboxy-terminal SOCS box, SOCSs target the Gp130 signalling complex for polyubiquitination and proteosomal degradation [6,83]. The SOCS box is a C-terminal sequence of almost 40 amino acids that contains 2 conserved regions [43, 217]. It is believed that the SOCS box is essential for the stability

of the SOCS proteins [43,218]. Over-expression studies reveals that SOCS box, together with the PEST sequence of SOCS3, facilitates the degradation of the SOCS3 [17]. Experiments show that SOCSs act as the coordinators of the biological responses to the specific cytokines, as well as, their role in attenuating the cytokine signalling (by degradation of the active complexes on the membrane [201,379]) [83].

SOCSs proteins also compete with STATs for binding to the phosphorylated sites on the Gp130 receptor [322,477]. Thus SOCS3 can interact with both JAK and Gp130 simultaneously. This property creates a ternary complex with high overall affinity [16]. Consequently, if the binding cytokine signals through receptors with the same binding sites as the SOCS3 (such as $IL-6/Gp130$), its signal transduction will be suppressed by SOCS3 [16,479]. It is also important to note that SOCS3 interacts with JAK1, JAK2 and TYK2 but not JAK3 [16]. This selectivity is because of a motif in the JAK insertion loop [16]. Through this interaction, SOCS3 is able to identify the target JAK and distinguish between them. The lack of this specific motif (motif$^{1071-1073}$ GQM) in JAK3 removes the SOCS3 feedback inhibition of its signalling [16].

2.3.5 $\mathrm{IL}-6$ and Cancer

Historically, $\mathrm{IL}-6$ was first discovered by Hirano and Kishimoto in 1986 as a B cell stimulating IgG production [186,327]. $\mathrm{IL}-6$ is produced by many tumors, for example: melanoma [214,316], multiple myeloma [214,228]and prostate cancer [214,407]. $\mathrm{IL}-6$ can act as autocrine and/or paracrine growth factor to stimulate tumor growth. Additionally, $\mathrm{IL}-6$ levels change in age-related diseases (e.g. Alzheimer's [508]). It has been assumed that the decrease in the level of sex hormones which occurs in aging, increases the $\mathrm{IL}-6$ levels [111,214].

As mentioned before, because of the Gp130 involvement in the $\mathrm{IL}-6$ transduction, any deregulated production of $\mathrm{IL}-6$ can induce distributed undesired inflammation in the organs. Many diseases progress via $\mathrm{IL}-6$ over-expression, e.g. Alzheimer's disease [99, 333], type 2 diabetes [92, 356]and some carcinomas [64,221]. A recent study reveals a direct relationship between the ulcerative colitis, developing colon cancer, over-expression of $\mathrm{IL}-6$ and the level of activated STAT3 [270]. Similar findings suggest that inhibition of $\mathrm{IL}-6$ signalling may prevent the progression of chronic inflammatory diseases and inflammation associated cancers [327].

2.3.6 Crosstalk

One of the features of $\mathrm{IL}-6$ signalling is that it interacts with other signalling pathways via its receptor, Gp130, and the alternatives in its downstream signalling (JAK/STAT and MAPK). There is evidence that $\mathrm{IL}-6$ crosstalks with cytokines such as BMP [493], NF-$\kappa\beta$ [31], Wnt/β-catenin [47]and $\mathrm{TGF}-\beta$ [207].

The focus of this project is on the IL−6 and TGF−β crosstalk, with an emphasis on the role of SMAD7. This relationship is supported by the interaction between STAT3/SMAD7/TGF−β in tumors where the EGFR was over-expressed and activated [287]. Persistent activation of STAT3 stimulates the SMAD7 expression, which then desensitizes TGF−β signal transduction [207,287]. Luwor et al. (2012) showed that this relationship occurs *in vivo* as well as *in vitro*. Yao et al [495] have reported that both TGF−β and IL − 6 are hyper-activated in Erlotinib-resistant cells and are essential for the survival of cancerous lung cells.

The concept of this thesis is the report on IL − 6:TGF−β interactions by Jenkins et al. (2005) [207] . They used "MEF" (mouse embryonic fibroblast) cells and mutated Gp130 in order to over- express STAT3 or STAT1. Cells with STAT3-hyperactivation illustrate impaired activation and nuclear translocation of SMAD2. Therefore, the TGF−β signal transduction was down-regulated in mutated MEFs . They tested their hypothesis using a PSMAD7-luc reporter to follow the SMAD7 transcription levels in mutated cells. They have also repeated the experiment *in vivo* with the same result [207].

The interaction between the TGF−β and IL − 6 signalling systems is very important in inflammatory, auto-immune diseases and cancers. As a result, it is essential to study both pathways quantitatively, and identify their precise possible interactions and predict ways to modulate the pathological signalling.

2.3.7 Mathematical Approach to the Modelling IL−6 Signalling

There are several mathematical ODE models of the JAK/STAT [70,320,402] signalling pathway. Most of the models of IL − 6 signalling concentrate on MAPK signalling through Shp2 [402]. For our purposes, we have developed a mathematical model with precisely quantified components for JAK/STAT signalling.

Singh et al. [402] proposed a model of IL − 6 signalling based on the literature data sets. The roles of SOCS3, Shp2 and PP2 (nuclear phosphatase) were studied subsequently by knock out studies [402]. Singh et al. [402] compared the responses of the model for perturbations of specific components in order to specify their functions. Although their model is comprehensively designed, there was no validation of the model. In addition a number of details that were overlooked in their model (such as transcription and protein synthesis). No mathematical compensations were applied to the model to compensate for these omissions. This model, notwithstanding, is one of the first attempts to develop a mathematical formulation from biological models of the IL − 6 signalling. I have used some of the kinetic values and initial conditions from Sing et al. [402] for this project.

Another IL − 6 model has been proposed by Huang et al. in 2010 [70]. They based their model on Singh et al. [402], but used sensitivity analysis and parameter clustering to simplify the model. They provided evidence that their simplification method was valid by comparing their results with the results of

the original Singh's model. Their work has identified the most important and effective components in the original model, however, the validation of the model against experimental data was not attempted.

The most recent mathematical model of the $\mathrm{IL}-6$ signalling pathway was published in 2010 by Moya et al. [320]. Again, the foundation of their model was Singh's model. They repeated the sensitivity analysis and used some new parameter estimates. They also used an implicit model of dynamics for the MAPK pathway. Finally, they applied same analysis and methods to IL-10 signal transduction. Experimental data were used in the MAPK signalling analysis. The $\mathrm{IL}-6$ and IL-10 models were used to investigate their roles in the regulation of STAT3. The paper perfectly filled the gap lacking in the mathematical and statistical analyses of the previous models, however, including MAPK signalling, all signalling pathways which activate MAPK must have been considered in the model.

Therefore, a model of the $\mathrm{IL}-6$/JAK/STAT signalling which focuses on the signalling crosstalks via activated STAT3 is not yet available. In this thesis I propose such a model and integrated $\mathrm{IL}-6$ signalling with the $\mathrm{TGF}-\beta$ model to investigate interactions between these pathways.

2.4 Summary

Intracellular signalling pathways play essential roles in regulation of the cell functions. Many diseases, such as different cancer types, are developed by the deregulation of the signalling pathways. Because of the close connection of inflammation and cancer, it is important to study the crosstalk between the inflammatory the growth signalling pathways. Additionally, the complexity of the intracellular signalling networks highlights the need for Systems biology approach and quantitative modelling of the networks. Two specific signalling pathways are studied in the current thesis: $\mathrm{IL}-6$ signalling which is upregulated while inflammatory responses and $\mathrm{TGF}-\beta$ signalling which causes anti-growth responses. Individual studies have identified the major components involved in each signalling system qualitatively. However, no quantitative analysis and modelling are reported which emphasizes on the crosstalk between $\mathrm{IL}-6$ and $\mathrm{TGF}-\beta$ signalling pathways.

This points to the need for development of two separate mathematical models which follow Systems biology principles in order to quantitatively identify the components of each signalling system and their role in the final output of the system. Next, mathematical models are experimentally validated individually. The $\mathrm{IL}-6$ and $\mathrm{TGF}-\beta$ signalling models are combined together to develop an integrated mathematical model which inspects the crosstalk between the two pathways.

This literature review has covered four major aspects of this project:

First, the Systems biology approach and its different methods were reviewed as the main theme of studying the $\mathrm{IL}-6$, $\mathrm{TGF}-\beta$ and the integrated models. Second, $\mathrm{TGF}-\beta$ signalling pathway and its key signalling components were reviewed, focusing on the role of $\mathrm{TGF}-\beta$ signalling in cancer. Previous mathematical models of $\mathrm{TGF}-\beta$ signal transduction in the literature were reviewed to specify the contribution of this project. Third, $\mathrm{IL}-6$ signalling pathway and the interaction between its components were studied, emphasizing on the literature mathematical models of $\mathrm{IL}-6$ signalling. Fourth, the crosstalk between $\mathrm{IL}-6$ and other signalling pathways were analysed, focusing on Jenkins et al. (2005) [206] first discovery of the attenuation of $\mathrm{TGF}-\beta$ signalling via $\mathrm{IL}-6$ up-regulation.

Chapter 3

Methods

- All methods in this Chapter were performed by the applicant.
- In the revised thesis, all abbreviations are either explained in full or detailed in the "Abbreviations" section on pages vii-ix.

3.1 Measurement of Key Signalling Components

MEFs were grown to confluence and the proteins extracted with detergent buffers. The method we used to quantitate the levels of SMAD2, STAT3, SMAD7, PSTAT3 and PSMAD2 was Western blotting. Where needed the experimental data set and the kinetic rates used to set initial parameters for the model were elicited from the literature [72,74,308,386,402,449,479,511,513].

Once the initial concentrations for the key signalling components were determined for MEFs, the cells were fractionated into plasma membrane, cytosol and nuclear compartments to measure the sub-cellular concentrations of each key signalling component. The proteins from cultured cells were harvested from 5 minutes to 2 days after stimulation and the levels of the key signalling components in the three subcellular compartments were measured quantitatively. The measurements are compared to the predicted values from the computer modelling.

3.1.1 Cell Culture and Cell Lysis

Mouse embryonic fibroblasts (MEFs) cells were isolated from day 13 to 15 embryos. Wild type MEFs and MEF Gp130$^{F/F}$ [206] and SV40-immortalized MEFs [147] cells were cultured in DMEM containing 15 $\%$ FCS . The cells were typsinazed and washed with DMEM + 15 $\%$ FCS before plating. Passage 3 cells were seeded at 1×10^6 MEFs/well in 60 mm plates for 0-4 hour, 0.5×10^6 MEFs/well for 24 hour and 0.25×10^6 MEFs/well for 48 hour treatment with 1 ng/ml $\mathrm{IL}-6$ (Ref 1661.F33. WEHI) and/or 5 ng/ml $\mathrm{TGF}-\beta$ respectively (for Gp130$^{F/F}$ MEFs the cell numbers changes as: 1.2×10^6 MEFs/well for 0-4 hours, 0.6×10^6

MEFs/well for 24 hours and 0.3×10^6 MEFs/well for 48 hours). After washing with cold PBS for two times, cells were lysed in ice-cold 200 ul RIPA lysis buffer, containing 1M Tris/HCL, 0.5 M EDTA , 5M NaCl, 10 % Na-Doc , 10 % TX-100, 10 % SDS , protease inhibitor 100 $\times$ and H_2O. The cell lysates were passed through 27 G needle for 5 times, then incubated in ice for 20 min. After incubation the samples were spun at 13,000 rpm for 30 min at 4^oC. The supernatant was transferred to new tubes where 20 ul of sample was used for a BCA protein assay using sigma BCA assay kit (product No. B9643). 20 ul $5\times$ SDS sample buffer was added to 80 ul of the lysate and the samples were heated at 95^oC for 10 min. The following steps were followed to prepare the samples for Western blot experiment.

Cell Collection

- Aspirate (remove the medium by vacuum suction) the medium.
- Add 5 ml PBS to remove all FCS. Wash and aspirate it. Repeat this step once more to remove all the medium (FCS neutralizes the trypsin therefore any traces of media will inhibit the action of the trypsin on the cells)
- Add 2 ml TV .
- Put the plate in the incubator for about 30 sec - 1 min.
- Label cell culture flasks. (Usually 3 or 4 flasks would be needed when learning to seed cells at a particular cell density or number)
- Use 50 ml Falcon tube. Label it with cell name.
- Add 10 ml medium to the cells and transfer them all to the 50 ml tube.
- Re-suspend the mixture for about 5 times
- Spin the mixture for 5 minute and aspirate the above medium then re-suspend the pellet in 10 ml fresh medium.

Cell Count

- Take a 100 ul sample of the cells. Use the 1.5 ml Eppendorf tubes
- Add 30 ul of the TB liquid to 1 well of a 96 well dish.
- Mix the 100 ul aliquot (sample) of cells and add to 30 ul of the cells to the trypan blue volume.
- This is a 1:2 dilution (dilution factor should be considered when calculating cell number/ml)
- Insert 10 ul of the mixture on to the cover-slip of the heamocytometer.
- Count each of the 4 square separately and take the average.

- Multiply the dilution factor and the zooming factor (1e4).This is the number of cells per ml.
- Multiply the amount of the medium (2 ml TB + 10 ml FCS DME). This would be the total number of cells.

Cell Culture Set-up

- In order to have different cell concentrations in each flasks/dishes calculate the volume of the cells for different numbers of cells per ml (i.e.: 0.5e6, 1e6, 2e6, 4e6).
- Add those calculated volumes to 10 ml of medium
- Label the flasks/dishes with cell line, passage number, date, type of medium, total cell count added to the flask/dish and volume

3.1.2 Western Blotting

According to the protein concentration results from the protein assay, Novex NuPAGE® 4-12%-Bis-Tris (life technologies NP0335 Box) gels were used for loading the lysates for each time point. PSTAT3 (XP^{TM} Rabbit mAb) antibodies were provided by Cell Signalling Technology (product No. 9145) and were used at a dilution 1:500 in 3% BSA-TBS-T . Antibody directed against SMAD7 was purchased from Santa Cruz Biotechnology and was diluted according to the manufacture's instructions. PSMAD2 antibody (rabbit polyclonal anti-phospho-Smad2 antibody (1:1000 for Western blot)) was a gift from Prof. Peter ten Dijke (Leiden University Medical Center, Netherlands). PSTAT3 (XP^{TM} Rabbit mAb) antibodies were provided by Cell Signalling Technology and were used at a dilution 1:500 in 3% BSA-TBS-T.

β-tubulin, Lamin B1 and transferrin receptor were used as loading control depending on the protein to be expressed. The gels were transferred onto nitrocellulose stained membrane via iBlot 2 gel transfer device (life technologies) and the membranes were scanned quantitatively using Odyssey infrared scanner (LI-COR). The following describes step by step procedure of Western blotting.

- Prepare a gel. Put it inside the western blot container.
- Use the MOPS as the liquid of the western blot if the proteins are quit big in size.
- Dilute the MOPS 1:20 (25 ml of MOPS in 500 ml of DDT).
- Pour the diluted liquid in the centre of the western blot container. Let it to redound to the sides spaces.

- Wash the wells of the gel using a syringe.
- Leave one of the wells for the standard sample. Here it is see-blue. Add 7 ul of the see-blue to the well.
- Use your pre boiled samples and fill all the wells in turn.
- Apply voltage to the container for about 1 hour.(The applied voltage should be between 150-180 V)
- Take the gel out and open it gently.
- Transfer the gel to the membrane and leave it about 6-8 min.
- Put the membrane in milk and cover it with aluminium foil and leave it on the shaker for a night. (we use the milk to block all the empty spaces between the layers to avoid unwanted bindings)
- Use TTBS (TBS-T) to wash the membrane. First rinse the milk. Then repeat the washing 4 times with 10 ml of TTBS following with 5 min moving on the shaker.
- Dilute 0.01 of the first anti body in 10 ml TTBS in Falcon tube.
- Add the 1st Ab to the membrane.
- Put the membrane on the shaker for another one hour.
- Another 4 time wash with 5 min shaking.
- Dilute 1ul of the second anti body in 10 ml TBS.
- Add the secondary Ab to the membrane and cover it with aluminium foil in order to avoid unwanted bindings caused by light.
- Put it on the shaker for another 1 hour.
- Repeat the 4 time wash and 5 min shaking.
- The last wash is with the 10 ml PBS to remove TTBS itself.
- Scan the result using Odyssey infrared scanner (LI-COR).

3.1.3 Protein Quantitation

The western blot images were quantitated using ImageJ 1.49p [140]. The signals for each protein were normalised using the loading controls.

3.2 Computer Modelling

The program used in this project was PYTHON 2.7 and MATLAB 7.10. PYTHON is known as a high-level multi-paradigm, object-oriented programming language. It also uses fully dynamic type system which benefits from an automatic memory management in addition to a comprehensive standard library. There are also several interpreters used for PYTHON which are suitable for almost every operating system. MATLAB is a well known and wildly used programming tool. It is a high-level language and interactive environment for numerical computation, visualization, and programming. Using MATLAB, you can analyze data, develop algorithms, and create models and applications. The curve fitting tool box of MATLAB is used for fitting the Hill equation to Figure 6,7,8 and 9 and deriving the Hill coefficients.

The other program that has been applied for the model development is CellDesigner [302] which is a structured diagram editor used to develop models of biochemical networks. The graphical notation system is stored in the form of Systems biology Markup Language (SBML) files but, it also supports simulations with Copasi [450]. Figures describing the model were produced via CellDesigner4.3 and Microsoft Power Point.

3.3 Design and Modelling Methods

3.3.1 Mathematical Modelling of the Intracellular Protein-Protein Reactions

Most common computer representations of cytokine signalling pathways use a set of ordinary differential equations (ODE) [20, 249]. In this method, the reaction rates are a representation of mass action kinetics and are proportional to the reactant concentrations. The ODE modelling method, when all of the components are known, is a reliable interpretation of dynamic behaviour of the system components. The parameters of this model need to be estimated quantitatively using mass spectrometry, mass immunoblotting or protein microarrays. For complex dynamic systems, such as cell signalling pathways, it is not possible to solve the ODEs analytically. Consequently, numerical integration solutions are required and hence, sensitivity analysis become more vital to identify the critical signalling components which regulate the output of the system. Furthermore, numerical integration can result in large changes even where changes in parameter values are small; therefore, by identifying the components to which the system is more sensitive, a more robust and reliable model of the system can be developed [177].

As mentioned earlier, the ODE modelling method is based on a mass-action kinetics assumption in which the rate of a reaction is defined to be proportional

to the concentration of the species of the reaction. In cases where this assumption breaks down- for example when spatial gradients of the species are important or when the concentrations are so low that stochastic fluctuations in the system can affect the steady-state and the states are not continuous, other modelling methods are normally used (PDEs or stochastic modelling) [292, 305].

Classical modelling of biochemical reactions decompose the complex signalling networks to a series of simple one or two direction reactions. For each reaction (both reversible and irreversible) the changes in the concentration of each component are described by a specific differential equation. Whenever two successive reactions share a component, the concentration of that component appear on the RHSs (right hand side) of the differential equations as a positive or negative term. For a review on the modelling of intracellular reaction kinetics see [154, 408, 409].

As an example for the mathematical modelling of a biochemical reaction using differential equations, a reversible protein-protein binding reaction is illustrated in Figure 3.1.

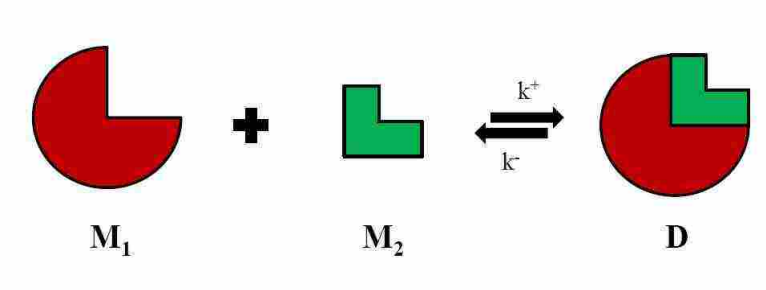

Figure 3.1: *A reversible biochemical reaction which shows the binding of two proteins. M_1 and M_2 bind together to produce D with the rate of k^+. Similarly, k^- specifies the rate of dissociation of D to M_1 and M_2.*

The corresponding biochemical reaction can be written as:

$$M_1 + M_2 \underset{k^-}{\overset{k^+}{\rightleftharpoons}} D,$$

where k^- and k^+ represent the kinetic rates of the reaction. Below are the corresponding differential equations for every component in this reaction:

$$\begin{aligned}
\frac{\mathrm{d}M_1}{\mathrm{d}t} &= -k^+ M_1 M_2 + k^- D \\
\frac{\mathrm{d}M_2}{\mathrm{d}t} &= -k^+ M_1 M_2 + k^- D \\
\frac{\mathrm{d}D}{\mathrm{d}t} &= k^+ M_1 M_2 - k^- D
\end{aligned}$$

Each differential equation describes the change of the concentration of a component with time. The kinetic rate constants appear on the RHSs.

3.3.2 Reduction, Scaling and Non-dimensionalization Methods

Complexity and the multiplicity of the components involved in a signalling network (more specifically intracellular signalling networks), often make models difficult to solve [146]. To tackle this problem, several reduction and simplification methods have been developed [115, 146]. Separating the reactions according to their time-scales and dividing the system to two subsystems (fast and slow) is one effective way of reducing the model variables and equations. In biochemistry, this method (the time-scale based reduction method) is known as the "rapid equilibrium assumption" [115, 203]. The rapid equilibrium assumption is based on the "singular perturbation" theory for nonlinear systems [272]. Both mass-action and Michaelis-Menten kinetics in biochemistry can be treated using singular perturbation methods (see [272] for more details). In an enzymic reaction, the small dimensionless parameter (ε), which appears in the singular perturbation format of the equations, is defined as the ratio of the initial concentrations of the enzyme and substrate [272].

In signalling networks, the system often evolves on different timescales, this allows us to benefit from the rapid equilibrium assumption in order to reduce and simplify the equations. We have used this method to decrease the complexity of our models.

One of the most important and challenging part of modelling signalling pathways is the matching of dimensions and units for the variables and kinetic rates in the model equations. To avoid mistakes in calculating the units of the variables and kinetic rates, we have used a non-dimensionalization method to substitute dimensionless variables in the equations [65,115]. Non-dimensionalization [65,115] can be used to ensure that every term in a model is consistent and all parameters are defined in appropriate units, this process is often followed by scaling of the variables and their coefficients. The parametrization of a model (specifically, the models described by differential equations) can be simplified via non-dimensionalization method. The non-dimensionalization method and its benefits are described in more detail in Chapter 4, section 4.4.

Due to the different levels of protein concentrations, detected during Western blot quantitation, it is important to use scaling methods. The experimental data are scaled to allow comparison with the simulation results.

Reduction Method

The greatest advantage of reduction methods in Systems biology is that they reduce the number of components and elements involved in the model and thus, the complexity of the model. It is possible to eliminate the components that do not significantly affect the dynamics and steady-state of the system and are difficult to measure quantitatively. The reduction method used in this thesis is "rapid equilibrium assumption". This method relies on the separation of the variables (or the reactions) in the system into "fast" and "slow". Time-scale separation

of the biochemical reactions allows one to simplify the kinetics at steady-state (or equilibrium). This section provides examples of applying rapid equilibrium assumption on biochemical systems in Chapters 4 and 5.

For instance, consider the high affinity dimerization process of $\mathrm{R2}$ ($\mathrm{TGF}-\beta$ receptor type two, see Chapter 4 for more details) that is much faster than the other $\mathrm{TGF}-\beta$ signalling reactions. In comparison to every other reaction in the $\mathrm{TGF}-\beta$ system, $\mathrm{R2}$ dimerization time scale is large enough to enable us to use the rapid equilibrium assumptions.

The time scale of each biochemical reaction can be calculated from the corresponding differential equations of the participating components. The time scale of a conversion reaction ($A \underset{k^-}{\overset{k^+}{\rightleftharpoons}} B$), for instance, is defined as the following:

$$\tau = \frac{1}{k^- + k^+},$$

which is calculated via solving the differential equation of A, i.e. $dA/dt = -k^+A + k^-B$, considering the fact that the total amount of $A + B$ is constant in time. Note that $\tau \ll 1$ if and only if $\begin{cases} k^- \gg 1 \\ or \\ k^+ \gg 1 \end{cases}$. However, it is easier for biologists to work with off rate, k^-. When, $k^- \gg 1$, τ can be estimated with the inverse k^-:

$$\tau \simeq \frac{1}{k^-}$$

In case of $\tau \gg T_i$ it is allowed to implement rapid equilibrium assumptions into our system. Here, T_i represents time scales of all other reactions of the system.

Our initial receptor model is illustrated in the following reactions: (In this section all primes denote the differentiation with respect to time.)

$$\mathrm{R2} + \mathrm{R2} \overset{K_2}{\rightleftharpoons} \mathrm{R2_2} \tag{3.1}$$

$$\mathrm{R1} + \mathrm{R1} + \mathrm{R2_2} \overset{K_{\mathrm{RC}}}{\rightleftharpoons} \mathrm{RC} \tag{3.2}$$

Equation 3.2 consists of two successive steps. In fact, the effect of $\mathrm{R1}$ dimerization is hidden in equation 3.2. In order to apply the rapid equilibrium assumption on our system, equation 3.2 should break into two steps:

$$\mathrm{R1} + \mathrm{R1} \overset{K_1}{\rightleftharpoons} \mathrm{R1_2} \tag{3.3}$$

$$\mathrm{R2} + \mathrm{R2} \overset{K_2}{\rightleftharpoons} \mathrm{R2_2} \tag{3.4}$$

$$\mathrm{R1_2} + \mathrm{R2_2} \overset{K_{\mathrm{RC}}}{\rightleftharpoons} \mathrm{RC} \tag{3.5}$$

We assume all these reactions are fast. According to equations 3.3, the differential equations describing $\mathrm{R1}$ and $\mathrm{R1_2}$ dynamics will be as the following:

$$\mathrm{R1}' = -2k^{+}\mathrm{R1}^{2} + 2\mathrm{k}^{-}\mathrm{R1_2} \tag{3.6}$$

$$\mathrm{R1_2}' = k^{+}\mathrm{R1}^{2} - \mathrm{k}^{-}\mathrm{R1_2}\,, \tag{3.7}$$

where r_{R1} and $r_{\mathrm{R1_2}}$ represent other terms of the equations such as, production and degradation of each substance or the association and dissociation of the successive components. k^{+} and k^{-} represent the forward and respectively, backward kinetic rates for the $\mathrm{R1}$ and $\mathrm{R2}$ dimerization reactions. Next, we apply the conservation law on $\mathrm{R1}$ as a substance of the reaction 3.3:

$$\mathrm{R1}_{\mathrm{T}} = \mathrm{R1} + 2\mathrm{R1_2} \tag{3.8}$$

The conservation law for $\mathrm{R1}$ states that the total amount of $\mathrm{R1}$, by definition, equals to the total amount of $\mathrm{R1}$ as monomers adding by twice of the amount of $\mathrm{R1}$ as dimmers (which is twice of $\mathrm{R1_2}$). This law is true in every condition. At equilibrium, the total flux for each reaction must be zero,i.e. the right arrow flux should be equal to left arrow flux (equation 3.3):

$$k^{+}\mathrm{R1}^{2} = \mathrm{k}^{-}\mathrm{R1_2}$$

A new term is defined; $K = \frac{k^{-}}{k^{+}}$ which is called the "equilibrium constant" and has units of "concentration". Consequently, $\mathrm{R1_2}$ can be rewritten in terms of $\mathrm{R1}$ and K, $\mathrm{R1_2} = \frac{\mathrm{R1}^{2}}{K}$.

At equilibrium, the equation 3.8 can be written as:

$$\mathrm{R1}_{\mathrm{T}} = \mathrm{R1} + 2\frac{\mathrm{R1}^{2}}{\mathrm{K}}$$

Now if we differentiate this equation with respect to time (the independent variable) and subsequently we will have:

$$\mathrm{R1}'_{\mathrm{T}} = \mathrm{R1}' + 4\frac{\mathrm{R1}}{\mathrm{K}}\mathrm{R1}' \tag{3.9}$$

On the other hand, $\mathrm{R1}'$ and $\mathrm{R1_2}'$ have already been defined via stoichiometry equations (equations 3.6 and 3.7). Substituting equations 3.6 and 3.7 into the recent equation for $\mathrm{R1}'_{\mathrm{T}}$ (equation 3.9), we would have another description for $\mathrm{R1}'_{\mathrm{T}}$:

$$\mathrm{R1}'_{\mathrm{T}} = -2k^{+}\mathrm{R1}^{2} + 2\mathrm{k}^{-}\mathrm{R1_2} + \mathrm{r_{R1}} + 2\mathrm{k}^{+}\mathrm{R1}^{2} - 2\mathrm{k}^{-}\mathrm{R1_2} + 2\mathrm{r_{R1_2}} \text{ or} \tag{3.10}$$

$$\mathrm{R1}'_{\mathrm{T}} = r_{\mathrm{R1}} + 2r_{\mathrm{R1_2}}$$

Combine the equations 3.9 and 3.10, a single equation will be derived:

$$\mathrm{R1}'(1+4\frac{\mathrm{R1}}{\mathrm{K}}) = \mathrm{r_{R1}} + 2\mathrm{r_{R1_2}} \tag{3.11}$$

This equation propose a differential equation for $\mathrm{R1}$. In fact, we have reduced a system of two coupled differential equations (equations 3.6 and 3.7) into a single differential equation for $\mathrm{R1}$ and hence, eliminated the direct dependence of the system on one of the variables,$\mathrm{R1_2}$.

The left hand side factor of equation 3.11, $(1+4\frac{\mathrm{R1}}{K})$, summarizes what happens during the dimerization process while, the right hand side describes the other reactions that affect the $\mathrm{R1}$ dynamics directly or through affecting $\mathrm{R1_2}$ dynamics, for instance $\mathrm{R1}$'s production and degradation reactions.

At equilibrium, the changes in the total amount of $\mathrm{R1}$ in time ($\mathrm{R1_T}'$) must be zero. Therefore, the left hand side of the equation equals zero and, it can be stated that equation below is the equilibrium condition of the dimerization reaction:

$$r_{\mathrm{R1}} = -2r_{\mathrm{R1_2}}$$

The nullclines in the slope field (phase portrait) is shown by $\mathrm{R1}' = 0$, thus it is only $r_{\mathrm{R1}} + 2r_{\mathrm{R1_2}}$ term that determines the nullclines. The velocity vectors longitude is proportional to K through the $\mathrm{R1}' = (\mathrm{r_{R1}} + 2\mathrm{r_{R1_2}})/(1+4\frac{\mathrm{R1}}{\mathrm{K}})$ equation.

The calculations above show the procedure of applying the rapid equilibrium assumptions on each fast reaction. We will benefit from this reduction method in Chapter 4 and 5 because of its advantages. These assumptions can be made only if the time scale of the reaction is remarkably greater than other reactions of the system.

Equations 3.3 and 3.4 follow the same model of dimerization. Therefore, the reductions applying to $\mathrm{R2}$ are the same as $\mathrm{R1}$. The final form of the reduced version of $\mathrm{R1}$ and $\mathrm{R2}$ dimerization would be as the following:

$$(1+4\frac{\mathrm{R1}}{K_1})\mathrm{R1}' = \mathrm{r_{R1}} + 2\mathrm{r_{R1_2}} \tag{3.12}$$

$$(1+4\frac{\mathrm{R2}}{K_2})\mathrm{R2}' = \mathrm{r_{R2}} + 2\mathrm{r_{R2_2}} \tag{3.13}$$

The dimerization reaction between identical species is called "fast homo-dimerization" (see equations 3.3 and 3.4). If we have a closer look at equation 3.5, it is clear that it can be interpreted as a dimerization reaction but, the substances $\mathrm{R1_2}$ and $\mathrm{R2_2}$ are not of the same kind. This type of dimerization is known as "fast hetero-dimerization". In spite of the distinction between fast homo and hetero dimerization reactions, they can be treated similarly. Therefore, we apply rapid equilibrium assumption on the reaction 3.5. The differential equations describing the reaction 3.5 are:

$$\mathrm{R1_2}' = -k^{+}\mathrm{R1_2\,R2_2} + k^{-}\mathrm{RC} + \mathrm{r_I} \tag{3.14}$$
$$\mathrm{R2_2}' = -k^{+}\mathrm{R1_2\,R2_2} + k^{-}\mathrm{RC} + \mathrm{r_{II}} \tag{3.15}$$
$$\mathrm{RC}' = \mathrm{k^{+}R1_2\,R2_2} - \mathrm{k^{-}RC} + \mathrm{r_C} \tag{3.16}$$

Similar to previous case ($\mathrm{R1}$ dimerization) r_I, r_{II} and r_C denote the other terms of the equations. Now, we have two equations for totals:

$$\mathrm{R1_{2\,}}_T = \mathrm{R1_2} + \mathrm{RC} \tag{3.17}$$
$$\mathrm{R2_{2\,}}_T = \mathrm{R2_2} + \mathrm{RC} \tag{3.18}$$

The final goal is to eliminate RC dependency of these two equations (equations 3.17 and 3.18), assuming that reaction 3.5 happens relatively fast. At equilibrium we have:

$$\mathrm{RC} = \frac{\mathrm{R1_2\,R2_2}}{\mathrm{K}}, \quad \mathrm{K} = \frac{\mathrm{k^{-}}}{\mathrm{k^{+}}}$$

Substituting RC to equations 3.17 and 3.18 we have:

$$\mathrm{R1_{2\,}}_T = \mathrm{R1_2} + \frac{\mathrm{R1_2\,R2_2}}{K}$$
$$\mathrm{R2_{2\,}}_T = \mathrm{R2_2} + \frac{\mathrm{R1_2\,R2_2}}{K}$$

Now we repeat the differentiation step for both equations.

$$\mathrm{R1_{2\,}}'_T = \mathrm{R1_2}' + \mathrm{RC}' \tag{3.19}$$
$$\mathrm{R2_{2\,}}'_T = \mathrm{R2_2}' + \mathrm{RC}' \tag{3.20}$$

We replace the terms from the equations 3.14 and 3.15:

$$\mathrm{R1_{2\,}}'_T = r_I + r_c$$
$$\mathrm{R2_{2\,}}'_T = r_{II} + r_c$$

Now we differentiate equations 3.19 and 3.20, while RC is replaced:

$$\mathrm{R1_{2\,}}'_T = \mathrm{R1_2}' + \frac{\mathrm{R2_2\,R1_2}'}{K} + \frac{\mathrm{R1_2\,R2_2}'}{K}$$
$$\mathrm{R2_{2\,}}'_T = \mathrm{R2_2}' + \frac{\mathrm{R2_2\,R1_2}'}{K} + \frac{\mathrm{R1_2\,R2_2}'}{K}$$

Therefore, we write the following equations:

$$(1+\frac{\mathrm{R2_2}}{K})\mathrm{R1_2}' + \frac{\mathrm{R1_2}}{K}\mathrm{R2_2}' = r_I + r_c$$
$$\frac{\mathrm{R2_2}}{K}\mathrm{R1_2}' + (1+\frac{\mathrm{R1_2}}{K})\mathrm{R2_2}' = r_{II} + r_c$$

At this point we use Cramer's rule to de-couple the system:

$$(1+\frac{\mathrm{R1_2}}{K}+\frac{\mathrm{R2_2}}{K})\mathrm{R1_2}' = (1+\frac{\mathrm{R1_2}}{K})r_I - \frac{\mathrm{R1_2}}{K}r_{II} + r_c \quad (3.21)$$
$$(1+\frac{\mathrm{R1_2}}{K}+\frac{\mathrm{R2_2}}{K})\mathrm{R2_2}' = -\frac{\mathrm{R2_2}}{K}r_{II} + (1+\frac{\mathrm{R2_2}}{K})r_{II} + r_c \quad (3.22)$$

The goal of section 3.3.2 is to demonstrate the reduction method. We have eliminated $\mathrm{R1_2}$ and $\mathrm{R2_2}$ from the corresponding differential equations of reactions 3.3 and 3.4 assuming that these reactions are fast. Later we have eliminated RC from the differential equations corresponding the fast reaction 3.5. In the next step we can substitute $\mathrm{R1_2}$ and $\mathrm{R2_2}$ variables in 3.21 and 3.22 and modify 3.12 and 3.13 in order to describe the whole receptor system via two differential equations ($\mathrm{R1}'$ and $\mathrm{R2}'$).

3.4 Validation Methods

The following methodologies are used and explained in more details in subsequent chapters (Chapter 4 (section 4.5), 5 (section 5.6) and 6 (section 6.4)).

3.4.1 Quantitation Methods

Quantification of protein expression using Western blot experiments is essential for mathematical modelling the signalling networks. ImageJ, a Java-based program, is one of the most common programs used for quantitation of blots. The blots can be converted to 8-bit grayscale in ImageJ analyses of standard Western blot figures in publications. Each row in a blot needs to be normalized to the relative loading control, however, normalization can also be performed with respect to a protein that remains constant e.g. total SMAD2/3 in TGF-$\beta$and total STAT3 in $\mathrm{IL}-6$ signalling pathways. The quantification methods are explained in [140, 429].

3.4.2 Estimation and Curve Fitting Methods

In order to validate our proposed models with experimental data, we have used the curve fitting toolbox of MATLAB [438, 467]. This toolbox lets the user perform data and regression analysis and provides adjustable initial conditions and parameter values to improve the fittings [157].

Chapter 4

$\mathrm{TGF}-\beta$ Receptor Model of Signal Switching in Cancer

4.0 Summary of the information included in Chapter 4

- Background

  Transforming growth factor β, $\mathrm{TGF}-\beta$, signalling regulates the development of embryos and tissue homeostasis in adults. In conjunction with other oncogenic changes long-term perturbation of $\mathrm{TGF}-\beta$ signalling is associated with cancer metastasis. Although $\mathrm{TGF}-\beta$ signalling can be complex, many of the signalling components are well defined by experiment; so it is possible to develop predictive models of $\mathrm{TGF}-\beta$ signalling using reduction and scaling methods. The parameterization of our $\mathrm{TGF}-\beta$ signalling model is consistent with the experimental results.

- Results

  By adding time-delayed positive feedback to the inherent time-delayed negative feedback for the $\mathrm{TGF}-\beta$ signalling - even when we used the minimal reaction set, we were able to simulate the sigmoidal, switch-like behaviour observed for the concentration dependence of long-term (> 3 hours) $\mathrm{TGF}-\beta$ stimulation. By using a "rapid equilibrium assumption" to reduce the network of $\mathrm{TGF}-\beta$ signalling reactions and the time scales of the individual reactions and the inclusion of both negative and positive feedback loops, we have developed a mathematical model for the $\mathrm{TGF}-\beta$ signalling pathway, i.e. the simplified model of $\mathrm{TGF}-\beta$ signalling. Computer simulations reveal the vital role of the coupling of positive and negative feedback loops on the regulation of the $\mathrm{TGF}-\beta$ signalling system. The incorporation of time-delays for the negative feedback loop improved the accuracy, stability and robustness of the model. This model reproduces

both the short-term and long-term switching responses for the intracellular signalling pathways at different $\mathrm{TGF}-\beta$ concentrations. We have tested the model against experimental data from MEF (mouse embryonic fibroblasts) WT, SV40-immortalized MEFs and Gp130$^{F/F}$ MEFs. The productions from the simplified model are consistent with the experimental data.

- Conclusions

  The signalling feedback loops are required to model $\mathrm{TGF}-\beta$ signal transduction and its effects on normal and cancer cells. We focus on the effects of time-delayed feedback loops and their coupling to ligand stimulation in this system. The model was simplified and reduced to its key components using standard methods and the rapid equilibrium assumption. We detected differences in short-term and long-term signal switching via consideration of positive and negative feedback loops in our simplified model of $\mathrm{TGF}-\beta$ signalling. The results from the model are compared to experimental data and provide predictions for $\mathrm{TGF}-\beta$ signalling in cancer cells with different mutations.

4.1 Introduction

$\mathrm{TGF}-\beta$ is a member of the transforming growth factor superfamily, which also includes other growth factors such as bone morphogenetic proteins, Mullerian inhibitory substance, activin, inhibin and Nodal [75,296,396]. Each family member controls a broad range of cellular processes, such as differentiation, proliferation, migration, life span and apoptosis [118,296]. $\mathrm{TGF}-\beta$ is secreted in an inactive form and sequestered in the extracellular matrix, but once activated by serine and metalloproteinases [208], $\mathrm{TGF}-\beta$ binds to cell surface $\mathrm{TGF}-\beta$ receptor complexes. The active ligand:receptor complex now initiates intracellular signalling that leads to SMAD activation and nucleocytoplasmic shuttling and, eventually, gene responses in the nucleus [300,433].

The $\mathrm{TGF}-\beta$ receptor complex is a tetramer comprised of Type 1 and Type 2 receptors that upon $\mathrm{TGF}-\beta$ binding becomes activated via autophosphorylation [178,296,471]. The activated $\mathrm{TGF}-\beta$ receptor complex is then internalized [169,301], where it phosphorylates and activates SMAD3 [178]. Activated SMAD3 then forms homotrimers, which bind to SMAD4 homotrimers and then imported into the nucleus [507]. These SMAD3:SMAD4 complexes function as transcription factors that up-regulate a number of target genes, including Jun, Fos, SNAIL1 and SMAD7, known inhibitor of $\mathrm{TGF}-\beta$ Type 1 receptors and $\mathrm{TGF}-\beta$ receptor signalling [323,451,507].

Recent studies indicate that $\mathrm{TGF}-\beta$ concentration, stimulation time, cell type and even the percentage of active signalling components can influence the

gene responses, giving a multi-functional aspect to TGF$-\beta$ signalling [75,297]. This is of particular interest in cancer, where SMAD signalling is the most critical pathway controlling the transition of normal epithelial cells to cancerous cells in the colon [206,297,299,330,396]. In spite of the myriad studies on the TGF$-\beta$ signalling pathway, there are still many unanswered questions concerning the impact of TGF$-\beta$ signalling at different stages of cancer cell progression [18]. In particular, there are two opposing reactions of cancer cells to TGF$-\beta$: the proliferation of cancer cells at an early stage is inhibited by TGF$-\beta$ [265], yet at more advanced stages of malignancy, proliferation of cancer cells is stimulated by this signalling protein [198].

Although TGF$-\beta$ signalling components were discovered decades ago [13], the quantitative aspects, dynamics and locations of the signalling components that occur within hours of TGF$-\beta$ stimulation [72,74,308,386,449,511,513] have been more difficult to understand. This has motivated the development of a number of mathematical models of TGF$-\beta$ signalling [19,72,74,75,308,386,449, 512,513] including a recent model [511]. In a comprehensive model, Zi et al. explains the high cooperativity and discontinuous cellular response to TGF$-\beta$ in terms of switch-like behaviour arising from ligand depletion. All of these models, however, lack inhibitory feedback mechanisms known to regulate the TGF$-\beta$ system, including feedback through SMAD7, a key inhibitor in TGF$-\beta$ signal transduction [323]. Furthermore, SMAD7 is an important component for mediating the crosstalk between TGF$-\beta$ signal transduction and other cytokine signalling pathways such as IL-6 or IL-11 [206].

These models also lack the more recently discovered positive feedback in TGF$-\beta$ signalling that acts by suppressing Azin1 via a microRNA (miR-433) [269]. Azin1 promotes polyamine synthesis [212,269], which suppresses TGF$-\beta$ signalling [269, 277, 345, 365]. Azin1 accomplishes this by inhibiting antizyme, thus preventing the degradation of ornithine decarboxylase (ODC) [212, 269]. ODC is essential for the biosynthesis of polyamines [212,269] (see Figure 4.1). Interestingly, over-expression of Azin1 suppresses the expression of TGF$-\beta$ and its Type 1 receptor [269]. The miR-433:Azin1:Antizyme:ODC reactions induce a positive feedback control of TGF$-\beta$ signalling.

Inclusion of such feedbacks is particularly important given that it is well understood that positive and negative feedback loops, particularly in the presence of time-delays (typically found in cellular signalling systems involving gene regulation and shuttling of signalling components between compartments) can also produce both cooperativity and switch-like behaviour even in the absence of ligand depletion [120, 121, 393]. As a prelude to improving our understanding of the TGF$-\beta$ signalling system we have developed a new mathematical model of the TGF$-\beta$ receptor system incorporating negative feedback control via SMAD signalling, positive feedback via Azin1 and transcriptional time-delays [248, 323]. To that end, here we present a detailed model incorporating the main mechanisms of TGF$-\beta$ and SMAD signalling, including feed-

backs and time-delays, but then reduce our model to a simpler system that is more amenable to both standard mathematical analysis techniques and simulation [459]. This permits us to fully characterise analytically the system at steady-state while also investigating the transient dynamics of the system in response to $\mathrm{TGF}-\beta$ signals.

4.2 Model Development

Signalling systems like the $\mathrm{TGF}-\beta$ pathway can be modelled using differential equations describing time rate of the concentration changes of the various cellular components (e.g $\mathrm{TGF}-\beta$ receptors, SMAD4) in terms of reaction rates corresponding to specific kinetic mechanisms, for example, first order or Henri-Michaelis-Menten [115]. These are shown for the $\mathrm{TGF}-\beta$ signalling system in Figure 4.1. $\mathrm{TGF}-\beta$ receptor activation starts with the dimerization of both components ($\mathrm{TGF}-\beta$ receptor type 1 and 2, called respectively $\mathrm{R1}$ and $\mathrm{R2}$). Extensive studies have discovered that receptor dimers initiate the signalling processes [102, 284]. The $\mathrm{R2}$ dimer binds to the $\mathrm{R1}$ dimer, resulting in the receptor complex RC. The RC complex binds $\mathrm{TGF}-\beta$ dimers in the medium around the cells (see Figure 4.1). This $\mathrm{TGF}-\beta$:RC complex (LC) contains all the components essential for signalling, however, $\mathrm{R1}$ s are not activated (phosphorylated) so LC is not the membrane transducer of the exogenous $\mathrm{TGF}-\beta$ signal. Activation of LC requires ligand stimulated phosphorylation of $\mathrm{R1}$ by $\mathrm{R2}$ to produce a fully phosphorylated ligand-receptor complex (PC). PC initiates SMAD signalling via stimulation of the SMAD phosphorylation processes. The activation processes start with the phosphorylation of SMAD2/3, the formation of $(\mathrm{PSMAD2/3})_3.(\mathrm{SMAD4})_3$ [481], the translocation $(\mathrm{Phospho\text{-}SMAD2/3})_3$ to the nucleus, stimulation of the SMAD7 gene and expression of the miR-433 microRNA. Accordingly, SMAD7 is transcribed, its mRNA translated and eventually the SMAD7/SMURF complex amplifies the degradation of the $\mathrm{R1}$ -associated membrane components (note that only SMAD3 is considered in Figure 4.1 due to its crucial role in SMAD7 and miR-433 activation). Note that the components and reactions are estimations of the most frequent occupance among all the possibilities in biology. For instance, receptor dimerizations of type1 and 2 receptors on the membrane are reported in different orders in the literature [156, 219, 237, 298], however, considering the significantly short time scale of the receptor dimerization reactions comparing to other intracellular reactions, altering among the different dimerization orders does not change the steady-state and equilibria of the system.

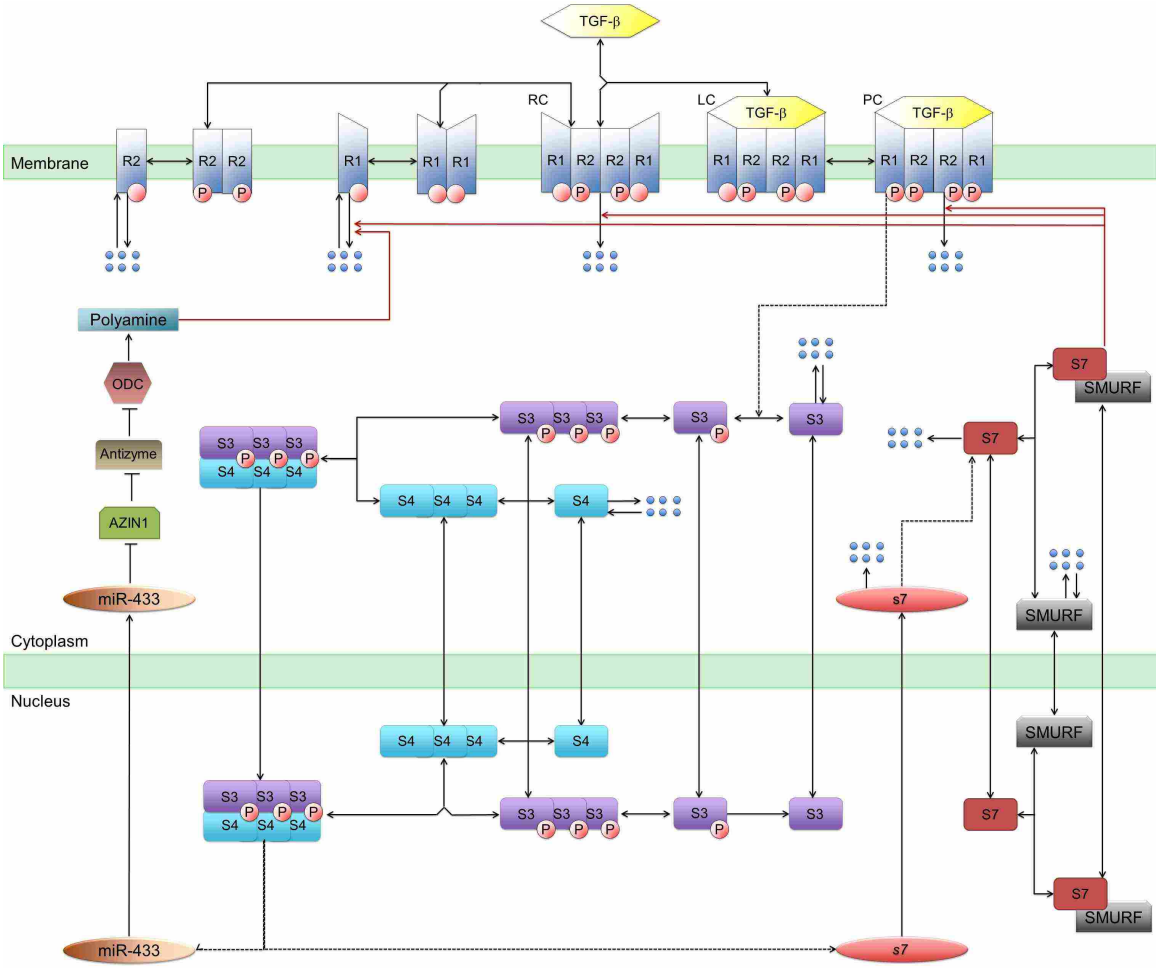

Figure 4.1: *The full* TGF$-\beta$ *signalling biological model. Potential phosphorylation sites of the receptors are specified with empty circles attached to* R1 *and* R2 *components. Arrows pointing to 6 blue dots represent degradation process. The red solid arrows originating from SMAD7/Smurf apply negative and/or positive feedback on the receptor components of the membrane. Oval-shaped components written in small letters represent micro-RNAs. In this figure,* S *represents the SMAD proteins. Note that the arrow from ODC to polyamine shows a stimulatory reaction rather than conversion.*

4.2.1 The Full Model

In order to simplify the intracellular reactions involving in TGF$-\beta$ signalling, we have focused on the receptor components and their interactions on the membrane. Simulation of these receptor processes is achieved by collapsing the SMAD signalling interactions (e.g. nucleocytoplasmic shuttling of activated SMAD complexes and transcription and translation of feedback-associated proteins, such as SMAD7) to a single ligand dependent feedback loop that is originated from PSMAD trimer, S_3. This simplifies the initial modelling equations and focusses the feedback reactions on membrane components. The real feed-

back loop in the Full Model of TGF$-\beta$ signalling is the result of a sequence of back-to-back, coupled reactions explained above (see Figure 4.1). Besides, each one of the intracellular processes happens within a specific time interval and at a defined kinetic rate. In order to summarize all the cytoplasmic and nuclear reactions in one stimulatory/inhibitory reaction, a significant time-delay needs to be included. Our model for TGF$-\beta$ signalling is shown in Figure 4.2.

Altering from Figure 4.1 to Figure 4.2 a few assumptions have been made. Primarily, $\hat{\mathrm{S}}$ is replaced with the all the phoshorylated SMAD3 in the cytoplasm, while the nuclear PSMAD3 is represented via $\mathrm{S_n}$ in Figure 4.2. SMAD4 is the common-mediator SMAD that participates in the TGF$-\beta$ signalling only by interacting with PSMAD2/3. Therefore, it is possible to summarize the SMAD4 role in TGF$-\beta$ signalling in $\hat{\mathrm{S}}$. Total $(\mathrm{PSMAD3})_3.(\mathrm{SMAD4})_3$ concentration is represented with $\mathrm{S_3}$ in Figure 4.2. The negative feedback cascade via SMAD7 is initiated from transcriptional active SMAD complex in the nucleus and is also reducible to $\mathrm{S_3}$ component. However, $\mathrm{S_3}$ is presented as a dimer in relative terms of negative feedback in the equations 4.1 in order to imitate the SMAD7:SMURF interaction. The positive feedback, on the other hand, consists of a chain of biochemical reactions which are triggered by nuclear $(\mathrm{PSMAD3})_3.(\mathrm{SMAD4})_3$. As a result, Azin1:Antizyme:ODC:Polyamine reactions can be represented via a single intermediate inhibitor, i.e. P.

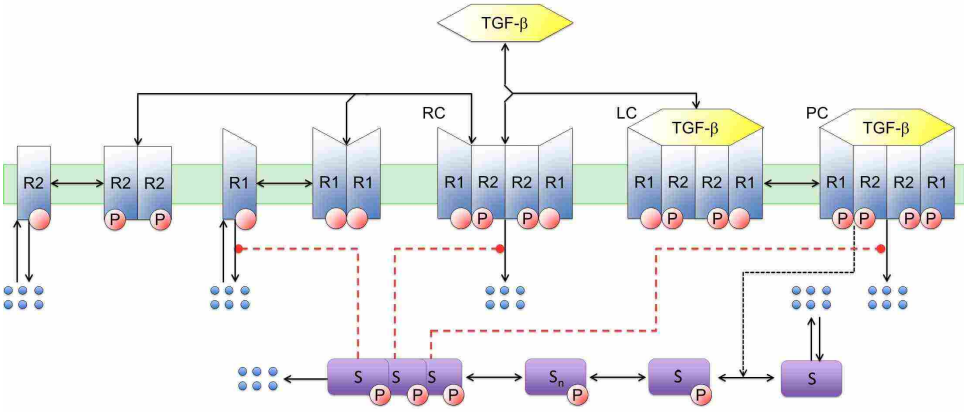

Figure 4.2: *The full receptor model,* TGF$-\beta$ *signal transduction. The red dashed lines which originate from phosphorylated SMAD trimer indirectly regulate the receptor levels. All the reactions from trimerization of phospho-SMAD2/3 to SMAD7 transcription and translation are reduced to the red dashed lines (see Figure 4.1 for clarification). The dotted ends of red dashed lines show that included reactions could lead to both inhibition and stimulation of their targeting reactions (demonstrating negative and positive feedback effects). In this figure S is specifically used for SMAD2/3*

Referring to the model Figure 4.2, the Full Model reactions are:

$$\mathrm{R1} + \mathrm{R1} \underset{k_1^-}{\overset{k_1^+}{\rightleftharpoons}} \mathrm{R1_2} \qquad \mathrm{R1} \underset{v_1}{\overset{k_1}{\rightleftharpoons}} ::: \qquad \mathrm{S} \underset{k_\mathrm{S}^-}{\overset{k_\mathrm{S}^+}{\rightleftharpoons}} \hat{\mathrm{S}} \qquad \mathrm{S} \underset{v_\mathrm{S}}{\overset{k_\mathrm{S}}{\rightleftharpoons}} :::$$

$$\mathrm{R2} + \mathrm{R2} \underset{k_2^-}{\overset{k_2^+}{\rightleftharpoons}} \mathrm{R2_2} \qquad \mathrm{R2} \underset{v_2}{\overset{k_2}{\rightleftharpoons}} ::: \qquad \hat{\mathrm{S}} \underset{k_n^-}{\overset{k_n^+}{\rightleftharpoons}} \mathrm{S_n}$$

$$\mathrm{R1_2} + \mathrm{R2_2} \underset{k_\mathrm{RC}^-}{\overset{k_\mathrm{RC}^+}{\rightleftharpoons}} \mathrm{RC} \qquad \mathrm{RC} \xrightarrow{k_\mathrm{RC}} ::: \qquad \mathrm{S_n} \underset{k_3^-}{\overset{k_3^+}{\rightleftharpoons}} \mathrm{S_3} \qquad \mathrm{S_3} \xrightarrow{k_3} :::$$

$$\mathrm{RC} + \mathrm{TGF_2} \underset{k_\mathrm{LC}^-}{\overset{k_\mathrm{LC}^+}{\rightleftharpoons}} \mathrm{LC}$$

$$\mathrm{LC} \underset{k_\mathrm{PC}^-}{\overset{k_\mathrm{PC}^+}{\rightleftharpoons}} \mathrm{PC} \qquad \mathrm{PC} \xrightarrow{k_\mathrm{PC}} :::$$

This leads to the following system of differential equations:

$$\begin{aligned}
\frac{\mathrm{d}\,[\mathrm{R1}]}{\mathrm{d}t} &= v_1 - k_1\,[\mathrm{R1}] - k_1^{\mathrm{f}-}\,[N]^2\,\frac{[\mathrm{R1}]}{[\mathrm{R1}]+K} - \\
&\quad 2k_1^+\,[\mathrm{R1}]\,[\mathrm{R1}] + 2k_1^-\,[\mathrm{R1_2}] - k_1^{\mathrm{f}+}\,[P]\,\frac{[\mathrm{R1}]}{[\mathrm{R1}]+K} \\
\frac{\mathrm{d}\,[\mathrm{R2}]}{\mathrm{d}t} &= v_2 - k_2\,[\mathrm{R2}] - 2k_2^+\,[\mathrm{R2}]\,[\mathrm{R2}] + 2k_2^-\,[\mathrm{R2_2}] \\
\frac{\mathrm{d}\,[\mathrm{R1_2}]}{\mathrm{d}t} &= k_1^+\,[\mathrm{R1}]\,[\mathrm{R1}] - k_1^-\,[\mathrm{R1_2}] - k_\mathrm{RC}^+\,[\mathrm{R1_2}]\,[\mathrm{R2_2}] + k_\mathrm{RC}^-\,[\mathrm{RC}] \\
\frac{\mathrm{d}\,[\mathrm{R2_2}]}{\mathrm{d}t} &= k_2^+\,[\mathrm{R1}]\,[\mathrm{R1}] - k_2^-\,[\mathrm{R2_2}] - k_\mathrm{RC}^+\,[\mathrm{R1_2}]\,[\mathrm{R2_2}] + k_\mathrm{RC}^-\,[\mathrm{RC}] \\
\frac{\mathrm{d}\,[\mathrm{RC}]}{\mathrm{d}t} &= k_\mathrm{RC}^+\,[\mathrm{R1_2}]\,[\mathrm{R2_2}] - k_\mathrm{RC}^-\,[\mathrm{RC}] - \\
&\quad k_\mathrm{LC}^+\,[\mathrm{RC}]\,[\mathrm{TGF_2}] + k_\mathrm{LC}^-\,[\mathrm{LC}] - k_\mathrm{RC}\,[\mathrm{RC}] - k_\mathrm{RC}^{\mathrm{f}-}\,[N]^2\,\frac{[\mathrm{RC}]}{[\mathrm{RC}]+K} \\
\frac{\mathrm{d}\,[\mathrm{LC}]}{\mathrm{d}t} &= k_\mathrm{LC}^+\,[\mathrm{RC}]\,[\mathrm{TGF_2}] - k_\mathrm{LC}^-\,[\mathrm{LC}] - k_\mathrm{PC}^+\,[\mathrm{LC}] + k_\mathrm{PC}^-\,[\mathrm{PC}] \qquad (4.1) \\
\frac{\mathrm{d}\,[\mathrm{PC}]}{\mathrm{d}t} &= k_\mathrm{PC}^+\,[\mathrm{LC}] - k_\mathrm{PC}^-\,[\mathrm{PC}] - k_\mathrm{PC}\,[\mathrm{PC}] - k_\mathrm{PC}^{\mathrm{f}-}\,[N]^2\,\frac{[\mathrm{PC}]}{[\mathrm{PC}]+K} \\
\frac{\mathrm{d}\,[\mathrm{S}]}{\mathrm{d}t} &= v_\mathrm{S} - k_\mathrm{S}\,[\mathrm{S}] - k_\mathrm{S}^+\,[\mathrm{PC}]\,\frac{[\mathrm{S}]}{[\mathrm{S}]+K_\mathrm{S}} + k_\mathrm{S}^-\,[\hat{\mathrm{S}}] \\
\frac{\mathrm{d}[\hat{\mathrm{S}}]}{\mathrm{d}t} &= k_\mathrm{S}^+\,[\mathrm{PC}]\,\frac{[\mathrm{S}]}{[\mathrm{S}]+K_\mathrm{S}} - k_\mathrm{S}^-\,[\hat{\mathrm{S}}] - k_n^+\,[\hat{\mathrm{S}}] + k_n^-\,[\mathrm{S_n}] \\
\frac{\mathrm{d}\,[\mathrm{S_n}]}{\mathrm{d}t} &= k_n^+\,[\hat{\mathrm{S}}] - k_n^-\,[\mathrm{S_n}] - 3k_3^+\,[\mathrm{S_n}]^{\,3} + 3k_3^-\,[\mathrm{S_3}] \\
\frac{\mathrm{d}\,[\mathrm{S_3}]}{\mathrm{d}t} &= k_3^+\,[\mathrm{S_n}]^{\,3} - k_3^-\,[\mathrm{S_3}] - k_3\,[\mathrm{S_3}]
\end{aligned}$$

where $[P] = {K_\mathrm{I}}^2/({K_\mathrm{I}}^2 + [\mathrm{S_3}\,(\mathrm{t}-\tau)]^2)$ and $[N] = [\mathrm{S_3}]\,(t-\tau)$, the positive and negative feedback intermediate components, respectively.

The purpose of the full model is to document all of the reactions we considered to be significant in the regulation of $\mathrm{TGF}{-}\beta$ signalling. Analysis of the reactions determines which reactions should remain in the reduced model and

which could be eliminated via the rapid equilibrium assumption. We will not solve the full model because it is not necessary to consider parameters which do not contribute in the determination of the steady-state of the model. Having the full model allows the readers to appreciate why and how the model is reduced.

4.2.2 The Simplified Model

The procedure of designing an effective mathematical model of the $\mathrm{TGF}-\beta$ signalling pathway incorporates several consecutive steps. The modelling was started from a very detailed, complex model of all the protein interactions and reactions on the membrane, in the cytoplasm and the nucleus (see Figure 4.1). In the full receptor model, several reactions with long time scales became summarized into feedback loops which originate from PSMAD trimer. We then simplified the receptor model to 6 differential equations. It is assumed that the $\mathrm{R1}$ and $\mathrm{R2}$ dynamics are similar, hence the individual components were replaced by a receptor block, R. R then become dimerized to form RC. Besides, LC and PC are assumed to to combine in one parameter, i.e. PC, since they approximately follow the same kinetics. In the SMAD activation section, an intermediate step, $\mathrm{S_n}$, has been added so as to mimic the nuclear accumulation of phosphorylated SMAD, in comparison with the abundance of unphosphorylated SMAD in the cytosol. Note that these assumptions are used in order to provide a simplified view of the Full model (Figure 4.1). No reduction method has been used up to this point. Eventually, the reactions describing the Simplified Model could be represented as below:

$$
\begin{aligned}
\mathrm{R} + \mathrm{R} &\underset{k^-_{\mathrm{RC}}}{\overset{k^+_{\mathrm{RC}}}{\rightleftharpoons}} \mathrm{RC} & \mathrm{R} &\underset{v_2}{\overset{k_2}{\rightleftharpoons}} ::: \\
& & \mathrm{RC} &\xrightarrow{\mathrm{k_{RC}}} ::: \\
\mathrm{RC} + \mathrm{TGF_2} &\underset{k^-_{\mathrm{PC}}}{\overset{k^+_{\mathrm{PC}}}{\rightleftharpoons}} \mathrm{PC} & \mathrm{PC} &\xrightarrow{\mathrm{k_{PC}}} ::: \\
\mathrm{S} &\underset{k^-_{\mathrm{S}}}{\overset{k^+_{\mathrm{S}}}{\rightleftharpoons}} \hat{\mathrm{S}} & \mathrm{S} &\underset{v_{\mathrm{S}}}{\overset{k_{\mathrm{S}}}{\rightleftharpoons}} ::: \\
& & \hat{\mathrm{S}} &\xrightarrow{\mathrm{k_{\hat{S}}}} ::: \\
\hat{\mathrm{S}} &\underset{k^-_n}{\overset{k^+_n}{\rightleftharpoons}} \mathrm{S_n} & \mathrm{S_n} &\xrightarrow{\mathrm{k_{S_n}}} :::
\end{aligned}
\tag{4.2}
$$

Figure 4.3 highlights the assumptions we used to simplify our receptor model. Here, Figure 4.3A describes the reaction system corresponding to Figure 4.2, these reactions are used to determine the equations defining the mathematical model of $\mathrm{TGF}-\beta$ signalling. By comparing the full receptor model (Figure 4.3A) and the simplified receptor model (Figure 4.3B), the key components in the $\mathrm{TGF}-\beta$ receptor signalling model are specified. In other words, our reduction/simplification method functions similar to sensitivity analysis in keeping

the critical components in a signalling pathway.

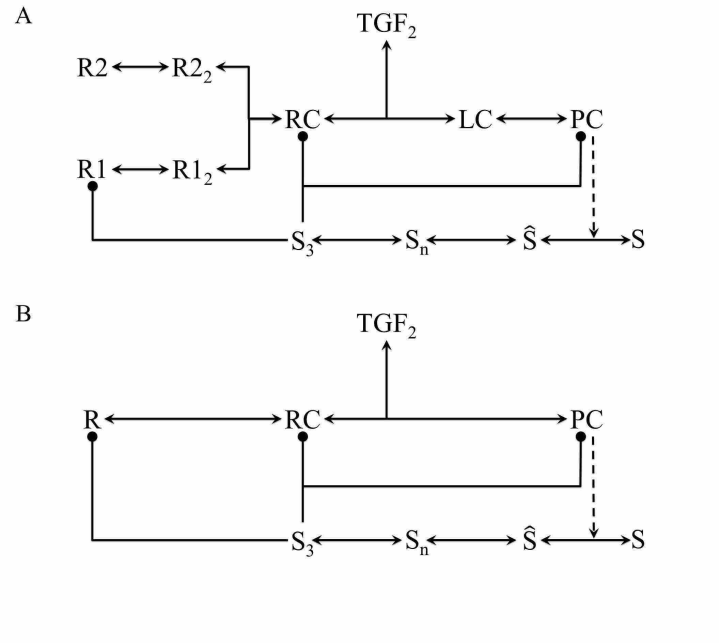

Figure 4.3: $\mathrm{TGF}-\beta$ *receptor signalling system. A) The schematic receptor model,* $\mathrm{TGF}-\beta$ *signal transduction. TGF and* $\hat{\mathrm{S}}+3\mathrm{S}_3$ *represent the input and the output of the model, respectively. B) A Simplified Model of* $\mathrm{TGF}-\beta$ *signal transduction.* $\mathrm{TGF}-\beta$ *and* $\hat{\mathrm{S}}+\mathrm{S_n}+3\mathrm{S}_3$ *represent the input and the output of the model, respectively.*

A set of delayed differential equations describing the Simplified Model are introduced via equations 4.3. The solutions to these equations are at equilibrium when the left hand value is zero, i.e. where the derivatives of each variable are zero with respect to time. The component P represents the molecules through which the positive feedback acts on the receptors (Azin1:Antizyme:ODC:Polyamine in Figure 4.1). The positive feedback is indirect, being affected by two coupled, inhibitory processes.

To achieve the most biologically compatible and robust model of $\mathrm{TGF}-\beta$ signalling, the place of action of the individual feedback reactions contains information which affects the responses of the system. Sensitivity analysis identify LC as the negative feedback action point. SMAD7 binds to receptors and participates in the induction of E3 ubiquitin (Ub) ligase-mediated receptor ubiquitination [101,226]. Michaelis-Menten kinetics is used to model the negative feedback inhibitory function. It is been reported that polyamine depletion increases the $\mathrm{TGF}-\beta$ type 1 receptor mRNA and increases the sensitivity of cells to $\mathrm{TGF}-\beta$-mediated growth inhibition [269,277,365]. Consequently, we have modelled the positive feedback successive reactions using two inhibitory reactions: first, the inhibition the intermediate inhibitor Pvia miR-433 and second, the inhibition of R via P.

Although some cooperativity within the system originates from several dimer-

izations and trimerizations on the membrane, in the cytosol and in the nucleus, the most critical cooperativity comes from the trimerization of the Phosphorylated SMAD3 and the binding of these oligomers to the SMAD4 trimer and the consequential stimulation of the miR-433 and SMAD7 nuclear transcription. It should be noted that the trimerization of Phospho-SMADs influences cooperativity in both the positive and negative feedback loops (see Figure 4.1 for more details).

The time-delay is considered in the equations representing the dynamics of $\mathrm{S_3}$. Hence, time-delays have been applied to both the positive and negative feedbacks. The time-delay compensates for the SMAD nucleocytoplasmic shuttling and other reactions that have been consolidated in the reduced and simplified model (e.g. SMAD7 transcription and translation and the miR-433/Azin1/Antizyme/ODC reactions).

For simplification, the time-delays and amplitudes of the positive and negative feedbacks are assumed to be identical, however, it is always feasible to adjust these parameters when reliable experimental data becomes available.

$$
\begin{aligned}
\frac{\mathrm{d}\,[\mathrm{R}\,]}{\mathrm{d}t} &= v_1 - k_1\,[\mathrm{R}\,] - 2k^{+}_{\mathrm{RC}}\,[\mathrm{R}\,]^{\,2} + 2k^{-}_{\mathrm{RC}}\,[\mathrm{RC}\,] - k_1^{\mathrm{f}+}\,[P]\,\frac{[\mathrm{R}\,]}{[\mathrm{R}\,]+K} - \\
&\quad k_1^{\mathrm{f}-}\,[N]^2\,\frac{[\mathrm{R}\,]}{[\mathrm{R}\,]+K} \\
\frac{\mathrm{d}\,[\mathrm{RC}\,]}{\mathrm{d}t} &= k^{+}_{\mathrm{RC}}\,[\mathrm{R}\,]^{\,2} - k^{-}_{\mathrm{RC}}\,[\mathrm{RC}\,] - k_{\mathrm{RC}}\,[\mathrm{RC}\,] - k^{+}_{\mathrm{PC}}\,[\mathrm{TGF_2}\,]\,[\mathrm{RC}\,] + \\
&\quad k^{-}_{\mathrm{PC}}\,[\mathrm{PC}\,] - k_{\mathrm{RC}}^{\mathrm{f}-}\,[N]^2\,\frac{[\mathrm{RC}\,]}{[\mathrm{RC}\,]+K} \qquad (4.3) \\
\frac{\mathrm{d}\,[\mathrm{PC}\,]}{\mathrm{d}t} &= k^{+}_{\mathrm{PC}}\,[\mathrm{TGF_2}\,]\,[\mathrm{RC}\,] - k^{-}_{\mathrm{PC}}\,[\mathrm{PC}\,] - k_{\mathrm{PC}}\,[\mathrm{PC}\,] - k_{\mathrm{PC}}^{\mathrm{f}-}\,[N]^2\,\frac{[\mathrm{PC}\,]}{[\mathrm{PC}\,]+K} \\
\frac{\mathrm{d}\,[\mathrm{S}\,]}{\mathrm{d}t} &= v_{\mathrm{S}} - k_{\mathrm{S}}\,[\mathrm{S}\,] - k^{+}_{\mathrm{S}}\,[\mathrm{PC}\,]\,\frac{[\mathrm{S}\,]}{[\mathrm{S}\,]+K_{\mathrm{S}}} + k^{-}_{\mathrm{S}}\,[\hat{\mathrm{S}}\,] \\
\frac{\mathrm{d}[\hat{\mathrm{S}}\,]}{\mathrm{d}t} &= k^{+}_{\mathrm{S}}\,[\mathrm{PC}\,]\,\frac{[\mathrm{S}\,]}{[\mathrm{S}\,]+K_{\mathrm{S}}} - k^{-}_{\mathrm{S}}\,[\hat{\mathrm{S}}\,] - k^{+}_{n}\,[\hat{\mathrm{S}}\,] + k^{-}_{n}\,[\mathrm{S_n}\,] - k_{\hat{\mathrm{S}}}\,[\hat{\mathrm{S}}\,] \\
\frac{\mathrm{d}\,[\mathrm{S_n}\,]}{\mathrm{d}t} &= k^{+}_{n}\,[\hat{\mathrm{S}}\,] - k^{-}_{n}\,[\mathrm{S_n}\,] - k_{\mathrm{S_n}}\,[\mathrm{S_n}\,]
\end{aligned}
$$

where again, $[\mathrm{S_3}\,] = [\mathrm{S_n}\,]^{\,3}/K_3$, $[N] = [\mathrm{S_3}\,]\,(t-\tau)$ and $[P] = {K_{\mathrm{I}}}^{\,2}/({K_{\mathrm{I}}}^{\,2} + [\mathrm{S_3\,(t} - \tau)]^2)$.

The parameters $k_1^{\mathrm{f}-}$, $k_{\mathrm{RC}}^{\mathrm{f}-}$ and $k_{\mathrm{PC}}^{\mathrm{f}-}$ represent, respectively, the strength of the negative feedback on R, RC and PC, the $\mathrm{R1}$-associated membrane complexes. Although we have applied the negative feedback on R, RC and PC simultaneously and with identical strengths and binding constants, the feedback on PC is what produces the switching behaviour (see section 4). The positive feedback is on R only, where Polyamine acts [269, 365], so that the cooperativity of the system originates from the coupling of the self-regulatory positive and negative feedback rather than from extracellular effects such as ligand dimerization or depletion.

In the work that follows, all calculations are performed with the simplified model where concentrations are dimensionless and scaled such that $v_1 = 1$. The details of the scaling and the dimension-less parameters are described in section 4.4 The most interesting changes in total PSMAD concentration occur between O(0.1) and O(1), $\mathrm{TGF}-\beta$ varies between 0 and O(10) and receptor concentration varies between 0 and O(1). This is reasonable given that there is insufficient data to constrain the model, particularly for the membrane bound receptor components.

Total PSMAD concentration $[\hat{\mathrm{S}}]$ is defined as:

$$[\hat{\mathrm{S}}] + \frac{Vn}{Vc}([\mathrm{S_n}] + [\mathrm{S_3}])$$

, where Vn and Vc are defined as the volume of the nucleus and the cytoplasm compartment, respectively. $[\mathrm{S_3}] = [\mathrm{S_n}]^3/K_3$ and $[\mathrm{S_n}]$ is calculated from the final equation of 4.3.

4.3 Numerical Simulations

Analyses of the reduced equations and scaling make it possible to study the performance of the model at steady-state in detail (also see "The Importance of Feedback" in Supplementary Material). Our model uses six coupled differential equations to represent all the reactions occurring on the membrane and within the SMAD signalling cascade.

The Zi et al. model produced sigmoidal $\mathrm{TGF}-\beta$ concentration dependence for the cellular responses to long-term stimulation [511]. The total concentration of SMAD was used as an interpretation of the final cell response. According to their results [511], the Hill coefficient of the fitted curve to the cell responses to long-time $\mathrm{TGF}-\beta$ stimulation was approximately 4.5. The Zi et al. model's short-term (transient) responses to $\mathrm{TGF}-\beta$ followed the Hill equation with an approximate coefficient of 0.8 [511]. Zi et al. proposed that the reason for such a dramatic change in the behaviour of the system was due to a significant time-dependent ligand depletion through ligand-receptor interaction [511]. Moreover, the level of total PSMAD concentration should be higher in the short-term response comparing to the long-term. This difference in the level of responses is due to the demanding overshoot of the PSMAD concentration time course (the peak of PSMAD concentration in Figure 4.4).

In order to test our hypothesis that the positive feedback is responsible for the change of the behaviour of the system from short-term to long-term cellular responses, we repeated the simulations for the same $\mathrm{TGF}-\beta$ and stimulation times. The parameter values used to produce the following figures are shown in Table 4.3 of "Supplementary Material". Figure 4.4 shows the predicted changes in the PSMAD concentration at different $\mathrm{TGF}-\beta$ concentrations. It is evident that the steady-state level of PSMAD is 40% less than its short-term peak

value. The predicted results shown in Figure 4.4 are consistent with the literature (e.g. [199, 511]) where the total PSMAD concentration peaks one hour after the ligand stimulation. Figure 4.5 and Figure 4.6 show the predicted transient and steady-state responses to the changes in $\mathrm{TGF}-\beta$ concentration in the system. Note that the x axis in Figure 4.5 and Figure 4.6 denote different concentration of $\mathrm{TGF}-\beta$. Therefore, the simulation time is the same for every point in each figure. The Hill coefficients are 0.85 for the short-term and 3.87 for the long-term stimulation, i.e. similar to Zi et al. [511] (In order to compare the reproduction results see the Figure 5.A and 5.B of [511]. The parameter values are fitted to a single term (Hill coefficient) for Figures 4.5, 4.6, 4.15 and 4.16.). These results support our hypothesis that the coupling of time-delayed positive and negative feedbacks in the $\mathrm{TGF}-\beta$ signal transduction system can account for ultra-sensitivity responses to the ligand concentrations.

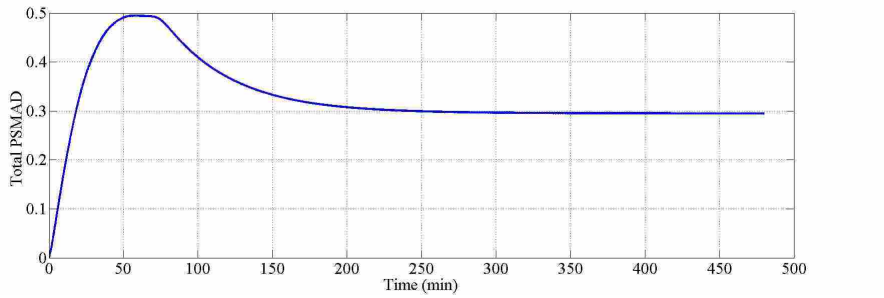

Figure 4.4: *Total PSMAD time course for* $\mathrm{TGF}-\beta = 5$. *The peak in the total PSMAD concentration occurs 50-60 min after the stimulation and corresponds to the short-term (transient) response. The constant level of PSMAD at 0.3 represents the long-term (steady-state) response of the system.*

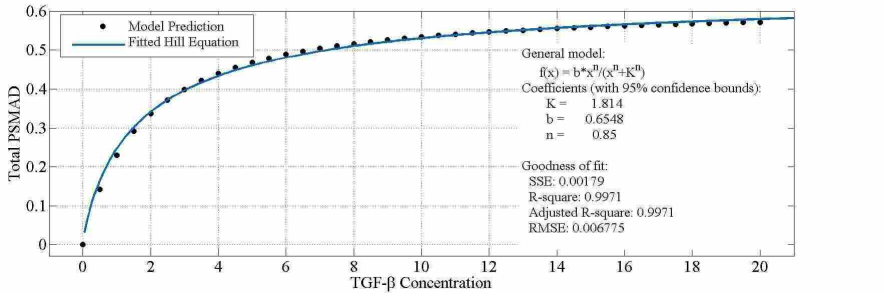

Figure 4.5: *Short-term responses of PSMAD levels to different concentrations of* $\mathrm{TGF}-\beta$*; transient response. The simulation time for each point in this figure is 50 min. The only parameter of the model which is being changed in this figure is the* $\mathrm{TGF}-\beta$ *concentration, meaning that each point has a different* $\mathrm{TGF}-\beta$ *input.*

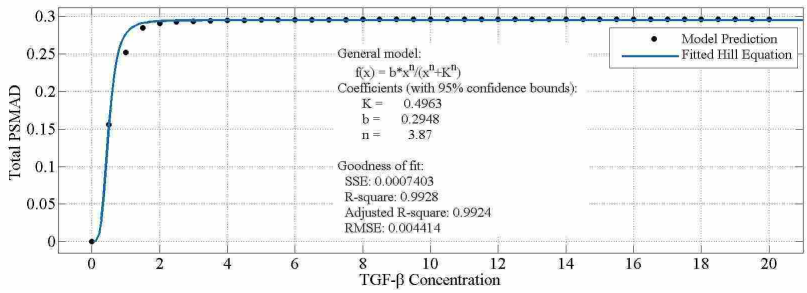

Figure 4.6: *Long-term responses of PSMAD levels to different concentrations of* $\mathrm{TGF}-\beta$*; steady-state response. The simulation time for each point in this figure is 1000 min. The only parameter of the model which is being changed in this figure is the* $\mathrm{TGF}-\beta$ *concentration, meaning that each point has a different* $\mathrm{TGF}-\beta$ *input.*

The negative feedback operates on all of the $\mathrm{R1}$ -associated complexes on the membrane. We suggest that it is the negative feedback through PC which regulates the system. PC is the only $\mathrm{TGF}-\beta$-associated complex in the simplified model for $\mathrm{TGF}-\beta$ signalling. The total $\mathrm{TGF}-\beta$ ligand concentration (extracellular $\mathrm{TGF}-\beta$, which is constant, and that which is bound within the PC complex) decreases because of the degradation of PC via the basal degradation of, and negative feedback on, PC. The saturation of the system with $\mathrm{TGF}-\beta$ flattens the $\mathrm{TGF}-\beta$ concentration response curves at high concentrations of ligand (Figure 4.5 and 4.6). In order to examine our hypothesis, we conducted a set of simulations with feedback on R and RC removed (Figures 1 and 2 in Supplementary Material). To accomplish this, $k_1^{\mathrm{f}-}$ and $k_{\mathrm{RC}}^{\mathrm{f}-}$ are set to zero. These simulation results corroborates our initial hypothesis that negative feedback acts almost entirely through PC.

We speculate that PSMAD concentration time course in response to $\mathrm{TGF}-\beta$ stimulation is modified in cancer cells due to the possible mutations in SMADs and different receptor levels [124,235,264,462]. Figure 4.7 simultaneously shows the model results of the responses of- what we have called- early and late stage cancer cells to $\mathrm{TGF}-\beta$ stimulation. We simulated the biochemical conditions of the early-stage tumors by reducing the membrane receptor and the SMAD concentrations. More precisely, the production rates of receptors (v_1 in Table 4.3) and SMADs (v_s in Table 4.3) were decreased. The simulation response of the total PSMAD time course in cells with lower receptor and SMAD concentrations is plotted in Figure 4.7A. A comparison of Figure 4.7A with Figure 4.4 reveals that PSMAD concentration peaks to a higher level (0.67 rather than 0.5) but flattens to a lower level at steady-state (0.13 v.s. 0.3). This result confirms the compatibility of our simplified receptor model of $\mathrm{TGF}-\beta$ signalling with both normal and cancer cell lines.

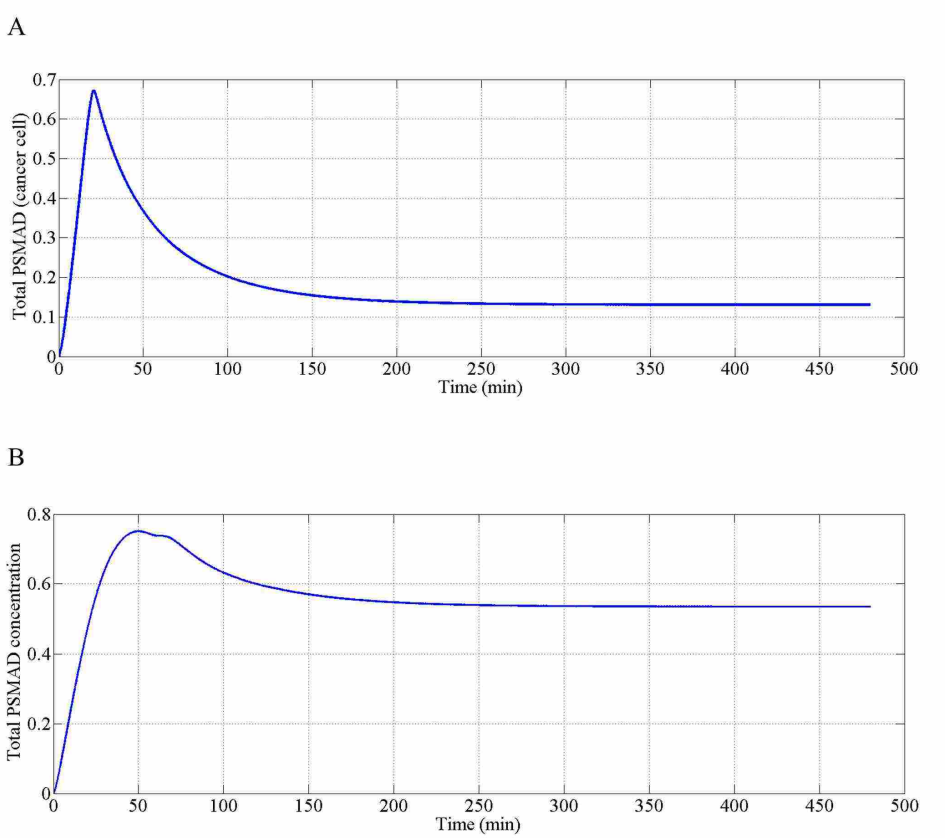

Figure 4.7: *Total PSMAD time course for a certain* $\mathrm{TGF}-\beta$ *concentration. A) simulation results for low membrane receptor concentration condition (or so called early-stage tumors) B) simulation results for high membrane receptor concentration condition (or so called late-stage tumors). These conditions were simulated via altering the receptor production rate on the membrane.*

In contrast, late-stage tumors express more responsiveness to $\mathrm{TGF}-\beta$ signalling. In order to establish late tumor environment, the receptors and SMADs levels are increased, using relative production rates. Predicted response of late tumors to $\mathrm{TGF}-\beta$ stimulation is shown in Figure 4.7B. Although total PSMAD concentration peaks at a higher level in late tumors, its steady-state level is not significantly lower than the peak, showing that the signalling remains high.

To investigate the role of receptor level in the signalling, we have simulated the behaviour of PSMAD concentration while the receptor concentration increases monotonically. Receptor production rate was increased to achieve an increase in receptor concentration. $\mathrm{TGF}-\beta$ concentration was maintained at a constant level during the experiment. This simulation was conducted for two distinct values of $\mathrm{TGF}-\beta$: 5 and 2. The second value of $\mathrm{TGF}-\beta$ concentration is located approximately where the switch in the long-term steady-state PSMAD concentration occurs (see Figure 4.6 and Figure 4.16 in Supplementary Material). There was no distinguishable change in the PSMAD steady-state concentration when $\mathrm{TGF}-\beta$ concentration was reduced (Figure 4.8). Low receptor concen-

tration simulate the cancer cell (see Figure 4.8). The flat starts in both panels of Figure 4.8 show that the cells are insensitive to $\mathrm{TGF}-\beta$ signalling when the receptor copy numbers are very low, i.e. the situation in cancer cells. The peak determines the receptor concentration in which the highest level of signal occurs. At high concentration of the receptors, the PSMAD level reaches a saturation level and stays there as the receptor concentration increases. When the $\mathrm{TGF}-\beta$ concentration is higher (Figure 4.8A) the peak levels of PSMAD shift to the left and all the changes happen at lower receptor levels. According to the model formulation, negative feedback term is directly proportional to $-{\mathrm{S}_3}^2$, while positive feedback element changes proportional to $-\frac{1}{{\mathrm{S}_3}^2}$. As a result, negative feedback dominates the positive feedback at highest S_3 concentration (i.e. the peak value of PSMAD) and decreases the PSMAD level until it reaches a balanced and stable state (see Figure 4.8).

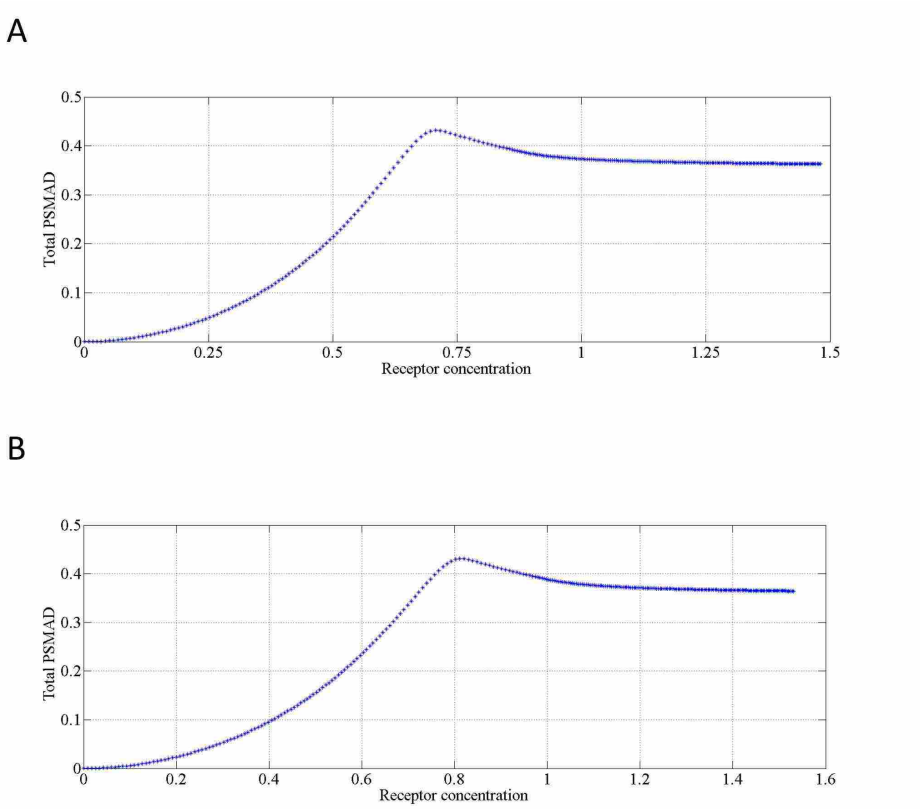

Figure 4.8: *The effects of receptor concentration on the long-term response of PSMAD. A)* $\mathrm{TGF}-\beta$ *= 5. B)* $\mathrm{TGF}-\beta$ *= 2. Approximately, no difference is observed between the two panels of this figure.*

We have repeated the above simulation with changing by SMAD concentration (see Figure 4.9). In neither panel of Figure 4.9 (corresponding to $\mathrm{TGF}-\beta = 5$ and 2) is sensitivity to the $\mathrm{TGF}-\beta$ concentration evident at low SMAD levels. PSMAD concentration level increases with SMAD concentration level until the

saturation region. Moreover, decreasing the TGF$-\beta$ value dramatically suppressed the signal of all SMAD concentrations. At the higher concentration of TGF$-\beta$, PSMAD levels increased even of low SMAD concentration (Figure 4.9A compared to Figure 4.9B). The distinct saturation levels of panel A and B of Figure 4.9 are relative to the distinct steady-state levels of Figure 4.5 and Figure 4.6. More specifically, PSMAD steady-state value in Figure 4.9A varies between 0.63 and 0.74, corresponding to the saturation level of PSMAD in short-term TGF$-\beta$ stimulation. In Figure 4.9B instead, total PSMAD changes from 0.415 to 0.43, corresponding to PSMAD saturation level in long-term responses. Consequently, total PSMAD concentration at higher TGF$-\beta$ stimulation varies with SMAD concentration levels as the system is stimulated with the ligand for a short time and vise versa.

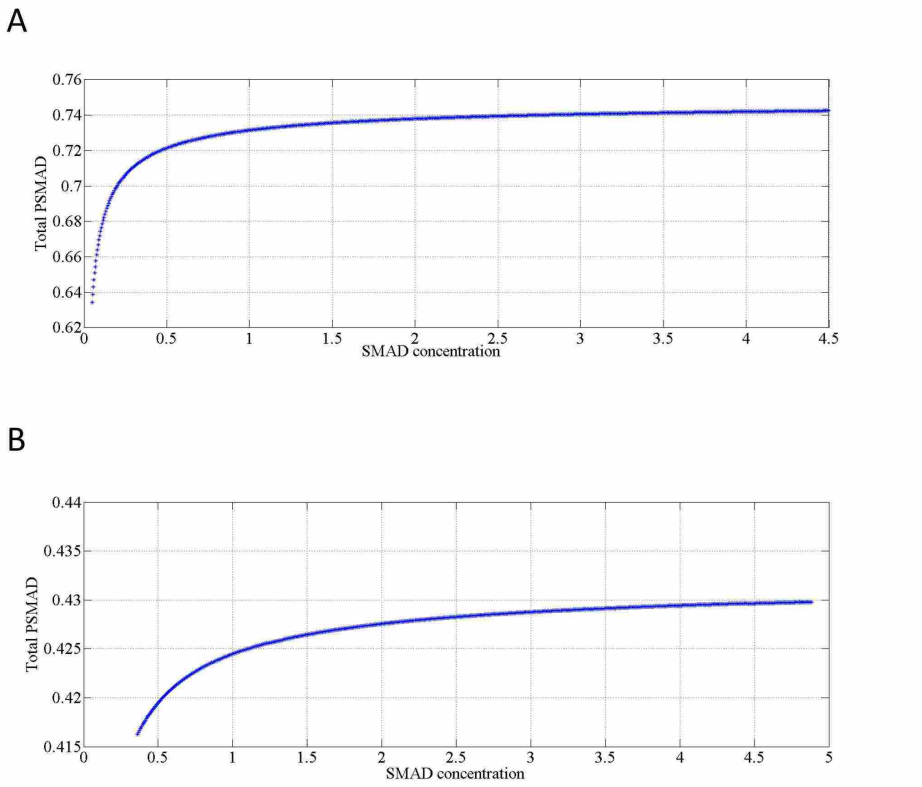

Figure 4.9: *The effects of SMAD concentration on the long-term response of PSMAD. A)* TGF$-\beta$ *= 5 B)* TGF$-\beta$ *= 2. The steady-state level of total PSMAD rises higher in Figure 4.9A than in Figure 4.9B.*

Figure 4.10 shows that the results of the simplified model of TGF$-\beta$ signalling are consistent with the experimental data from different cell lines (wild type MEFs and SV40-immortalized MEFs). Note that the blue line is not a fit of the experimental data (dots). We have compared the output of the model with the experimental data for different cell lines. Identical model parameters are used to produce Figure 4.10A, Figure 4.10B and Figure 4.7B (the blue curves).

For the wild type MEFs (Figure 4.10C), however, we have used the same model parameters as in Figure 4.4

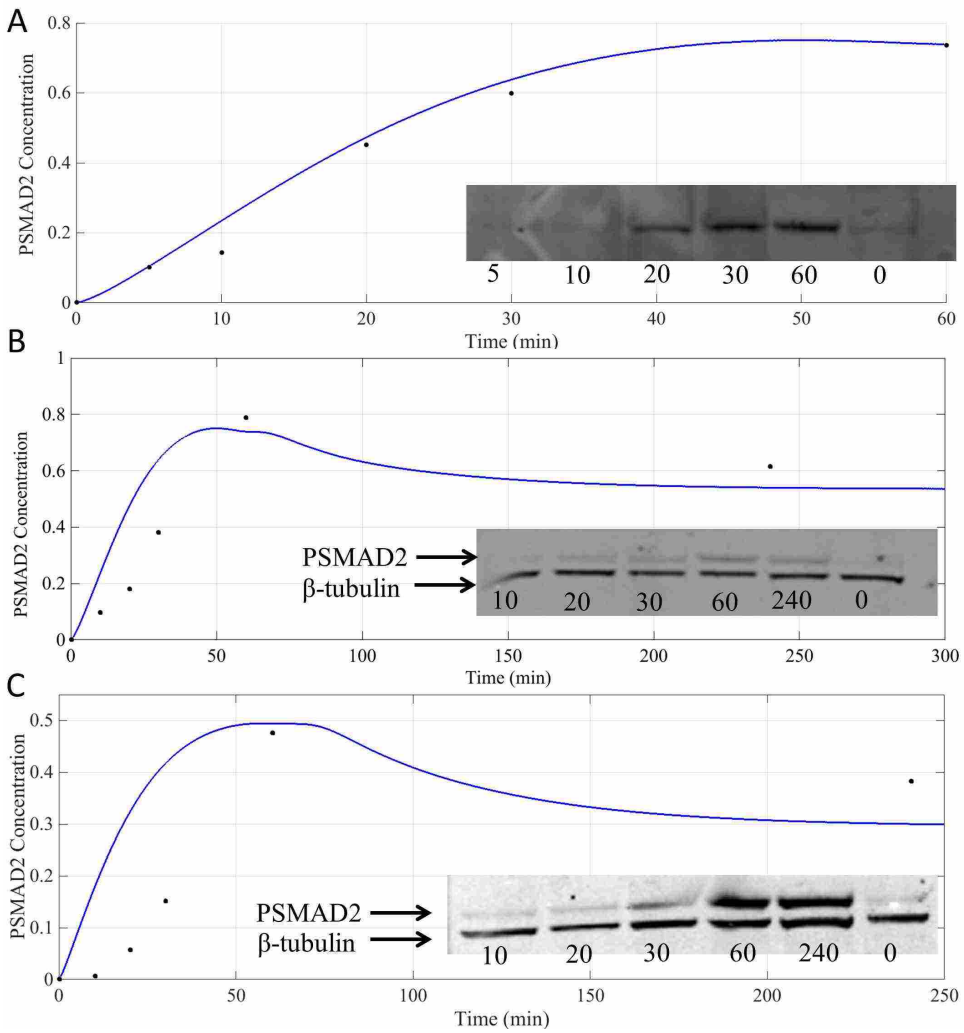

Figure 4.10: *The validation of the simplified model with experimental data. The dots show the level of PSMAD2 concentration obtained from experiment and the curves specify the model predictions. A) PSMAD2 time course for 0-1h on SV40-immortalized MEFs cell line stimulated with* $\mathrm{TGF}-\beta$ *and its corresponding blot B) PSMAD2 time course for 0-4h on SV40-immortalized MEFs cell line stimulated with* $\mathrm{TGF}-\beta$ *and its corresponding blot C) PSMAD2 time course for 0-4h on wild type MEFs stimulated with* $\mathrm{TGF}-\beta$ *and its corresponding blot*

Our simplified $\mathrm{TGF}-\beta$ signalling model was tested experimentally against the data collected in our lab, by the applicant. Figure 4.11 shows the ability of the model to predict the trend of the different experimental sets. The difference between the experimental data and the simulation curves can be explained by the errors associated by the experiments. The error bars for the experimental data in Figure 4.11 suggest a broad range of values for each time point. However, the model simulation result (blue curve) provides a good approximation to the general trend of the experimental data sets. Similarly, in Figure 4.12 the sim-

plified model is fitted to the experimental data set from Gp130$^{F/F}$ MEFs [207]. In order to achieve this fit the parameters of the model had to be adjusted. The level of the SMAD7 concentration is higher in Gp130$^{F/F}$ MEFs due to their gene modification. As is shown in Figure 4.12, the steady-state level of PSMAD2 is lower than in Figure 4.11. Note that the error bars are smaller in Figure 4.12 for the longer time points.

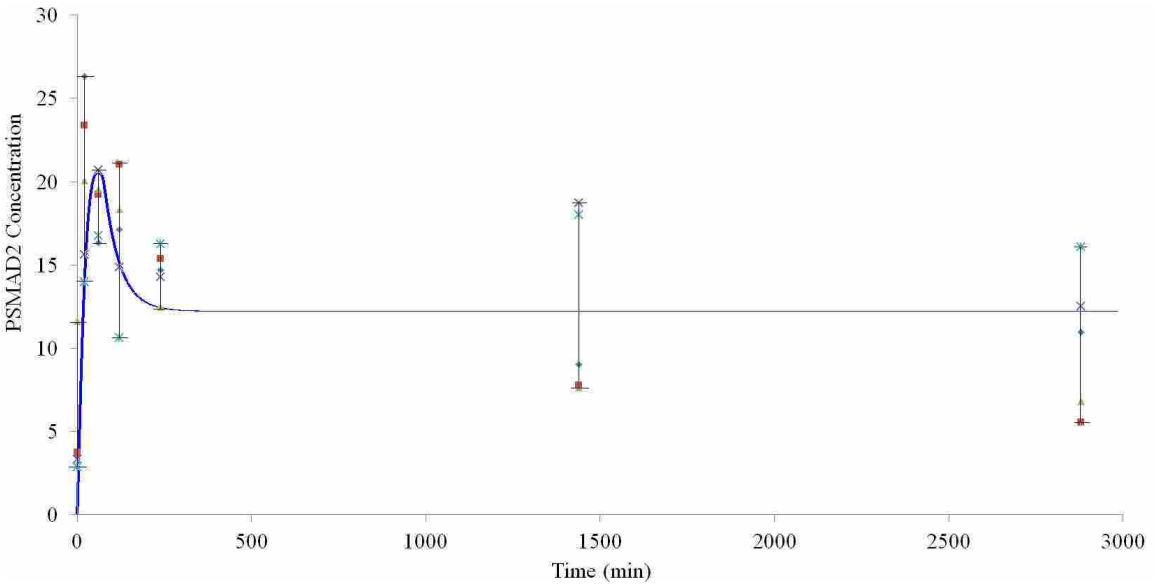

Figure 4.11: *PSMAD2 time course validation with experimental data sets from wild type MEFs. Different dot colors specify different experiments. The curve shows the model prediction of PSMAD2 dynamics.*

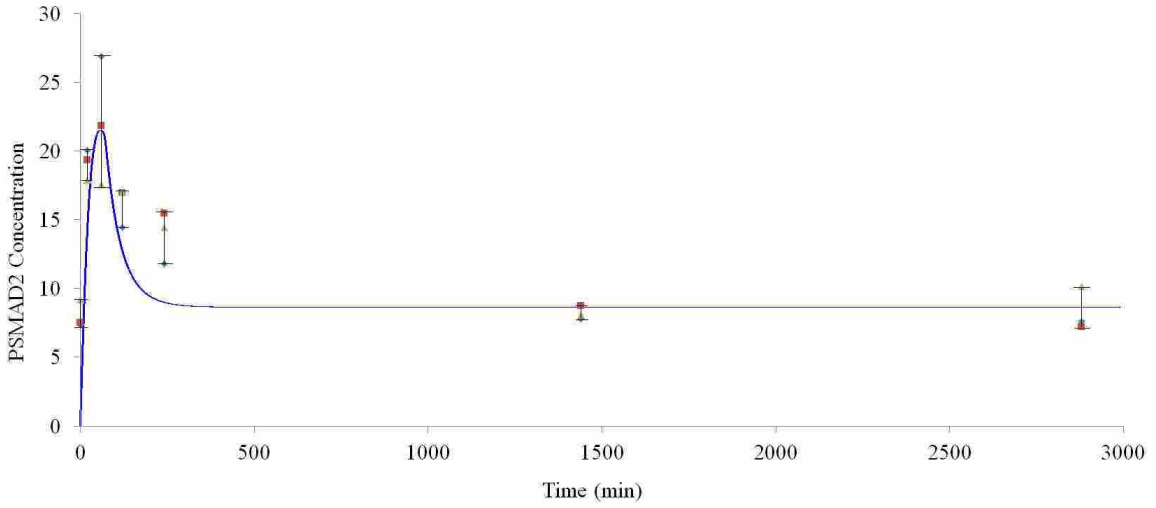

Figure 4.12: *PSMAD2 time course validation with experimental data sets from Gp130$^{F/F}$ MEFs. The SMAD7 level is higher in Gp130$^{F/F}$ MEFs and the PSMAD2 steady-state level is lower compared to wild type MEFs. Different dot colors specify different experiments. The curve shows the model prediction of PSMAD2 dynamics.*

4.4 Discussion

The importance of $\mathrm{TGF}-\beta$ signalling in the progression of cancer heralded in a new era of cell biology research [9,88,350,378]. Several models for $\mathrm{TGF}-\beta$ signalling have been proposed [72,74,308,386,449,511,513]. In each case the models were attempting to study the complex responses of the intracellular signalling reactions to different concentrations of $\mathrm{TGF}-\beta$. In one of the most comprehensive mathematical models Zi et al. [511] predicted that ligand depletion contributed to the long-term response levels of PSMAD. Zi et al. suggested that at higher concentrations of $\mathrm{TGF}-\beta$, it was not depleted in the medium; as a result there was a transfer from a transient to a switch-like response to $\mathrm{TGF}-\beta$ concentration. They also noted the possibility that negative feedback mechanisms might also contribute to the switch-like response [511].

Our $\mathrm{TGF}-\beta$ model expresses less complexity than Zi et al., but at the same time it contains the critical components that lead to robust responses to $\mathrm{TGF}-\beta$ stimulation. The robustness of our model originates from the fact that the cooperative output does not rely on the depletion of the ligand but is built into the network. It is known that time-delayed positive and negative coupled feedbacks can create robust stable signalling [120, 121, 460, 461]. In order to show the critical role of feedback loops in the signalling networks we introduced a reduced model whose steady-state and equilibria were studies in the absence and presence of a linear negative feedback. Steady-state studies with our reduced model predict that feedback considerations can lead to a major improvement in mathematical modelling of $\mathrm{TGF}-\beta$ signalling. One of the objectives of our study was to design quantitative mathematical model that not only is applicable to normal cells but also cancer cells. In cancer cells the number of $\mathrm{TGF}-\beta$ receptors decreases significantly [235,264,462], thus the signalling will be downregulated. The time-dependent ligand depletion model of Zi et al. [511] does not simulate the decrease in the receptor copy numbers.

We have shown that the PSMAD response of the cells is insensitive to $\mathrm{TGF}-\beta$ stimulation for low receptor concentration. This situation could be interpreted as $\mathrm{TGF}-\beta$ signal suppression in cancer cell lines. The relevant concentration of receptors via which the most signal is delivered to the cells was also predicted. Furthermore, our simulations show that the SMAD level reduction also causes a global suppression of signalling in response to $\mathrm{TGF}-\beta$. Due to mutations of SMADs, many cancer cells have reduced levels of $\mathrm{TGF}-\beta$ signalling [124]. These results are consistent with the picture of early-stage tumors being associated with the loss of $\mathrm{TGF}-\beta$ sensitivity and the decrease of $\mathrm{TGF}-\beta$ receptor expression, a prediction that may have recently been validated in endothelial cells and several cancer cell lines [97].

However, $\mathrm{TGF}-\beta$ transduction is stimulated in late-stage tumors (termed "The $\mathrm{TGF}-\beta$ Paradox," for reviews refer to [3, 165]). Our self-regulatory model can produce simulation results consistent with both roles of $\mathrm{TGF}-\beta$ in tumori-

genesis. We simulated loss of responsiveness to $\mathrm{TGF}-\beta$ seen in early tumors via reducing the production rates of the receptors and SMADs and the reacquiring of late tumors responsiveness to $\mathrm{TGF}-\beta$ via increasing their production rates. According to our model predictions, the overshoot peak of PSMAD in response to $\mathrm{TGF}-\beta$ is higher in early tumors and the steady-state levels of PSMAD are lower generally, while in late tumors both steady-state and peak levels are higher than normal cells. Additionally, the difference between the PSMAD peak and steady-state levels becomes less in late-stage tumors to keep the signalling on for longer time. This work can be used as a guide for future experimental research on $\mathrm{TGF}-\beta$ effects on tumor progression.

In addition to reproducing the data in the literature ([511]), new experiments were designed. To validate our model for the abnormal receptor concentration level, we have conducted experiments on an immortal cell line (SV40-immortalized MEFs). Figure 4.10, Figure 4.11 and Figure 4.12 demonstrate how the experimental data on immortal cells are explained via low receptor concentration level (Figure 4.10A and Figure 4.10B) and how the signalling changes for genetically modified cell lines (Figure 4.12). Concluding Figure 4.10, Figure 4.11 and Figure 4.12, they confirm that the model is compatible with the normal and/or the abnormal conditions inside a cell. Such robustness originates from the rigorous system analysis applied on the model (see the "The Simplified Model" and "The Importance of Feedback" in "Supplementary Material").

This model provides the basis for a mathematical study of $\mathrm{TGF}-\beta$ signal transduction and its influence on cancer cells. By considering of a model where coupled, positive-negative feedback loops modulate signalling, $\mathrm{TGF}-\beta$ signal transduction can be studied more precisely using control theory analysis including system identification methods [59, 68].

4.5 Materials and Methods

The experimental data set and the kinetic rates used to set initial parameters for the model were elicited from the literature [72, 74, 308, 386, 449, 511, 513]. More precisely, for the initial conditions, parameter estimated values and the interpretation of some experimental we have benefitted from Zi et al. proposed model [511]. The values for all model parameters are documented in Table 4.3 of the Supplementary Material.

Computer modelling and simulations The programs used for these simulation where PYTHON 2.7 and MATLAB 7.10. The curve fitting tool box of MATLAB is used for fitting the Hill equation to Figure 4.5 and Figure 4.15 in Supplementary Material, and deriving the Hill coefficients.

Mathematical and biochemical analysis The biochemical kinetics, equilibrium analysis, feedback analysis, reduction analysis using rapid equilibrium assumption, time-delayed analysis, asymptotic expansions and sensitivity analysis have

been performed on the model [115].

Cell culture and cell lysis Mouse embryonic fibroblasts (MEFs) cells were isolated from day 13 to 15 embryos. Wild type MEFs, SV40-immortalized MEFs (Simian vacuolating virus 40) and Gp130$^{F/F}$ MEFs cells were cultured in DMEM containing 15% FCS. The cells were typsinazed and washed with DMED + 10% FCS before plating. Passage 3 cells with 1×10^6 MEFs/well were seeded in 60 mm plates for 0-4 hours, 0.5×10^6 MEFs/ well for 24 hour and 0.25×10^6 MEFs/ well for 48 hour treatment with 5 ng/ml $\mathrm{TGF}-\beta$ respectively (for Gp130$^{F/F}$ MEFs the cell numbers changes as: 1.2×10^6 MEFs/well for 0-4 hours, 0.6×10^6 MEFs/well for 24 hours and 0.3×10^6 MEFs/well for 48 hours). After washing with cold PBS for two times, cells were lysed in ice-cold 200 ul RIPA lysis buffer, containing 1M Tris/HCL, 0.5 M EDTA, 5M NaCl, 10 % Na Doc, 10 % TX-100, 10 % SDS, proteinase inhibitor 100 $\times$ and H_2O. The cell lysits were passed through 27 G needle for 5 times, then incubated in ice for 20 min. After incubation the samples were span at 13,000 rpm for 30 min at 4^{o}C. The supernatant was transferred to new tubes where 20 ul of samples were saved for BCA protein assay using sigma BCA assay kit (B9643). 20 ul $5x$ sample buffer was added to 80 ul loading sample and the samples were heated at 95^{o}C for 10 min.

Western blotting According to the protein concentration results from the protein assay, Novex NuPAGE® 4-12%-Bis-Tris (life technologies NP0335 Box) gels were used for loading proper amount of sample lysate for each time point. PSTAT3 (XP^{TM} Rabbit mAb) antibodies were provided by Cell Signalling Technology and were used at a dilution 1:500 in 3% BSA-TBS-T. Antibody directed against SMAD7 was provided via Santa Cruz Biotechnology and was diluted 1:1000. PSMAD2 antibody (rabbit polyclonal anti-phospho-Smad2 antibody (1: 1000 for Western blot)) was a gift from Prof. Peter ten Dijke (Leiden University Medical Center, Netherlands). β-tubulin, actin, Lamin b1 or transferrin receptor are used as loading control depending on the protein to be expressed. Eventually, the gels were transformed onto nitrocellulose membrane via iBlot 2 gel transfer device (life technologies) and the membranes were scanned using Odyssey infrared scanner (LI-COR).

Protein Quantitation The western blot images were quantitated using ImageJ 1.49p. The signals of each protein were normalised to the loading control protein.

4.6 Supplementary Material

4.6.1 The Reduced Model

The full model described by equations 4.1 consists of two subsystems, separated according to the participating components. The membrane subsystem is represented by the first 7 equations and nucleocytoplasmic subsystem is described by the remaining 4 differential equations. At this stage we are focusing on the receptor subsystem only. The equations of the $\mathrm{TGF}-\beta$ system in this section (equations 4.5 and 4.6) are different from our simplified model described in Chapter 4 (equations 4.3). More specifically, we have reduced the $\mathrm{TGF}-\beta$ system differently in this section in order to describe the behaviour of the $\mathrm{TGF}-\beta$ signalling via only two differential equations and study the phase portrait of the system. In reducing the $\mathrm{TGF}-\beta$ system, the rapid equilibrium assumption was used.

As mentioned earlier in a dimerization reaction, it is almost impossible to measure k^+ (the forward reaction rate). Although k^- (the backward reaction rate) is measurable, the easiest parameter to be quantified is K (K = $\frac{k^-}{k^+}$), i.e. the equilibrium constant. The dimerization process of $\mathrm{R1}$ or $\mathrm{R2}$ is much faster than the other receptor reactions. Furthermore, as discussed earlier the symbolic feedback loop was replaced with a number of relatively slow reactions. In comparison to every other reaction in the receptor system, the time scales of $\mathrm{R1}$ and $\mathrm{R2}$ dimerization and RC formation are fast, thus justifying the "rapid equilibrium assumption" [115, 203, 459].

Based on the above assumptions, we apply the conservation law to $\mathrm{R1}$ and $\mathrm{R2}$, so the final form of the reduced version of the $\mathrm{R1}$, $\mathrm{R2}$ and PC are:

$$\begin{aligned} \mathrm{R1}_{\mathrm{T}} &= \mathrm{R1} + 2\mathrm{R1}_2 + 2\mathrm{RC} \\ \mathrm{R2}_{\mathrm{T}} &= \mathrm{R2} + 2\mathrm{R2}_2 + 2\mathrm{RC} \\ \mathrm{PC}_{\mathrm{T}} &= \mathrm{LC} + \mathrm{PC} \end{aligned} \tag{4.4}$$

The conservation law for $\mathrm{R1}$ and $\mathrm{R2}$ states that the total amount of $\mathrm{R1}$ and $\mathrm{R2}$, by definition, equals to the total amount of $\mathrm{R1}$ and $\mathrm{R2}$ as monomers adding by twice of the amount of $\mathrm{R1}$ and $\mathrm{R2}$ as dimers (which is twice of $\mathrm{R1}$ and $\mathrm{R2}$). The same definition applies for PC_T.

According to the experimentalists, we know that the dimerization reactions, the binding reactions of the two dimers and the phosphorylation of the two $\mathrm{R1}$s inside LC (PC association) are relatively fast comparing to the ligand binding reaction [115]. Inside the cytosol the trimerization of the phosphorylated SMAD occurs more rapidly than the SMAD phosphorylation processes. Pursuant to the rapid equilibrium assumption, at equilibrium the forward and the backward terms of the fast reactions can be considered to be equal. Therefore, the equations describing the reduced model are:

$$\begin{aligned}
\beta_{11}\,[\mathrm{R1}\,]\,' + \beta_{12}\,[\mathrm{R2}\,]\,' &= v_1 - k_1\,[\mathrm{R1}\,] - 2k_{\mathrm{RC}}\,[\mathrm{RC}\,] - k_1^{\mathrm{f}-}\,[N]^2\,\frac{[\mathrm{R1}\,]}{\mathrm{R1}+\mathrm{K}} - \\
&\quad 2k_{\mathrm{RC}}^{\mathrm{f}-}\,[N]^2\,\frac{[\mathrm{RC}\,]}{[\mathrm{RC}\,]+K} - k_1^{\mathrm{f}+}\,[P]\,\frac{[\mathrm{R1}\,]}{[\mathrm{R1}\,]+K} \\
\beta_{21}\,[\mathrm{R1}\,]\,' + \beta_{22}\,[\mathrm{R2}\,]\,' &= v_2 - k_2\,[\mathrm{R2}\,] - 2k_{\mathrm{RC}}\,[\mathrm{RC}\,] - 2k_{\mathrm{RC}}^{\mathrm{f}-}\,[N]^2\,\frac{[\mathrm{RC}\,]}{[\mathrm{RC}\,]+K} \\
(1+K_{\mathrm{PC}}\,)\,[\mathrm{PC}\,]\,' &= k_{\mathrm{LC}}^{+}\,[\mathrm{TGF_2}\,]\,[\mathrm{RC}\,] - k_{\mathrm{LC}}^{-}\,K_{\mathrm{PC}}\,[\mathrm{PC}\,] - k_{\mathrm{PC}}^{-}\,[\mathrm{PC}\,] - \\
&\quad k_{\mathrm{PC}}^{\mathrm{f}-}\,[N]^2\,\frac{[\mathrm{PC}\,]}{[\mathrm{PC}\,]+K} \\
[\mathrm{S}\,]\,' &= v_{\mathrm{S}} - k_{\mathrm{S}}\,[\mathrm{S}\,] - k_{\mathrm{S}}^{+}\,[\mathrm{PC}\,]\,\frac{[\mathrm{S}\,]}{[\mathrm{S}\,]+K_{\mathrm{S}}} + k_{\mathrm{S}}^{-}\,[\hat{\mathrm{S}}\,] \\
[\hat{\mathrm{S}}\,]' &= k_{\mathrm{S}}^{+}\,[\mathrm{PC}\,]\,\frac{[\mathrm{S}\,]}{[\mathrm{S}\,]+K_{\mathrm{S}}} - k_{\mathrm{S}}^{-}\,[\hat{\mathrm{S}}\,] - 3k_3^{+}\,[\hat{\mathrm{S}}\,]^3 + 3k_3^{-}\,[\mathrm{S}_3\,]
\end{aligned} \tag{4.5}$$

$$\beta_{11} = 1 + 4\frac{[\mathrm{R1}\,]}{K_1} + \frac{4}{K_1\,K_2\,K_{\mathrm{RC}}}\,[\mathrm{R1}\,]\,[\mathrm{R2}\,]^{\,2} \quad \beta_{12} = \frac{4}{K_1\,K_2\,K_{\mathrm{RC}}}\,[\mathrm{R1}\,]^{\,2}\,[\mathrm{R2}\,]$$
$$\beta_{21} = \frac{4}{K_1\,K_2\,K_{\mathrm{RC}}}\,[\mathrm{R1}\,]\,[\mathrm{R2}\,]^{\,2} \quad \beta_{22} = 1 + 4\frac{[\mathrm{R2}\,]}{K_2} + \frac{4}{K_1\,K_2\,K_{\mathrm{RC}}}\,[\mathrm{R1}\,]^{\,2}\,[\mathrm{R2}\,]$$

and again, $[N] = [\mathrm{S}_3\,]\,(t-\tau)$ and $[P] = {K_{\mathrm{I}}}^2/({K_{\mathrm{I}}}^2 + [\mathrm{S}_3\,(\mathrm{t}-\tau)]^2)$. Note that the equilibrium equations that formulate the reduced model can be written as:

$$\begin{aligned}
[\mathrm{R1_2}\,] &= \frac{[\mathrm{R1}\,]^{\,2}}{K_1} & [\mathrm{LC}\,] &= K_{\mathrm{PC}}\,[\mathrm{PC}\,] \\
[\mathrm{R2_2}\,] &= \frac{[\mathrm{R2}\,]^{\,2}}{K_2} & [\mathrm{RC}\,] &= \frac{[\mathrm{R1}\,]^{\,2}\,[\mathrm{R2}\,]^{\,2}}{K_1\,K_2\,K_{\mathrm{RC}}}
\end{aligned}$$

$$[\mathrm{S}_3\,] = \frac{[\hat{\mathrm{S}}\,]^3}{K_3} = \frac{1}{K_3}\left(\frac{[\mathrm{LC}\,]\,k_{\mathrm{S}}^{+}\,[\mathrm{S}\,]}{K_{\mathrm{PC}}\,k_{\mathrm{S}}^{-}\,([\mathrm{S}\,]+K_{\mathrm{S}}\,)}\right)^3$$

The Importance of Feedback

This section aims to demonstrate the effects of a negative feedback loop on the steady-state of the $\mathrm{TGF}-\beta$ signalling system. The corresponding equations can be shown as the following.

$$\begin{aligned}
\frac{\mathrm{d}\,[\mathrm{R1}\,]}{\mathrm{d}t} &= v_1 - k_1\,[\mathrm{R1}\,] - 2k_{\mathrm{RC}}\,[\mathrm{RC}\,] - k_1^{\mathrm{f}-}\,[\mathrm{S}_3\,]^{\,2}\,[\mathrm{R1}\,] - 2k_{\mathrm{RC}}^{\mathrm{f}-}\,[\mathrm{S}_3\,]^{\,2}\,[\mathrm{RC}\,] \\
\frac{\mathrm{d}\,[\mathrm{R2}\,]}{\mathrm{d}t} &= v_2 - k_2\,[\mathrm{R2}\,] - 2k_{\mathrm{RC}}\,[\mathrm{RC}\,] - 2k_{\mathrm{RC}}^{\mathrm{f}-}\,[\mathrm{S}_3\,]^{\,2}\,[\mathrm{RC}\,] \\
\frac{\mathrm{d}\,[\mathrm{PC}\,]}{\mathrm{d}t} &= k_{\mathrm{LC}}^{+}\,[\mathrm{TGF_2}\,]\,[\mathrm{RC}\,] - k_{\mathrm{LC}}^{-}\,K_{\mathrm{PC}}\,[\mathrm{PC}\,] - k_{\mathrm{PC}}^{-}\,[\mathrm{PC}\,] \\
\frac{\mathrm{d}\,[\mathrm{S}\,]}{\mathrm{d}t} &= v_{\mathrm{S}} - k_{\mathrm{S}}\,[\mathrm{S}\,] - k_{\mathrm{S}}^{+}\,[\mathrm{PC}\,]\,\frac{[\mathrm{S}\,]}{[\mathrm{S}\,]+K} + k_{\mathrm{S}}^{-}\,[\hat{\mathrm{S}}\,] \\
\frac{\mathrm{d}[\hat{\mathrm{S}}\,]}{\mathrm{d}t} &= k_{\mathrm{S}}^{+}\,[\mathrm{PC}\,]\,\frac{[\mathrm{S}\,]}{[\mathrm{S}\,]+K} - k_{\mathrm{S}}^{-}\,[\hat{\mathrm{S}}\,]
\end{aligned} \tag{4.6}$$

As is shown in equations 4.6, we have assumed that the dimerization of $\mathrm{R1}$, dimerization of $\mathrm{R2}$, association of RC and the association of PC are fast. Consequently, $\mathrm{R1_2}$, $\mathrm{R2_2}$, RC and LC are evaluated based on $\mathrm{R1}$, $\mathrm{R2}$ and PC. Furthermore, there is no $\mathrm{S_n}$ defined in this system and it is assumed that $\hat{\mathrm{S}}$ represents both nuclear and cytoplasmic phospho-SMAD.

These equations are also different from the reduced model (equations 4.5. Specifically, we have assumed that K_1, K_2 and K_{RC} are large enough such that $\beta_{11} = \beta_{22} = 1$ and $\beta_{12} = \beta_{21} = 0$. Additionally, the production of PC from LC and trimerization of $\hat{\mathrm{S}}$ occur relatively fast. Therefore, $[\mathrm{LC}] = K_{\mathrm{PC}}\ [\mathrm{PC}]$ and $[\mathrm{S_3}] = \frac{[\hat{\mathrm{S}}]}{K_3}$ at equilibrium. In our toy model (equations 4.8), we assumed that the negative feedback loops are applied only to $\mathrm{R1}$ and RC and follow linear kinetics (instead of Michaelis-Menten kinetics). We did not include a time-delay in the system. With these assumptions we can write the following set of equations to represent the system at equilibrium.

$$\begin{aligned}
[\mathrm{S}] &= \frac{v_{\mathrm{S}}}{k_{\mathrm{S}}} \\
[\hat{\mathrm{S}}] &= \frac{k_{\mathrm{S}}^{+}}{k_{\mathrm{S}}^{-}}\,[\mathrm{LC}]\ K_{\mathrm{PC}}\ \frac{[\mathrm{S}]}{[\mathrm{S}] + K_{\mathrm{S}}} \\
[\mathrm{PC}] &= \frac{k_{\mathrm{LC}}^{+}\ [\mathrm{TGF_2}]}{k_{\mathrm{LC}}^{-}\ + \frac{k_{\mathrm{PC}}^{-}}{K_{\mathrm{PC}}}} \\
[\mathrm{S_3}] &= \frac{[\hat{\mathrm{S}}]^{3}}{K_3} = \frac{1}{K_3}\left(\frac{[\mathrm{LC}]\ k_{\mathrm{S}}^{+}\ [\mathrm{S}]}{K_{\mathrm{PC}}\ k_{\mathrm{S}}^{-}\ ([\mathrm{S}] + K)}\right)^{3} \\
[\mathrm{RC}] &= \frac{[\mathrm{R1}]^{\,2}[\mathrm{R2}]^{\,2}}{K_1\,K_2\,K_{\mathrm{RC}}}
\end{aligned} \tag{4.7}$$

We have non-dimensionalized the model (equations 4.6) in order to simplify our equations without elimination of any information from the system. According to [273], scaling does not change the solution of the original system. Non-dimensionalization is often used to simplify and reduce the number of effective parameters (without changing the number of variables and equations), to analyse the behaviour of a system without considering the units of its components and to re-scale the variables whose amounts have vastly different magnitudes [76, 273]. The simplifications preserve the essential features of our model. After applying the non-dimensionalization method, at equilibrium, the system in equation 4.6 can be reduced to (we have named it the toy model):

$$\begin{aligned}
0 &= 1 - r_1 - c_1 r_1^2 r_2^2 - \delta r_1^{13} r_2^{12} - \varepsilon_1 r_1^{14} r_2^{14} \\
0 &= 1 - r_2 - c_2 r_1^2 r_2^2 \qquad\qquad - \varepsilon_2 r_1^{14} r_2^{14}
\end{aligned} \tag{4.8}$$

, with the dimension-less variables and components defined as:

$$
\begin{aligned}
r_1 &= k_1\,[\mathrm{R1}]\,/v_1 & r_2 &= k_2\,[\mathrm{R2}]\,/v_2 \\
c_1 &= \frac{2k_{\mathrm{RC}}\,v_1\,{v_2}^2}{K_1\,K_2\,K_{\mathrm{RC}}\,{k_1}^2{k_2}^2} & c_2 &= \frac{2k_{\mathrm{RC}}\,{v_1}^2v_2}{K_1\,K_2\,K_{\mathrm{RC}}\,{k_1}^2{k_2}^2} \\
\varepsilon_1 &= 2\frac{k_b}{v_1\,{K_3}^2}\frac{{v_1}^{14}{v_2}^{14}}{{k_1}^{14}{k_2}^{14}}\left(\frac{k_{\mathrm{S}}^{+}\,v_{\mathrm{S}}\,k_{\mathrm{LC}}^{+}\,[\mathrm{TGF_2}]}{K_{\mathrm{PC}}\,k_{\mathrm{S}}^{-}\,k_{\mathrm{S}}\,(\frac{v_{\mathrm{S}}}{k_{\mathrm{S}}}+K)(k_{\mathrm{LC}}^{-}+\frac{k_{\mathrm{PC}}}{K_{\mathrm{PC}}})}\right)^6\frac{1}{(K_1\,K_2\,K_{\mathrm{RC}}\,)^7} \\
\varepsilon_2 &= 2\frac{k_b}{v_2\,{K_3}^2}\frac{{v_1}^{14}{v_2}^{14}}{{k_1}^{14}{k_2}^{14}}\left(\frac{k_{\mathrm{S}}^{+}\,v_{\mathrm{S}}\,k_{\mathrm{LC}}^{+}\,[\mathrm{TGF_2}]}{K_{\mathrm{PC}}\,k_{\mathrm{S}}^{-}\,k_{\mathrm{S}}\,(\frac{v_{\mathrm{S}}}{k_{\mathrm{S}}}+K)(k_{\mathrm{LC}}^{-}+\frac{k_{\mathrm{PC}}}{K_{\mathrm{PC}}})}\right)^6\frac{1}{(K_1\,K_2\,K_{\mathrm{RC}}\,)^7} \\
\delta &= \frac{k_a}{v_1\,{K_3}^2}\frac{{v_1}^{13}{v_2}^{12}}{{k_1}^{13}{k_2}^{12}}\left(\frac{k_{\mathrm{S}}^{+}\,v_{\mathrm{S}}\,k_{\mathrm{LC}}^{+}\,[\mathrm{TGF_2}]}{K_{\mathrm{PC}}\,k_{\mathrm{S}}^{-}\,k_{\mathrm{S}}\,(\frac{v_{\mathrm{S}}}{k_{\mathrm{S}}+K})(K_1\,K_2\,K_{\mathrm{RC}}\,)(k_{\mathrm{LC}}^{-}+\frac{k_{\mathrm{PC}}}{K_{\mathrm{PC}}})}\right)^6
\end{aligned}
\tag{4.9}
$$

Note that $k_1^{\mathrm{f}-} = k_a$ and $k_{\mathrm{RC}}^{\mathrm{f}-} = k_b$. Equation 4.8 was derived after applying the reduction method explained in Chapter 3.

The system (equations 4.6) was reduced to two effective equations as functions of the concentrations of $\mathrm{R1}$ and $\mathrm{R2}$. In this section, equations 4.8 are solved and analyzed in the steady-state (equilibrium). First, we study the system in the absence of feedback ($\delta = \varepsilon_1 = \varepsilon_2 = 0$) - the simplest, symmetric system. Then, we investigate the effects of the negative, regulatory feedback loop on the equilibria of the system. This negative feedback is only applied on $\mathrm{R1}$ and RC. In fact, the importance of the positive feedback and the resulted ultra-sensitivity feature of the system are included in the "The Simplified Model". The most critical advantage of the toy model (equations 4.8) is to analytically (since we reduced all the equations to two) study the effects of a feedback loop (here negative feedback loop) on the steady-state and equilibria of a system. Based on feedback study of this system, we can speculate changes in the system's operating point after adding complementary positive and/or negative feedbacks.

As mentioned in the introduction, previous models on $\mathrm{TGF}-\beta$ signalling lacked the consideration of the feedback loops. In other words, the steady-state analysis of $\mathrm{TGF}-\beta$ transduction in the absence of feedback corresponds to the previous mathematical models of $\mathrm{TGF}-\beta$ in the literature. In this section, we demonstrate the importance of a simple, linear negative feedback on the steady-state of the $\mathrm{TGF}-\beta$ signalling system.

The equations describing the reduced model in the absence of feedback (the no-feedback toy model) are:

$$\frac{\mathrm{d}r_1}{\mathrm{d}t} = 1 - r_1 - c_1 r_1^2 r_2^2 \tag{4.10}$$

$$\frac{\mathrm{d}r_2}{\mathrm{d}t} = 1 - r_2 - c_2 r_1^2 r_2^2 \tag{4.11}$$

This equation can be written as:

$$\frac{\mathrm{d}r_1}{\mathrm{d}t} = f_1 \tag{4.12}$$

$$\frac{\mathrm{d}r_2}{\mathrm{d}t} = f_2 \tag{4.13}$$

Here, r_1 and r_2 are the scaled values of $\mathrm{R1}$ and $\mathrm{R2}$ respectively. We have assumed β_{12} and β_{21} are zero, e.g. K_{RC} is very large (see Table 4.3). The clearest way to appreciate the dynamics of the systems at equilibrium is to consider the phase plane. In phase plane analysis of the differential equations we normally consider the nullclines. The nullclines of f_1, respectively f_2, are defined by setting $f_1(r_1, r_2) = 0$, respectively $f_2(r_1, r_2) = 0$. The steady-state of the system is defined by a set of (r_1, r_2) such that $f_1(r_1, r_2) = 0$ and $f_2(r_1, r_2) = 0$. The intersection of each pair of nullclines represents a fixed point of the system at steady-state. The pattern achieved via connecting fixed points for a set of parameters shows the equilibrium curve that describes the system at steady-state. In the absence of feedback ($\delta = \varepsilon_1 = \varepsilon_2 = 0$) the nullclines are given by,

$$\begin{aligned} r_1 &= \frac{-1 \pm \sqrt{1 + 4c_1 r_2^2}}{2c_1 r_2^2} \\ r_2 &= \frac{-1 \pm \sqrt{1 + 4c_2 r_1^2}}{2c_2 r_1^2} \end{aligned} \tag{4.14}$$

and the steady-state is the solution of,

$$\begin{aligned} 1 - r_1 - c_1 r_1^2 r_2^2 &= 0 \\ 1 - r_2 - c_2 r_1^2 r_2^2 &= 0 \end{aligned} \tag{4.15}$$

which can be solved for:

$$\frac{1 - r_2}{1 - r_1} = \frac{c_2}{c_1} \equiv c. \tag{4.16}$$

c is the slope of the curve in the (r_1, r_2) phase plane. It is important to note that equation 4.16 does not define the steady-state of the system completely, though it is sufficient for plotting the phase plane (phase portrait) to visualise the behaviour of the system.

The steady-state analysis of the reduced model in the absence of feedback is summarized in Figure 4.13. Figure 4.13A shows the steady-state curves for five different values of c. It shows how the steady-state curve varies with c. Note that for all values of c the steady-state curves are straight lines which pass through 1,1. Scaled total S_3 (here designated as s_3) is plotted against the logarithm of c to base 2 for different values of c when δ and ε values are zero (see Figure 4.13B). Here, s_3 is a representative of the output. According to the reduced model design in "The Reduced Model", c is a ratio of v_1 and v_2, the production rates of

R1 and R2 respectively. Therefore, Figure 4.13B specifies how the abundance of the receptors on the membrane can upregulare/downregulate the TGF$-\beta$ signalling in the absence of feedback. Experimentally, v_1 and v_2 are estimated to have similar values. So we expect the working point of the system to be in the middle part of the Figure 4.13B ($c = 1$, $\log c = 0$), at which the output dramatically changes. This explains the importance of the receptor concentrations in TGF$-\beta$ signalling.

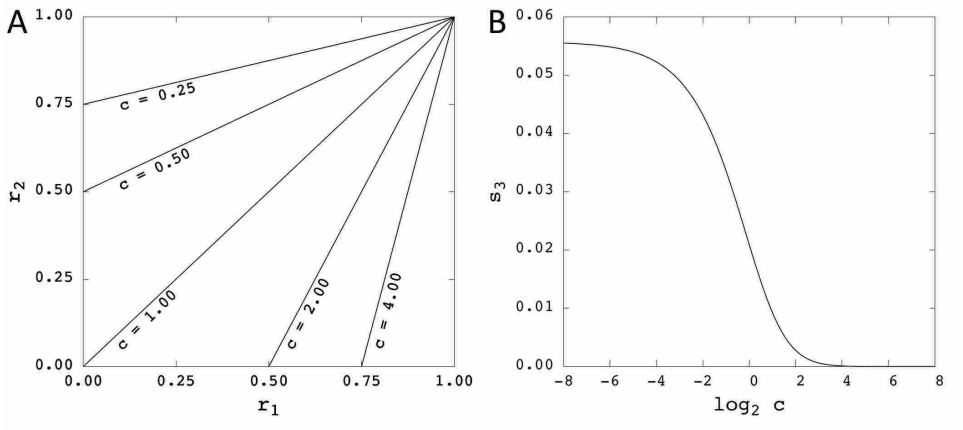

Figure 4.13: *Steady-state analysis of the reduced model in the absence of feedback. A) The phase plane plots of the reduced receptor system at equilibrium for different values of c. B) The scaled total PSMAD trimer, s_3, value against different values of c, where* $\log c = 0$ *corresponds to* $c = 1$.

To understand the effects of feedback in this system, we then consider the toy model (equations 4.8) with its simplest negative feedback loops. For the sake of presentation, r_1 and r_2 are changed to x and y, respectively. As mentioned earlier these negative feedback terms correspond to those in equations 4.5, but with the Michaelis-Menten terms linearized. The 4.8 equations can be presented by one 14th order polynomial which characterizes the full receptor system at steady-state.

$$\varepsilon x^{14}y^{14} + c\delta x^{13}y^{12} - y + cx - c + 1 = 0 \qquad \varepsilon = \frac{c_2\varepsilon_1 - c_1\varepsilon_2}{c_1}, c = \frac{c_2}{c_1} \tag{4.17}$$

There is no straight forward procedure for solving an 14th-order equation. However, we can approximate the solution via asymptotic expansion of y as a function of x. Perturbation expansion is used, assuming that the two parameters of δ and ε are small. We have ignored the second order term for δ and/or ε (first order approximation).

$$y(x) = cx - c + 1 + \varepsilon x^{14}(cx - c + 1)^{14} - \delta c x^{13}(cx - c + 1)^{12} + 14\varepsilon^2 x^{28}(cx - c + 1)^{27}$$
$$-26c\varepsilon\delta x^{27}(cx - c + 1)^{25} + 12c^2\delta^2 x^{26}(cx - c + 1)^{23} + O(n^3), n \in \{\varepsilon, \delta\} \tag{4.18}$$

The final result is illustrated in Figure 4.14 which shows how the solution from the asymptotic expansion changes a with different set of values for δ and ε. This figure shows the deviation of the steady-state curves when negative feedback is input to the system compared to no-feedback. Feedback considerations altered the straight lines to curves which no longer pass through the (1,1) point of the phase plane (see Figure 4.14A). In Figure 4.14A, the solid curves demonstrate the least and highest value of the δ, while the value of ε remains zero. The grey curves simply cover the range between these two limits. By comparing Figure 4.14A with Figure 4.13A (where $\delta = 0$ and $\varepsilon = 0$), it could be seen how the addition of a weak negative feedback, only on $\mathrm{R1}$, change the steady-state of the reduced model. A complete sensitivity analysis of the receptor system is displayed in Figure 4.14B. It is apparent that for non-zero values of ε the system is less sensitive to the changes in δ. Significantly, for the c_1/c_2 ratio of the second order of magnitude, the system is very sensitive to small changes in the feedback strength (ε and δ). A comparison between Figure 4.13B and Figure 4.14B reveals how the steady-state of a system can be affected via insertion of a linear negative feedback.

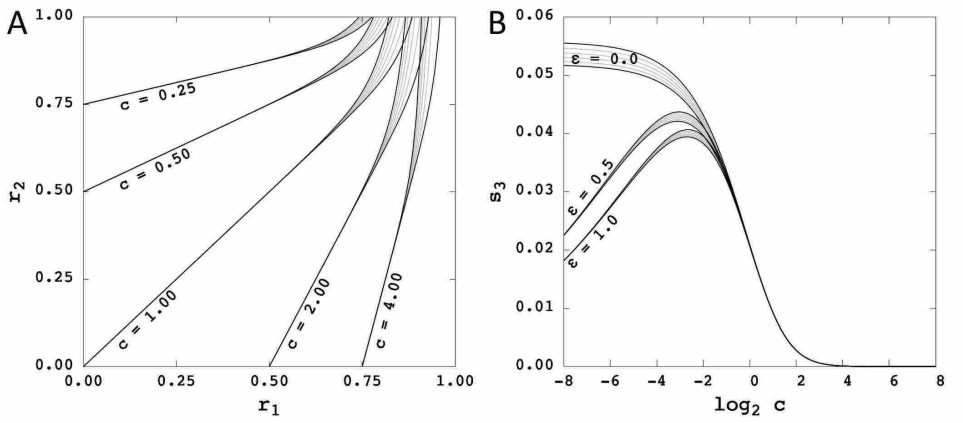

Figure 4.14: *The steady-state of the receptor system for different range of parameters. A) ε = 0.5 δ = 0(0.2)1 In these panels A,B and C $c = 2^n$ for n = -2(1)2. B) δ = 0(0.2)1, In this panel ε changes as labeled.*

It is important to note that the steady-state diagrams of Figure 4.14 are acquired using the asymptotic expansion estimation of the exact solution (4.18). As a result, the curves may behave differently for large values of ε and δ. Also note that r_1, r_2 and s_3 in this section represent scaled receptor variables and the level of total PSMAD trimer in the reduced model. We can follow all the scaling steps reversely to derive receptor concentrations in terms of the production/degradation rates and reaction binding constants. However, the functionality of one variable with respect to the other remains the same. We do not expect significant divergence in the actual $\mathrm{R1}$ -$\mathrm{R2}$ plot (and S_3 plot verses v_1 and v_2 ratio) from the results shown in Figure 4.14. The changes due to negative feed-

back considerations are close to expectation. The negative feedback on $\mathrm{R1}$ and RC does not extremely change the steady-state of r_1 and r_2 (note the operating point of $\log c \approx 0$ in Figure 4.14B). Such an insensitivity might be due to the lack of positive feedback and/or negative feedback on LC (refer to the numerical simulation, section 4).

4.6.2 Model Parameters

Components as variables	Components symbols in simulation and codes
$\mathrm{TGF}-\beta$ receptor type 1	$\mathrm{R1}$
$\mathrm{TGF}-\beta$ receptor type 2	$\mathrm{R2}$
$\mathrm{TGF}-\beta$ receptor type 1 dimer	$\mathrm{R1_2}$
$\mathrm{TGF}-\beta$ receptor type 2 dimer	$\mathrm{R2_2}$
Receptor complex	RC
Ligand-receptor complex	LC
Completely phosphorylated ligand-receptor complex	PC
Cytoplasmic SMAD	S
Phosphorylated SMAD in the cytoplasm	$\hat{\mathrm{S}}$
Phosphorylated SMAD in the nucleus	$\mathrm{S_n}$
Phosphorylated SMAD trimer	$\mathrm{S_3}$
Delayed Phosphorylated SMAD trimer	N
Positive feedback intermediate inhibitor	P
Extracellular $\mathrm{TGF}-\beta$ ligand	$\mathrm{TGF}-\beta$ Dimer

Table 4.1: Components of the $\mathrm{TGF}-\beta$ receptor signalling model

Kinetic rates	Description	Unit
	$\mathrm{TGF}-\beta$ Receptor	
v_1	Production rate of $\mathrm{TGF}-\beta$ receptor type 1	$nMmin^{-1}$
k_1	Degradation rate of $\mathrm{TGF}-\beta$ receptor type 1	min^{-1}
v_2	Production rate of $\mathrm{TGF}-\beta$ receptor type 2	$nMmin^{-1}$
k_2	Degradation rate of $\mathrm{TGF}-\beta$ receptor type 2	min^{-1}
k_1^+	Association rate of type 1 receptor homo-dimer complex	$nM^{-1}min^{-1}$

k_1^-	Dissociation rate of type 1 receptor homo-dimer complex	min^{-1}
k_2^+	Association rate of type 2 receptor homo-dimer complex	$nM^{-1}min^{-1}$
k_2^-	Dissociation rate of type 2 receptor homo-dimer complex	min^{-1}
k_{RC}^+	Association rate of receptor tetramer complex	$nM^{-1}min^{-1}$
k_{RC}^-	Dissociation rate of receptor tetramer complex	min^{-1}
k_{RC}	Degradation rate of receptor tetramer complex	min^{-1}
k_{LC}^+	Association rate of ligand-receptor complex	$nM^{-1}min^{-1}$
k_{LC}^-	Dissociation rate of ligand-receptor complex	min^{-1}
k_{PC}^+	Association rate of phosphorylated ligand-receptor complex	min^{-1}
k_{PC}^-	Dissociation rate of phosphorylated ligand-receptor complex	min^{-1}
k_{PC}	Degradation rate of phosphorylated ligand-receptor complex	min^{-1}

SMAD Proteins

v_{S}	Production rate of cytoplasmic SMAD	$nMmin^{-1}$
k_{S}	Degradation rate of SMAD in the cytoplasm	min^{-1}
k_{S}^+	Phosphorylation rate of SMAD in the cytoplasm	min^{-1}
k_{S}^-	Dephosphorylation rate of SMAD in the cytoplasm	min^{-1}
$k_{\mathrm{S_n}}$	Degradation rate of PSMAD in the nucleus	min^{-1}
k_n^+	Import rate of PSMAD into the nucleus	min^{-1}
k_n^-	Export rate of PSMAD from the nucleus	min^{-1}
k_3^+	Association rate of PSMAD homo-trimer complex	$nM^{-2}min^{-1}$
k_3^-	Dissociation rate of PSMAD homo-trimer complex	min^{-1}
K_{RC}	The receptor complex binding constant	nM
K_{S}	The phsphorylation binding constant	nM
K_3	PSMAD trimer binding constant	nM^2

Feedback

$k_1^{\mathrm{f}+}$	Positive feedback on $\mathrm{TGF}-\beta$ receptor type 1	$nMmin^{-1}$
$k_1^{\mathrm{f}-}$	Negative feedback on $\mathrm{TGF}-\beta$ receptor type 1	$nM^{-1}min^{-1}$
$k_{\mathrm{RC}}^{\mathrm{f}-}$	Negative feedback on receptor tetramer complex	$nM^{-1}min^{-1}$

$k_{\mathrm{PC}}^{\mathrm{f}-}$	Negative feedback on phosphorylated ligand-receptor complex	$nM^{-1}min^{-1}$
K	Negative feedback inhibitory binding constant	nM
K_{I}	Inhibition of the intermediate inhibitor binding constant	nM

Table 4.2: Kinetic rates and binding constants of the model

Parameters	Symbol	Literature value	Reference	Scaled data for our model
R production rate	v_1	$0.0137\ nMmin^{-1}$	[462]	$1\ nMmin^{-1}$
R degradation rate	k_1	$0.00256\ min^{-1}$	[225,513]	$0.2\ min^{-1}$
R positive stimulated degradation rate	$k_1^{\mathrm{f}+}$	–		$1\ min^{-1}$
R negative stimulated degradation rate	$k_1^{\mathrm{f}-}$	–		$0.4\ nM^{-1}min^{-1}$
RC association rate	k_{RC}^{+}	–		$0.5\ nM^{-1}min^{-1}$
RC dissociation rate	k_{RC}^{-}	–		$0.5\ min^{-1}$
RC degradation rate	k_{RC}	–		$1\ min^{-1}$
RC negative stimulated degradation rate	$k_{\mathrm{RC}}^{\mathrm{f}-}$	$0.00256\ nM^{-1}min^{-1}$	[93]	$0.4\ nM^{-1}min^{-1}$
PC association rate	k_{PC}^{+}	–		$1.6\ nM^{-1}min^{-1}$
PC dissociation rate	k_{PC}^{-}	–		$0.2\ min^{-1}$
PC degradation rate	k_{PC}	–		$0.4\ min^{-1}$

PC negative stimulated degradation rate	$k_{\mathrm{PC}}^{\mathrm{f}-}$	–	-	0.4 $nM^{-1}min^{-1}$
S production rate	v_{S}	–		0.01 $nMmin^{-1}$
S degradation rate	k_{S}	–		0.008 min^{-1}
$\hat{\mathrm{S}}$ association rate	k_{S}^{+}	$0.049\ nM^{-1}min^{-1}$	[511]	$0.1\ min^{-1}$
$\hat{\mathrm{S}}$ dissociation rate	k_{S}^{-}	–		$0.1\ min^{-1}$
$\hat{\mathrm{S}}$ degradation rate	$k_{\hat{\mathrm{S}}}$	$0.394\ min^{-1}$	[386]	0.035 min^{-1}
$\mathrm{S_n}$ association rate	k_{n}^{+}	$0.156\ min^{-1}$	[386,513]	$10\ min^{-1}$
$\mathrm{S_n}$ dissociation rate	k_{n}^{-}	$0.739\ min^{-1}$	[386,513]	$8\ min^{-1}$
$\mathrm{S_n}$ degradation rate	$k_{\hat{\mathrm{S}}}$	–		$0.01\ min^{-1}$
positive/negative feedback constant	K	–		2
Inhibition of the intermediate inhibitor binding constant	K_{I}	–		0.4
SMAD phsphorylation binding constant	K_{S}	–		0.008
R initial value		–		$0.83\ nM$
RC initial value		–		$0.23\ nM$
S initial value		$60.6\ nM$	[511]	$1\ nM$
$\mathrm{TGF}-\beta$ initial value		to be specified	[511]	to be specified

Table 4.3: The parameter values of simplified $\mathrm{TGF}-\beta$ model

4.6.3 Figures

By comparing Figure 4.15 and Figure 4.16 with Figure 4.5 and Figure 4.6 in the numerical simulation section, we confirmed that the effects of the system's negative feedback is almost entirely on LC .

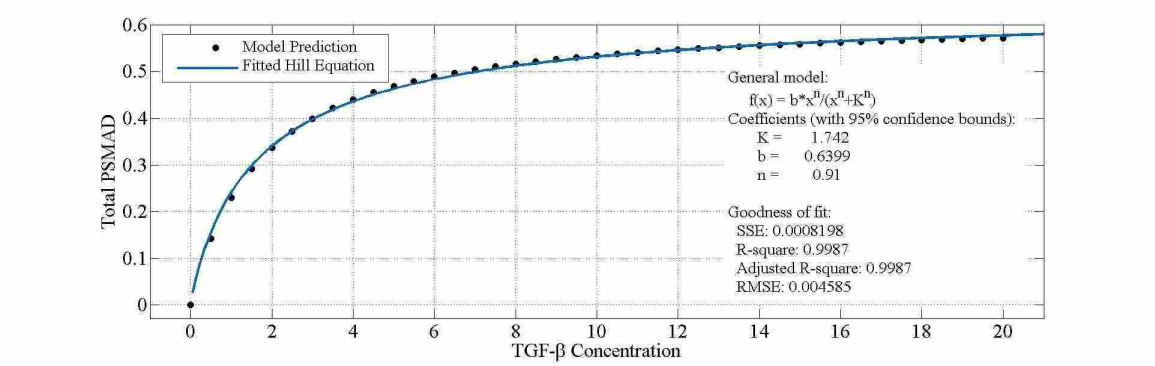

Figure 4.15: *The predicted effects of different concentrations of* TGF$-\beta$ *on the short-term responses of total PSMAD when the negative feedback influences* LC *only.*

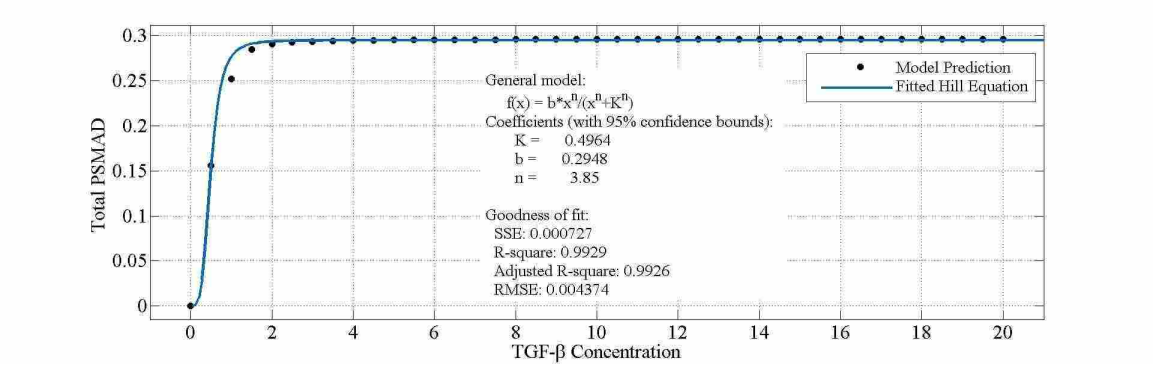

Figure 4.16: *The predicted effects of different concentrations of* TGF$-\beta$ *on the long-term responses of total PSMAD when the negative feedback influences* LC *only.*

4.6.4 Steady-state Analysis of the Simplified Model

There are two possible methods to solve a system of differential equations at steady-state (or equilibrium in this case), analytical and numerical analysis. Analytical analysis defines the equilibria (whether it is single or multiple equilibrium points) explicitly. I attempted to develop analytical solutions for the equilibrium and/or steady-state of the simplified TGF$-\beta$ model.

The simplified model of TGF$-\beta$ consists of 6 differential equations which can be categorized into 2 subsystems (see equations 4.3). The first 3 equations

belong to the membrane subsystem and the last 3 equations belong to the nucleocytoplasmic subsystem. The coupling between the two subsystems is defined such that nucleocytoplasmic subsystem feeds back on the membrane subsystem. In order to solve the steady-state of the system analytically, we equate the RHSs of the equations 4.19 to zero. This provides us with 6 algebraic equations whose solution is defines the equilibrium of the whole system. In the following calculations, the variables of the system are substituted with x_1 to x_6 respectively, for the sake of presentation.

$$\begin{aligned}
\frac{\mathrm{d}x_1}{\mathrm{d}t} &= v_1 - k_1\, x_1 - 2k^+_{\mathrm{RC}}\, x_1^2 + 2k^-_{\mathrm{RC}}\, x_2 - k_1^{\mathrm{f}+}\, [P]\, \frac{x_1}{x_1 + K} - \\
&\quad k_1^{\mathrm{f}-}\, [N]^2\, \frac{x_1}{x_1 + K} \\
\frac{\mathrm{d}x_2}{\mathrm{d}t} &= k^+_{\mathrm{RC}}\, x_1^2 - k^-_{\mathrm{RC}}\, x_2 - k_{\mathrm{RC}}\, x_2 - k^+_{\mathrm{PC}}\, [\mathrm{TGF_2}]\, x_2 + \\
&\quad k^-_{\mathrm{PC}}\, x_3 - k^{\mathrm{f}-}_{\mathrm{RC}}\, [N]^2\, \frac{x_2}{x_2 + K} \\
\frac{\mathrm{d}x_3}{\mathrm{d}t} &= k^+_{\mathrm{PC}}\, [\mathrm{TGF_2}]\, x_3 - k^-_{\mathrm{PC}}\, x_3 - k_{\mathrm{PC}}\, x_3 - k^{\mathrm{f}-}_{\mathrm{PC}}\, [N]^2\, \frac{x_3}{x_3 + K} \\
\frac{\mathrm{d}x_4}{\mathrm{d}t} &= v_{\mathrm{S}}\, - k_{\mathrm{S}}\, x_4 - k^+_{\mathrm{S}}\, x_3 \frac{x_4}{x_4 + K_{\mathrm{S}}} + k^-_{\mathrm{S}}\, x_5 \\
\frac{\mathrm{d}x_5}{\mathrm{d}t} &= k^+_{\mathrm{S}}\, x_3 \frac{x_4}{x_4 + K_{\mathrm{S}}} - k^-_{\mathrm{S}}\, x_5 - k^+_n\, x_5 + k^-_n\, x_6 - k_{\hat{\mathrm{S}}}\, x_5 \\
\frac{\mathrm{d}x_6}{\mathrm{d}t} &= k^+_n\, x_5 - k^-_n\, x_6 - k_{\mathrm{S_n}}\, x_6
\end{aligned} \tag{4.19}$$

where again, $[\mathrm{S_3}] = x_6^3/K_3$, $x_6 = [\mathrm{S_3}]\ (t-\tau)$ and $[P] = {K_{\mathrm{I}}}^2/({K_{\mathrm{I}}}^2 + {[\mathrm{S_3}]}^2)$.

In nucleocytoplasmic subsystem, x_6 can be written in terms of x_5 soling the last equation of 4.19 for its roots. Second last equation defines x_5 in terms of x_3 and x_4. Considering the fact the two thermodynamic terms are in common between fourth and fifth equations we can also write x_4 in terms of x_5 and x_6. All together, the nucleocytoplasmic subsystem can be represented by a single nonlinear algebraic equation:

$$v_{\mathrm{S}}\, - k_{\mathrm{S}}\, x_4 = (k^+_n\, + k_{\hat{\mathrm{S}}}\, - \frac{k^-_n\, k^+_n}{k^-_n\, + k_{\mathrm{S_n}}})k^+_{\mathrm{S}}\, x_3 \frac{x_4}{(x_4 + K_{\mathrm{S}}\,)(k^-_{\mathrm{S}}\, + k^+_n\, + k^-_n \frac{k^+_n}{k^-_n + k_{\mathrm{S_n}}} + k_{\hat{\mathrm{S}}}\,)},$$

where

$$\begin{aligned}
x_6 &= \frac{k^+_n}{k^-_n\, + k_{\mathrm{S_n}}} x_5 \\
x_5 &= k^+_{\mathrm{S}}\, x_3 \frac{x_4}{(x_4 + K_{\mathrm{S}}\,)(k^-_{\mathrm{S}}\, + k^+_n\, + k^-_n \frac{k^+_n}{k^-_n + k_{\mathrm{S_n}}} + k_{\hat{\mathrm{S}}}\,)}
\end{aligned} \tag{4.20}$$

However, reducing the algebraic equations of the membrane subsystem is more complex than the nucleocytoplasmic subsystem. Such complexity is mainly

due to their high nonlinearity. The third equation of 4.19 suggests that x_2 can be written in terms of x_3 and x_6. Therefore, x_2 can be eliminated in the first and second equilibrium equations, giving 2 equations based on x_1, x_3 and x_6:

$$0 = v_1 - k_1 x_1 - 2k^+_{\mathrm{RC}} x_1^2 + 2k^-_{\mathrm{RC}} \frac{k^-_{\mathrm{PC}} + k_{\mathrm{PC}}}{k^+_{\mathrm{PC}} [\mathrm{TGF_2}]} x_3 + k^{\mathrm{f}-}_{\mathrm{PC}} \frac{x_6^6 x_3}{{K_3}^2 (x_3 + K) k^+_{\mathrm{PC}} [\mathrm{TGF_2}]} - k_1^{\mathrm{f}+} \frac{{K_{\mathrm{I}}}^2 x_1}{({K_{\mathrm{I}}}^2 + x_6^6/{K_3}^2)(x_1 + K)} - k_1^{\mathrm{f}-} \frac{x_6^6 x_1}{{K_3}^2 (x_1 + K)} \tag{4.21}$$

$$\begin{aligned} 0 &= k^+_{\mathrm{RC}} x_1^2 - (k^-_{\mathrm{RC}} + k_{\mathrm{RC}} + k^+_{\mathrm{PC}} [\mathrm{TGF_2}]) \\ &\left(\frac{k^-_{\mathrm{PC}} + k_{\mathrm{PC}}}{k^+_{\mathrm{PC}} [\mathrm{TGF_2}]} x_3 + k^{\mathrm{f}-}_{\mathrm{PC}} \frac{x_6^6 x_3}{{K_3}^2 (x_3 + K) k^+_{\mathrm{PC}} [\mathrm{TGF_2}]} \right) \\ &+ k^-_{\mathrm{PC}} x_3 - k^{\mathrm{f}-}_{\mathrm{RC}} \frac{x_6^6 \left(\frac{k^-_{\mathrm{PC}} + k_{\mathrm{PC}}}{k^+_{\mathrm{PC}} [\mathrm{TGF_2}]} x_3 + k^{\mathrm{f}-}_{\mathrm{PC}} \frac{x_6^6 x_3}{{K_3}^2 (x_3 + K) k^+_{\mathrm{PC}} [\mathrm{TGF_2}]} \right)}{{K_3}^2 \left(\frac{k^-_{\mathrm{PC}} + k_{\mathrm{PC}}}{k^+_{\mathrm{PC}} [\mathrm{TGF_2}]} x_3 + k^{\mathrm{f}-}_{\mathrm{PC}} \frac{x_6^6 x_3}{{K_3}^2 (x_3 + K) k^+_{\mathrm{PC}} [\mathrm{TGF_2}]} \right) + K}, \end{aligned} \tag{4.22}$$

where

$$x_2 = \frac{k^-_{\mathrm{PC}} + k_{\mathrm{PC}}}{k^+_{\mathrm{PC}} [\mathrm{TGF_2}]} x_3 + k^{\mathrm{f}-}_{\mathrm{PC}} \frac{x_6^6 x_3}{{K_3}^2 (x_3 + K) k^+_{\mathrm{PC}} [\mathrm{TGF_2}]} \tag{4.23}$$

On the other hand, equating the identical thermodynamic terms in the membrane subsystem provides another algebraic equation in terms of x_1, x_3 and x_6:

$$\begin{aligned} 2 \quad & (k_{\mathrm{RC}} + k^+_{\mathrm{PC}} [\mathrm{TGF_2}]) \left(\frac{k^-_{\mathrm{PC}} + k_{\mathrm{PC}}}{k^+_{\mathrm{PC}} [\mathrm{TGF_2}]} x_3 + k^{\mathrm{f}-}_{\mathrm{PC}} \frac{x_6^6 x_3}{{K_3}^2 (x_3 + K) k^+_{\mathrm{PC}} [\mathrm{TGF_2}]} \right) - \\ 2 \quad & k^-_{\mathrm{PC}} x_3 + 2k^{\mathrm{f}-}_{\mathrm{RC}} \frac{x_6^6 \left(\frac{k^-_{\mathrm{PC}} + k_{\mathrm{PC}}}{k^+_{\mathrm{PC}} [\mathrm{TGF_2}]} x_3 + k^{\mathrm{f}-}_{\mathrm{PC}} \frac{x_6^6 x_3}{{K_3}^2 (x_3 + K) k^+_{\mathrm{PC}} [\mathrm{TGF_2}]} \right)}{{K_3}^2 \left(\left(\frac{k^-_{\mathrm{PC}} + k_{\mathrm{PC}}}{k^+_{\mathrm{PC}} [\mathrm{TGF_2}]} x_3 + k^{\mathrm{f}-}_{\mathrm{PC}} \frac{x_6^6 x_3}{{K_3}^2 (x_3 + K) k^+_{\mathrm{PC}} [\mathrm{TGF_2}]} \right) + K \right)} = \\ v_1 \quad & -k_1 x_1 - k_1^{\mathrm{f}+} \frac{{K_{\mathrm{I}}}^2}{{K_{\mathrm{I}}}^2 + x_6^6/{K_3}^2} \frac{x_1}{x_1 + K} - k_1^{\mathrm{f}-} \frac{x_6^6}{{K_3}^2} \frac{x_1}{x_1 + K} \end{aligned} \tag{4.24}$$

Equations 4.21, 4.22 and 4.24 should be solved simultaneously for x_1, x_3 and x_6 so that the equilibrium point or the equilibria of the system would be identified rigorously. However, the complexity of these algebraic equations makes it hard to introduce an analytical solution for the steady-state of the simplified system. Therefore in order to study the behaviour of the system with different inputs, numerical methods were used (instead of analytical methods). These numerical methods are constrained with the biological data. Several limitations are applied to the model parameters and the initial values of the variables. For instance, none of the components of the model can be negative since they are concentrations, kinetic rates or binding constants, or most of the cytoplasmic and nuclear variables are zero at the beginning of the stimulation. The equilibria cannot be located in the whole $\mathbb{R}^6$ space.

Chapter 5

Modelling the $\mathrm{IL}-6$ Signal Transduction System

5.0 Summary of the information included in Chapter 5

Interleukin-6 is a pleiotropic cytokine that can act as both an anti- and a pro-inflammatory regulator. Signalling via $\mathrm{IL}-6$ plays a pivotal role in many the tissue regulation mechanisms including cell proliferation, apoptosis and immune responses during inflammation. Importantly, excess $\mathrm{IL}-6$ signalling is associated with a diverse range of tumors. A robust mathematical model is required for predicting the likely cellular responses to $\mathrm{IL}-6$ signalling. We have analysed the $\mathrm{IL}-6$ signalling pathway, identified the critical components and developed the minimal systems model capable of quantitative simulation of the network in response to perturbations. Our reduced $\mathrm{IL}-6$ signalling model is compatible with experimental data on changes in STAT3, phospho-STAT3 and SOCS3 levels at different sub-cellular locations in response to continuous or pulsed $\mathrm{IL}-6$ stimulation. Interestingly, appropriately pulsed signalling is expected to increase phospho-STAT3 levels more than continuous stimulation with the same concentration of $\mathrm{IL}-6$. The model also provides a platform for predicting the responses of the network to mutations or inhibitors of $\mathrm{IL}-6$ signalling components. $\mathrm{IL}-6$ induced changes in $\mathrm{TGF}-\beta$ signalling can be predicted with the model.

5.1 Introduction

Interleukin-6 ($\mathrm{IL}-6$) is a multifunction cytokine which influences both acute and chronic inflammation [134]. As a pro-inflammatory cytokine $\mathrm{IL}-6$ can stimulate B cells [186]. Beside the auto-immune responses and cellular growth regulation, $\mathrm{IL}-6$ signalling acts as a mediator in many chronic inflammatory diseases,

including multiple sclerosis and cancer [11,213]. Since the up-regulation of $\mathrm{IL}-6$ has been reported in different types of human cancer (including renal, ovarian, breast, pancreatic and lung cancer), many anti-cancer treatments now aim to target the $\mathrm{IL}-6$ cytokine or its signalling pathways (see [202] for a review). Despite its pro-inflammatory role in chronic inflammatory diseases, $\mathrm{IL}-6$ can decrease inflammation during viral infections [353].

$\mathrm{IL}-6$-type cytokines participate in many cellular processes including differentiation, apoptosis, proliferation, inflammation and immune responses [175, 431]. $\mathrm{IL}-6$ signalling activates intracellular biochemical cycles from the plasma membrane to the nucleus. Signalling occurs when $\mathrm{IL}-6$ binds to its specific receptor IL-6R (also called Gp80) [448]. The $\mathrm{IL}-6$:IL-6R complex then binds a common signal transduction, 130 kDa glycoprotein (Gp130) [253]. All members of $\mathrm{IL}-6$ family of cytokines ($\mathrm{IL}-6$, IL-11, leukaemia inhibitory factor (LIF), oncostatin M (OSM), ciliary neurotrophic factor (CNTF) and cardiotrophin-1 (CT-1)) use Gp130 to transfer the signalling from the cell surface to the cytoplasm [191]. All $\mathrm{IL}-6$-type cytokines induce their signalling through the activation of Janus kinases (JAK) [474]. Deregulation in the signalling pathways stimulated by $\mathrm{IL}-6$ member cytokines (e.g. $\mathrm{IL}-6$ and IL-11) is often associated with human hematological and epithelial malignancies [109]. Moreover, $\mathrm{IL}-6$ is also known as a pleiotropic cytokine that can potentially promote or inhibit tumors [251].

$\mathrm{IL}-6$ signalling interacts with other signalling pathways due to the involvement with Gp130, and the alternative downstream signalling (JAK/STAT and MAPK). There is evidence that $\mathrm{IL}-6$ crosstalks with cytokines such as, BMP [493], NF$-\kappa\beta$ [31], Wnt/β-catenin [47]and $\mathrm{TGF}-\beta$ [207]. The focus of our study is on the $\mathrm{IL}-6$ and $\mathrm{TGF}-\beta$ crosstalk which involves the role of SMAD7 [207]. The interactions between $\mathrm{TGF}-\beta$ and $\mathrm{IL}-6$ signalling are important due to their involvement in inflammatory, auto-immune diseases and cancer. Jenkins et al. [207] used "MEF" (mouse embryonic fibroblast) cells with mutated Gp130 in order to over-express STAT3. STAT3 hyperactivated MEF cells have impaired activation and nuclear translocation of SMAD2 in response to $\mathrm{TGF}-\beta$ [207]. Both $\mathrm{TGF}-\beta$ and $\mathrm{IL}-6$ signalling are over-activated in Erlotinib-resistant cells [495] and both signalling systems are essential for the survival of lung cancer cells [495]. The crosstalk of $\mathrm{TGF}-\beta$ and $\mathrm{IL}-6$ has also been studied by Luwor et al. [287]: the STAT3/SMAD7/$\mathrm{TGF}-\beta$ interactions are also affected by the activation of the EGFR. Persistent activation of STAT3 induces SMAD7 expression, which then desensitizes $\mathrm{TGF}-\beta$ transduction [207,287].

Considering the network of processes responsible for the regulation of $\mathrm{IL}-6$ signalling, it is important to study this signal transduction quantitatively. Since the final responses of the cells will vary with respect to the strength and timing of the initial signal, understanding the temporal changes in the $\mathrm{IL}-6$ signalling components is critical [174, 406]. Models in Systems biology are defined as a mapping from a biological system to a more accessible, immediate and con-

crete system [44, 406]. Modelling of complex signalling networks helps explain the intracellular biological mechanisms, in addition to providing predictions for the responses of the system when it undergoes perturbations (such as environmental perturbations and/or gene mutations) [174, 406]. The significant role of mathematical modelling of signalling pathways is highlighted when it is studied in the context of cancer research. Cancer is a multi-scale, multi-pathway, complex disease that involves many cellular functions [136, 295, 469].

Most of the models of $\mathrm{IL}-6$ signalling concentrate on MAPK signalling through Shp2 (see [175] for a review). We have now developed a reduced model which predicts quantitatively the behaviour of the components of JAK/STAT signalling. The roles of SOCS3, Shp2 and PP2 (nuclear phosphatase) have been studied subsequently by gene knock out studies [402]. Singh et al. [402] compare the responses of the components of $\mathrm{IL}-6$ signalling for each knock out in order to specify the function of each component. Huang et al. in 2010 [70] extended this model and applied sensitivity analysis and parameter clustering in order to simplify the model. Moya et al. [320] also built on Singh's model but re-estimated some of the parameters and included a simulation of the transcription factor dynamics of the MAPK pathway. We focus on IL-6/Gp130/JAK/STAT/SMAD7 signalling, simplifying and reducing the model by removing reactions that do not affect the equilibrium state. Our modelling results are compared to the experimentally derived cell responses of mouse embryonic fibroblasts and mouse liver hepatocytes to $\mathrm{IL}-6$ stimulation.

5.2 Model Development

As mentioned above, $\mathrm{IL}-6$ signals via two separate pathways, Jak/STAT and MAPK. The latter has been studied several times in the literature (for a review see [214]). MAPK is activated by other signalling pathways including receptor kineses such as the EGFR [185, 222, 258, 263, 375]. We examine the crosstalk between $\mathrm{IL}-6$ and $\mathrm{TGF}-\beta$ signalling [207], and focus on the STAT3/SMAD7 connection via the Jak/STAT pathway.

Based on recent data [402, 479], we have designed a detailed model of the initial phases of $\mathrm{IL}-6$ signalling which focuses on the receptor configuration and membrane reactions (Figure 5.1).

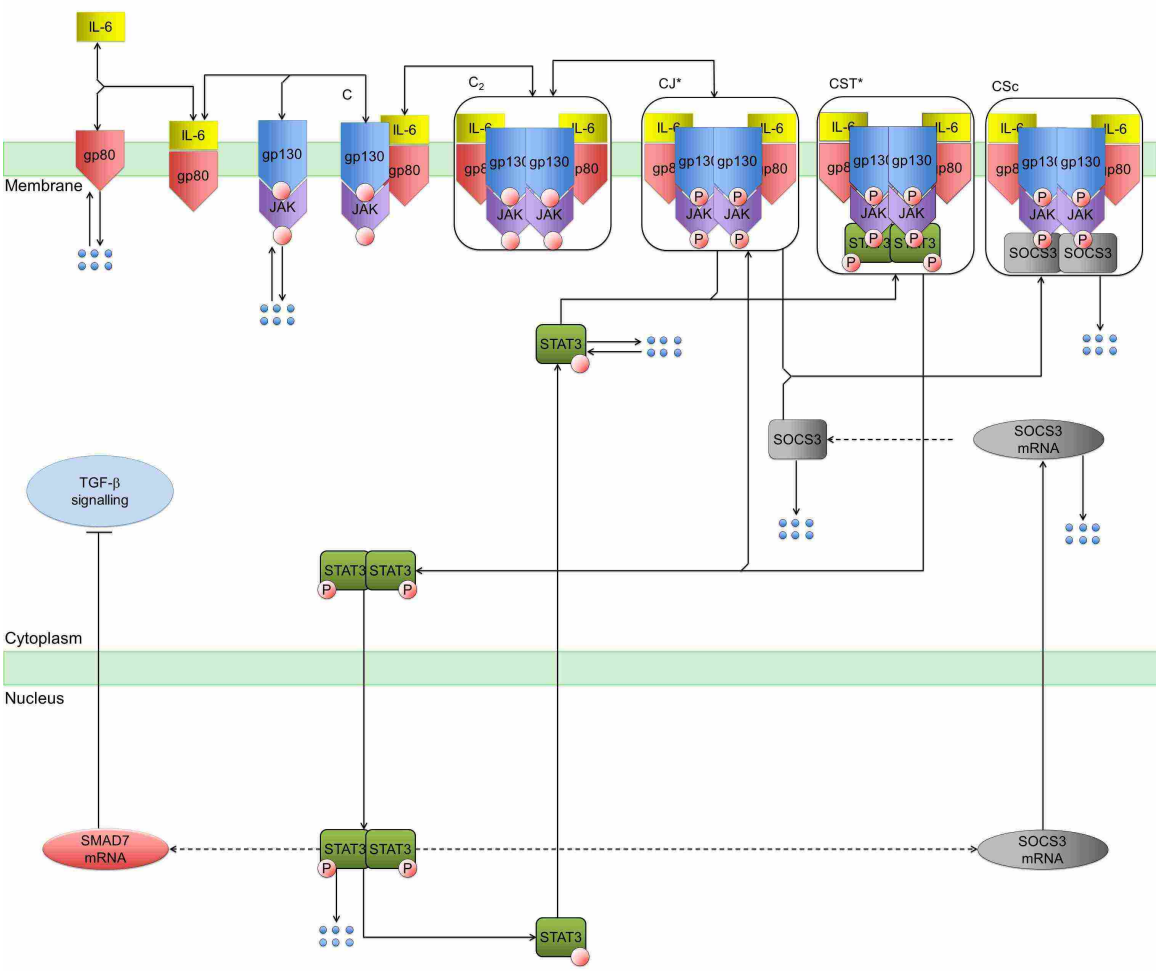

Figure 5.1: *Topology of the* IL − 6 *signalling pathway model. Potential phosphorylation sites of the components are specified with empty circles. Arrows pointing to 6 blue dots represent degradation process. Oval-shaped components represent micro-RNAs. The dot arrows represent the transcription and translation reactions.*

The IL − 6 cytokine first interacts with the Gp80 receptor (also called IL-6Rα chain) [37, 176, 317, 382, 404, 405]. Then, the IL − 6/Gp80 complex binds with the JAK-associated Gp130, resulting in a ligand receptor complex. The complex dimerizes and activates JAK through an autophosphorylation process [317]. Phosphorylated JAK subsequently phosphorylates Gp130 and leads to STAT3 binding [79, 138, 478]. After phosphorylation STAT3 dimerizes, leaves the receptor complex and starts a nucleocytoplasmic shuttling cycle that involves activation of transcription and dephosphorylation of the STAT3 in the nucleus [232, 490]. Phosphorylated Gp130 can bind SOCS3 [15] which blocks STAT3 phosphorylation. The SOCS3 gene is activated by the phosphorylated STAT3 dimer [103, 321].

The components of the IL − 6 signalling pathway are listed as Table 5.1:

Components as variables	Components signs in simulation and codes
$\mathrm{IL}-6$ receptor, Gp80	[Gp80]
$\mathrm{IL}-6$ receptor, Gp130	[Gp130]
Gp80/$\mathrm{IL}-6$ complex	[Gp80/L]
JAK associated Gp130	[Gp130/J]
Ligand-receptor complex	[C]
Ligand-receptor complex dimer	[C_2]
Ligand-receptor complex with activated JAKs	[CJ^*]
Ligand-receptor complex with activated STAT3s	[CST^*]
Ligand-receptor complex binding with SOCS3s	[CSc]
STAT3	[STAT3]
STAT3 dimer	[$STAT3_2$]
PSTAT3	[PSTAT3]
PSTAT3 dimer	[$PSTAT3_2$]
SOCS3	[SOCS3]
SOCS3 mRNA	[socs3]
Extracellular $\mathrm{IL}-6$ ligand	[$\mathrm{IL}-6$]
SMAD7 mRNA	[S7mRNA]
SMAD7	[S7]

Table 5.1: List of the components of the $\mathrm{IL}-6$ signalling model shown in Figure 5.1 and the standard initial conditions for the model which were constructed from the literature

Based on the $\mathrm{IL}-6$ signalling model in Figure 5.1, the differential equations of the reaction network are of the following form. Note that we have never solved the full model of $\mathrm{IL}-6$ signalling which is described by Table 5.2, however, the table is useful for understanding the reduction methodology.

Diff. eq. based on kinetics	Raw diff. Eq. for simulation
$d/dt[Gp80] = v1 - v2 - v3$	$d/dt[Gp80] = v_{80} - k_{\emptyset 80}[Gp80] - k_{a80/L}[IL-6][Gp80] + k_{d80/L}[Gp80/L]$
$d/dt[Gp80/L] = v3 - v4$	$d/dt[Gp80/L] = k_{a80/L}[IL-6][Gp80] - k_{d80/L}[Gp80/L] - k_{ac}[Gp80/L][Gp130J] + k_{dc}[C]$
$d/dt[Gp130/J] = v5 - v6 - v4$	$d/dt[Gp130/J] = v_{130} - k_{\emptyset 130}[Gp130/J] - k_{ac}[Gp80/L][Gp130/J] + k_{dc}[C]$
$d/dt[C] = v4 - 2v7$	$d/dt[C] = k_{ac}[Gp80/L][Gp130/J] - k_{dc}[C] - 2k_{a2}[C][C] + 2k_{d2}[C_2]$
$d/dt[C_2] = v7 - v8$	$d/dt[C_2] = k_{a2}[C][C] - k_{d2}[C_2] - k_{aJ}[C_2] + k_{dJ}[CJ^*]$
$d/dt[CJ^*] = v8 - v9$	$d/dt[CJ^*] = k_{aJ}[C_2] - k_{dJ}[CJ^*] - k_{ph}[STAT3][STAT3][CJ^*] + k_{dst}[CST^*] - k_{aCSc}[CJ^*][SOCS3][SOCS3]$
$d/dt[CST^*] = v13 - v11$	$d/dt[CST^*] = k_{ph}[CJ^*][STAT3][STAT3] - k_{d130}[CST^*]$
$d/dt[CSc] = v12 - v14$	$d/dt[CSc] = v_{ST} - k_{\emptyset CSc}[CSc] + k_{aCSc}[CJ^*][SOCS3][SOCS3]$
$d/dt[STAT3] = -v10 + v15 - v16$	$d/dt[STAT3] = -k_{ph}[STAT3][STAT3][CJ^*] + k_{eST}[STAT3in] - k_{\emptyset ST}[STAT3]$
$d/dt[PSTAT3_2] = v11 - v17$	$d/dt[PSTAT3_2] = k_{dst}[CST^*] - k_{iST}[PSTAT3_2]$
$d/dt[PSTAT3_{2in}] = v17 - v18$	$d/dt[PSTAT3_{2in}] = k_{iST}[PSTAT3_2] - k_{dph}[PSTAT3_{2in}]$
$d/dt[STAT3_{in}] = 2v18 - v15$	$d/dt[STAT3_{in}] = 2k_{dph}[PSTAT3_{2in}] - k_{eST}[STAT3in]$
$d/dt[socs3_{in}] = v19 - v20$	$d/dt[socs3_{in}] = k_{trac}\frac{[PSTAT3_{2in}]}{[PSTAT3_{2in}]+K_{Sc}} - k_{emRNA}[socs3_{in}]$
$d/dt[socs3] = v20 - v21 - v22$	$d/dt[socs3] = k_{emRNA}[socs3_{in}] - k_{\emptyset mRNA}[socs3] - k_{trnsl}[socs3]$
$d/dt[SOCS3] = -v23 + v22 - v12$	$d/dt[SOCS3] = k_{\emptyset Sc}[SOCS3] + k_{trnsl}[socs3] - 2k_{aCSc}[C130^*][SOCS3][SOCS3]$

Table 5.2: Differential equations used to model the reactions of the $\mathrm{IL}-6$ signalling pathway shown in Figure 5.2

The critical components and reactions for $\mathrm{IL}-6$ signalling are summarized in Figure 5.2. The dashed line represents a complex series of interactions, including genetic expression and mRNA processes (see [15] for a review) and the two headed arrows specify reversible reactions.

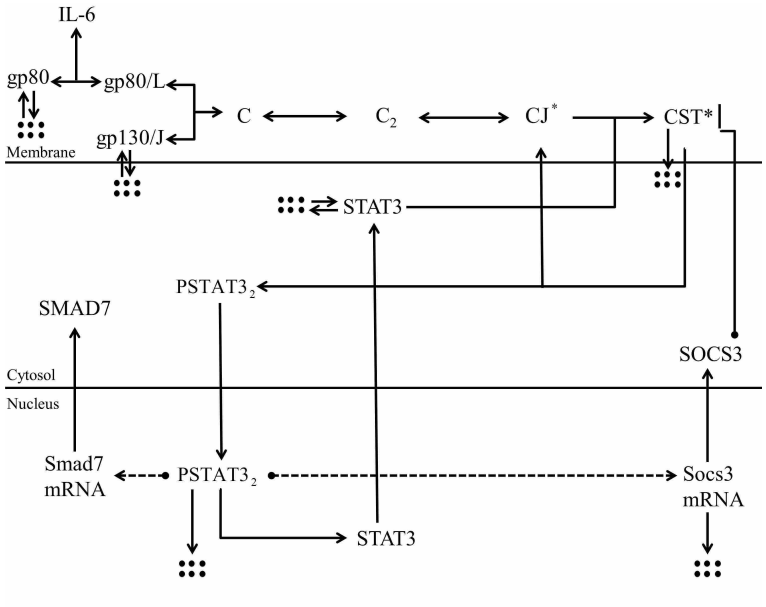

Figure 5.2: *A reduced model representing the* $\mathrm{IL}-6$ *signal transduction network. Arrows pointing to 6 blue dots represent degradation process. The stars represent for the phosphorylated species. The dot arrows represent the transcription and translation reactions.*

5.3 Analysis

5.3.1 Reduction Implementation on the Receptor Part

In accordance with to the rapid equilibrium assumption [115, 203], the membrane components of the $\mathrm{IL}-6$ transduction can be reduced to the main components $\mathrm{IL}-6$, Gp80 and Gp130. The relatively fast kinetic rates of the interactions on the membrane compared to the other reactions (such as import, export, transcription and translation of the intracellular proteins) enables us to apply the reduction process. It is reported that the order of magnitudes for signalling processes can be categorized as Table 5.3 [340].

Process	Order of magnitude	References
Signalling reactions	$< 10^0$s	[150,271]
Transcriptional regulation	10^2s	[304,367,515]
Receptor internalization	10^2s	[119,211]
ligand dimerization ans receptor dimerization	10^{-3}s	[374]

Table 5.3: Separation of the intracellular reactions based on their timescale [340]

The following reactions on the membrane are fast and consequently at equilibrium these reactions can be reduced:

$$\mathrm{IL}-6+\mathrm{Gp80} \overset{K_{80}}{\rightleftharpoons} \mathrm{Gp80/L} \tag{5.1}$$

$$J+Gp130 \overset{K_{130}}{\rightleftharpoons} Gp130/J \tag{5.2}$$

$$Gp80/L+Gp130/J \overset{K_1}{\rightleftharpoons} C \tag{5.3}$$

$$C+C \overset{K_2}{\rightleftharpoons} C_2 \tag{5.4}$$

$$C_2 \overset{K_2^*}{\rightleftharpoons} CJ^* \tag{5.5}$$

In IL-6:JAK:STAT signalling, Gp130/JAK are pre-associated before binding of $\mathrm{IL}-6$ [15, 176]. However in the equations above, we added a pre-step to simulate Gp130 and JAK binding. Consequently, the equations 5.1 and 5.2 can be treated similarly. Based on the fast reactions above, the equilibrium values of the components can be written as:

$$\begin{aligned}
[Gp80/L] &= \frac{[IL-6]\,[Gp80]}{K_{80}} \\
[Gp130/J] &= \frac{[J]\,[Gp130]}{K_{130}} \\
[C] &= \frac{[Gp80/L]\,[Gp130/J]}{K_1} = \frac{[IL6]\,[Gp80]\,[J]\,[Gp130]}{K_{80}K_{130}K_1} \\
[C_2] &= \frac{[C]^2}{K_2} = \frac{[IL6]^2\,[Gp80]^2\,[J]^2\,[Gp130]^2}{K_{80}^2K_{130}^2K_1^2K_2} \\
[CJ^*] &= \frac{[C_2]}{K_2^*} = \frac{[IL6]^2\,[Gp80]^2\,[J]^2\,[Gp130]^2}{K_{80}^2K_{130}^2K_1^2K_2K_2^*}
\end{aligned} \tag{5.6}$$

Now we can write the equations for the total concentrations of Gp80 and Gp130 based on the conservation law. These equations are written according to the participation of each receptor in the membrane complexes:

$$\begin{aligned}
[Gp80]_T &= [Gp80]+[Gp80/L]+[C]+2\,[C_2]+2\,[CJ^*] \\
[Gp130]_T &= [Gp130]+[Gp130/J]+[C]+2\,[C_2]+2\,[CJ^*]
\end{aligned} \tag{5.7}$$

On the other hand, we can write the following equations for the derivation of the receptors with respect to time:

$$\begin{aligned}
\frac{\mathrm{d}[Gp80]}{\mathrm{d}t} &= v_{80}-k_{\emptyset 80}[Gp80]-2(k_{aCSc}[SOCS3]\frac{[CJ^*]}{[CJ^*]+K} \\
&\quad +k_{dJ}[CJ^*]+k_{d2}[C_2]) \\
\frac{\mathrm{d}[Gp130]}{\mathrm{d}t} &= v_{130}-k_{\emptyset 130}[Gp130]-2(k_{aCSc}[SOCS3]\frac{[CJ^*]}{[CJ^*]+K} \\
&\quad +k_{dJ}[CJ^*]+k_{d2}[C_2])
\end{aligned} \tag{5.8}$$

We define f_1 and f_2 as the RHSs of $\frac{\mathrm{d}[Gp80]}{\mathrm{d}t}$ and $\frac{\mathrm{d}[Gp130]}{\mathrm{d}t}$ in equations 5.8, respectively. By differentiating the right hand sides of the conservation equations

(equations 5.7) and equating them with the reactions by which the total number of receptors vary (f_1 and f_2), we have:

$$\begin{aligned} A_{11} frac\mathrm{d}[Gp80]\mathrm{d}t + A_{12}\frac{\mathrm{d}[Gp130]}{\mathrm{d}t} &= f_1 \\ A_{21}\frac{\mathrm{d}[Gp80]}{\mathrm{d}t} + A_{22}\frac{\mathrm{d}[Gp130]}{\mathrm{d}t} &= f_2 \end{aligned} \tag{5.9}$$

where,

$$\begin{aligned} A_{11} &= 1 + \frac{[L]}{K_{80}} + \frac{[L][J][Gp130]}{K_{80}K_{130}K_1} + \frac{4[L]^2[Gp80][J]^2[Gp130]^2}{K_{80}^2K_{130}^2K_1^2K_2}(1+1/K_2^*) \\ A_{21} &= \frac{[L][J][Gp130]}{K_{80}K_{130}K_1} + \frac{4[L]^2[Gp80][J]^2[Gp130]^2}{K_{80}^2K_{130}^2K_1^2K_2}(1+1/K_2^*) \\ A_{12} &= \frac{[L][Gp80][J]}{K_{80}K_{130}K_1} + \frac{4[L]^2[Gp80]^2[J]^2[Gp130]}{K_{80}^2K_{130}^2K_1^2K_2}(1+1/K_2^*) \\ A_{22} &= 1 + \frac{[J]}{K_{130}} + \frac{[L][Gp80][J]}{K_{80}K_{130}K_1} + \frac{4[L]^2[Gp80]^2[J]^2[Gp130]}{K_{80}^2K_{130}^2K_1^2K_2}(1+1/K_2^*) \end{aligned} \tag{5.10}$$

and,

$$\begin{aligned} f_1 &= v_{80} - k_{\emptyset 80}[Gp80] - 2R \\ f_2 &= v_{130} - k_{\emptyset 130}[Gp130] - 2R \end{aligned} \tag{5.11}$$

and, R is given by:

$$R = k_{aCSc}[SOCS3]\frac{[CJ^*]}{[CJ^*]+K} + k_{dJ}[CJ^*] + k_{d2}[C_2]. \tag{5.12}$$

Note that we have substituted the equilibrium values for all membrane components, equation 5.9 can be decoupled using Cramer's rule [355].

5.3.2 Modelling of the Nucleocytoplasmic Reactions

According to our $\mathrm{IL}-6$ signalling model, STAT3 phosphorylation occurs after binding to the IL-6:IL-6R:Gp130 complex. The biochemical reactions can be represented as:

$$CJ^* + 2STAT3 \rightarrow CST^* \rightarrow CJ^* + PSTAT3_2 \tag{5.13}$$

Assuming that the intermediate reactions are sufficiently fast, this can be reduced to:

$$2STAT3 \xrightarrow{CJ^*} PSTAT3_2 \tag{5.14}$$

CJ^* represents the enzyme that catalyses the phosphorylation process. The enzymatic reaction is modelled using Michaelis–Menten kinetics.

5.3.3 Simplified Model

The rapid equilibrium assumption [115, 203] significantly decreases the complexity of the $\mathrm{IL}-6$ signalling network. Gp130 uses a specific mechanism to phosphorylate STAT3 and transfer the signal to the nucleus: As shown in Figures 5.1 and 5.2, STAT3 becomes phosphorylated, activated and dimerized after binding with the JAK-associated Gp130 complex. Next, the phosphorylated STAT3 dimer dissociates from the membrane receptor complex. Using the mass action law for STAT3 phosphorylation adds extra complexity to the system, however, the membrane receptor complex can be considered as an enzyme and the STAT3 phosphorylation process an enzymic reaction. Michaelis–Menten kinetics replaces the mass action kinetics in Figure 5.3.

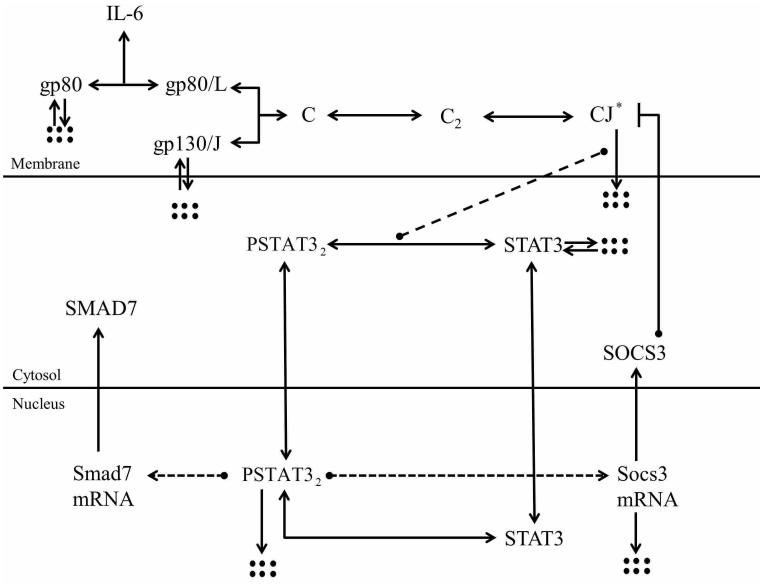

Figure 5.3: *Simplified model of* $\mathrm{IL}-6$ *signal transduction. The dashed line specifies an enzymic reaction. Arrows pointing to 6 blue dots represent degradation process. The stars represent for the phosphorylated species. The dot arrows represent the transcription and translation reactions.*

The equations used for the Numerical Simulations and Validation sections are (the equations of the simplified model):

$$
\begin{aligned}
\frac{\mathrm{d}[Gp80]}{\mathrm{d}t} &= (f_1 A_{22} - f_2 A_{12})/(A_{11}A_{22} - A_{21}A_{12}) \\
\frac{\mathrm{d}[Gp130]}{\mathrm{d}t} &= (f_2 A_{11} - f_1 A_{21})/(A_{11}A_{22} - A_{21}A_{12}) \\
\frac{\mathrm{d}[STAT3]_C}{\mathrm{d}t} &= v_{ST} - k_{\emptyset ST}[STAT3]_C - 2k_{phc}[CJ^*]\frac{[STAT3]_C^2}{[STAT3]_C^2 + K^2} - \\
&\qquad 2k_{dph}[PSTAT3_2]_C + k^e Vnc[STAT3]_N - k^i[STAT3]_C \\
\frac{\mathrm{d}[PSTAT3_2]_C}{\mathrm{d}t} &= k_{phc}[CJ^*]\frac{[STAT3]_C^2}{[STAT3]_C^2 + K^2} - k_{dph}[PSTAT3_2]_C - \\
&\qquad k^i[PSTAT3_2]_C + k^e Vnc[PSTAT3_2]_N) \\
\frac{\mathrm{d}[SOCS3]_C}{\mathrm{d}t} &= k_{trnsl}k^e Vnc[socs3]_N - k_{\emptyset Sc}[SOCS3]_C \\
\frac{\mathrm{d}[STAT3]_N}{\mathrm{d}t} &= 2k_{dph}[PSTAT3_2]_N - 2k_{phn}[STAT3]_N^2 - k^e[STAT3]_N \\
&\qquad + k^i Vcn[STAT3]_C \\
\frac{\mathrm{d}[PSTAT3_2]_N}{\mathrm{d}t} &= k^i Vcn[PSTAT3_2]_C - k_{dph}[PSTAT3_2]_N + k_{phn}[STAT3]_N^2 - \\
&\qquad k_{\emptyset PSn}[PSTAT3_2]_N - k^e[PSTAT3_2]_N \\
\frac{\mathrm{d}[socs3]_N}{\mathrm{d}t} &= -k_{\emptyset mRNA}[socs3]_N - k_{trnsl}k^e[socs3]_N + k_{trac}\frac{[PSTAT3_2]_N}{[PSTAT3_2]_N + K_{Sc}}
\end{aligned}
\tag{5.15}
$$

In these equations we assumed all the import and export kinetic rates are the same for different components. Vnc and Vcn are defined as the (volume of the nucleus)/(volume of the cytoplasm) and (volume of the cytoplasm)/(volume of the nucleus), respectively. The kinetic rates and their units are listed in Tables 5.4 and 5.5

Kinetic rates	Description	Unit
	IL − 6 Receptor	
v_{80}	Production rate of Gp80 receptor	$nMmin^{-1}$
$k_{\emptyset 80}$	Degradation rate of Gp80 receptor	min^{-1}
v_{130}	Production rate of Gp130 receptor	$nMmin^{-1}$
$k_{\emptyset 130}$	Degradation rate of Gp130 receptor	min^{-1}
K_{80}	Ligand:Gp80 binding constant	nM
K_{130}	Gp130:JAK binding constant	nM
K_1	Ligand-Gp80 binding constant	nM
K_2	Gp80/L:Gp130/J binding constant	nM
K_2^*	C_2:CJ^* binding constant	$-$
	STAT Proteins	
v_{ST}	Production rate of cytoplasmic STAT3 receptor	$nMmin^{-1}$
$k_{\emptyset ST}$	Degradation rate of cytoplasmic STAT3 receptor	min^{-1}

k_{phc}	Phosphorylation and dimerization rate of STAT3 protein in the cytoplasm	min^{-1}
k_{dph}	Dephosphorylation rate of PSTAT3 protein dimer	min^{-1}
k_{phn}	Phosphorylation and dimerization rate of STAT3 protein in the nucleus	$nM^{-1}min^{-1}$
$k_{\emptyset PSn}$	Degradation rate of phosphorylated STAT3 dimer	min^{-1}
k^i	Nuclear import rate of cytoplasmic complexes	min^{-1}
k^e	Nuclear export rate of cytoplasmic complexes	min^{-1}
K	Phosphorylation of STAT3 binding constant	nM
	Feedback	
k_{trnsl}	Translation rate of SOCS3	$-$
$k_{\emptyset Sc}$	Degradation rate of SOCS3 in the cytoplasm	min^{-1}
$k_{\emptyset mRNA}$	Degradation rate of socs3 mRNA in the nucleus	min^{-1}
k_{trac}	Transcription rate of socs3 mRNA	$nMmin^{-1}$
k_{dJ}	Basal degradation rate of CJ^* on the membrane	min^{-1}
k_{aCSc}	Degradation rate of CJ^* stimulated with negative feedback	min^{-1}
k_{d2}	Basal degradation rate of C_2 on the membrane	min^{-1}
K_{Sc}	Transcription of socs3 mRNA binding constant	$nMmin^{-1}$

Table 5.4: Kinetic rates and binding constants of the model

Parameters symbol	Literature value	Reference	Scaled data for our model
v_{80}	$-$		$0.17\ nMmin^{-1}$
$k_{\emptyset 80}$	$-$		$0.01\ min^{-1}$
v_{130}	$-$		$0.15\ nMmin^{-1}$
$k_{\emptyset 130}$	$-$		$0.01\ min^{-1}$
K_{80}	0.5	[402]	$1\ nM$
K_{130}	0.5	[402]	$1\ nM$
K_1	1	[402]	$1\ nM$
K_2	5	[402]	$5\ nM$
K_2^*			0.5
v_{ST}	$-$		$0.25\ nMmin^{-1}$

$k_{\emptyset ST}$	$-$		$0.4\ min^{-1}$
k_{phc}	$-$		$0.0005\ min^{-1}$
k_{dph}	$-$		$0.005\ min^{-1}$
k_{phn}	$-$		$0.005\ nM^{-1}min^{-1}$
$k_{\emptyset PSn}$	$-$		$0.1\ min^{-1}$
k^i	$0.005\ min^{-1}$	[402]	$0.5\ min^{-1}$
k^e	$-$		different for different components min^{-1}
K	$-$		$0.5\ nM$
k_{trnsl}	$0.01\ min^{-1}$	[402]	0.5
$k_{\emptyset Sc}$	$-$		$0.15\ min^{-1}$
$k_{\emptyset mRNA}$	$-$		$1\ min^{-1}$
k_{trac}	$0.01\ nMmin^{-1}$	[402]	$6\ nMmin^{-1}$
k_d	$-$		$0.01\ min^{-1}$
k_{aCSc}	$-$		$0.01\ min^{-1}$
k_{d2}	$-$		$0.01\ min^{-1}$
K_{Sc}	$400\ nM$	[402]	$6\ nM$

Table 5.5: The parameter values of simplified $\mathrm{IL}-6$ model

Similar to the Chapter 4, the complexity and non-linearity of the simplified $\mathrm{IL}-6$ model make us to use numerical methods rather than analytical methods.

5.4 Numerical Simulations and Validation

We have quantitated the published experimental [479] Western blot results for STAT3, PSTAT3 and SOCS3 protein expression levels in mouse liver cells. These quantitative results were compared with the levels of these components predicted by our $\mathrm{IL}-6$ signalling model. Due to STAT3 and PSTAT3 nucleocytoplasmic shuttling, our model design requires total STAT3 concentration level (including Phosphorylated STAT3 in the cytosol and nucleus) to be constant in time. Experimental results from Wormald et al. [479] support the model assumption that total STAT3 concentration is relatively stable (see Figure 5.4). The slight decrease in the level of total STAT3 at the beginning of the simulation is due to the time-scale of the STAT3 phosphorylation process. By increasing the time-scale of phosphorylation reaction, the simulation curve converges to the total, experimental STAT3 steady-state level faster. Note that total STAT3 (monomer) concentration is defined as $[STAT3]_C + 2[PSTAT3_2]_C + V_{nc}([STAT3]_N + 2[PSTAT3_2]_N)$.

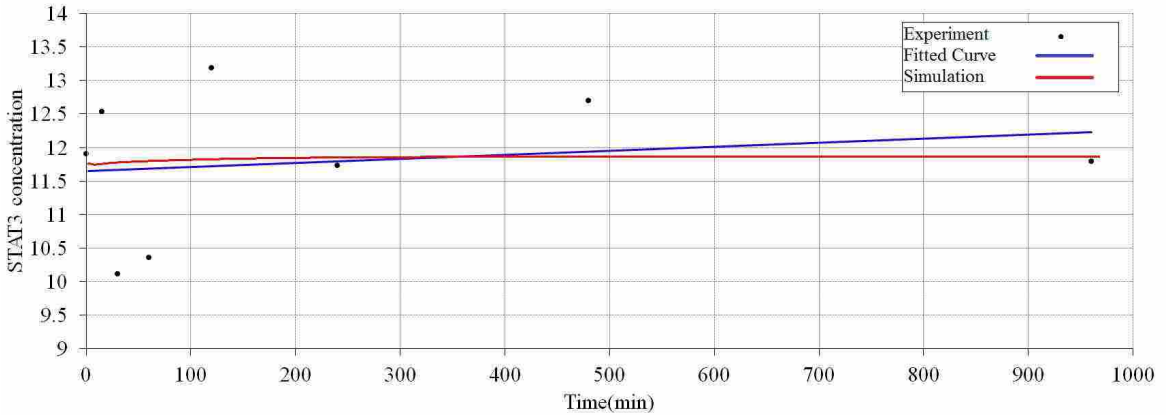

Figure 5.4: *Total STAT3 concentration in liver extracts after* IL − 6 *stimulation. The dots represent the experimental values derived from figure 1 of Wormald et al. [479]. The blue and red curves represent the fitted curve for the experimental data and the predicted values from the model, respectively. The fitted curve is plotted via trendline tool of Microsoft Excel.*

In order to study the changes in STAT3 concentration level in the shorter time-scale, the simulation results as a function of STAT3 concentration have been plotted in a semi log graph (see Figure 5.5). The x axis in Figure 5.5 is a log scale and the y axis is magnified in order to elaborate the short-term variations of STAT3. The steady-state level of total STAT3 is slightly higher that its initial value. As mentioned earlier, the difference in the time-scale of the phosphorylation and dephosphorylation kinetic rates in the model is the main reason for the protein level variation.

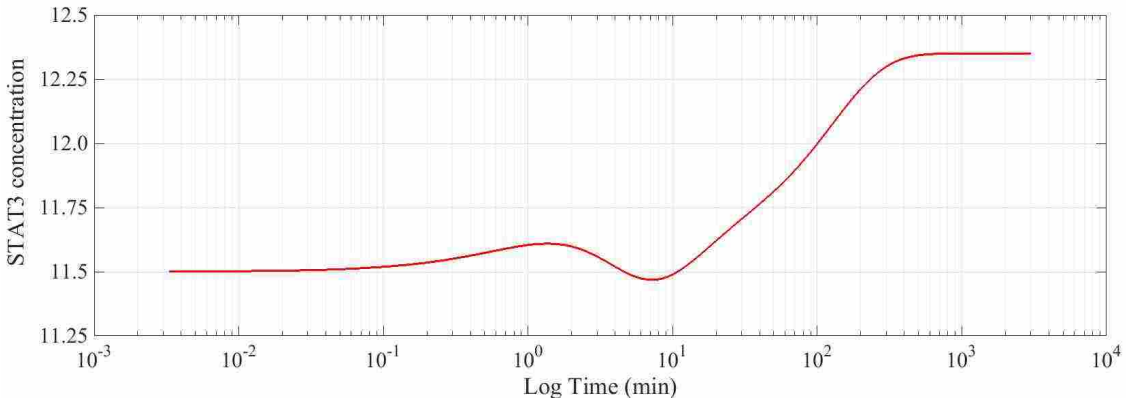

Figure 5.5: *Total STAT3 concentration time course in liver extracts after* IL − 6 *stimulation in log timescale. The red curve is the simulation result. The figure suggests a difference between the initial level of total STAT3 and its steady-state level. The fitted curve is plotted via trendline tool of Microsoft Excel.*

The levels of total PSTAT3 and SOCS3 were shown by Wormald et al. [479]. Figures 5.6 and 5.7 show the experimentally measured levels of total PSTAT3

and SOCS3. The predicted trends for these protein concentrations simulated via our model are shown in Figures 5.6 and 5.7. Although the Wormald's published data was not quantitated [479], we were able to use their gel images to estimate the total STAT3, total PSTAT3 and SOCS3 levels. The original photographic films were kindly provided by S. Wormald. The dots show the experimental values from Wormald et al. data [479]

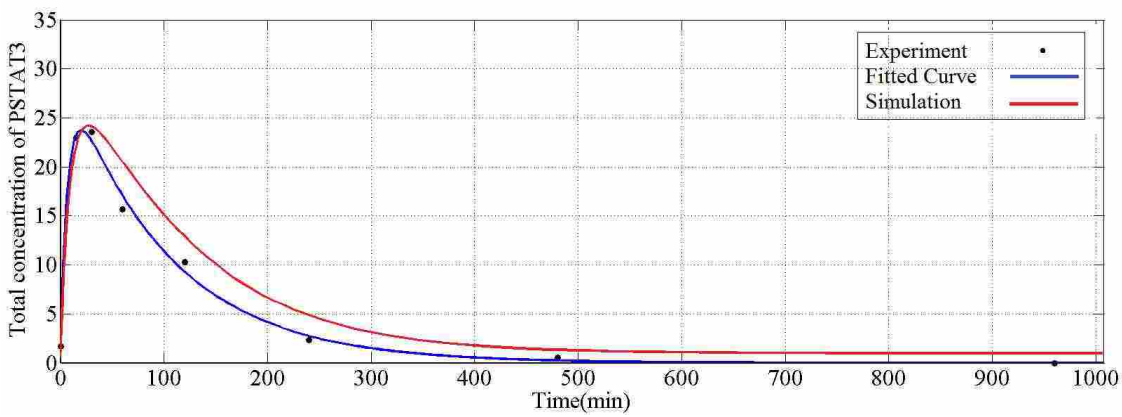

Figure 5.6: *Total PSTAT3 concentration in liver extracts after* $\mathrm{IL}-6$ *stimulation. The dots represent the experimental values derived from figure 1 of Wormald et al. [479]. The blue and red curves represent the fitted curve for the experimental data and the predicted values from the model, respectively. The fitted curve is plotted via trendline tool of Microsoft Excel.*

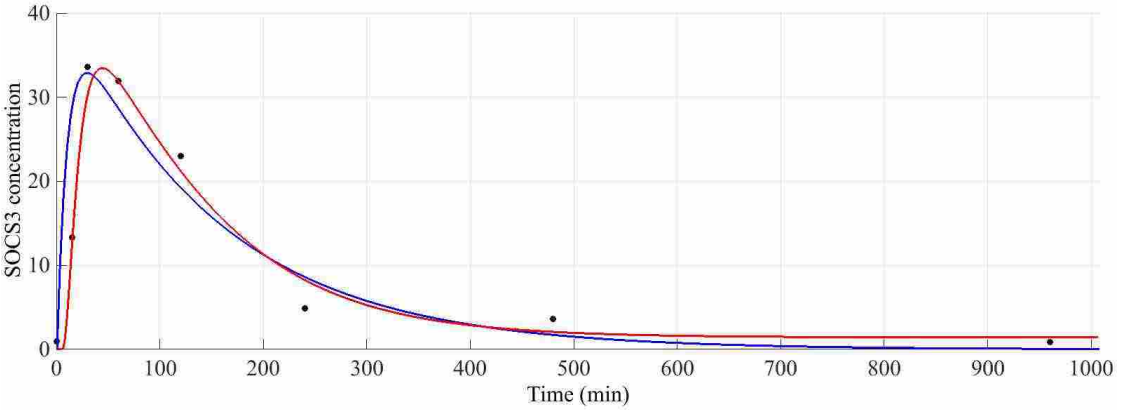

Figure 5.7: *SOCS3 concentration in liver extracts after* $\mathrm{IL}-6$ *stimulation. The dots represent the experimental values derived from figure 1 of Wormald et al. [479]. The blue and red curves demonstrate the fitted curve for the experimental data and the predicted values from the model, respectively.*

The final results for our simulations demonstrate that our simplified model of $\mathrm{IL}-6$ signalling pathway can predict the protein and phospho-protein levels accurately.

The general trend of the experimental and modelling curves for total STAT3, PSTAT3, and SOCS3 are similar. PSTAT3 measured by experiment peaks at 50 min and the peak value is almost 10 times larger than its steady-state value. The modelling predicts differences in the total concentration of PSTAT3 verses time. The simulation predicts protein levels up to 1000 min. Due to the lack of data on the absolute amount of each protein on the gels in Wormald's paper, PSTAT3 and SOCS3 levels were normalized to the total STAT3 loadings.

Figure 5.7 shows the SOCS3 time course for both the experiment and the simulation. The simulation shows a peak signal approximately an hour after IL-6 stimulation which is consistent with the results from the experiment. In both the experimental and simulation curves, the peak value is more than 15 fold higher than the steady-state value for the concentration of SOCS3.

SMAD7 level can be predicted using our $\mathrm{IL}-6$ model. More specifically, the SMAD7 level varies proportional to the PSTAT3 dimer in the nucleus i.e. the transcription factor. Consequently, the SMAD7 concentration is defined as $[PSTAT3_2]_N^2/([PSTAT3_2]_N^2+1)$ in Figure 5.8 and Figure 5.9. Figure 5.8 shows time dependent changes in SMAD7 concentration for both linear and non-linear PSTAT3/SMAD7 relation. The linear relation is modeled using mass-action kinetics, while Michaelis-Menten kinetics are used to show non-linear stimulation of SMAD7 via PSTAT3 transcription factor. Furthermore, the $\mathrm{IL}-6$ ligand concentration changes the SMAD7 dynamics. Specifically, SMAD7 seems to decay later at higher ligand concentration (see Figure 5.9).

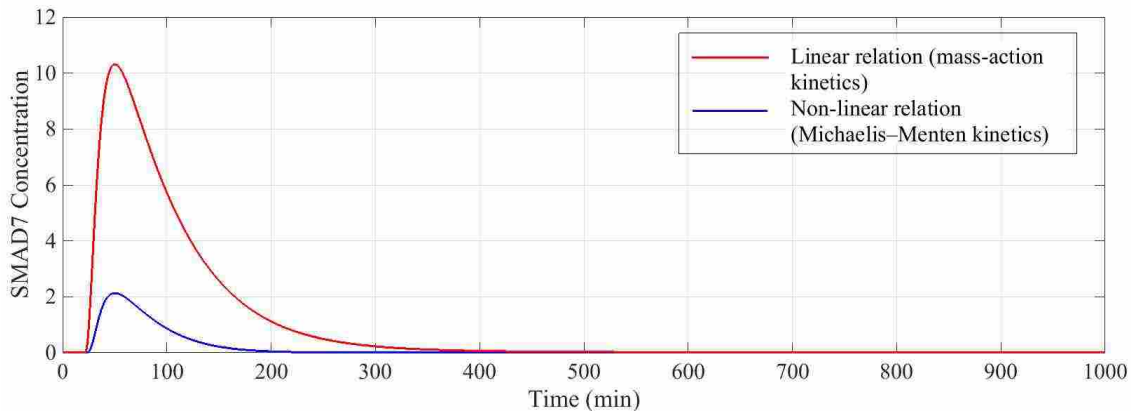

Figure 5.8: *SMAD7 concentration time course for linear and non-linear stimulation via nuclear PSTAT3.*

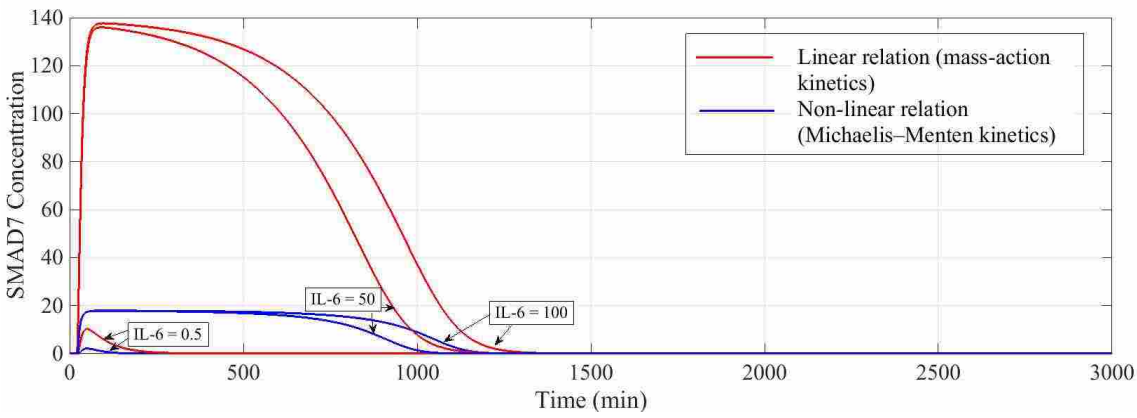

Figure 5.9: *SMAD7 concentration time course dynamics for* $\mathrm{IL}-6$ *concentration input = 0.5, 100 and 400 (the concentration units are arbitrary).*

An advantage of a signalling model is that its predictions are not specific to a single cell line. To show the compatibility of our model we have validated the simplified $\mathrm{IL}-6$ signalling model with a set of experimental data extracted from wild type mouse embryonic fibroblasts (MEFs). Figure 5.10 shows how the model simulation of PSTAT3 dynamics explains the experimental within 1 hour after $\mathrm{IL}-6$ stimulation. For data extraction method of Figure 5.10 see "Material and Methods" section. Changes in PSTAT3 concentration level to long-time $\mathrm{IL}-6$ stimulation is shown in Figure 5.11. Dots with the same colour belong to the same experimentally collected data set. The model simulation curve explains the experimental results more precisely for short-time rather than long-time $\mathrm{IL}-6$ stimulation (see Figure 5.10 and Figure 5.11).

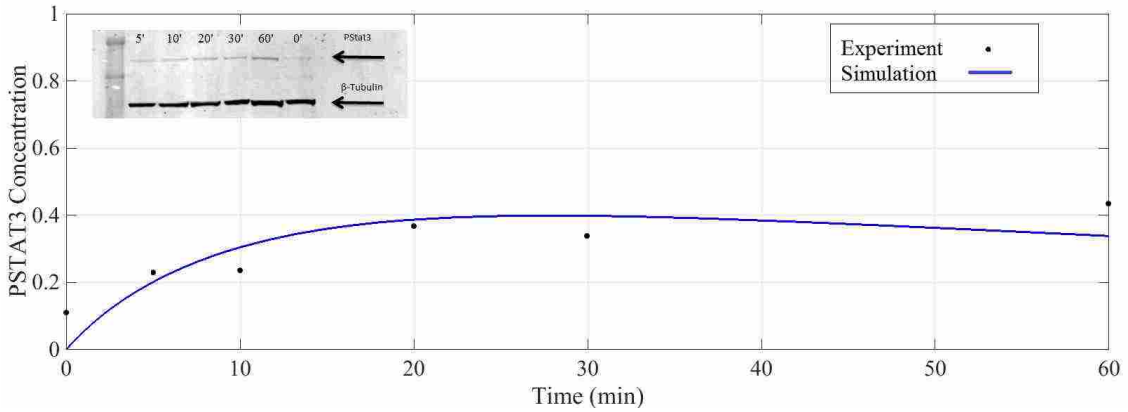

Figure 5.10: *Short-time simulation of total PSTAT3 dynamics. The blue curve shows the simulation results and the dots represent the relative experimental data for 0-1 h* $\mathrm{IL}-6$ *stimulation.*

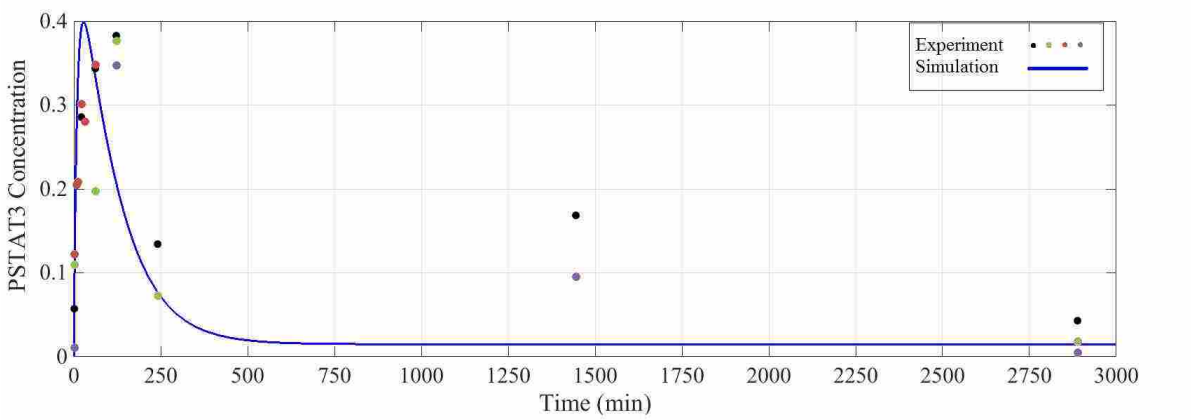

Figure 5.11: *Experimental and simulation results for long-time* $\mathrm{IL}-6$ *stimulation. Different colored dots show different experiments.*

Another interesting experiment which can be conducted via modelling is to investigate the response of the signalling system to pulsatile $\mathrm{IL}-6$ inputs. Figure 5.12 shows how PSTAT3 concentration follows different $\mathrm{IL}-6$ stimulations patterns. It is noticeable that the PSTAT3 steady-state changes reversely with the "on" time increase of the stimuli. This observable phenomenon can be explained from the topology of the $\mathrm{IL}-6$ signalling network (see Figure 5.3). 20 min almost equals the time for $\mathrm{IL}-6$ signalling to reach the activated nuclear PSTAT3 and hence, the transcription of socs3 and activation of the feedback. The degradation of PSTAT3 happens only in the nucleus and is linearly proportional to the nuclear PSTAT3 concentration (Mass Action kinetics). However, the production rate of PSTAT3 (the STAT3 phosphorylation rate) is a nonlinear function of the cytoplasmic PSTAT3 (Michaelis–Menten kinetics). Additionally, the "off" time is not long enough to return all the signalling components to zero, including cytoplasmic and nuclear PSTAT3. Therefore, total PSTAT3 accumulates in the cell and peaks when the cytoplasmic and nuclear PSTAT3 peaks around 60 min. Since the activated receptor complex is limited, the signalling becomes attenuated gradually and total PSTAT3 concentration decreases after an hour.

As the stimulation "on" time decreases, the signalling affects the down-stream components less. The accumulated level PSTAT3 in the nucleus reduces comparing to longer "on" time stimulations, while cytoplasmic PSTAT3 production follows the same pattern. Consequently, the transient (at each pulse) and steady-state levels of total PSTAT3 increase globally. Figure 5.12 also suggests that a pulsatile stimulation pattern may provide an alternative to the production of genetically modified cell lines, such as MEF $\mathrm{Gp130}^{F/F}$, in which the SOCS3 feedback loop is knocked out in order to over-express STAT3.

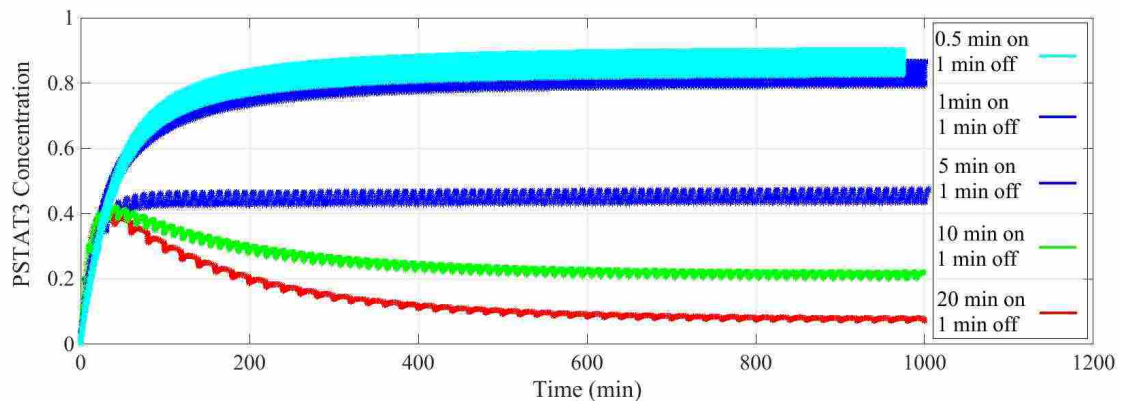

Figure 5.12: *PSTAT3 responses of* $\mathrm{IL}-6$ *signalling system to a pulsatile input. Different curves correspond to distinct pulsation patterns.*

By increasing the level of receptors concentration on the membrane, the $\mathrm{IL}-6$ signalling attenuation which occurs after 1 hour, can be avoided. Therefore, the steady-state level of PSTAT3 increases by increasing the total receptor concentration (see Figure 5.13). In order to vary the membrane receptor concentration in Figure 5.13, we changed the production rates Gp80 and Gp130 simultaneously. Variable 'm' in Figure 5.13 is proportional to the production rates of Gp80 and Gp130 at the membrane. Additionally, the effect of SOCS3 negative feedback loop was decreased to decrease the degradation rate of both receptors.

Continual high level of total PSTAT3 concentration represents the responses of cells in chronic inflammation. Our $\mathrm{IL}-6$ signalling model predicts that chronic inflammation and hence cancer occur when the level of total receptor concentration increases.

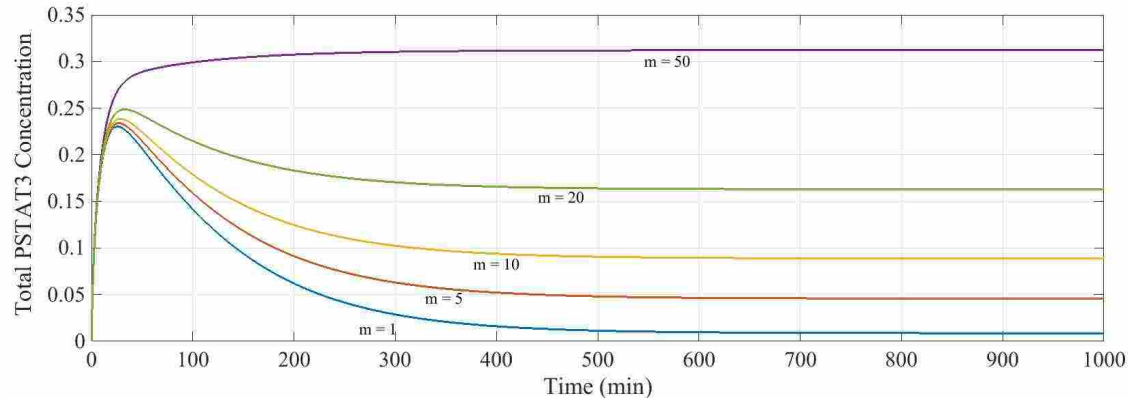

Figure 5.13: *PSTAT3 responses of* $\mathrm{IL}-6$ *signalling system to different levels of membrane receptors. "m" represents the level of receptor concentrations on the membrane.*

5.5 Discussion

Understanding the $IL-6$ signalling pathways and its components has attracted the interest of scientists for decades [186, 327]. Due to its roles in inflammation, $IL-6$ signalling influences the progression of tumors, such as: melanoma [214, 316], multiple myeloma [214, 228], prostate cancer [214, 407] and colon cancer [32, 359].

A detailed mathematical models of $IL-6$ signalling was proposed via Singh et al. [402]. Although their model is comprehensive, no comparison with experimental data was attempted by the authors. Subsequent models of $IL-6$ signalling have used more mathematical and statistical analyses on the basis of Singh's $IL-6$ model [70, 320], however, these more recent reports focus on MAPK signalling which adds an extra complexity to the system but ignores the major specific action of $IL-6$ signalling, i.e. the activation of the JAK/STAT system.

We have focused on JAK/STAT signal transduction. Our reduction method simplifies the complexity of the intracellular protein interactions and allows an extended time-scale for the simulations. This reduction method is used in biochemical engineering and non-linear dynamical systems analysis [115, 158, 422]. The final simplified model was reduced to 8 differential equations and was solved numerically. The initial values of the parameters and scaling were based on reported experimental data [464, 479].

Model predictions of changes in total STAT3, total PSTAT3 and SOCS3 concentrations compared favourably with the experimental results of Wormald et al. [479]. Small differences between the experiments and simulations may occur because of the lack of absolute quantitation from the Western blots of Wormald et al. [479]. We have also tested the model results with a set of experimental data from another cell line (MEFs) in order to demonstrate the robustness of our model to changes in the initial conditions. Our model validates and supports our parameter estimations, the model logistics and the reduction method [115]. Furthermore, using this model, predictions can be made for the pulsatile signal inputs and their influences on the ultimate steady-state of the system. Pulsatile responses to $IL-6$ stimulation are confirmable in future by designing a new experimental set up. The high level of $IL-6$ signalling in chronic inflammation and cancer was predicted by our model, which shows the robustness of this model against different perturbations. This work can be used as a foundation for an integrated model designed to include the $IL-6$-JAK-STAT3 signalling in more complex simulations of combined signalling pathways.

In conclusion, modelling of the $IL-6$ signalling network has helped us understand the importance of the negative feedback loop for the functionality and stability of the $IL-6$ signalling network. It is interesting to see how one signalling pathway can influence and regulate another signalling network. The importance of time-delays in such networks, caused by slow sets of reactions

or protein complex translocations is also evident in our simulations. We also predict how pulsatile stimulation of a signalling network can affect the strength and the duration of $\mathrm{IL}-6$ signalling.

5.6 Material and Methods

Three major types of data analysis have been used in this project:

- **Model design**

  In order to model the $\mathrm{IL}-6$ signalling pathways we have written ordinary differential equations for the concentration of each component using mass action or Michaelis–Menten kinetic equations [249]. The reduction method [115] was applied to the $\mathrm{IL}-6$ model using rapid equilibrium assumptions. Time-delays were considered in the equations for the PSTAT3-induced SMAD7 stimulation.

- **Computer modelling**

  The simulation of the mathematical model of $\mathrm{IL}-6$ signalling was performed via MATLAB. We used the curve fitting package from the MATLAB platform and trendline tool of Microsoft Excel in order to fit the model predictions to compare with the experimental data from Wormald et al. [479]. The $\mathrm{IL}-6$ signalling model figure (Figure 5.1) was first designed via CellDesigner [132] and later with Microsoft Power Point. The MATLAB codes are available on request.

- **Experimental data**

  The experimental data set and the kinetic rates were extracted by data analysis from Wormald et al. published in 2006 [479] in addition to a set of experimental data obtained in the following manner:

  Cell culture and cell lysis

  Mouse embryonic fibroblasts (MEFs) cells were isolated from day 13 to 15 embryos. Wild type MEF cells were cultured in DMEM containing 15% FCS. The cells were trypsinized and washed with DMED + 15% FCS before plating. Passage 3 cells with 1×10^6 MEFs/well were seeded in 60 mm plates for 0-1 hour, treatment with 1 ng/ml $\mathrm{IL}-6$ (Ref 1661.F33. WEHI). After washing with cold PBS for two times, cells were lysed in ice-cold 200 ul RIPA lysis buffer, containing 1M Tris/HCL, 0.5 M EDTA, 5M NaCl, 10 % Na Doc, 10 % TX-100, 10 % SDS, proteinase inhibitor 100 $\times$ and H_2O. The cell lysits were passed through 27 G needle for 5 times, then incubated in ice for 20-30 min. After incubation the samples were span at 13,000 rpm for 30 min at 4^oC. The supernatant was transferred to new tubes where 20 ul of samples were saved for BCA protein assay using sigma BCA assay

kit (B9643). 20 ul $5x$ sample buffer was added to 80 ul loading sample and the samples were heated at 95^oC for 10 min.

Western blotting

The protein concentrations were determined using the sigma BCA assay kit (B9643), Novex NuPAGE® 4-12%-Bis-Tris (life technologies NP0335 Box) gels were used for loading proper amount of sample lysate for each time point. PSTAT3 (XP^{TM} Rabbit mAb) antibodies were provided by Cell Signalling Technology and were used at a dilution 1:500 in 3% BSA-TBS-T. β-tubulin is used as loading control. Eventually, the gels were transformed onto nitrocellulose membrane via iBlot 2 gel transfer device (life technologies) and the membranes were scanned using Odyssey infrared scanner (LI-COR).

Protein Quantitation

The western blot images were quantitated using ImageJ 1.49p. The signals of each protein were normalised to the loading control protein where possible.

Chapter 6

$\mathrm{TGF}-\beta$ and $\mathrm{IL}-6$ Signalling Crosstalk: an integrated model

6.0 Summary of the information included in Chapter 6

Crosstalk studies are inseparable parts of Systems biology approach. Systems biology studies the crosstalk between the components of a system, emphasizing on how the ultimate systems's function is influenced by such interactions. Particularly in the case of intracellular signalling networks, in which individual signalling pathways share several components, it is crucial to study other interacting signalling pathways.

Last two chapters were dedicated to individual $\mathrm{TGF}-\beta$ and $\mathrm{IL}-6$ signalling and their self-regulation. In this chapter, we introduce an "integrated" model by which we study the regulation of $\mathrm{TGF}-\beta$ signalling via $\mathrm{IL}-6$ stimulation. The integrated model makes predictions for the formulation and the strength of the crosstalk between the $\mathrm{TGF}-\beta$ and $\mathrm{IL}-6$ signalling pathways.

6.1 Introduction

Cell signalling in complex biological systems regulates cellular functions. Each signalling pathway targets a specific range of genes and consequently controls a set of system's characteristics. However, signalling pathways do not function as isolated systems, rather many proteins often participate in two or more signalling pathways. The Systems biology approach can be used to study the intracellular signalling networks as an interconnected complex system, where the properties of the system are governed by several mutual interactions. Colorectal cancer, the third most common cancer in the world [362], occurs due to an accumulation of specific genetic alterations. Wnt, PGE2, EGF, $\mathrm{TGF}-\beta$, TNF-α, $\mathrm{IL}-6$ and IFNg are among the signalling pathways that interfere with the growth of

stomach or colon cancers [80, 362, 369, 412, 494, 498, 501]. All of these signalling pathways have been studied individually in the literature. In Chapters 4 and 5 we modelled and analyzed two of these signalling pathways ($\mathrm{TGF}-\beta$ and $\mathrm{IL}-6$ signalling). This chapter focuses on $\mathrm{TGF}-\beta$ and $\mathrm{IL}-6$ signalling crosstalk and the role of this crosstalk in gastrointestinal tumors.

$\mathrm{TGF}-\beta$ is a pleiotropic cytokine which regulates a broad range of cell's characteristics i.e. differentiation, proliferation, migration, life time and apoptosis [118, 296]. This cytokine plays a crucial role in tumorigenesis [104, 312, 350]. Acting on early-tumors, $\mathrm{TGF}-\beta$ functions as an anti-proliferative factor that causes tumor suppression [357, 434]. Notwithstanding, late-tumors become stimulated by $\mathrm{TGF}-\beta$ signalling [107, 357]. Mathematical modelling and computational analysis of $\mathrm{TGF}-\beta$ signalling help identify the conditions and components which cause its dual-behaviour. There are reports of $\mathrm{TGF}-\beta$ signalling crosstalk with many other pathways, such as MAPK, PI3K/Akt, Wnt, Hedeghog (Hh), Notch, ILs (including $\mathrm{IL}-6$), TNF-β, and IFN-γ [159]. Extensive crosstalk between individual signalling pathways and $\mathrm{TGF}-\beta$ is due to the potential ability of $\mathrm{TGF}-\beta$ signalling components (e.g. SMADs) to interact with other proteins outside their own direct signalling pathways [159]. Furthermore, $\mathrm{TGF}-\beta$ signal transduction has multiple transcriptional and non-transcriptional targets which are also influenced by other signalling pathways [159]. SMADs participate in the $\mathrm{TGF}-\beta$ signalling responsible for signal delivery from the ligand activation of the receptor to the nuclear activation events. $\mathrm{TGF}-\beta$ downstream signalling is also regulated via its inherent negative feedback originated from one of the SMAD family members, SMAD7 [155, 179, 261, 315, 400, 492].

$\mathrm{IL}-6$ signalling targets genes involved in inflammation and immune responses [175,190,337,421]. $\mathrm{IL}-6$ signals via the JAK-STAT and MAPK signalling pathways (see Chapter 5), which makes $\mathrm{IL}-6$ signalling potentially appropriate for the analysis of crosstalk with other cytokine signalling. STAT3 is the target intracellular protein which connects $\mathrm{TGF}-\beta$ and $\mathrm{IL}-6$ signallings [206]. Similar to $\mathrm{TGF}-\beta$ signalling, the $\mathrm{IL}-6$ system has an intrinsic negative regulatory feedback loop, SOCS3 [15, 176]. Signalling through JAK/STAT pathway and hence STAT3 level is controlled by the level of the SOCS3 protein [206].

Key parameters and mechanism of the $\mathrm{TGF}-\beta$ and $\mathrm{IL}-6$ signallings crosstalk can change dramatically depending on the cell-lines, spatial location of the intracellular proteins and the developmental stage of the cells [4, 159, 402, 511]. Experimental evidence shows that $\mathrm{TGF}-\beta$ signalling can affect $\mathrm{IL}-6$ signal transduction through the MAPK pathway in an autocrine loop [10,204,275,437]. Additionally, $\mathrm{TGF}-\beta$ expression can increase in T helper cells via activation of STAT3 [223,238]. A $\mathrm{TGF}-\beta$ and $\mathrm{IL}-6$ signalling crosstalk via a STAT3-SMAD7 pathway interaction was first proposed via Jenkins et al. [206]. Jenkins et al. have analyzed Gp130/JAK/STAT3 signalling and the SOCS3 negative feedback in mouse gastric epithelial cells in order to determine the role of $\mathrm{IL}-6$ induced

SMAD7-negative feedback on $\mathrm{TGF}-\beta$ signalling possible interactions [206]. Using the inherent feedback loops controlled by SOCS3, SMAD7 and miR-433 we have connected our previously proposed mathematical models of $\mathrm{TGF}-\beta$ and $\mathrm{IL}-6$ signalling to study the gastric tumour model described by Jekins et al. [207].

6.2 Model Development

According to the Jenkins et al. proposed signal exchange between the $\mathrm{TGF}-\beta$ and $\mathrm{IL}-6$ signalling pathways [206], we have developed an integrated mathematical model that connects these two signal transduction systems. Our integrated model is based on our previous individual models for $\mathrm{TGF}-\beta$ and $\mathrm{IL}-6$. Figure 6.1 illustrates how the two systems combine. A positive inherent feedback on $\mathrm{TGF}-\beta$ signalling [269] was added to the recommended model suggested by Jenkins et al. The red arrow accentuates the main interaction between the two pathways.

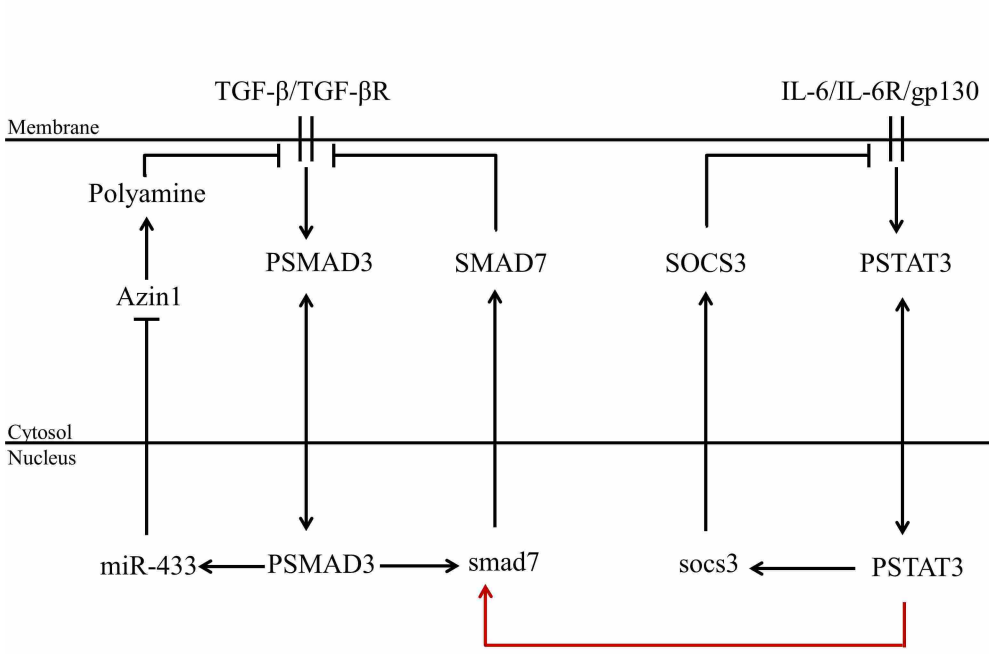

Figure 6.1: *The schematic diagram of* $\mathrm{TGF}-\beta$ *and* $\mathrm{IL}-6$ *crosstalk. the redarrow is the focus of the current thesis.*

The parameters of each signalling model were re-evaluated and the initial values of variables in $\mathrm{TGF}-\beta$ and $\mathrm{IL}-6$ systems were adjusted according to experimental data in the literature [206]. The scaled parameters are mainly the kinetic rates and binding constants of the $\mathrm{IL}-6$ signalling part of the inte-

grated model. In scaling these parameters we have considered the smoothness of the curves, non-negative values for the variables, stability and robustness of the integrated model. We have compared two different kinetics models for the PSTAT3/SMAD7 interaction system: mass-action and Michaelis-Menten kinetics. PSTAT3 is considered to act as a transcription factor in the pathway and activate SMAD7 transcription (Michaelis-Menten enzymic kinetics).

The equations representing the integrated model are listed below. The negative feedback terms of the $[\mathrm{R}]$, $[\mathrm{RC}]$ and $[\mathrm{PC}]$ differential equations have been changed such that the phosphorylated PSTAT3 dimer in the nucleus considered as the initiator.

$$
\begin{aligned}
\frac{\mathrm{d}[Gp80]}{\mathrm{d}t} &= (f_1 A_{22} - f_2 A_{12})/(A_{11}A_{22} - A_{21}A_{12}) \\
\frac{\mathrm{d}[Gp130]}{\mathrm{d}t} &= (f_2 A_{11} - f_1 A_{21})/(A_{11}A_{22} - A_{21}A_{12}) \\
\frac{\mathrm{d}[STAT3]_C}{\mathrm{d}t} &= v_{ST} - k_{\emptyset ST}[STAT3]_C - 2k_{phc}[CJ^*]\frac{[STAT3]_C^2}{[STAT3]_C^2 + K^2} - \\
&\quad 2k_{dph}[PSTAT3_2]_C + k^e Vnc[STAT3]_N - k^i[STAT3]_C \\
\frac{\mathrm{d}[PSTAT3_2]_C}{\mathrm{d}t} &= k_{phc}[CJ^*]\frac{[STAT3]_C^2}{[STAT3]_C^2 + K^2} - k_{dph}[PSTAT3_2]_C - \\
&\quad k^i[PSTAT3_2]_C + k^e Vnc[PSTAT3_2]_N) \\
\frac{\mathrm{d}[SOCS3]_C}{\mathrm{d}t} &= k_{trnsl}k^e Vnc[socs3]_N - k_{\emptyset Sc}[SOCS3]_C \\
\frac{\mathrm{d}[STAT3]_N}{\mathrm{d}t} &= 2k_{dph}[PSTAT3_2]_N - 2k_{phn}[STAT3]_N^2 - k^e[STAT3]_N \\
&\quad + k^i Vcn[STAT3]_C \\
\frac{\mathrm{d}[PSTAT3_2]_N}{\mathrm{d}t} &= k^i Vcn[PSTAT3_2]_C - k_{dph}[PSTAT3_2]_N + k_{phn}[STAT3]_N^2 - \\
&\quad k_{\emptyset PSn}[PSTAT3_2]_N - k^e[PSTAT3_2]_N \\
\frac{\mathrm{d}[socs3]_N}{\mathrm{d}t} &= -k_{\emptyset mRNA}[socs3]_N - k_{trnsl}k^e[socs3]_N \\
&\quad + k_{trac}\frac{[PSTAT3_2]_N}{[PSTAT3_2]_N + K_{Sc}} \\
\frac{\mathrm{d}\,[\mathrm{R}\,]}{\mathrm{d}t} &= v_1 - k_1\,[\mathrm{R}\,] - 2k^+_{\mathrm{RC}}\,[\mathrm{R}\,]^{\,2} + 2k^-_{\mathrm{RC}}\,[\mathrm{RC}\,] - k_1^{\mathrm{f}+}\,[P]\,\frac{[\mathrm{R}\,]}{[\mathrm{R}\,] + K} - \\
&\quad k_1^{\mathrm{f}-}\,k^-_{PS}\,[N]^2\,\frac{[PSTAT3_2]^2_{N(t-\tau_1)}\,[\mathrm{R}\,]}{([PSTAT3_2]^2_{N(t-\tau_1)} + K^2_{PS})([\mathrm{R}\,] + K\,)} \\
\frac{\mathrm{d}\,[\mathrm{RC}\,]}{\mathrm{d}t} &= k^+_{\mathrm{RC}}\,[\mathrm{R}\,]^{\,2} - k^-_{\mathrm{RC}}\,[\mathrm{RC}\,] - k_{\mathrm{RC}}\,[\mathrm{RC}\,] \\
&\quad -k^+_{\mathrm{PC}}\,[\mathrm{TGF_2}\,]\,[\mathrm{RC}\,] + k^-_{\mathrm{PC}}\,[\mathrm{PC}\,] \\
&\quad -k^{\mathrm{f}-}_{\mathrm{RC}}\,k^-_{PS}\,[N]^2\,\frac{[PSTAT3_2]^2_{N(t-\tau_1)}\,[\mathrm{RC}\,]}{([PSTAT3_2]^2_{N(t-\tau_1)} + K^2_{PS})([\mathrm{RC}\,] + K\,)} \\
\frac{\mathrm{d}\,[\mathrm{PC}\,]}{\mathrm{d}t} &= k^+_{\mathrm{PC}}\,[\mathrm{TGF_2}\,]\,[\mathrm{RC}\,] - k^-_{\mathrm{PC}}\,[\mathrm{PC}\,] - k_{\mathrm{PC}}\,[\mathrm{PC}\,] - \\
&\quad k^{\mathrm{f}-}_{\mathrm{PC}}\,k^-_{PS}\,[N]^2\,\frac{[PSTAT3_2]^2_{N(t-\tau_1)}\,[\mathrm{PC}\,]}{([PSTAT3_2]^2_{N(t-\tau_1)} + K^2_{PS})([\mathrm{PC}\,] + K\,)} \\
\frac{\mathrm{d}\,[\mathrm{S}\,]}{\mathrm{d}t} &= v_{\mathrm{S}} - k_{\mathrm{S}}\,[\mathrm{S}\,] - k^+_{\mathrm{S}}\,[\mathrm{PC}\,]\,\frac{[\mathrm{S}\,]}{[\mathrm{S}\,] + K_{\mathrm{S}}} + k^-_{\mathrm{S}}\,[\hat{\mathrm{S}}\,] \\
\frac{\mathrm{d}[\hat{\mathrm{S}}\,]}{\mathrm{d}t} &= k^+_{\mathrm{S}}\,[\mathrm{PC}\,]\,\frac{[\mathrm{S}\,]}{[\mathrm{S}\,] + K_{\mathrm{S}}} - k^-_{\mathrm{S}}\,[\hat{\mathrm{S}}\,] - k^+_n\,[\hat{\mathrm{S}}\,] + k^-_n\,[\mathrm{S_n}\,] - k_{\hat{\mathrm{S}}}\,[\hat{\mathrm{S}}\,] \\
\frac{\mathrm{d}\,[\mathrm{S_n}\,]}{\mathrm{d}t} &= k^+_n\,[\hat{\mathrm{S}}\,] - k^-_n\,[\mathrm{S_n}\,] - k_{\mathrm{S_n}}\,[\mathrm{S_n}\,]
\end{aligned}
\tag{6.1}
$$

,where we have the followings are defined:

$$[\mathrm{S}_3\,] = [\mathrm{S}_\mathrm{n}\,]^{\,3}/K_3 \tag{6.2}$$

$$[N] = [\mathrm{S}_3\,]_{\,(t-\tau_2)} \tag{6.3}$$

$$[P] = {K_\mathrm{I}}^{\,2}/({K_\mathrm{I}}^{\,2} + [\mathrm{S}_3\,]^{\,2}_{(t-\tau_2)}) \tag{6.4}$$

$$\begin{aligned}
A_{11} &= 1 + \frac{[L]}{K_{80}} + \frac{[L][J][Gp130]}{K_{80}K_{130}K_1} + \frac{4[L]^2[Gp80][J]^2[Gp130]^2}{K_{80}^2K_{130}^2K_1^2K_2}(1+1/K_2^*) \\
A_{21} &= \frac{[L][J][Gp130]}{K_{80}K_{130}K_1} + \frac{4[L]^2[Gp80][J]^2[Gp130]^2}{K_{80}^2K_{130}^2K_1^2K_2}(1+1/K_2^*) \\
A_{12} &= \frac{[L][Gp80][J]}{K_{80}K_{130}K_1} + \frac{4[L]^2[Gp80]^2[J]^2[Gp130]}{K_{80}^2K_{130}^2K_1^2K_2}(1+1/K_2^*) \\
A_{22} &= 1 + \frac{[J]}{K_{130}} + \frac{[L][Gp80][J]}{K_{80}K_{130}K_1} + \frac{4[L]^2[Gp80]^2[J]^2[Gp130]}{K_{80}^2K_{130}^2K_1^2K_2}(1+1/K_2^*)
\end{aligned} \tag{6.5}$$

$$\begin{aligned}
f_1 &= v_{80} - k_{\emptyset 80}[Gp80] - 2R \\
f_2 &= v_{130} - k_{\emptyset 130}[Gp130] - 2R
\end{aligned} \tag{6.6}$$

$$R = k_{aCSc}[SOCS3]\frac{[CJ^*]}{[CJ^*]+K} + k_{dJ}[CJ^*] + k_{d2}[C_2]. \tag{6.7}$$

6.3 Results from $\mathrm{IL}-6$:$\mathrm{TGF}-\beta$ Crosstalk Model and Discussion

Different stimulation patterns are used in this section to predict the responses of the integrated model to various perturbations. For the first experiment, the integrated system is stimulated simultaneously with $\mathrm{IL}-6$ and $\mathrm{TGF}-\beta$, i.e. "double stimulation". The levels of PSTAT3 and PSMAD2 are studied as the outputs of the integrated system when it is double stimulated. Figure 6.2 compares the PSMAD2 time course in the absence of the $\mathrm{IL}-6$ stimulation with double stimulation. Due to the induced expression of SMAD7 (the negative feedback loop for the $\mathrm{TGF}-\beta$ signalling) via PSTAT3 nuclear accumulation in double stimulation experiment, the PSMAD2 concentration curve decreases to a lower level after its first peak. The lower level of PSMAD2 leads to lower nuclear SMAD7 production in $\mathrm{TGF}-\beta$ signal transduction, so the PSMAD2 level rises again, but peaks at a lower level than the first $\mathrm{TGF}-\beta$ induced peak (see Figure 6.2). The dampening of the PSMAD2 peaks is because of the loss of activated $\mathrm{IL}-6$ receptors at the membrane, which leads to the reduction of the PSTAT3 signal an hour after $\mathrm{IL}-6$ stimulation. The positive feedback loop for $\mathrm{TGF}-\beta$ signalling is weakened as the $\mathrm{TGF}-\beta$ signalling becomes down-regulated by SMAD7 activation. As a result, each peak of PSMAD2 is weaker than the previous peak. The steady-state level of PSMAD2 is the same in both stimulation patterns.

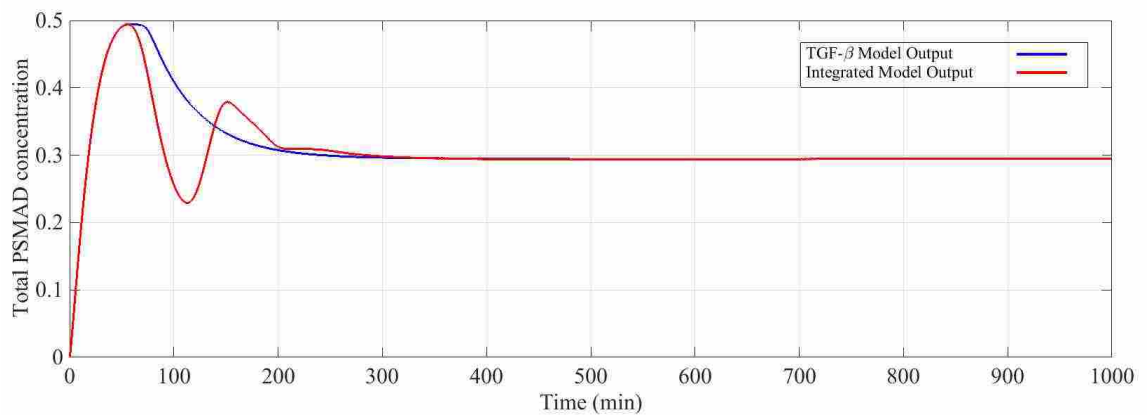

Figure 6.2: *A comparison between the PSMAD2 response of the* $\mathrm{TGF}-\beta$ *signalling system and the integrated* $\mathrm{IL}-6$:$\mathrm{TGF}-\beta$ *signalling system. The integrated model output follows the* $\mathrm{TGF}-\beta$ *model output for the first 60 minutes, however it diverges afterwards. The steady-state PSMAD2 levels of both models are identical.*

Our second stimulation scenario includes a two-hour "pre-stimulation" of the integrated system with $\mathrm{IL}-6$ followed by the $\mathrm{TGF}-\beta$ stimulation which is started one hour after the $\mathrm{IL}-6$ stimulation. Again the total PSTAT3 and PSMAD2 levels are considered to be the outputs of the $\mathrm{IL}-6$:$\mathrm{TGF}-\beta$ crosstalk system. Figure 6.3 compares the response of the system to pre-stimulation and the double stimulation patterns. The second peak of PSMAD2 response is stronger in pre-stimulation compared to the double stimulation. When the $\mathrm{IL}-6$ signalling is terminated after 2 hours,there is a rapid decay in total PSTAT3 concentration and hence SMAD7 levels. Consequently, SMAD7 is only produced through $\mathrm{TGF}-\beta$ signalling after 2 hours and PSMAD2 levels rise to higher levels at the second peak. Again, the steady-state level of PSMAD2 for both stimulation patterns is the same.

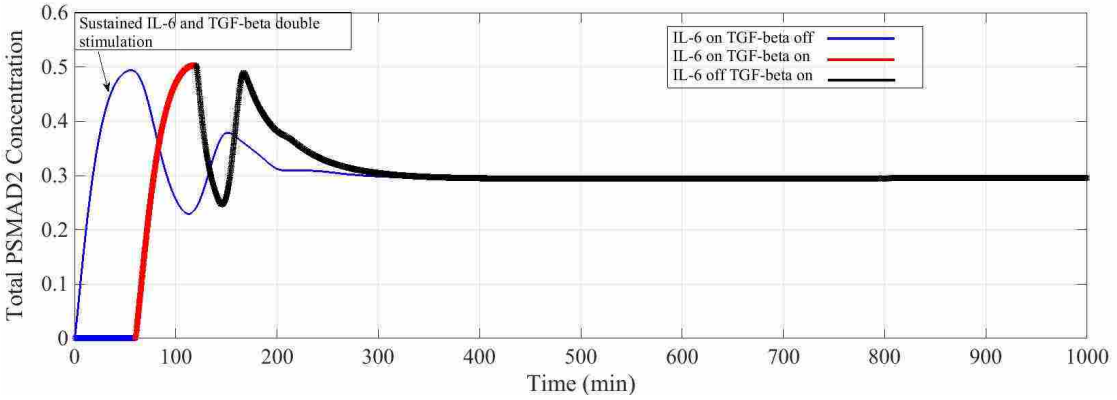

Figure 6.3: *The integrated model output for the double stimulation and pre-stimulation scenarios of* $\mathrm{IL}-6$:$\mathrm{TGF}-\beta$ *signalling.*

We have also examined the response of the integrated model to a pulsatile

stimulation of IL − 6 (the TGF−β stimulus is constant, see Figure 6.4). The same pulsation patters in Figure 5.12 in chapter 5 are used in this experiment. As the "on time" of the pulses increases, the PSMAD2 response trends closer to the output of the sustained response model (see Figure 6.3 for comparison). Studying Figure 5.12, it is clear that the PSTAT3 response is closer to sustained IL − 6 stimulation with pulses of longer "on" duration.

The PSMAD2 dynamics in response to short IL−6 pulsation is comparable to the system's output in the absence of IL − 6 signalling (see Figure 6.4 and Figure 6.2). Because of the steady PSTAT3 levels at short IL − 6 pulses (see Figure 5.12), the SMAD7 level stays high and the PSMAD2 level does not peak for a second or third time. Furthermore, the level of PSMAD2 first peak is lower in response to short IL − 6 pulses because of the higher level of the PSTAT3 peak (see Figure 5.12).

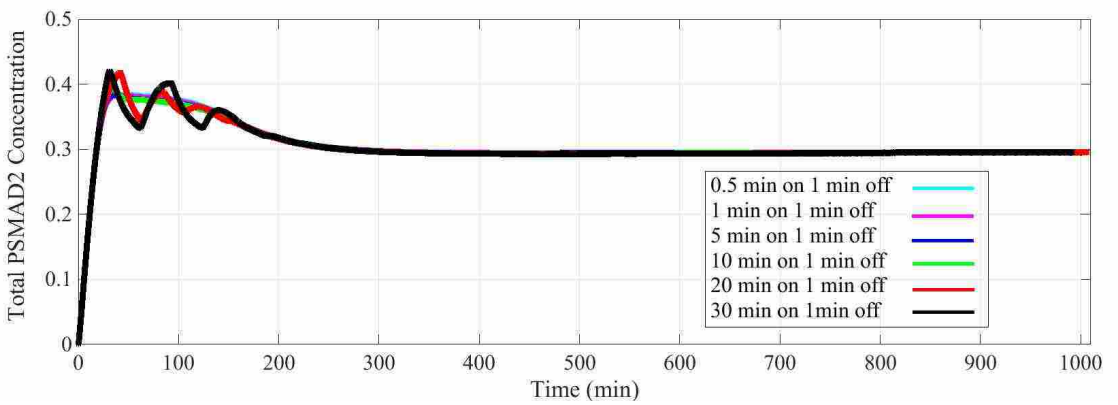

Figure 6.4: *PSMAD2 responses of the integrated model to different pulsatile inputs of* IL − 6. *The* TGF−β *level is kept constant for the entire duration of the simulation.*

In the next experiment, we have kept IL − 6 signalling constant and input TGF−β pulses to the integrated system. The TGF−β pulse patterns are identical to the previous experiment (IL − 6 pulsatile stimulation). Figure 6.6 demonstrates the responses of the integrated system to the TGF−β pulsatile stimulation. A comparison between Figure 6.6 and Figure 6.5 reveals that the peaks in the PSMAD2 transient response of the integrated model to IL − 6 and TGF−β stimulation appear because of the PSTAT3/SMAD7 interaction between the functions of the two proteins rather than changes to the positive feedback loop within the TGF−β pathway. Clearly, TGF−β signalling plays the main role in determining the steady-state level of PSMAD2 in the integrated model, since the equilibrium PSMAD2 levels are equivalent in both Figure 6.6 and 6.5. As expected and in a similar fashion to the previous pulsatile stimulation experiments using the integrated model, as the "on" time of the pulses increases, the model response approaches the output level of PSMAD2 for the sustained stimulation condition.

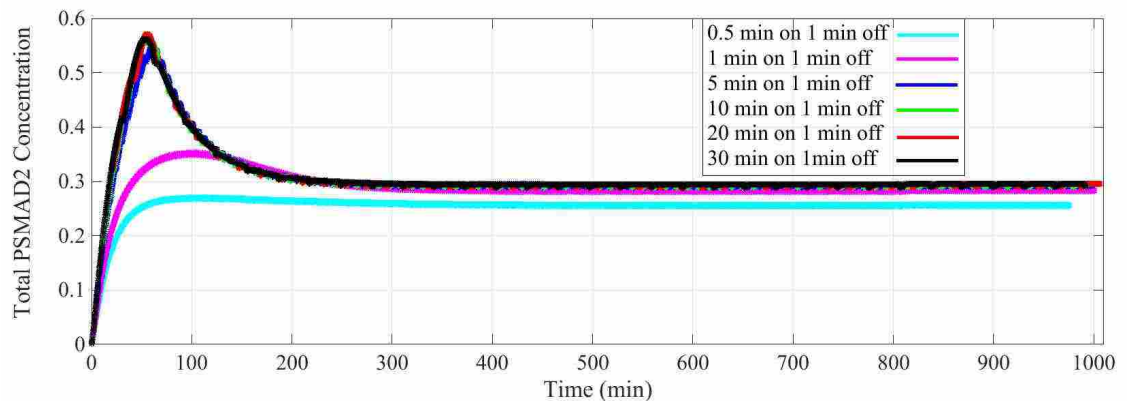

Figure 6.5: *The simplified* $\mathrm{TGF}-\beta$ *model response (proposed in Chapter 4) to pulsatile* $\mathrm{TGF}-\beta$ *input.*

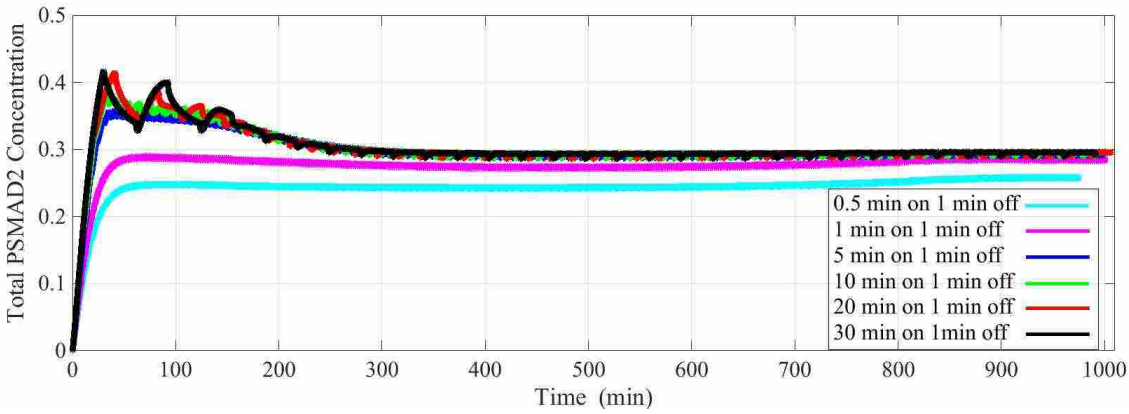

Figure 6.6: *The integrated model response to pulsatile* $\mathrm{TGF}-\beta$ *stimulation.*

Figure 6.7 shows the SMAD7 dynamics in the double stimulation of the integrated system with both $\mathrm{IL}-6$ and $\mathrm{TGF}-\beta$. Because of the incorporation of time-delay in PSTAT3/SMAD7 and PSMAD2/SMAD7 reactions, the SMAD7 level does not start increasing instantly, i.e. there is a 10-min delay. SMAD7 concentration decreases after 60-70 min due to the lost of activated receptors in both signalling pathways. However, the SMAD7 level rises for the second time. As mentioned above, the second peak is caused mainly by the non-zero but low level of PSTAT3 produced in response to the $\mathrm{IL}-6$ stimulation. Figure 6.7 compares how the different kinetics for PSTAT3/SMAD7 reactions affects the total SMAD7 dynamics.

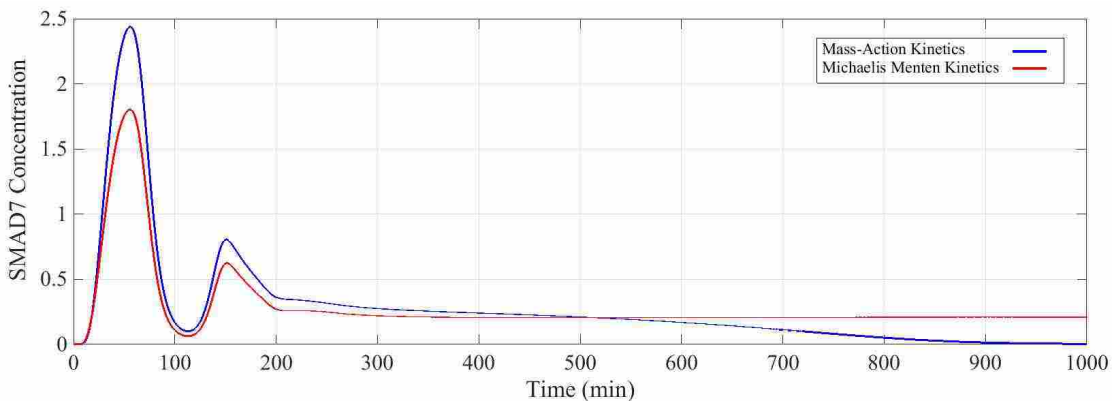

Figure 6.7: *SMAD7 dynamics when the integrated model is stimulated with constant levels of* IL − 6 *and* TGF−β.

SMAD7 dynamics is studied in a pre-stimulation experiment (see Figure 6.8). Comparing Figure 6.8 with Figure 6.7, the second peak of SMAD7 vanishes as the result of pre-stimulation. The existence of the second SMAD7 peak in the double stimulation experiment was due to the non-zero level of PSTAT3. When the system is pre-stimulated, the PSTAT3 level reduces to zero within 120 minutes (see Figure 6.8).

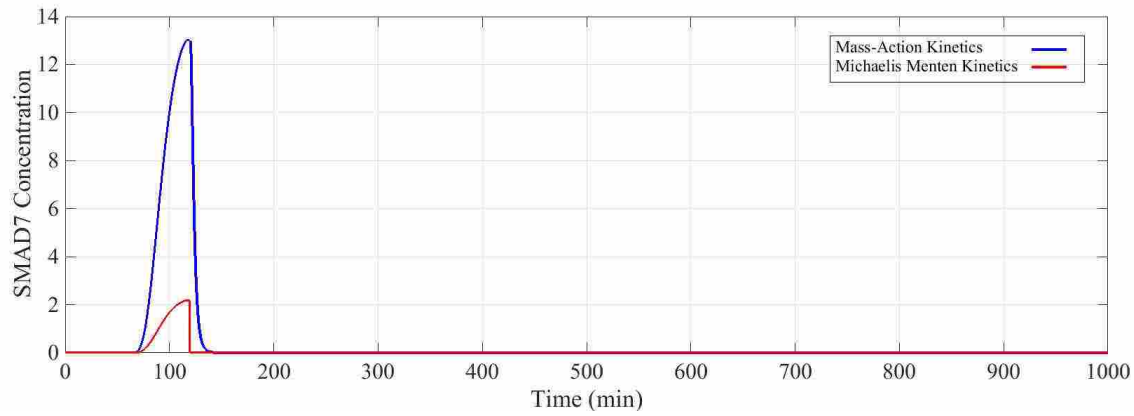

Figure 6.8: *Two models of the SMAD7 dynamics when the integrated model is pre-stimulated with* IL − 6 *for 2 hours and with* TGF−β *an hour after* IL − 6 *stimulation.*

It is important to note that the SMAD7 level peaks around 100 min in the mass-action model of PSTAT3/SMAD7 kinetics, compared to the Michaelis-Menten kinetics. Whereas, the curve corresponding to Michaelis-Menten kinetics experiences a sudden decrease at 120 min.

In order to measure how sensitive the integrated model is to the PSTAT3/-SMAD7 functional interaction, we have plotted the PSMAD2 response of the integrated model to pre-stimulation, while varying the strength of the activation of SMAD7 via PSTAT3 (see Figure 6.9). The "coefficient" in Figure 6.9 is used as a representative of the strength of the PSTAT3/SMAD7 interaction. Greater coef-

ficient leads to stronger stimulation of SMAD7 via PSTAT3. As shown in Figure 6.9, the reduction of the PSMAD2 output after its first peak is extremely sensitive to PSTAT3-dependent stimulation of SMAD7. The steady-state of the model remains unchanged via the PTAT3/SMAD7 reactions, which confirms our previous hypothesis that the TGF−β signalling determines the ultimate steady-state level of SMAD7 in the integrated model.

The results in Figure 6.9 support the initial hypothesis of this research, i.e. the activated form of PSTAT3 induces the down-regulation of TGF−β signalling and suppresses the PSMAD2 activation through over-expression of SMAD7, the PSMAD2 level is suppressed significantly after 150 min (see Figure 6.9). After the first peak, the effect of IL−6 signalling is eliminated and the PSMAD2 curves loose their sensitivity to PSTA3 and IL − 6 signalling.

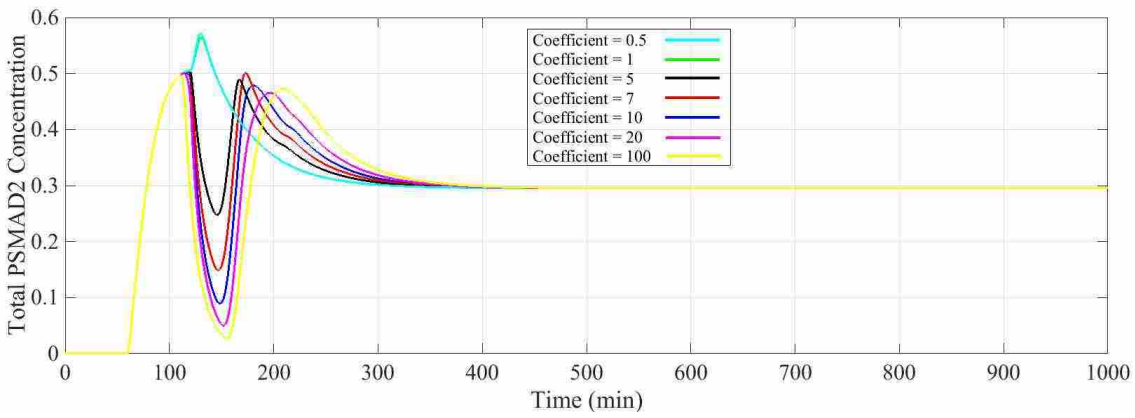

Figure 6.9: *The variation in the integrated model output as the PSTAT3/SMAD7 interaction is being reinforced gradually. Different coefficients represent different strength of the PSTAT3-induced stimulation of SMAD7.*

In order to test experimentally our integrated model we have developed and designed an experimental protocol. In this protocol, wild type MEFs were stimulated with IL − 6 for 1 hour before their double-stimulation with TGF−β and IL − 6. The one hour pre-stimulation with IL − 6 acts as the time-delay used in the IL − 6:TGF−β signalling connection. The 0 time point represents the initial time of the double-stimulation with TGF−β and IL−6. According to Figure 6.3, the total PSMAD2 concentration undergoes a double-peak fluctuation in the first 300 min, before reaching the steady-state. We have measured the level of total PSMAD2 for 0 to 4 hour after the double-stimulation. This experiment has been designed to test the double-peak appearance in the stimulation of TGF−β and IL − 6.

Figure 6.10 shows how the predictions of the integrated model (the blue curve) are in accordance with the experimental data. Each replicates of the experiment is illustrated with a specific colour and marker shape. The points specified by a "cross" are the average of the 3 experimental sets extracted for each time point.

Figure 6.11 is the representative blot of the data shown in the Figure 6.10. It is clear that PSMAD2 level rises for the second time after its minimum at 150 min. The data points in Figure 6.10 are normalised to the loading control, e.g. actin.

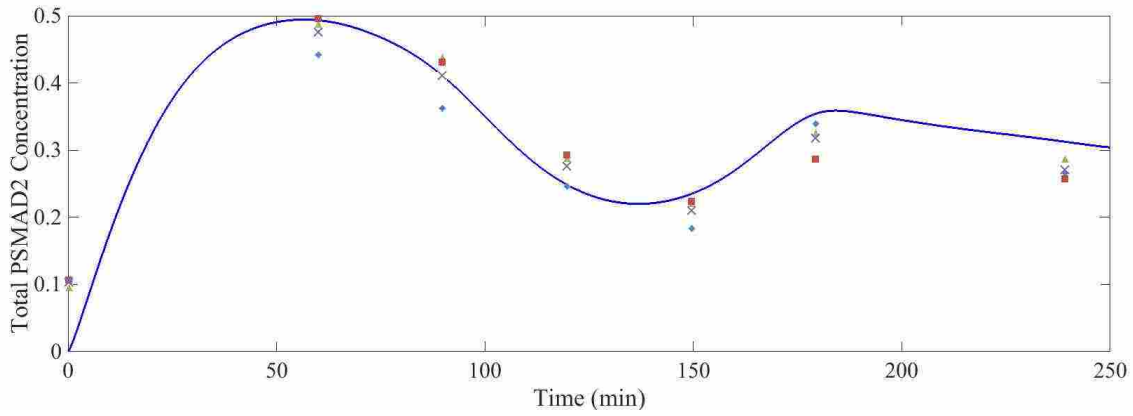

Figure 6.10: *The experimental validation of the integrated model. The blue curve is the model prediction of the double-stimulation of* TGF−β *and* IL − 6*. The colored dots represent the experimental data from wild type MEFs. Each set of experimental data is specified with a color. The "cross"es represent the average of the 3 experimental replicates.*

It is important to note that I needed to revise the time-delay parameter considered in the feedback terms of TGF−β-part of the integrated model. A proportion of the SMAD7 is induced by IL−6 signalling which also has a time-delay of 20 min and had to be added to the time-delay of the SMAD7-induced feedback terms.

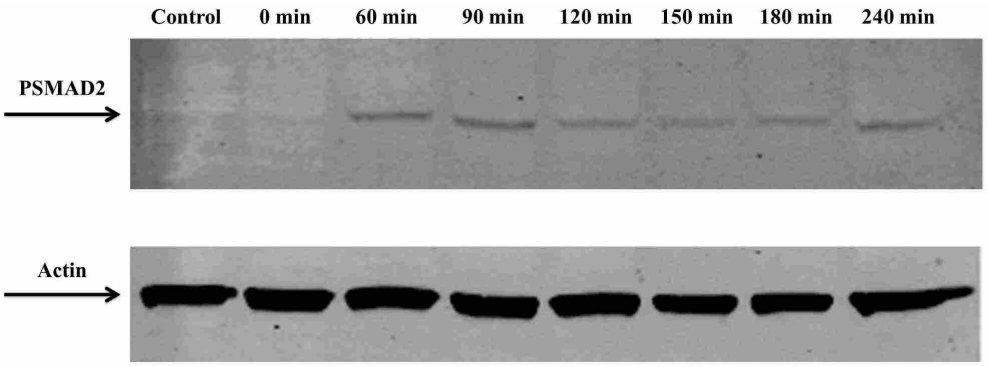

Figure 6.11: *The representative blots of Figure 6.10. The top bands show the total PSMAD2 concentration level of the double-stimulation experiment. The bottom bands represent the loading control to which the PSMAD2 levels are normalised.*

6.4 Material and Methods

Three major types of data analysis have been used in this project:

- **Model design**

  In order to combine the $\mathrm{TGF}-\beta$ and $\mathrm{IL}-6$ signalling pathways we have written ordinary differential equations for the concentration of each component using mass action or Michaelis–Menten kinetic equations [249]. Two different time-delays were considered in the equations for feedback loops in order to compensate for the transcription and translation processes and the connecting reaction of the two pathways.

- **Computer modelling**

  The simulation of the mathematical model of the integrated $\mathrm{IL}-6$:$\mathrm{TGF}-\beta$ signalling was performed via MATLAB. The equations are represented by equations 6.1. The MATLAB codes are available on request. The experimental data points are produced using Microsoft Excel 2010 [352].

- **Experimental data**

  The experimental data set and the kinetic rates were extracted by the applicant in Walter and Eliza Hall Institute of Medical research, Burgess Lab:

  Cell culture and cell lysis

  Mouse embryonic fibroblasts (MEFs) cells were isolated from day 13 to 15 embryos. Wild type MEF cells were cultured in DMEM containing 15% FCS. The cells were trypsinized and washed with DMED + 15% FCS before plating. Passage 3 cells with 1×10^6 MEFs/well were seeded in 60 mm plates for 0-1 hour, treatment with 1 ng/ml $\mathrm{IL}-6$ (Ref 1661.F33. WEHI). After washing with cold PBS for two times, cells were lysed in ice-cold 200 ul RIPA lysis buffer, containing 1M Tris/HCL, 0.5 M EDTA, 5M NaCl, 10 % Na Doc, 10 % TX-100, 10 % SDS, proteinase inhibitor 100 $\times$ and H_2O. The cell lysits were passed through 27 G needle for 5 times, then incubated in ice for 20-30 min. After incubation the samples were span at 13,000 rpm for 30 min at 4^oC. The supernatant was transferred to new tubes where 20 ul of samples were saved for BCA protein assay using sigma BCA assay kit (B9643). 20 ul $5x$ sample buffer was added to 80 ul loading sample and the samples were heated at 95^oC for 10 min.

  Western blotting

  The protein concentrations were determined using the sigma BCA assay kit (B9643), Novex NuPAGE® 4-12%-Bis-Tris (life technologies NP0335 Box) gels were used for loading proper amount of sample lysate for each time point. PSMAD2 antibody was provided by was used at a dilution 1:500 in 3% BSA-TBS-T. PSMAD2 antibody (rabbit polyclonal anti-phospho-Smad2 antibody (1:1000 for Western blot)) was a gift from Prof. Peter ten

Dijke (Leiden University Medical Center, Netherlands). β-tubulin is used as loading control. Eventually, the gels were transformed onto nitrocellulose membrane via iBlot 2 gel transfer device (life technologies) and the membranes were scanned using Odyssey infrared scanner (LI-COR).

Protein Quantitation

The western blot images were quantitated using ImageJ 1.49p. The signals of each protein were normalised to the loading control protein where possible.

6.5 Summary and Conclusions

The complexity of cancer and the growing rate of cancer diagnosis make this disease one of the greatest challenges for the health sciences worldwide. Strong correlations between cancer and other diseases of cell regulatory systems, such as chronic inflammation, increase the complexity in developing targeted treatments. Systems biology provides us a holistic approach to study biological systems and their components function-wise. Mathematical modelling, as one of methods defined in Systems biology, allows predictions for biological systems.

Two specific cytokine signalling pathways were studied individually and together, in this project: $\mathrm{TGF}-\beta$ and $\mathrm{IL}-6$ signalling. Separate mathematical models were developed for $\mathrm{TGF}-\beta$ and $\mathrm{IL}-6$ signalling and each system was parameterized and validated experimentally. Chapter 4 describes the model development, model analysis, model validation and model predictions for $\mathrm{TGF}-\beta$ signal transduction. The importance of feedback loops and time-delays in signal regulation are discussed in chapter 4. The contribution of a novel positive feedback loop in $\mathrm{TGF}-\beta$ signalling system and the effects of the feedback coupling in this system are studied in Chapter 4. A systematic reduction method was introduced to simplify the number of components and variables of the $\mathrm{TGF}-\beta$ signalling system without influencing the steady-state and transient response of the system. Eventually, the $\mathrm{TGF}-\beta$ model was validated with a combination of experimental data extracted from the literature and the data produced by the applicant. Developing a rigorous and precise mathematical model for $\mathrm{TGF}-\beta$ signalling equipped us with the predictions for the response of the cells in cancerous conditions (see Chapter 4).

Similar steps were repeated to develop a mathematical model for $\mathrm{IL}-6$ signalling based on Systems biology principles. In Chapter 5 our methodology for designing, developing and simplifying $\mathrm{IL}-6$/Gp130/JAK/STAT3 signalling is presented along with the experimental validation of the model. For the first time, the time-delay is incorporated in the equations of the $\mathrm{IL}-6$ system. Two experimental data sets were used to verify our proposed mathematical model of $\mathrm{IL}-6$ signalling. Chapter 5 also provides model predictions for different stimulation patterns and perturbations. These predictions introduce the idea of the crosstalk between the $\mathrm{IL}-6$ and $\mathrm{TGF}-\beta$ signalling pathway via the negative feedback loop of $\mathrm{TGF}-\beta$ signalling network, which is studied in Chapter 6. In another novel prediction of Chapter5, it is proposed that pulsatile input of $\mathrm{IL}-6$ to the system can regulate the steady-state level of the output of the system. This method can be used to amplify the $\mathrm{IL}-6$ signalling to eliminate signalling the negative feedback effects through SOCS3.

In order to examine our initial hypothesis concerning the suppression of $\mathrm{TGF}-\beta$ signalling by $\mathrm{IL}-6$ over-stimulation, we combined our proposed models of $\mathrm{TGF}-\beta$ and $\mathrm{IL}-6$ signalling and designed our integrated $\mathrm{IL}-6$:$\mathrm{TGF}-\beta$ model, in Chapter 6. The previous models were re-evaluated and re-parameterized

to capture all the properties of both signalling networks. For instance, the time-delay incorporated in the feedback terms of the $\mathrm{TGF}-\beta$ signalling equations has been modified in the integrated model. The integrated model was tested against different stimulation patterns and the responses of the models were interpreted according to the network connections. The sensitivity and robustness of the integrated model against the strength of the crosstalk were studied. The simulation results from the integrated model are compatible with our assumptions and interpretation of the down-regulation of $\mathrm{TGF}-\beta$ signalling due to the hyper-activation of $\mathrm{IL}-6$ JAK/STAT signalling pathway. In the final part of this thesis, the integrated $\mathrm{IL}-6$:$\mathrm{TGF}-\beta$ signalling model is examined against experimental data from the double-stimulation of wild type MEFs. These results strongly support the biological logistics of our models, our modelling approaches, the simplification and reduction methods and the parameterization of our model.

The results from the integrated model predict that PSMAD2 levels will oscillate in the first two hours due to the $\mathrm{IL}-6$ stimulation (short-term response), while the steady-state levels (long-term response) depend on the level of the $\mathrm{TGF}-\beta$ stimulation. Specifically, the appearance of the double peak in the dynamics of total PSMAD2 concentration (which has been experimentally proven for the first time) is due to the $\mathrm{IL}-6$ signalling.

6.6 Overall Conclusions and Future Work

The work described in this thesis has focussed on the development of mathematical models of two signalling pathways ($\mathrm{TGF}-\beta$ and $\mathrm{IL}-6$) that are compatible with the latest logistical analysis of these pathways. Chapter 4 and 5 provide well-designed models of $\mathrm{TGF}-\beta$ and $\mathrm{IL}-6$ signal transduction with minimum sets of equations which specify the critical reactions in these signalling pathways. In our model of $\mathrm{TGF}-\beta$ signalling, the coupling of the positive and negative feedback loops and its important effects on the regulation of the $\mathrm{TGF}-\beta$ signalling are proposed for the first time. This implies that more consideration should be made when studying systems with feedback loops e.g. signalling systems. Moreover, corporation of time-delays in order to distinguish between the fast and slow reactions is introduced for the first time in our models of $\mathrm{TGF}-\beta$ and $\mathrm{IL}-6$ signalling. In this thesis the interactions between two distinct regulatory signalling pathways are studied quantitatively for the first time, which paves the road for future studies of the relationship between chronic inflammation and tumor development.

While this thesis proposed a comprehensive study of the crosstalk between two different signalling pathways in line with Systems biology approach, many opportunities for extending the scope of this thesis remain. First, we want to experimentally explore the predictions from our model e.g. the behaviour of

the two signalling pathways with pulsatile input. This requires the development of more experimental protocols. Furthermore, more experimental data is required in order to parameterize the time-delays incorporated in the integrated model. Considering the fact that MAPK signalling is closely related to $\mathrm{TGF}{-}\beta$ and $\mathrm{IL}-6$, the immediate future step is to model MAPK signalling and study its influences on the integrated $\mathrm{IL}-6{:}\mathrm{TGF}{-}\beta$ model. Inclusion of MAPK signalling in our integrated model would make it possible to study the effects of other signalling receptors such as EGFR family members on $\mathrm{TGF}{-}\beta$ and $\mathrm{IL}-6$ signalling. Other modelling approaches (such as stochastic or PDE modelling) could also be studied and compared with the results from our ODE models.

Chapter 7

Appendices

7.1 A Differential Equation Overview

Differential equations are common tools used in mathematical modelling of physical, chemical or biological systems [41, 45, 52, 53, 236, 282]. When the components of a system vary with respect to time, differential equations are used to describe, formulate and solve the system. Examples of differential equations in different areas include mass-spring systems in Physics which follows Hooke's law or tumor growth dynamics [45].

7.1.1 Initial Conditions and Solutions

Regardless of the type of the differential equation, there might be a set of solutions to a single differential equation. These solutions differ in their starting points. Depending on the integration constant or the arbitrary private solution, the solutions follow different curves. Occasionally, single solution among the family of solution curves is important for our purpose. The solution curves can be identified based on their "initial conditions". Initial condition is written in the form of $y(t_0) = y_0$ and the problems which provide initial conditions are called "initial value problems" [41, 236, 282].

7.1.2 Ordinary VS. Partial

Differential equations can be categorized into "ordinary" and "partial" differential equations. Ordinary differential equations, also known as ODEs, are defined when the dependent variable (the variable whose derivative is appeared on the left hand side of the differential equation, e.g. u) of a system is a function of a single independent variable (e.g. t) [41, 282].

$$u = u(t), \tag{7.1}$$

$$u' = f(u, t) \tag{7.2}$$

Whereas, the dependent variable in partial differential equations (PDEs) is a function of multiple independent variables (e.g. t_is) [41,282].

$$u = u(t_1, ..., t_n), \tag{7.3}$$

$$f(u, t_1, ..., t_n, \frac{\partial u}{\partial t_1}, ..., \frac{\partial u}{\partial t_n}, \frac{\partial^2 u}{\partial t_1^2}, ..., \frac{\partial^2 u}{\partial t_n^2}, ...) = 0 \tag{7.4}$$

7.1.3 Order of Differential Equations; Autonomous and Non-autonomous Differential Equations

Both ODEs and PDEs are further classified by the order of derivatives they contain. Order of a differential equation is specified by the number of the highest derivative on the RHS. The general form of a first-order differential equation is illustrated as $u' = f(t, u)$, where f is a function of t and u. The solution of equation 7.2 is defined to be $u = u(t)$ whose derivative is defined as $u' = f(t, u)$. If f does not depend directly on t, then the differential equation is called "autonomous", otherwise, it is a "non-autonomous" differential equation. The autonomous equations are self-governing. This means that the dynamics described by autonomous differential equation will not change by altering the time origin (the starting point of time) [41,53,282].

7.1.4 Linearity VS. Non-linearity

Differential equations are classified into "linear" and "non-linear", depending on the power of the variables appearing on the RHS. If the variables appear only with power one, the differential equation is called linear, otherwise it is a non-linear differential equation [41,282].

Pendulum, for instance, is a classic mechanical system which is formulated by a nonlinear differential equation (because $\sin(\theta)$ is not a first power in 7.5) [41,53,282].

$$\frac{\mathrm{d}^2\theta}{\mathrm{d}t^2} + \sin(\theta) = 0 \tag{7.5}$$

7.1.5 Systems of Differential Equations

Many problems in science involve multiple differential equations and cannot be described by one differential equation (if they are not simplified and reduced). Depending on the number of variables, different systems of differential equations are used to describe such systems. Similar to single differential equation, systems of differential equations are linear or non-linear. As an example of a system of non-linear, first-order ODE, consider a simple protein dimerization system where two monomers combine to form a dimmer:

$$M + M \underset{a}{\overset{b}{\rightleftharpoons}} D$$
$$\emptyset \rightarrow M$$
$$M \rightarrow \emptyset$$
$$D \rightarrow \emptyset$$

The non-linear ODE system with two variables is of the form:

$$\begin{aligned} M' &= p - 2aM^2 + 2bD - mM \\ D' &= aM^2 - bD - dD, \end{aligned}$$

where p, m and d are production and degradation rates.

There is no certain method or algorithm for solving non-linear systems of differential equations. It becomes more complicated when the equations that describe the system are "coupled" [41, 53, 282]. In coupled system of equations, the right hand sides of the equations are functions of two or more variables (including the variables whose derivative are appeared on the left):

$$u' = f(t, u, v)$$
$$v' = g(t, u, v)$$

All systems of ordinary differential equations can be written as systems of first-order ODEs. Most of the biological systems can be modeled with a set of first-order ordinary differential equations. That is the reason for using ODEs in order to model biological systems.

Having formulated the desired system into an appropriate model of differential equation, the next step is to find a solution, $u(t)$, which provides the dynamics of the system. The majority of the natural systems are explained by coupled non-linear systems of differential equations and may not have analytical solutions. Analytic solutions or "closed-form" are said to be found when mathematical manipulations lead to a formula for $u(t)$. In cases where an analytic solution cannot be found, numerical methods are used. A numerical solution is an approximate solution derived via different algorithms of approximation. Non-linear systems can often be solved through numerical methods. Qualitative methods illustrate important features of the solution without solving the system explicitly and are useful in sketching a graphical representation of the system [41, 53, 282].

Having the system solved, analytically or numerically, a number of "equilibrium points" must be found. Physical systems arising from physical phenomena often result in a number of equilibrium points. Consequent stability analysis illuminates whether the equilibrium points are stable and can be explained by a physical explanation.

7.1.6 Qualitative Analysis; Fixed Points, Equilibrium Points and Stability

In order to gain an understanding of the solution of first-order differential equations, we can sketch the "direction field" or "slope field". In direction field, the slope of each small vector (slope mark) is in the direction of $f(t,u)$ for all points in t,u-plane. A line in the direction field which is obtained by setting f equal to a constant is called "isocline" and the lines along which the slope field is zero are "nullclines" [41,282]. As an example, consider the system of first-order ODEs:

$$\begin{cases} x_1' = f_1(x_1,...,x_n) \\ x_2' = f_2(x_1,...,x_n) \\ \vdots \vdots \vdots \\ x_n' = f_n(x_1,...,x_n) \end{cases}$$

The set of x_js ($j = 1,...,n$)) that satisfies $f_j(x_1,...x_n) = 0$ is the nullcline set of the system. The intersection where all nullclines meet is the "fixed point" or the "equilibrium point". The origin $(0,0)$ is a fixed point of all linear systems of ordinary differential equation, while a non-linear system may have neither fixed points nor nullclines. In general, a fixed point is a state of the system where the variables are constant with time. This state is called "steady-state" [41,282].

Stability of a system is defined based on the perturbations applied to the system near its fixed or equilibrium points. If the system converges to its equilibrium point after applying perturbation, the equilibrium is "stable". If the system deviates from its equilibrium point rapidly after applying perturbations, the equilibrium is called "unstable".

Studying the direction field of an equation is important in problems that the changes in the rate of the variables are crucial (such as equations describing cytokine signalling pathways where the system can be reduced based on the reaction rates). However, it is hard to visualize the slope field for systems with more than three time-varying variables. Therefore, this feature is not applicable to most of the biological system studies.

7.1.7 Linearization of Non-linear ODEs

As mentioned previously, most of the real world systems are non-linear and hard to solve analytically. However, if a non-linear system has an equilibrium, its stability can be assessed by studying the stability of an approximated linear system near the equilibrium point. Linear systems are easier to solve. Their behaviours are determined by their associated matrix of eigenvalues and eigenvectors. The general idea of linearization is to approximate a non-linear system by the relative linear system in a neighborhood of the equilibria and use the linear system's features to find a proper approximated solution [41,53,236,282].

Linearization starts by defining small perturbations around the equilibrium point for each variable of the system. As an example, consider the system below as the initial non-linear system:

$$x' = f(x, y)$$
$$y' = g(x, y)$$

If $x^* = (x_e, y_e)$ is an isolated equilibrium, $u = x - x_e$ and $v = y - y_e$ will be defined as the small perturbations around x^*. Therefore, the equation can be rewritten to the form:

$$u' = f(x_e + u, y_e + v)$$
$$v' = g(x_e + u, y_e + v)$$

Now, we can use the "Taylor series" to expand the right side of the equations.

$$u' = f(x_e, y_e) + f_x(x_e, y_e)u + f_y(x_e, y_e)v$$
$$v' = g(x_e, y_e) + g_x(x_e, y_e)u + g_y(x_e, y_e)v$$

The first term in each equation is zero. We can represent the above equations in matrix form:

$$\begin{pmatrix} u' \\ v' \end{pmatrix} = \begin{pmatrix} f_x(x_e, y_e) & f_y(x_e, y_e) \\ g_x(x_e, y_e) & g_y(x_e, y_e) \end{pmatrix} \begin{pmatrix} u \\ v \end{pmatrix}$$

The matrix that maps $\begin{pmatrix} u \\ v \end{pmatrix}$ to $\begin{pmatrix} u' \\ v' \end{pmatrix}$ is called "Jacobian" matrix and contains the first partial derivatives of f and g with respect to x and y. The eigenvalues of Jacobian matrix determine the stability status of the original non-linear system around the equilibrium point (only if the eigenvalues have nonzero real part) [41, 52, 53, 236, 282].

7.2 ODE Solving Methods; Numerical Consideration

Solution methods of ordinary differential equations are controlled either by "initial conditions" or "boundary conditions". The distinction between these two conditions is in the number of points by which the subsidiary conditions are given. In initial value problems, information about a certain point (normally at t = 0) guarantees the uniqueness of the solution, while this information is spread among a number of points (boundaries) in boundary value problems.

7.2.1 Analytical Solutions

Most of linear systems are solvable via analytical methods. The usual strategy to solve linear differential equations is to reduce their order by various algorithms and solve the reduced equation using different methods, depending on the equation type [41, 52, 53, 236, 282]. Two of the most common and general methods to deal with linear systems are: 1. Fourier transform and 2. Laplace transform [41, 282]

Fourier transform enables us to solve linear boundary value problems which might have solutions in the whole real line domain. Notwithstanding, Laplace transform is able to solve linear initial value problems with the help of Fourier transform [41, 282].

As mentioned before, in order to solve a nonlinear system of differential equation an optimal linear system should be found in the first place. This linear system of equations can be solved by one of the analytical methods later. There are a few methods to approximate a nonlinear system near a point of interest. Following subsections provide brief summary on the most applicable approximation methods used to solve nonlinear systems [41, 52, 53, 236, 282].

Iterative Methods

Picard iteration (E.Picard, 1856-1941) is the simplest approximation method for solving nonlinear differential equation by a recursive analytic process. This method of approximation is founded on the basis of a classical method in mathematics called "fixed point iteration" [41, 52, 282]. Fixed point iteration finds solutions for general algebraic equations of the form $x = g(x)$. Approximated solution x^* is generated through the iterative procedure,

$$x_{k+1} = g(x_k), \quad k = 0, 1, 2, ... \tag{7.6}$$

, provided $\mid g'(x^*) \mid < 1$ and the initial guess of the solution is close enough [41, 52, 282].

Picard iteration method is mostly applied to initial value problem, adopting the fixed pint iteration idea. Consider initial conditions as the following:

$$u' = f(t, u) \tag{7.7}$$
$$u(t_0) = u_0 \tag{7.8}$$

We integrate both sides of the first equation to derive an equation for the solution.

$$u(t) = u_0 + \int_{t_0}^{t} f(s, u(s))ds \tag{7.9}$$

Now Picard iteration is defined based on the fixed point iteration.

$$u_{k+1}(t) = u_0 + \int_{t_0}^{t} f(s, u_k(s))ds, \quad k = 0, 1, 2, ... \tag{7.10}$$

In this equation $u_0(t)$ is the initial approximation and is usually set to be the constant function $u_0(t) = u_0$. By applying this method, a sequence of $u_k(t)$ is generated which converges to the absolute solution.

Technically, any solution of $x = g(x)$ is the solution of $f(x) = 0$ and vise-versa. Therefore, this set of solution satisfies the below equation.

$$x = g(x) = x - \frac{f(x)}{h(x)} \tag{7.11}$$

$h(x)$ is a non-zero arbitrary function. By setting $h(x)$ equals to $f'(x)$, the iterative equation is defined as:

$$x_{n+1} = x_n - \frac{f(x_n)}{f'(x_n)}, \quad n = 0, 1, 2, ... \tag{7.12}$$

Now, using fixed point iteration method, x_n will converge to the real solution, only if the initial guess is close enough to it. In truth, replacing $h(x)$ with the first derivative of f has made the convergence as rapid as possible. In other words, the equation, known as "Newton method", is the optimal state of the equation.

Picard iteration is a functional method for acquiring the solution, however, the solution is guaranteed only if the right hand side function is regular. In any case, Using Picard iteration, the solution is still found locally. Therefore, other numerical methods are put into operation to solve initial value problem by means of computer algorithm [41, 52, 282].

7.2.2 Numerical Solutions

Up to this point, the differential equation types and some solution methods have been reviewed. Though, there are many important problems in engineering and science that are potentially unsolvable with analytical methods and it is impossible to derive from them an exact expression for the solution. As a result, alternative methods have been created to provide an accurate approximation to the solution of an initial value problem. These alternative methods are called "numerical methods" [41, 52, 53, 236].

- **Taylor Series Approach**

  Taylor series are the foundation of most of the numerical approximation methods since they define the function f in terms of its measured derivatives in a single point. The Taylor series of $f(x)$ in $x = a$ are of the form:

$$f(a) + \frac{1}{2!}f'(a)(x-a) + \frac{1}{3!}f''(a)(x-a)^2 + ... = \sum_{n=0}^{\infty} \frac{f^{(n)}(a)}{n!}(x-a)^n \tag{7.13}$$

Using the first two terms of Taylor series to extend $u'(t)$ in $u'(t) = f(t, u)$ is the basis of "Euler method" for solving nonlinear differential equations. In order to increase the order of cumulative error and obtain a more precise approximation of the solution, the most sensible way is to extend the Euler formula to the third term of the Taylor series. The result is the "three term Taylor series method":

$$u_{n+1} = u_n + hf(t_n, u_n) + \frac{h^2}{2}\left[\frac{\partial f}{\partial t} + f\frac{\partial f}{\partial u}\right](t_n, u_n), \quad n = 0, ..., N \tag{7.14}$$

Apparently, the error of the three term Taylor series method is of the order h^2 which, in comparison with Euler method, makes a great difference in the approximated solution if h is small.

- **Explicit VS. Implicit**

  In numerical methods approximations, whenever a point such as u_{n+1} can be approximated in a way that it only depends on the previous point approximations, the equation is solved "explicitly" and the approach is an "explicit method". Otherwise, the approximated measurement at each point depends on both itself and previous points and the approximation is acquired through an "implicit method". Implicit method such as, Newton's method, requires solving (nonlinear) equations to find u_{n+1} in terms of u_n. First-order implicit methods provide solutions which are "absolutely stable" while, the solutions derived via explicit methods are "conditionally stable".

  As an example of implicit and explicit methods, consider "Euler method" formula (for more details on this method refer to next section):

$$u_{n+1} = u_n + hf(t_n, u_n) \tag{7.15}$$

  This is in fact the explicit expression of Euler method, however, this method has implicit version as well:

$$u_{n+1} - hf(t_{n+1}, u_{n+1}) = u_n \tag{7.16}$$

  Choosing between implicit and explicit numerical methods is always a trade-off. As mentioned before, the solutions via implicit methods are absolutely stable. Thus, it is sensible if one chooses the implicit instead of the explicit Euler method. However, applying implicit methods on nonlinear and complex systems often leads to nonlinear equations to be solved. Numerical methods used to solve nonlinear equations result in approximated solutions. Yet, Obtaining approximated solutions means that we have already lost the stability of our solution.

All in one, implicit methods do not induce higher stability assigning to complex nonlinear systems. Therefore, in dealing with the majority of the nonlinear models in biology it is more preferred to use explicit numerical methods, such as explicit, forth-order "Runge-Kutta".

- **Error Analysis of Numerical Methods**

  Solving IVP (initial value problem) numerically raises a number of other properties to the solutions that need to be studied. One of these properties is the "convergence" of the solution. Convergence means how close the solution sequence $(u_1, u_2, ..., u_n)$ is to the actual solution or, how small the step size should be to give the maximum solution accuracy.

  In order to quantify the convergence property, two classes of errors have been defined. The difference between the solution obtained numerically and the actual solution (u_n^*) is known as "global truncation error", E_n.

$$E_n = u_n^* - u_n \tag{7.17}$$

  This error is caused by both the approximation formula to determine u_{n+1} used in each step and the approximated input to the approximation formula at the following step. Now, if we assume that the input in the last step is accurate, the only error is due to the approximation formula and is called "local truncated error", e_n.

- **Euler Method**

  Euler method, named after L. Euler (1707-1783), has got the simplest algorithm among numerical approximation methods. The basic idea of this method is to replace the continuous time model with an approximate discrete time model. To achieve this, the time span is divided into smaller intervals of the size h.

$$0 = t_0, t_1, t_2, ..., t_n = T \quad t_n = nh \quad n = 0, 1, 2, ..., N \tag{7.18}$$

  If we use the fundamental theorem of calculus, we can write:

$$u(t_{n+1}) - u(t_n) = \int_{t_n}^{t_{n+1}} f(t, u)dt. \tag{7.19}$$

  This can be approximated by the left-hand rule as the following:

$$u_{n+1} = u_n + hf(t_n, u_n) \tag{7.20}$$

  In the last step, $u(t_n)$ is substituted by u_n for the sake of presentation. Equation is the main Euler formula. Solution at time t is calculated based on solution at time $t - h$ and the slope of the solution curve at the previous

approximated point. The cumulative error is bounded by h over the time interval. As a result, the Euler method is of the order h.

Going back to our dimerization example in Section 3.3.1, we want to solve the system with Euler method $u_{n+1} = u_n + hf(t_n, u_n)$, up to two steps:

$$M' = p - 2a.M^2 + 2b.D - m.M \tag{7.21}$$
$$D' = a.M^2 - b.D - d.D, \tag{7.22}$$

where p, m and d represent production rate of M, degradation rate of M and degradation rate of D, respectively. First, we should set the initial conditions for M and D. We define $M(t_0) = M_0$ and $D(t_0) = D_0$. Now, in the first step when $n = 0$ Euler equation provides:

$$\begin{aligned} M_1 &= M_0 + h(p - 2a.M_0^2 + 2b.D_0 - m.M_0) \\ &= (2ha)M_0^2 + (1 - mh)M_0 + (hp + 2hbD_0) \\ D_1 &= D_0 + h(a.M_0^2 - b.D_0 - d.D_0) = (ha)M_0^2 + (1 - hb - hd)D_0 \end{aligned} \tag{7.23}$$

Having derived M_1 and D_1, we can obtain M_2 and D_2 successively, setting $n = 1$.

$$M_2 = M_1 + h(p - 2a.M_1^2 + 2b.D_1 - m.M_1) \tag{7.24}$$
$$D_2 = D_1 + h(a.M_1^2 - b.D_1 - d.D_1) \tag{7.25}$$

Substituting M_1 and D_1 from the previous step, we can calculate the state of the system in the second step of Euler method. The consequent steps are calculated similarly. In order to avoid complex calculation, it is better to set values for the constants and the initial conditions. Here, I have used the real values for $\mathrm{R2}$ dimerizarion in our model:

$$M_0 = 8.87,\ \ D_0 = 0,\ \ p = 0.019,\ \ m = 0.0132,\ \ a = 0.01,\ \ b = 0.001,\ \ d = 11.8 \tag{7.26}$$

Substituting $h = 0.5$ in equations , we will have:

$$M_1 = 8.03 \tag{7.27}$$
$$D_1 = 0.39 \tag{7.28}$$

Consequently, the solutions for $n = 1$ are as the following:

$$M_2 = 7.34 \tag{7.29}$$
$$D_2 = -3.57 \tag{7.30}$$

Similarly, next step ($n = 2$) provides subsequent solutions:

$$M_3 = M_2 + h(p - 2a.M_2^2 + 2b.D_2 - m.M_2) = 6.75 \tag{7.31}$$
$$D_3 = D_2 + h(a.M_2^2 - b.D_2 - d.D_2) = 17.76 \tag{7.32}$$

Steps can be continued as much as it is required. Though, taking more steps and more calculations do not increase the accuracy of the Euler method; they just provide a better approximated solution curve.

- **Modified Euler Method**

  The Euler method can be more accurate, using the "trapezoidal rule".

$$u(t_{n+1}) - u(t_n) = \frac{h}{2}\left[f(t_n, u_n) + f(t_{n+1}, u_{n+1})\right]. \tag{7.33}$$

  This equation is called implicit Euler equation and its cumulative error is of the order h^2. At each step of solving this equation, a nonlinear equation must be solved for u_{n+1}. To avoid such a complexity, u_{n+1} at each step is replaced by u_{n+1} derived from simple Euler method. Thus, the predictor can be calculated as:

$$\tilde{u}_{n+1} = u_n + hf(t_n, u_n) \tag{7.34}$$

  and the corrector is in the form of:

$$u(t_{n+1}) - u(t_n) = \frac{h}{2}\left[f(t_n, u_n) + f(t_{n+1}, \tilde{u}_{n+1})\right] \tag{7.35}$$

  This predictor-corrector algorithm is known as modified Euler method, Huen's method or second-order Runge-Kutta method. The cumulative error of modified Euler method is also of the order of h^2.

- **Runge-Kutta Method (A Class of Methods)**

  The extension of Euler method is possible either by contribution of higher order of derivatives calculated or by multiplicity of evaluation of the function f, at each step. The idea of the latter was first proposed by Runge in 1895. In collaboration with Heun (1900) and Kutta (1901) this method was developed to forth order and a few efforts for the fifth order was made.

Huta (1956, 1957) introduced the sixth-order of Runge-Kutta method. Recent studies are focussed on implicit Runge-Kutta methods to find numerical solutions for stiff differential equations (solutions derived through numerical methods are numerically unstable in stiff equations). This method is simple and accurate at the same time and thereupon, is the most widely used method in science and engineering.

The Runge-Kutta method is indeed a class of various methods with different calculation steps and different assumptions. They also can be explicit and implicit. The simple idea is that the average values of f accept different weights in the process of finding the next approximating point. Here, we only focus on the low-order explicit methods of standard Runge-Kutta. In general, the two-stage Runge-Kutta method can be formulated as below:

$$u_{n+1} = u_n + h[b_1 f(u_n) + b_2 f(u_n + h a_{21} f(u_n))] \tag{7.36}$$

where $t_{n+1} = t_n + h$. The constants b_1, b_2 and a_{21} should be chosen in a way that the order of the method is as high as possible. The optimal state for the first and second orders are:

$$First - Order : b_1 + b_2 = 1 \tag{7.37}$$

$$Second - order : b_1 + b_2 = 1 \ , \ b_2 a_{21} = \tfrac{1}{2} \tag{7.38}$$

at the same time.

Therefore, assuming $U(t)$ as the approximated value of $u(t)$, the method is illustrated as:

$$U_i(x) = u(t_0) + (t - t_0) \sum_{j=1}^{s} a_{ij} f(U_j(t)) \quad i = 1, 2, ..., s, ... \tag{7.39}$$

$$U(t) = u(t_0) + (t - t_0) \sum_{j=1}^{s} b_j f(U_j(t)) \tag{7.40}$$

The above weights are identified by the Butcher Tableau:

$$\begin{array}{c|c} c_1 & a_{11} \ a_{12} ... a_{1s} \\ c_2 & a_{21} \ a_{22} ... a_{2s} \\ \vdots & \vdots \vdots \vdots \\ c_s & a_{s1} \ a_{s2} ... a_{ss} \\ \hline & b_1 \ b_2 \ ... b_s \end{array} \tag{7.41}$$

The numbers $c_i s$ are defined as $c_i = \sum_{j=1}^{s} a_{ij}$ for $i = 1, 2, ..., s$. These weights can be shown in a tree graph diagram as well.

Methods With Orders Less Than Four:

The Butcher Tableau for order 2 with two stages is provided below:

$$\begin{array}{c|cc} 0 & & \\ c_2 & a_{21} & \\ \hline & b_1 & b_2 \end{array} \tag{7.42}$$

Putting $b_1 + b_2 = 1$ and $b_2 c_2 = \frac{1}{2}$, c_2 will be equal to a_{21}. Two possible cases of the tableaus meeting these conditions are:

$$\begin{array}{c|cc} 0 & & \\ \frac{1}{2} & \frac{1}{2} & \\ \hline & 0 & 1 \end{array} \tag{7.43}$$

and

$$\begin{array}{c|cc} 0 & & \\ 1 & 1 & \\ \hline & \frac{1}{2} & \frac{1}{2} \end{array} \tag{7.44}$$

Reviewing previous sections, these represent the same modified Euler method.

In order to move to third-order Runge-Kutta, three stages are essential to fill up the tableau:

$$\begin{array}{c|ccc} 0 & & & \\ c_2 & a_{21} & & \\ c_3 & a_{31} & a_{32} & \\ \hline & b_1 & b_2 & b_3 \end{array} \tag{7.45}$$

The conditions that rise immediately are:

$$b_1 + b_2 + b_3 = 1, \quad b_2 c_2 + b_3 c_3 = \frac{1}{2}, \quad b_2 c_2^2 + b_3 c_3^2 = \frac{1}{3}, \quad b_3 a_{32} c_2 = \frac{1}{6} \tag{7.46}$$

If we solve all these equations simultaneously, three different cases would be created, depending on the arbitrary choices of the individual constants.

The classical forth-order Runge-Kutta can be written via Butcher Tableau as below. This is the most well-known version of Runge-Kutta method. This is remarkably because a_{31}, a_{41} and a_{42} are put to zero.

$$\begin{array}{c|cccc} 0 & 0 & 0 & 0 & 0 \\ \frac{1}{2} & \frac{1}{2} & 0 & 0 & 0 \\ \frac{1}{2} & 0 & \frac{1}{2} & 0 & 0 \\ 1 & 0 & 0 & 1 & 0 \\ \hline & \frac{1}{6} & \frac{1}{3} & \frac{1}{3} & \frac{1}{6} \end{array} \tag{7.47}$$

The equations for the classical forth-order Runge-Kutta are formulated as below:

$$u_{n+1} = u_n + \frac{h}{6}\left[k_{n,1} + 2k_{n,2} + 2k_{n,3} + k_{n,4}\right], \quad n = 0, 1, 2, ..., N \tag{7.48}$$

$$\begin{cases} k_{n,1} = f(t_n, u_n) \\ k_{n,2} = f(t_n + \frac{1}{2}h, u_n + \frac{1}{2}hk_{n,1}) \\ k_{n,3} = f(t_n + \frac{1}{2}h, u_n + \frac{1}{2}hk_{n,2}) \\ k_{n,4} = f(t_n + h, u_n + hk_{n,3}) \end{cases} \tag{7.49}$$

Four functional evaluations are performed at each step in this method while, in Euler method we evaluate only one function at a time.

The $\frac{h}{6}\left[k_{n,1} + 2k_{n,2} + 2k_{n,3} + k_{n,4}\right]$ is interpreted as the average slope, calculated in 4 different points. The error in fourth-order Runge-kutta method is of order h^4, which represents the degree of accuracy of this method compared to previous numerical methods.

It is time to return to the dimerization example and see how it is solved via forth-order classical Runge-Kutta.

$$M' = p - 2a.M^2 + 2b.D - m.M = f(t, M, D) \tag{7.50}$$

$$D' = a.M^2 - b.D - d.D = g(t, M, D) \tag{7.51}$$

In order to simplify the calculation, we give values to equation parameters and initial conditions. Here, I have used the same values for $\mathrm{R}2$ dimerizarion used in Euler method section:

$$M_0 = 8.87, \quad D_0 = 0, \quad p = 0.019, \quad m = 0.0132, \quad a = 0.01, \quad b = 0.001, \quad d = 11.8 \tag{7.52}$$

Putting $n = 0$ and $h = 0.5$, $k_{0,i} \quad i = 1, 2, 3, 4$ are calculated as the following:

$$
\begin{aligned}
k_{0,1} &= f(t_0, M_0, D_0) \\
&= p - 2a.M_0^2 + 2b.D_0 - m.M_0 = -1.67 \\
l_{0,1} &= g(t_0, M_0, D_0) \\
&= a.M_0^2 - b.D_0 - d.D_0 = 0.79 \\
k_{0,2} &= f(t_0 + \frac{1}{2}h, M_0 + \frac{1}{2}hk_{0,1}, D_0 + \frac{1}{2}hl_{0,1}) \\
&= p - 2a.[M_0 + \frac{1}{2}hk_{0,1}]^2 + 2b.[D_0 + \frac{1}{2}hl_{0,1}] - m.[M_0 + \frac{1}{2}hk_{0,1}] = -1.52 \\
l_{0,2} &= g(t_0 + \frac{1}{2}h, M_0 + \frac{1}{2}hk_{0,1}, D_0 + \frac{1}{2}hl_{0,1}) \\
&= a.[M_0 + \frac{1}{2}hk_{0,1}]^2 - b.[D_0 + \frac{1}{2}hl_{0,1}] - d.[D_0 + \frac{1}{2}hl_{0,1}] = -1.65 \\
k_{0,3} &= f(t_0 + \frac{1}{2}h, M_0 + \frac{1}{2}hk_{0,2}, D_0 + \frac{1}{2}hl_{0,2}) \\
&= p - 2a.[M_0 + \frac{1}{2}hk_{0,2}]^2 + 2b.[D_0 + \frac{1}{2}hl_{0,2}] - m.[M_0 + \frac{1}{2}hk_{0,2}] = -1.53 \\
l_{0,3} &= g(t_0 + \frac{1}{2}h, M_0 + \frac{1}{2}hk_{0,2}, D_0 + \frac{1}{2}hl_{0,2}) \\
&= a.[M_0 + \frac{1}{2}hk_{0,2}]^2 - b.[D_0 + \frac{1}{2}hl_{0,2}] - d.[D_0 + \frac{1}{2}hl_{0,2}] = 5.59 \\
k_{0,4} &= f(t_0 + h, M_0 + hk_{0,3}, D_0 + hl_{0,3}) \\
&= p - 2a.[M_0 + hk_{0,3}]^2 + 2b.[D_0 + hl_{0,3}] - m.[M_0 + hk_{0,3}] = -1.41 \\
l_{0,4} &= g(t_0 + h, M_0 + hk_{0,3}, D_0 + hl_{0,3}) \\
&= a.[M_0 + hk_{0,3}]^2 - b.[D_0 + hl_{0,3}] - d.[D_0 + hl_{0,3}] = -32.33
\end{aligned}
\tag{7.53}
$$

M_1 and D_1 can be derived from M_0 and D_0 with the help of $k_{0,i}s$ and $l_{0,i}s$:

$$M_1 = M_0 + \frac{1}{6}(k_1 + 2k_2 + 2k_3 + k_4) = 7.31 \tag{7.54}$$

$$D_1 = D_0 + \frac{1}{6}(l_1 + 2l_2 + 2k_3 + k_4) = 0.29 \tag{7.55}$$

The same procedure should be followed for the successive steps ($n = 1, 2, ...$). Each n represents single point in the slope plane. The curve that connects all the points gives the solution of the system with mentioned initial conditions and assumptions.

7.3 Review of the Mathematical Models on TGF$-\beta$ Signalling

- A Rate Equation Approach to Elucidate the Kinetics and Robustness of the TGF$-\beta$ Pathway, Melke et al. 2006 [308]

A minimalist model of the $\mathrm{TGF}-\beta$ family signal transduction is provided in this paper. The aim is to study the aspects of $\mathrm{TGF}-\beta$ signalling which have not been studied in detail previously, to identify the key components and modules (specifically SMAD7) in the pathway and gain the ability to predict the quantities which have not been measured yet. The signalling through ALK5 ($\mathrm{TGF}-\beta\ \mathrm{R1}$) and ALK1 (BMP signalling pathway receptor) are compared, while the effects of inhibitory feedback of SMAD7 on both signalling pathways have been modeled. Compared to the Vilar et al. [449] model, the mathematical modelling equations (17 ODE equations) of Melk et al. [308] are simple and are unable to simulate the topology of $\mathrm{TGF}-\beta$ signal transduction. However, as the first attempt to model a complex signalling pathway such as $\mathrm{TGF}-\beta$, Melke et al. [308] succeeded to introduce a robust model and discovered that SMAD7 presence as a negative feedback for the pathway is essential to maintain this robustness. No experimental data is provided by Melke et al. [308].

- Signal Processing in the $\mathrm{TGF}-\beta$ Superfamily Ligand-Receptor Network, Vilar et al. 2006 [449]

  In this paper Vilar et al. [449] mathematically model the $\mathrm{TGF}-\beta$ superfamily receptor trafficking. This model is based on 6 ODEs. In order to justify the dual-responding of cancer cells to $\mathrm{TGF}-\beta$ stimulation, it has been suggested that there are two different ways for $\mathrm{TGF}-\beta$ receptors to be internalized in response to ligand binding: receptor internalization through a lipid-raft-caveolar degradation pathway [449] in which there is no signalling initiated from the internalized receptor, and the standard internalization clathrin pathway which leads to the normal signalling degradation of the receptors. Vilar et al [449] conclude that the imbalances between the rates of the receptor internalization pathways are the key component responsible for the duality in the role of $\mathrm{TGF}-\beta$ stimulation.

Parameters derived by Vilar et al. [449]	Parameters from the literature	Experimental data
Receptor internalization rate (kint = 0.334 min-1)	Experimental data sets	[200]
Ligand-induced receptor degradation rate (klid = 0.25 min-1)		[313]
Constitutive degradation rate (kcd = 0.028 min-1)		[93]
Receptor recycling rate (krec = 0.034 min-1)		
Ligand receptor complex association rate (ka = 1; ligand concentration = 0.01 nM)		
Steady and quasi-steady-state analysis		

- Systems theory of SMAD signalling, Clarke et al. 2009 [74]

  In contrast to the Vilar et al. [449] model, the Clarke et al. TGF$-\beta$ signalling model focuses on intracellular interactions rather than the receptor trafficking on the cell surface. A total of 9 ODEs are used to parameterise the TGF$-\beta$ signalling system. SMAD7 inhibitory effects are not included in this model. Clark et al. [74] conclude that the system is more sensitive to the parameters regulating the R-SMAD phosphorylation and dephosphorylation processes. The importance of the role of SMAD4 in TGF$-\beta$ signal transduction is pointed in this paper. It is postulated that the imbalance between the phosphorylation and dephosphorylation rates of the R-SMADs (see Chapter 2) is the critical determinant of SMAD2, 3 and 4 nuclear accumulation.

Parameters derived by Clarke et al. [73]	Parameters from the literature	Experimental data
Number of receptors: 1000	Other experimental data sets	[351]
Number of SMAD2/3 in the cytoplasm: 1.62e+5		[456]
Number of SMAD2/3 in nucleus: 1.8e+4		
Number of SMAD4 in the cytoplasm: 1.2e+5		
Number of SMAD4 in the nucleus: 3e+4		

- Constraint-Based Modelling and Kinetic Analysis of the SMAD Dependent $\mathrm{TGF}-\beta$ Signalling Pathway, Zi at al 2007 [513]

  In this model, both receptor trafficking and SMAD nucleocytoplasmic shuttling are included explicitly. The aim is to study the dynamic responses to $\mathrm{TGF}-\beta$ signalling via system biology approach. Steady-state analysis has been performed prior to a dynamic study of the signalling components. However, the model appears to be over-fitted. Since all of the experimental data is used for parameter estimation, no predictive analysis is compared with experimental data. This model uses one of the most comprehensive topographies for modelling the $\mathrm{TGF}-\beta$ signalling pathway (it is based on 16 ODEs) and provides access to experimental data for initial data parameterization and the dynamics of the signalling components. Zi et al. [513] develop a constraint-based modelling approach and conclude that the most effective regulator of $\mathrm{TGF}-\beta$ signalling is the balance between clatherin dependent endocytosis and non-clatherin mediated endocytosis.

Parameters derived by Zi et al. [513]	Parameters from the literature	Experimental data
Type I receptor at cell surface: 0.237 nM	The volume of the epithelial cells	[93]
Type I receptor in caveolar lipid-raft: 2.092 nM	Internalization, degradation and recycling rates of the receptor	[93, 449]
Type I receptor in early endosome: 2.06 nM	SMAD nucleocytoplasmic rates	[384]
Type II receptor at cell surface: 0.202 nM	PSMAD nuclear import rate	[486]
Type II receptor in caveolar lipid-raft: 1.778 nM	Total amount of SMADs	[173]
Type II receptor in early endosome: 1.148 nM	Total receptor number	[462]
SMAD2/3 in the cytoplasm: 492.61 nM	Experimental data sets (time course of stimulated PSMAD2, nuclear PSMAD2)	[21, 151, 200, 274]
SMAD2/3 in the nucleus: 236.45 nM		
SMAD4 in the cytoplasm: 1149.4 nM		
SMAD4 in the nucleus: 551.72 nM		
V(HaCaT): 1.4e-12		
Vcyt: 1.05e-12		
Vnuc: 3.5e-13		

- Mathematical modelling identifies SMAD nucleocytoplasmic shuttling as a dynamic signal-interpreting system, Schmierer et al. 2008 [386]

A more developed mathematical model of $\mathrm{TGF}-\beta$ signal transduction is provided by Schmierer et al. [386]. They built a constrained mathematical model to quantify the components of $\mathrm{TGF}-\beta$ signalling pathway and predict the behaviour of a cell with an impaired SMAD2 mutant [386]. Having considered the receptor trafficking and SMAD nucleocytoplasmic shuttling, their model also includes the mechanisms of transcriptional activation by the SMAD nuclear complex, in addition to feedback control from the nucleus. However, the feedback control they use originates from an artificial small molecule (SB-431542) rather from the inherent feedback of the pathway, I-SMADs (see Chapter 2). By introducing this model, Schemierer et al. [386] derived quantitative kinetic rates and other components in $\mathrm{TGF}-\beta$ signalling system to which many subsequent modelling papers refer (such as [511]).

Parameters derived by Schmierer et al. [386]	Parameters from the literature	Experimental data
Concentration of receptors	Concentration of SMAD2 and SMAD3	[73]
Nucleocytoplasmic volume ratio (using experimental data)		[384]]
All the kinetic rates (from optimization)		[200]
Total PSMAD2		[5]
SMAD2/3 in the cytoplasm: 82800 molecules/cell = 60.6 nM		[173]
SMAD2/3 in the nucleus: 17200 molecules/cell = 28.5 nM		[462]
SMAD4 in the cytoplasm: 69400= 50.8 nM		[21,151,200,274]
SMAD4 in the nucleus: 30600 molecules/cell = 50.8 nM		
Receptors in the cytoplasm: 1400 molecules/cell = 1 nM		
Phosphatase in the nucleus: 600 molecules/cell = 1 nM		

- Quantitative Modelling and Analysis of the Transforming Growth Factor Signalling Pathway, Chung et al. 2009 [72]

  Chung et al. [72] aim to discover the changes in intracellular processes in cancer cells during exposure of TGF$-\beta$. Their final goal is to explain the duality of TGF$-\beta$ stimulation (see Chapter 2 and 4). The model has deficiencies when considering the feedback role of SMAD7; however, it is one of the most complete models that study the TGF$-\beta$ signalling pathway

with 17 ODEs. A variety of different databases are used for their parameter estimations. The latter causes disruptions in the predictive nature of the model, since the experimental conditions for the data sets were different. Finally, they propose a new hypothesis to justify the paradoxical effects of $\mathrm{TGF}-\beta$ treatment for cancer cells.

Parameters derived by Chung et al. [72]	Parameters from the literature	Experimental data
Model analysis and simulation	Experimental data sets (total nuclear PSMAD2 for short and long time stimulation of $\mathrm{TGF}-\beta$, total cytoplasmic PSMAD2, total nuclear and cytoplasmic SMAD2 and total SMAD4)	[200,351]
Sensitivity analysis	Model validation data set	[274,279,351]
The comparison between normal and cancerous cells in the level of nuclear PSMAD2-SMAD4	Experimental data set (cancerous cell line)	[267]
	Most of the kinetic rates	[130, 148, 274, 279, 347,384,388,463]
A set of experimental data of PSMAD2 level in prostate cancer cell line	10000 $\mathrm{TGF}-\beta$ receptors	[462]
kinetic rates	Total SMAD2 and SMAD4: 100000 each	[73,384]
	SMAD2 in the cytoplasm: 85000	
	SMAD2 in the nucleus: 15000	
	SMAD4 in the cytoplasm: 87000	
	SMAD4 in the nucleus: 13000	

- Quantitative analysis of transient and sustained transforming growth factor-β signalling dynamics, Zi et al. 2011 [511]

  Zi et al. [511] have provided the most recent mathematical model of the $\mathrm{TGF}-\beta$ signalling. This model uses switch-like responses as outputs of the signalling system. Their model has 19 ODEs and its main goal is to specify the dose-dependency and time-dependency of the $\mathrm{TGF}-\beta$ signalling responses. The authors believe long-term switch-like responses to $\mathrm{TGF}-\beta$ stimulation determine the cellular behaviours. It is because of the different sensitivities the pathway displays in response to different ligand doses and ligand stimulation time-scales. However, the assumptions used to design this model are not complete and do not explain the signalling details precisely (see Chapter 4 for more details).

Parameters derived by Zi et al. [511]	Parameters from the literature	Experimental data
Experimental data sets (6 sets)	Initial values for the ratio and the exact values of cytoplasmic and nuclear SMAD2 and SMAD4	[384,386]
Model analysis and model validation	Volume estimation of the cell's compartment	[386]
A few of the kinetic rates and initial values (estimation via SBML estimation tools)	Most of the kinetic rates	[93, 215, 225, 313,386,449,462, 513]
	Two experimental data sets for validation	[386]
	Receptor type I on the surface: 0.702 nM	[386]
	Receptor type I in the endosome: 6.523 nM	
	Receptor type II on the surface: 0.201 nM	
	Receptor type II in the endosome: 1.440 nM	
	SMAD2/3 in the cytoplasm: 60.6 nM	
	SMAD2/3 in the nucleus: 28.5 nM	
	SMAD4 in the cytoplasm: 50.8	
	SMAD4 in the nucleus: 50.8	
	Vcyt: 2.3e-12	
	Vnuc: 1e-12	

In order to compare the information derived from the mathematical models above, Table 7.1 is created. Having a closer look at the data below, a large diversity is detected in the range of data provided by each model. As an example, the concentration of receptors on the cell surface varies from 1 nM to 112 nM. One explanation for such diversity may be the fact that the initial values for the components at steady-state are estimated. Depending on the demanding accuracy of the model and its relative predictions, estimation methods are different. In the explanations column, the units of the values are listed so that it is easier to compare them. The data has been aligned in a way that is more consistent with the hypothesis of our own model (see Figure 4.1). For instance, individual internalization of the $\mathrm{TGF}-\beta$ receptors has not been included and it is assumed that receptors can stimulate signal transduction only through the ligand-receptor complex on the membrane. In order to align the data with our model, I have included the receptor internalization rate in the receptor degradation rate and similarly, the receptor recycle rate in the receptor production rate (see "Explanations" column of Table 7.1). Looking through all the data provided in Table 7.1, Schmierer et al. [386] approach to data analysis and estimation is more reliable to establish the basis of our model. Schmierer et al. [386] data extraction, including protein concentrations or kinetic rates, follow a logical algorithm. Furthermore, there is no obviously out of range data detected in the following table in Schmierer et al. [386] experimental data (see Table 7.1).

Components	Value	Models	Reference	Explanations
Concentration of receptors on the membrane (in steady-state)		Melke et al. [308]		Mouse embryonic endothelial cells
	1.1 nM	Vilar et al. [449]	estimate	HaCaT cells, 103 receptors per cell
	17 nM	Clarke et al [74]	estimate	HaCaT cells (Vcyt = 9e-13, Vnuc = 1e-13), 104 receptors per cell
	7.5 nM	Zi et al. 2007 [513]	estimate	HaCaT cells (Vcyt = 1.05e-12, Vnuc = 3.5e-13)

	112 nM	Schmierer et al [386]	estimate	HaCaT cells (Vcyt = 2.3e-12, Vnuc = 10e-13), 105 type2 receptors per cell + 1 nM type 1 receptor per cell
	11 nM	Chung et al [72]	estimate	HaCaT cells (Vcyt =1.13e-12, Vnuc = 3.75e-13), 104 total receptors per cell
	8.87 nM	Zi et al. 2011 [511]	estimate	HaCaT cells (Vcyt =2.3e-12, Vnuc = 1e-13)
Concentration of SMAD2/3 in the cytoplasm(in steady-state)		Melke et al [308]		
		Vilar et al [449]		Vilar et al [449] study the receptor trafficking only. No data on nuclearcytoplasmic shuttling of SMADs is provided.
	300 nM	Clarke et al [74]	estimate	
	492.61 nM	Zi et al. 2007 [513]	estimate	
	121.2 nM	Schmierer et al [386]	estimate	
	124.9 nM	Chung et al [72]	estimate	
	60.6 nM	Zi et al. 2011 [511]	estimate	

Concentration of SMAD2/3 in the nucleus(in steady-state)		Melke et al. [308]		
		Vilar et al [449]		Vilar et al [449] study the receptor trafficking only. No data on nuclearcytoplasmic shuttling of SMADs is provided.
	300 nM	Clarke et al [74]	estimate	
	236.45 nM	Zi et al. 2007 [513]	estimate	
	57 nM	Schmierer et al [386]	estimate	
	66 nM	Chung et al [72]	estimate	
	28.5 nM	Zi et al. 2011 [511]	estimate	
Concentration of SMAD4 in the cytoplasm(in steady-state))		Melke et al. [308]		
		Vilar et al [449]		Vilar et al [449] study the receptor trafficking only. No data on nuclearcytoplasmic shuttling of SMADs is provided.

	230 nM	Clarke et al [74]	estimate	
	1149.4 nM	Zi et al. 2007 [513]	estimate	
	50.8 nM	Schmierer et al [386]	estimate	
	127.8 nM	Chung et al [72]	estimate	
	50.8 nM	Zi et al. 2011 [511]	Schmierer et al [386]	
Concentration of SMAD4 in the nucleus(in steady-state)		Melke et al [308]		
		Vilar et al [449]		Vilar et al [449] study the receptor trafficking only. No data on nuclearcytoplasmic shuttling of SMADs is provided.
	500 nM	Clarke et al [74]	estimate	
	551.72 nM	Zi et al. 2007 [513]	estimate	
	50.8 nM	Schmierer et al [386]	estimate	
	57 nM	Chung et al [72]	estimate	
	50.8 nM	Zi et al. 2011 [511]	Schmierer et al [386]	

Receptor (type1, type2) production rate		Melke et al [308]		
	0.125, 0.25 min^{-1}	Vilar et al [449]	estimate	0.408 min^{-1} for the total receptor production rate plus the receptor recycle rate.
		Clarke et al [74]		
	0.0103, 0.029 min^{-1}	Zi et al. 2007 [513]	estimate	0.0433 min^{-1} and 0.06169 min^{-1} for the each receptor production rate plus its recycle rate.
		Schmierer et al [386]		
	0.009 min^{-1}	Chung et al [72]	calculation	
	0.0137, 0.019 nM^{-1} min^{-1}	Zi et al. 2011 [511]	Wakefield et al. [462], calculation	0.01 min^{-1} for type 1 receptor and 0.004 min^{-1} for type 2 receptor
Receptor (type1, type2) degradation rate	0.0001 min^{-1}	Melke et al [308]		
	0.028 min^{-1}	Vilar et al [449]		This is the constitutive degradation of the receptors. (0.361 min^{-1} for the rate of constitutive degradation plus internalization rate)

		Clarke et al [74]		
	0.005, 0.025 min^{-1}	Zi et al. 2007 [513]	Kavasak et al [225]	0.335 min^{-1} and 0.355 min^{-1} for the rate of constitutive degradation plus internalization rate of the receptors.
		Schmierer et al [386]		
	0.00003 min^{-1}	Chung et al. [72]	Vilar et al [449]	
	0.00256, 0.0132 min^{-1}	Zi et al. 2011 [511]	Kavasak et al [225] , Zi et al. [513]	
Ligand-receptor complex association rate		Melke et al [308]		
	1 min^{-1}	Vilar et al [449]		The units of ligand concentration are chosen so that the association rate constant is the unit.
	0.000012 nM^{-1} min^{-1}	Clarke et al [74]		
	2197 nM^{-2} min^{-1}	Zi et al. 2007 [513]	estimate	Around 175.76 nM min^{-1} and 351.52 min^{-1}
	0.11 nM^{-1} min^{-1}	Schmierer et al [386]		Around 0.96 min^{-1}.
	0.0000102 nM^{-1} min^{-1}	Chung et al [72]	estimate	Around 0.000000816 min^{-1}

	117.897 nM^{-2} min^{-1}	Zi et al. 2011 [511]	calculation	Around 16.55 min^{-1}
PSMAD nuclear import rate		Melke et al [308]		
		Vilar et al [449]		Vilar et al [449] study the receptor trafficking only. No data on nuclearcytoplasmic shuttling of SMADs is provided.
	16.6 min^{-1}	Clarke et al [74]		
	0.16 min^{-1}	Zi et al. 2007 [513]	Schmierer et al [386] , Xu et al. [486]	
	5.7 min^{-1}	Schmierer et al [386]		
	0.081 min^{-1}	Chung et al [72]	estimate	
	0.889 min^{-1}	Zi et al. 2011 [511]	Schmierer et al [386]	

Table 7.1: Comparison of all the existing models for $\mathrm{TGF}-\beta$ transduction in terms of included components and their values

7.4 Equations Describing the $\mathrm{TGF}-\beta$ and $\mathrm{IL}-6$ Signalling Systems

7.4.1 $\mathrm{TGF}-\beta$ Receptor Model

$$\begin{aligned} A_{11}\,[\mathrm{R1}\,]' + A_{12}\,[\mathrm{R2}\,]' &= f_1 \\ A_{21}\,[\mathrm{R1}\,]' + A_{22}\,[\mathrm{R2}\,]' &= f_2 \end{aligned}$$

$$A_{11} = 1 + 4\frac{[\mathrm{R1}]}{K_1} + \frac{4\alpha}{K_1K_2K_{RC}}[\mathrm{R1}]\,[\mathrm{R2}]^{\,2} \qquad A_{12} = \frac{4\alpha}{K_1K_2K_{RC}}[\mathrm{R1}]^{\,2}[\mathrm{R2}]$$
$$A_{21} = 1 + 4\frac{[\mathrm{R2}]}{K_2} + \frac{4\alpha}{K_1K_2K_{RC}}[\mathrm{R1}]^{\,2}[\mathrm{R2}] \qquad A_{22} = \frac{4\alpha}{K_1K_2K_{RC}}[\mathrm{R1}]\,[\mathrm{R2}]^{\,2}$$

$$f_1 = v_1 - k_1[\mathrm{R1}] - 2\left(k_{RC} + k_{\mathrm{LRC^*}}\frac{[TGF]}{K_{LRC}K_{\mathrm{LRC^*}}} + k_b[\mathrm{SMAD7}]_{\mathrm{C}}\right)\frac{[\mathrm{R1}]^{\,2}[\mathrm{R2}]^{\,2}}{K_1K_2K_{RC}} - k_a[\mathrm{SMAD7}]_{\mathrm{C}}[\mathrm{R1}]$$
$$f_2 = v_2 - k_2[\mathrm{R2}] - 2\left(k_{RC} + k_{\mathrm{LRC^*}}\frac{[TGF]}{K_{LRC}K_{\mathrm{LRC^*}}} + k_b[\mathrm{SMAD7}]_{\mathrm{C}}\right)\frac{[\mathrm{R1}]^{\,2}[\mathrm{R2}]^{\,2}}{K_1K_2K_{RC}}$$

Note that the activated receptor complex, $[\mathrm{LRC^*}]$, is given by:

$$[\mathrm{LRC^*}] = \frac{[TGF][\mathrm{R1}]^{\,2}[\mathrm{R2}]^{\,2}}{K_1K_2K_{RC}K_{LRC}K_{\mathrm{LRC^*}}}.$$

$$\alpha = \left(1 + \frac{[TGF]}{K_{LRC}} + \frac{[TGF]}{K_{LRC}K_{LRCp}}\right).$$

7.4.2 Cytoplasmic SMAD Model

$$\frac{d[\mathrm{SMAD2}]_{\mathrm{C}}}{dt} = v_2 - k_2[\mathrm{SMAD2}]_{\mathrm{C}} - k_2^*[\mathrm{LRC^*}]\frac{[\mathrm{SMAD2}]_{\mathrm{C}}}{[\mathrm{SMAD2}]_{\mathrm{C}} + K_2^*} - k_2^{\mathrm{i}}[\mathrm{SMAD2}]_{\mathrm{C}} + k_2^{\mathrm{e}}V_{\mathrm{C}}^{\mathrm{N}}[\mathrm{SMAD2}]_{\mathrm{N}}$$
$$\frac{d[\mathrm{SMAD3}]_{\mathrm{C}}}{dt} = v_3 - k_3[\mathrm{SMAD3}]_{\mathrm{C}} - k_3^*[\mathrm{LRC^*}]\frac{[\mathrm{SMAD3}]_{\mathrm{C}}}{[\mathrm{SMAD3}]_{\mathrm{C}} + K_3^*} - k_3^{\mathrm{i}}[\mathrm{SMAD3}]_{\mathrm{C}} + k_3^{\mathrm{e}}V_{\mathrm{C}}^{\mathrm{N}}[\mathrm{SMAD3}]_{\mathrm{N}}$$

$$\begin{aligned}
A_{11}\frac{d[\mathrm{SMAD2^*}]_{\mathrm{C}}}{dt} + A_{12}\frac{d[\mathrm{SMAD3^*}]_{\mathrm{C}}}{dt} + A_{13}\frac{d[\mathrm{SMAD4}]_{\mathrm{C}}}{dt} &= f_1\\
A_{21}\frac{d[\mathrm{SMAD2^*}]_{\mathrm{C}}}{dt} + A_{22}\frac{d[\mathrm{SMAD3^*}]_{\mathrm{C}}}{dt} + A_{23}\frac{d[\mathrm{SMAD4}]_{\mathrm{C}}}{dt} &= f_2\\
A_{31}\frac{d[\mathrm{SMAD2^*}]_{\mathrm{C}}}{dt} + A_{32}\frac{d[\mathrm{SMAD3^*}]_{\mathrm{C}}}{dt} + A_{33}\frac{d[\mathrm{SMAD4}]_{\mathrm{C}}}{dt} &= f_3
\end{aligned}$$

$$\frac{d[\mathrm{SMAD7}]_{\mathrm{C}}}{dt} = v_7 - k_7[\mathrm{SMAD7}]_{\mathrm{C}} + k_7^{\mathrm{t}}V_{\mathrm{C}}^{\mathrm{N}}[\mathrm{SMAD7}]_{\mathrm{N}}$$

$$
\begin{aligned}
A_{11} &= 1 + 9\frac{[\text{SMAD2}^*]_\text{C}^2}{K_2} + 9\frac{[\text{SMAD2}^*]_\text{C}^2\,[\text{SMAD4}]_\text{C}^3}{K_2K_4K_{24}} \\
A_{13} &= 9\frac{[\text{SMAD2}^*]_\text{C}^3\,[\text{SMAD4}]_\text{C}^2}{K_2K_4K_{24}} \\
A_{22} &= 1 + 9\frac{[\text{SMAD3}^*]_\text{C}^2}{K_3} + 9\frac{[\text{SMAD3}^*]_\text{C}^2\,[\text{SMAD4}]_\text{C}^3}{K_3K_4K_{34}} \\
A_{23} &= 9\frac{[\text{SMAD3}^*]_\text{C}^3\,[\text{SMAD4}]_\text{C}^2}{K_3K_4K_{34}} \\
A_{31} &= 9\frac{[\text{SMAD2}^*]_\text{C}^2\,[\text{SMAD4}]_\text{C}^3}{K_2K_4K_{24}} \\
A_{32} &= 9\frac{[\text{SMAD3}^*]_\text{C}^2\,[\text{SMAD4}]_\text{C}^3}{K_3K_4K_{34}} \\
A_{33} &= 1 + 9\frac{[\text{SMAD4}]_\text{C}^2}{K_4} + 9\frac{[\text{SMAD2}^*]_\text{C}^3\,[\text{SMAD4}]_\text{C}^2}{K_2K_4K_{24}} + 9\frac{[\text{SMAD3}^*]_\text{C}^3\,[\text{SMAD4}]_\text{C}^2}{K_3K_4K_{34}}
\end{aligned}
$$

$$
\begin{aligned}
f_1 &= k_2^*\,[\text{LRC}^*]\,\frac{[\text{SMAD2}]_\text{C}}{[\text{SMAD2}]_\text{C} + K_2^*} - 3k_{24}^\text{i}\frac{[\text{SMAD2}^*]_\text{C}^3\,[\text{SMAD4}]_\text{C}^3}{K_2K_4K_{24}} \\
f_2 &= k_3^*\,[\text{LRC}^*]\,\frac{[\text{SMAD3}]_\text{C}}{[\text{SMAD3}]_\text{C} + K_3^*} - 3k_{34}^\text{i}\frac{[\text{SMAD3}^*]_\text{C}^3\,[\text{SMAD4}]_\text{C}^3}{K_3K_4K_{34}} \\
f_3 &= v_4 - \left(k_4 + k_4^\text{i}\right)[\text{SMAD4}]_\text{C} + k_4^\text{e}V_\text{C}^\text{N}\,[\text{SMAD4}]_\text{N} - 3k_{24}^\text{i}\frac{[\text{SMAD2}^*]_\text{C}^3\,[\text{SMAD4}]_\text{C}^3}{K_2K_4K_{24}} \\
&\quad -3k_{34}^\text{i}\frac{[\text{SMAD3}^*]_\text{C}^3\,[\text{SMAD4}]_\text{C}^3}{K_3K_4K_{34}}
\end{aligned}
$$

Note that $A_{12} = A_{21} = 0$.

7.4.3 Nuclear SMAD Model

$$
\begin{aligned}
\frac{d\,[\text{SMAD2}]_\text{N}}{dt} &= k_2^*\,[\text{SMAD2}^*]_\text{N} + k_2^\text{i}V_\text{N}^\text{C}\,[\text{SMAD2}]_\text{C} - k_2^\text{e}\,[\text{SMAD2}]_\text{N} \\
\frac{d\,[\text{SMAD3}]_\text{N}}{dt} &= k_3^*\,[\text{SMAD3}^*]_\text{N} + k_3^\text{i}V_\text{N}^\text{C}\,[\text{SMAD3}]_\text{C} - k_3^\text{e}\,[\text{SMAD3}]_\text{N}
\end{aligned}
$$

$$
\begin{aligned}
A_{11}\frac{d\,[\text{SMAD2}^*]_\text{N}}{dt} + A_{12}\frac{d\,[\text{SMAD3}^*]_\text{N}}{dt} + A_{13}\frac{d\,[\text{SMAD4}]_\text{N}}{dt} &= f_1 \\
A_{21}\frac{d\,[\text{SMAD2}^*]_\text{N}}{dt} + A_{22}\frac{d\,[\text{SMAD3}^*]_\text{N}}{dt} + A_{23}\frac{d\,[\text{SMAD4}]_\text{N}}{dt} &= f_2 \\
A_{31}\frac{d\,[\text{SMAD2}^*]_\text{N}}{dt} + A_{32}\frac{d\,[\text{SMAD3}^*]_\text{N}}{dt} + A_{33}\frac{d\,[\text{SMAD4}]_\text{N}}{dt} &= f_3
\end{aligned}
$$

$$
\begin{aligned}
\frac{d\,[\text{SMAD7}]_\text{N}}{dt} &= v_7 + \left(v_\text{A} + v_\text{B}\frac{[\text{STAT3}_2^*]_\text{N}^2}{[\text{STAT3}_2^*]_\text{N}^2 + K_\text{B}^2}\right)\frac{[\text{SMAD3}_3^* \cdot \text{SMAD4}_3]_\text{N}^2}{[\text{SMAD3}_3^* \cdot \text{SMAD4}_3]_\text{N}^2 + K_\text{A}^2} \\
&\quad -k_7\,[\text{SMAD7}]_\text{N}
\end{aligned}
$$

$$
\begin{aligned}
A_{11} &= 1 + 9\frac{[\mathrm{SMAD2^*}]_\mathrm{N}^2}{K_2} + 9\frac{[\mathrm{SMAD2^*}]_\mathrm{N}^2\,[\mathrm{SMAD4}]_\mathrm{N}^3}{K_2K_4K_{24}} \\
A_{13} &= 9\frac{[\mathrm{SMAD2^*}]_\mathrm{N}^3\,[\mathrm{SMAD4}]_\mathrm{N}^2}{K_2K_4K_{24}} \\
A_{22} &= 1 + 9\frac{[\mathrm{SMAD3^*}]_\mathrm{N}^2}{K_3} + 9\frac{[\mathrm{SMAD3^*}]_\mathrm{N}^2\,[\mathrm{SMAD4}]_\mathrm{N}^3}{K_3K_4K_{34}} \\
A_{23} &= 9\frac{[\mathrm{SMAD3^*}]_\mathrm{N}^3\,[\mathrm{SMAD4}]_\mathrm{N}^2}{K_3K_4K_{34}} \\
A_{31} &= 9\frac{[\mathrm{SMAD2^*}]_\mathrm{N}^2\,[\mathrm{SMAD4}]_\mathrm{N}^3}{K_2K_4K_{24}} \\
A_{32} &= 9\frac{[\mathrm{SMAD3^*}]_\mathrm{N}^2\,[\mathrm{SMAD4}]_\mathrm{N}^3}{K_3K_4K_{34}} \\
A_{33} &= 1 + 9\frac{[\mathrm{SMAD4}]_\mathrm{N}^2}{K_4} + 9\frac{[\mathrm{SMAD2^*}]_\mathrm{N}^3\,[\mathrm{SMAD4}]_\mathrm{N}^2}{K_2K_4K_{24}} + 9\frac{[\mathrm{SMAD3^*}]_\mathrm{N}^3\,[\mathrm{SMAD4}]_\mathrm{N}^2}{K_3K_4K_{34}}
\end{aligned}
$$

$$
\begin{aligned}
f_1 &= -k_2^*\,[\mathrm{SMAD2^*}]_\mathrm{N} + 3k_{24}^\mathrm{i}V_\mathrm{N}^\mathrm{C}\frac{[\mathrm{SMAD2^*}]_\mathrm{C}^3\,[\mathrm{SMAD4}]_\mathrm{C}^3}{K_2K_4K_{24}} \\
f_2 &= -k_3^*\,[\mathrm{SMAD3^*}]_\mathrm{N} + 3k_{34}^\mathrm{i}V_\mathrm{N}^\mathrm{C}\frac{[\mathrm{SMAD3^*}]_\mathrm{C}^3\,[\mathrm{SMAD4}]_\mathrm{C}^3}{K_3K_4K_{34}} \\
f_3 &= k_4^\mathrm{i}V_\mathrm{N}^\mathrm{C}\,[\mathrm{SMAD4}]_\mathrm{C} - k_4^\mathrm{e}\,[\mathrm{SMAD4}]_\mathrm{N} + 3k_{24}^\mathrm{i}V_\mathrm{N}^\mathrm{C}\frac{[\mathrm{SMAD2^*}]_\mathrm{C}^3\,[\mathrm{SMAD4}]_\mathrm{C}^3}{K_2K_4K_{24}} + \\
&\quad 3k_{34}^\mathrm{i}V_\mathrm{N}^\mathrm{C}\frac{[\mathrm{SMAD3^*}]_\mathrm{C}^3\,[\mathrm{SMAD4}]_\mathrm{C}^3}{K_3K_4K_{34}}
\end{aligned}
$$

Note that $A_{12} = A_{21} = 0$, and that the transcription factor complex $[\mathrm{SMAD3}_3^* \cdot \mathrm{SMAD4}_3]_\mathrm{N}$ is given by:

$$[\mathrm{SMAD3}_3^* \cdot \mathrm{SMAD4}_3]_\mathrm{N} = \frac{[\mathrm{SMAD3^*}]_\mathrm{N}^3\,[\mathrm{SMAD4}]_\mathrm{N}^3}{K_3K_4K_{34}}.$$

7.4.4 IL-6 Receptor Model

$$
\begin{aligned}
A_{11}[80]' + A_{12}[130]' &= f_1 \\
A_{21}[80]' + A_{22}[130]' &= f_2
\end{aligned}
$$

$$
\begin{aligned}
A_{11} &= 1 + \frac{[L]}{K_{80}} + \frac{[L][J][130]}{K_{80}K_{130}K_1} + \frac{4[L]^2[80][J]^2[130]^2}{K_{80}^2K_{130}^2K_1^2K_2}(1 + 1/K_2^*) \\
A_{21} &= \frac{[L][J][130]}{K_{80}K_{130}K_1} + \frac{4[L]^2[80][J]^2[130]^2}{K_{80}^2K_{130}^2K_1^2K_2}(1 + 1/K_2^*) \\
A_{12} &= \frac{[L][80][J]}{K_{80}K_{130}K_1} + \frac{4[L]^2[80]^2[J]^2[130]}{K_{80}^2K_{130}^2K_1^2K_2}(1 + 1/K_2^*) \\
A_{22} &= 1 + \frac{[J]}{K_{130}} + \frac{[L][80][J]}{K_{80}K_{130}K_1} + \frac{4[L]^2[80]^2[J]^2[130]}{K_{80}^2K_{130}^2K_1^2K_2}(1 + 1/K_2^*)
\end{aligned}
$$

$$\begin{aligned} f_1 &= v_{80} - k_{80}[80] - 2R \\ f_2 &= v_{130} - k_{130}[130] - 2R \end{aligned}$$

Note that R, is given by:

$$R = (k_{ac} + k_d[SOCS3])\frac{[L]^2[80]^2[J]^2[130]^2}{K_{80}^2 K_{130}^2 K_1^2 K_2^*}.$$

7.5 Review of the Positive Feedback Loop in $\mathrm{TGF}-\beta$ Signalling

This document investigates the existence and importance of a positive feedback on the $\mathrm{TGF}-\beta$ signal transduction via SMADs. $\mathrm{TGF}-\beta$ signalling pathway and its importance in cell responses have been known for decades. Previous mathematical and computational models of this pathway have noticed one or two inherent negative feedbacks (SMAD7 and TMEPAI) by which help to explain the long-term responses of cells to $\mathrm{TGF}-\beta$ stimulation. System analysis suggests detection of oscillation in $\mathrm{TGF}-\beta$ signalling with negative delayed feedbacks. These oscillations have not been reported experimentally. These clues have provided us a new hypothesis: there might be a (merely strong) positive feedback to $\mathrm{TGF}-\beta$ signalling which couples with the SMAD7 negative feedback. We speculate that interactions between the positive and negative feedback can explain the non-oscillatory behaviour of the cell response (here, PSMAD2) at both short and long times after stimulation by $\mathrm{TGF}-\beta$.

We have introduced a recently identified microRNA, miR-433, to initiate a positive feedback via a complex series reactions. It has been known that $\mathrm{TGF}-\beta$ is capable of regulating the expression of different groups of microRNAs. however, it was not clear which microRNA $\mathrm{TGF}-\beta$ regulates. Li et al. [269] have introduced miR-433 as the targeted microRNA via $\mathrm{TGF}-\beta$ in fibrotic kidneys. Using *invivo* and *invitro* studies, they have found antizyme inhibitor 1 (Azin1) is regulated by miR-433 in renal injuries.

miR-433 is reported to have two SMAD-binding sites (SBS)s at its 5'-end in the genomes of human, mouse and rat (at -1845 bp and - 582 bp) [269]. These SBSs, in addition to the binding of SMAD3 to SBS2 of miR-433 in mouse embryonic fibroblasts, these also appears to be a physical interaction between SMAD3 with miR-433. Li et al. show that treatment of TECs (thyroid epithelial cells) with $\mathrm{TGF}-\beta$ decreases the expression of Azin1 at the RNA and protein levels [269]. It is also reported that Azin1 affects the regulation of ECM expression in liver fibrosis [269, 354]. Applying knockdown experiments to TECs and analysis with the luciferase reporter assays, Li et al. proposed an inverse relationship between Azin1 and miR-433 expression. More precisely, miR-433 targets the 3'-untranslated region of Azin1 and negatively regulates its expression.

The role of Azin1 in promotion of polyamine synthesis has been known [212,269]. Indeed, Azin1 binds to the antizyme and inhibits its function, including the initiation of ornithine decarboxylase (ODC) degradation [212,269]. ODC is essential for biosynthesis of polyamines [212, 269]. Depletion of polyamine activates TGF$-\beta$ signalling [269,277,345,365]. We postulate that the Azin1 expression maintains cellular polyamine concentration, suppressing of TGF$-\beta$-induced expression of fibrotic markers [269]. Reports show that over-expression of Azin1 suppresses the expression levels of TGF$-\beta$ and its type 1 receptor while, it has no effects on the receptor type 2 expression levels [269].

A diagram of the positive stimulatory feedback for TGF$-\beta$ signal transduction is illustrated in figure 1. Since this positive feedback includes multiple stimulatory/inhibitory reactions, transcription/translation and possible change of compartments for some components, a noticeable time-delay needs to be included in the model.

The discovery of such a positive feedback would be an important factor for understanding the pathway modelling of TGF$-\beta$. We believe it is now possible to describe the dual behaviour of the cancer cell responses to TGF$-\beta$ stimulation with a mathematical model.

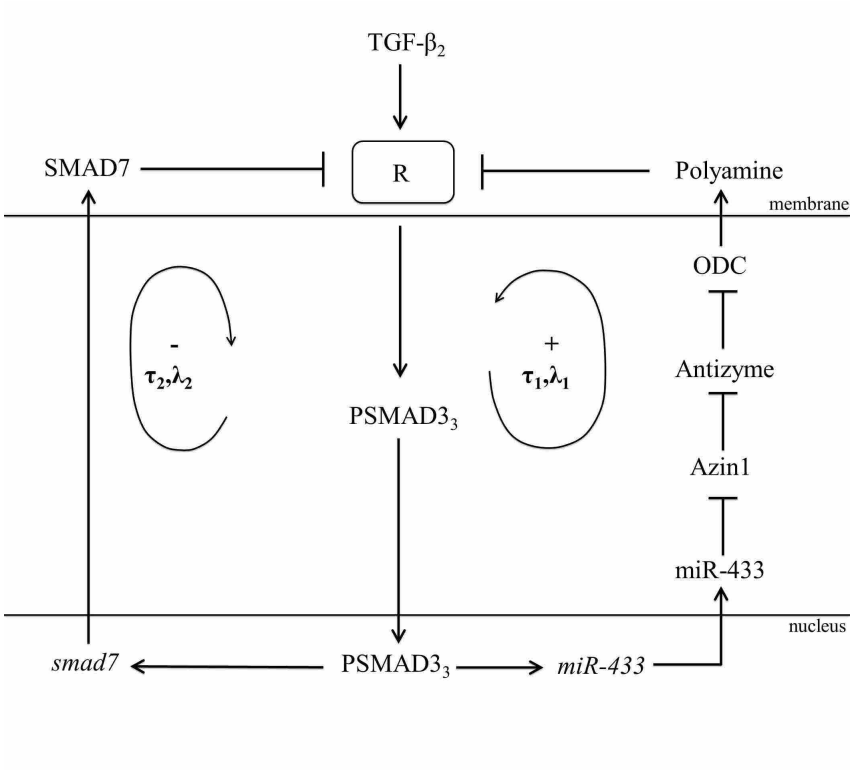

Figure 7.1: *The simplified cartoon of the feedbacks in* TGF$-\beta$ *signal transduction system*

7.5.1 Preliminary Experimental Data Integration

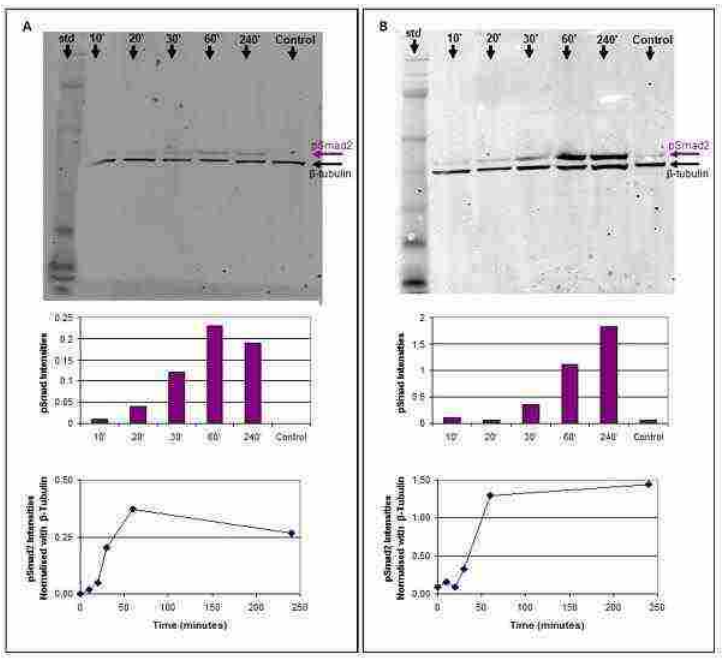

Figure 7.2: *A) Western blot analysis of SV40-immortalized MEF cells (immortal MEFs) stimulated by* TGF$-\beta$ *for different times, probed with PSMAD2 and* β*-tubulin anti-bodies. The results indicate that total PSMAD2 levels peak after 60 minutes of* TGF$-\beta$ *stimulation. B) Western blot analysis of wild type MEF cells (MEF* $Gp130^{F/F}$*) stimulated with* TGF$-\beta$ *for different duration, probed with PSMAD2 and* β*-tubulin anti-bodies. The results indicate that total PSMAD2 levels peaks after 20 minutes of* TGF$-\beta$ *stimulation.*

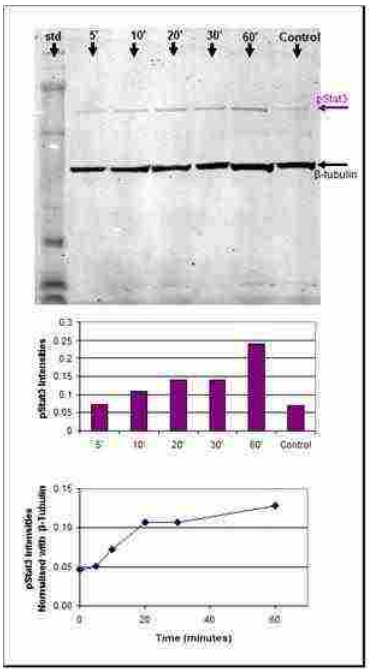

Figure 7.3: *Western blot analysis of wild type MEF cells (MEF Gp130$^{F/F}$) stimulated with* $\mathrm{IL}-6$ *(10% conditioned medium) for different duration, probed with PSTAT3 and* β*-tubulin anti-bodies. Results indicate that total PSTAT3 levels rise gradually until 60 minutes of* $\mathrm{IL}-6$ *stimulation.*

The first part of the experimental data extraction was obtained at the Ludwig Institute for Cancer Research, Parkville branch, Epithelial laboratory. Mouse embryo fibroblast cells (SV40-immortalized and WT MEFs) were analyzed using, protein assays and Western blot methods. Figure 7.2 shows the Western blot results of total PSMAD2 measured in the two cell lines. These cells were stimulated with $\mathrm{TGF}-\beta$ for different times. Stimulation activates the $\mathrm{TGF}-\beta$ signalling from the membrane to the nucleus of a cell. By altering the stimulation duration we can develop a time course for the PSMAD2 dynamic changes in the cells. A similar protocol has been followed for detecting total PSTAT3 in different cell lines, activating $\mathrm{IL}-6$ signalling pathway. The results of western blot analysis for wild type MEFs and the relative time course are shown in Figure 7.3. These experimental results are for the evaluation of our model.

Clearly, it is possible to detect PSMAD2 and PSTAT3 in MEF cells. Western blotting is not the most precise method for quantification of the experimental data; however, it does provide initial estimate of the PSMAD2 levels in a cell line.

Bibliography

[1] K. Aggarwal and J. Massagué. Ubiquitin removal in the TGF-β pathway. *Nature cell biology*, 14(7):656–657, 2012.

[2] A. Agrawal. Phenotypic plasticity in the interactions and evolution of species. *Science*, 294(5541):321–326, 2001.

[3] R. J. Akhurst and R. Derynck. TGF-β signaling in cancer–a double-edged sword. *Trends in cell biology*, 11(11):S44–S51, 2001.

[4] B. B. Aldridge, J. M. Burke, D. A. Lauffenburger, and P. K. Sorger. Physicochemical modelling of cell signalling pathways. *Nature cell biology*, 8(11):1195–1203, 2006.

[5] B. B. Aldridge, J. M. Burke, D. A. Lauffenburger, and P. K. Sorger. Physicochemical modelling of cell signalling pathways. *Nat Cell Biol*, 8(11):1195–1203, 2006.

[6] W. S. Alexander. Suppressors of cytokine signalling (SOCS) in the immune system. *Nature Reviews Immunology*, 2(6):410–416, 2002.

[7] U. Alon, M. Surette, N. Barkai, and S. Leibler. Robustness in bacterial chemotaxis. *Nature*, 397(6715):168–171, 1999.

[8] A. Ambade, D. Catalano, A. Lim, and P. Mandrekar. Inhibition of heat shock protein (molecular weight 90 kDa) attenuates proinflammatory cytokines and prevents lipopolysaccharide-induced liver injury in mice. *Hepatology*, 55(5):1585–1595, 2012.

[9] M. Anzano, A. Roberts, J. Smith, M. Sporn, and J. De Larco. Sarcoma growth factor from conditioned medium is composed of both type α and type β transforming growth factors. *Proc. Natl Acad. Sci. USA*, 80:6264–6268, 1983.

[10] H. Aoki, H. Ohnishi, K. Hama, S. Shinozaki, H. Kita, H. Yamamoto, H. Osawa, K. Sato, K. Tamada, and K. Sugano. Existence of autocrine loop between interleukin-6 and tranforming growth factor-β1 in activated rat pancreatic stellate cells. *Journal of cellular biochemistry*, 99(1):221–228, 2006.

[11] P. Ataie-Kachoie, M. H. Pourgholami, and D. L. Morris. Inhibition of the IL-6 signaling pathway: a strategy to combat chronic inflammatory diseases and cancer. *Cytokine & growth factor reviews*, 24(2):163–173, 2013.

[12] L. Attisano and S. T. Lee-Hoeflich. The Smads. *Genome Biol*, 2(8):3010.1––3010.8, 2001.

[13] L. Attisano and J. Wrana. Signal transduction by the TGF-β superfamily. *Science Signalling*, 296(5573):1646, 2002.

[14] L. Attisano and J. L. Wrana. Smads as transcriptional co-modulators. *Curr Opin Cell Biol*, 12(2):235–43, 2000.

[15] J. Babon, N. Kershaw, J. Murphy, N. Liau, and N. Nicola. S-3: Inhibition of IL-6 family cytokines by SOCS3: Characterizing the mode of inhibition and the basis of its specificity. *Cytokine*, 70(1):21, 2014.

[16] J. J. Babon, N. J. Kershaw, J. M. Murphy, L. N. Varghese, A. Laktyushin, S. N. Young, I. S. Lucet, R. S. Norton, and N. A. Nicola. Suppression of cytokine signaling by SOCS3: characterization of the mode of inhibition and the basis of its specificity. *Immunity*, 36(2):239–250, 2012.

[17] J. J. Babon, E. J. McManus, S. Yao, D. P. DeSouza, L. A. Mielke, N. S. Sprigg, T. A. Willson, D. J. Hilton, N. A. Nicola, M. Baca, et al. The structure of SOCS3 reveals the basis of the extended SH2 domain function and identifies an unstructured insertion that regulates stability. *Molecular cell*, 22(2):205–216, 2006.

[18] K. E. Bachman and B. H. Park. Duel nature of TGF-β signaling: tumor suppressor vs. tumor promoter. *Current Opinion in Oncology*, 17(1):49–54, 2005.

[19] J. Bachmann, A. Raue, M. Schilling, V. Becker, J. Timmer, and U. Klingmuller. Predictive mathematical models of cancer signalling pathways. *J Intern Med*, 271(2):155–65, 2012.

[20] J. Bachmann, A. Raue, M. Schilling, V. Becker, J. Timmer, and U. Klingmüller. Predictive mathematical models of cancer signalling pathways. *Journal of internal medicine*, 271(2):155–165, 2012.

[21] A. V. Bakin, A. K. Tomlinson, N. A. Bhowmick, H. L. Moses, and C. L. Arteaga. Phosphatidylinositol 3-kinase function is required for transforming growth factor beta-mediated epithelial to mesenchymal transition and cell migration. *J Biol Chem*, 275(47):36803–10, 2000.

[22] F. Balkwill, K. A. Charles, and A. Mantovani. Smoldering and polarized inflammation in the initiation and promotion of malignant disease. *Cancer cell*, 7(3):211–217, 2005.

[23] F. Balkwill and A. Mantovani. Inflammation and cancer: back to Virchow? *The lancet*, 357(9255):539–545, 2001.

[24] D. L. Barber, B. B. Andrade, C. McBerry, I. Sereti, and A. Sher. Role of IL-6 in Mycobacterium avium–associated immune reconstitution inflammatory syndrome. *The Journal of Immunology*, 192(2):676–682, 2014.

[25] E. Barillot, L. Calzone, P. Hupe, J.-P. Vert, and A. Zinovyev. *Computational systems biology of cancer*. 2012. ISBN:9781439831441.

[26] N. Barkal and S. Leibler. Robustness in simple biochemical networks. *Nature*, 387(6636):913–917, 1997.

[27] M. Beich-Frandsen, E. Aragón, M. Llimargas, J. Benach, A. Riera, J. Pous, and M. J. Macias. Structure of the N-terminal domain of the protein Expansion: an 'Expansion' to the Smad MH2 fold. *Biological Crystallography*, 71(4), 2015. doi:10.1107/S1399004715001443.

[28] U. Benary, B. Kofahl, A. Hecht, and J. Wolf. Mathematical modelling suggests a differential impact of β-transducin repeat-containing protein paralogues on wnt/β-catenin signalling dynamics. *FEBS Journal*, 282(6):1080–1096, 2015.

[29] A. Bernad, M. Kopf, R. Kulbacki, N. Weich, G. Koehler, and J. C. Gutierrez-Ramos. Interleukin-6 is required in vivo for the regulation of stem cells and committed progenitors of the hematopoietic system. *Immunity*, 1(9):725–731, 1994.

[30] A. Biernacka, M. Dobaczewski, and N. G. Frangogiannis. TGF-β signaling in fibrosis. *Growth factors*, 29(5):196–202, 2011.

[31] J. G. Bode, U. Albrecht, D. Häussinger, P. C. Heinrich, and F. Schaper. Hepatic acute phase proteins–regulation by IL-6-and IL-1-type cytokines involving STAT3 and its crosstalk with NF-κB-dependent signaling. *European journal of cell biology*, 91(6):496–505, 2012.

[32] J. Bollrath, T. J. Phesse, V. A. von Burstin, T. Putoczki, M. Bennecke, T. Bateman, T. Nebelsiek, T. Lundgren-May, Ö. Canli, S. Schwitalla, et al. gp130-mediated Stat3 activation in enterocytes regulates cell survival and cell-cycle progression during colitis-associated tumorigenesis. *Cancer cell*, 15(2):91–102, 2009.

[33] E. Bonavita, S. Gentile, M. Rubino, V. Maina, R. Papait, P. Kunderfranco, C. Greco, F. Feruglio, M. Molgora, I. Laface, et al. PTX3 is an extrinsic oncosuppressor regulating complement-dependent inflammation in cancer. *Cell*, 160(4):700–714, 2015.

[34] N. Bonito, J. Drechsler, S. Stoecker, C. Carmo, M. Seckl, H. Hermanns, and A. Costa-Pereira. Control of gp130 expression by the mitogen-activated protein kinase ERK2. *Oncogene*, 33(17):2255–2263, 2014.

[35] S. Bonni, H. R. Wang, C. G. Causing, P. Kavsak, S. L. Stroschein, K. Luo, and J. L. Wrana. TGF-β induces assembly of a Smad2-Smurf2 ubiquitin ligase complex that targets SnoN for degradation. *Nat Cell Biol*, 3(6):587–95, 2001.

[36] M. J. Boulanger, A. J. Bankovich, T. Kortemme, D. Baker, and K. C. Garcia. Convergent mechanisms for recognition of divergent cytokines by the shared signaling receptor gp130. *Molecular cell*, 12(3):577–589, 2003.

[37] M. J. Boulanger, D.-c. Chow, E. E. Brevnova, and K. C. Garcia. Hexameric structure and assembly of the interleukin-6/IL-6 α-receptor/gp130 complex. *Science*, 300(5628):2101–2104, 2003.

[38] M. J. Boulanger and K. C. Garcia. Shared cytokine signaling receptors: structural insights from the gp130 system. *Advances in protein chemistry*, 68:107–146, 2004.

[39] T. G. Boulton, N. Stahl, and G. D. Yancopoulos. Ciliary neurotrophic factor/leukemia inhibitory factor/interleukin 6/oncostatin M family of cytokines induces tyrosine phosphorylation of a common set of proteins overlapping those induced by other cytokines and growth factors. *Journal of Biological Chemistry*, 269(15):11648–11655, 1994.

[40] T. Bowman, M. A. Broome, D. Sinibaldi, W. Wharton, W. Pledger, J. M. Sedivy, R. Irby, T. Yeatman, S. A. Courtneidge, and R. Jove. Stat3-mediated Myc expression is required for Src transformation and PDGF-induced mitogenesis. *Proceedings of the National Academy of Sciences*, 98(13):7319–7324, 2001.

[41] W. E. Boyce, R. C. DiPrima, and C. W. Haines. *Elementary differential equations and boundary value problems*. Wiley New York, 7th edition, 1992. ISBN:0471319996.

[42] K. Boyle, P. Egan, S. Rakar, T. A. Willson, I. P. Wicks, D. Metcalf, D. J. Hilton, N. A. Nicola, W. S. Alexander, A. W. Roberts, et al. The SOCS box of suppressor of cytokine signaling-3 contributes to the control of G-CSF responsiveness in vivo. *Blood*, 110(5):1466–1474, 2007.

[43] K. Boyle, J.-G. Zhang, S. E. Nicholson, E. Trounson, J. J. Babon, E. J. McManus, N. A. Nicola, and L. Robb. Deletion of the SOCS box of suppressor of cytokine signaling 3 (SOCS3) in embryonic stem cells reveals SOCS box-dependent regulation of JAK but not STAT phosphorylation. *Cellular signalling*, 21(3):394–404, 2009.

[44] R. Brachman and H. Levesque. *Knowledge representation and reasoning*. Elsevier, 2004. ISBN:1558609326.

[45] M. Braun. *Differential Equations and Their Applications: An Introduction to Applied Mathematics*. Texts in Applied Mathematics. Springer, 1992. ISBN:9780387978949.

[46] J. Briscoe, D. Guschin, and M. Müller. Signal transduction: just another signalling pathway. *Current Biology*, 4(11):1033–1035, 1994.

[47] J. Bromberg and T. C. Wang. Inflammation and cancer: IL-6 and STAT3 complete the link. *Cancer cell*, 15(2):79–80, 2009.

[48] P. O. Brown and D. Botstein. Exploring the new world of the genome with DNA microarrays. *Nat Genet*, 21(1 Suppl):33–7, 1999.

[49] E. P. Böttinger and W. Ju. Gene Expression Signatures of TGF-β Smad-Induced Responses . In P. t. Dijke and C.-H. Heldin, editors, *Smad signal transduction: Smads in proliferation, differentiation and disease*, pages 335–360. Springer, 2006. ISBN:101402045425.

[50] M. Bugno, L. Graeve, P. Gatsios, A. Koj, P. C. Heinrich, J. Travls, and T. Kordula. Identification of the interleukin-6/oncostation M response element in the rat tissue inhibitor of metalloproteinases-1 (TIMP-1) Promoter. *Nucleic acids research*, 23(24):5041–5047, 1995.

[51] E. Bullinger, R. Findeisen, D. Kalamatianos, and P. Wellstead. *System and control theory furthers the understanding of biological signal transduction*, pages 123–135. Springer Berlin Heidelberg, 2007. ISBN:9783540719878, Book title:Biology and control theory: Current challenges, Editors:Isabelle Queinnec, Sophie Tarbouriech, Germain Garcia, Silviu-Iulian Niculescu.

[52] R. Burden and J. Faires. *Numerical Analysis*. Brooks/Cole, Cengage Learning, 9th edition, 2010. ISBN:9780538733519.

[53] J. Butcher. *The numerical analysis of ordinary differential equations: Runge-Kutta and general linear methods*. Wiley-Interscience publication. J. Wiley, 1987. ISBN:9780471910466.

[54] S. Camazine. *Self-organization in biological systems*. Princeton University Press, 2003. ISBN:0691012113.

[55] W. B. Cannon. *The wisdom of the body.* Number 312. WW Norton & Co, 1932. ISBN:0393002055.

[56] N. Caronni, B. Savino, and R. Bonecchi. Myeloid cells in cancer-related inflammation. *Immunobiology*, 220(2):249–253, 2015.

[57] B. Chacko, B. Qin, A. Tiwari, G. Shi, S. Lam, L. Hayward, M. De Caestecker, and K. Lin. Structural basis of heteromeric smad protein assembly in TGF-β signaling. *Molecular cell*, 15(5):813–823, 2004.

[58] A. Chakravorty, M. M. Awad, J. K. Cheung, T. J. Hiscox, D. Lyras, and J. I. Rood. The Pore-Forming α-Toxin from Clostridium septicum Activates the MAPK Pathway in a Ras-c-Raf-Dependent and Independent Manner. *Toxins*, 7(2):516–534, 2015.

[59] B.-S. Chen and C.-C. Wu. On the calculation of signal transduction ability of signaling transduction pathways in intracellular communication: systematic approach. *Bioinformatics*, 28(12):1604–1611, 2012.

[60] C.-R. Chen, Y. Kang, and J. Massagué. Defective repression of c-myc in breast cancer cells: a loss at the core of the transforming growth factor β growth arrest program. *Proceedings of the National Academy of Sciences*, 98(3):992–999, 2001.

[61] F. Chen, X. Lin, P. Xu, Z. Zhang, Y. Chen, C. Wang, J. Han, B. Zhao, M. Xiao, and X.-H. Feng. Nuclear Export of Smads by RanBP3L Regulates Bone Morphogenetic Protein Signaling and Mesenchymal Stem Cell Differentiation. *Molecular and cellular biology*, 35(10):1700–1711, 2015.

[62] F. Chen and R. A. Weinberg. Biochemical evidence for the autophosphorylation and transphosphorylation of transforming growth factor beta receptor kinases. *Proc Natl Acad Sci U S A*, 92(5):1565–9, 1995.

[63] K. Chen, L. Calzone, A. Csikasz-Nagy, F. Cross, B. Novak, and J. Tyson. Integrative analysis of cell cycle control in budding yeast. *Molecular biology of the cell*, 15(8):3841–3862, 2004.

[64] M.-F. Chen, P.-T. Chen, M. S. Lu, P. Y. Lin, W.-C. Chen, and K.-D. Lee. IL-6 expression predicts treatment response and outcome in squamous cell carcinoma of the esophagus. *Mol Cancer*, 12(1):26, 2013.

[65] W. W. Chen, M. Niepel, and P. K. Sorger. Classic and contemporary approaches to modeling biochemical reactions. *Genes & development*, 24(17):1861–1875, 2010.

[66] M. Chintamaneni and M. Bhaskar. Biomarkers in Alzheimer's disease: A review. *ISRN pharmacology*, 2012. doi:10.5402/2012/984786.

[67] S. W. Cho, F. Q. Pirih, A. J. Koh, M. Michalski, M. R. Eber, K. Ritchie, B. Sinder, S. Oh, S. A. Al-Dujaili, J. Lee, et al. The soluble interleukin-6 receptor is a mediator of hematopoietic and skeletal actions of parathyroid hormone. *Journal of Biological Chemistry*, 288(10):6814–6825, 2013.

[68] S. Choi. *Systems Biology Approaches: Solving New Puzzles in a Symphonic Manner*, pages 3–11. Springer, 2010.

[69] P. A. Chong, H. Lin, J. L. Wrana, and J. D. Forman-Kay. Coupling of tandem Smad ubiquitination regulatory factor (Smurf) WW domains modulates target specificity. *Proc Natl Acad Sci U S A*, 107(43):18404–9, 2010.

[70] Y. Chu, J. Hahn, et al. Model simplification procedure for signal transduction pathway models: An application to IL-6 signaling. *Chemical engineering science*, 65(6):1964–1975, 2010.

[71] D. Chuderland, A. Konson, and R. Seger. Identification and characterization of a general nuclear translocation signal in signaling proteins. *Molecular cell*, 31(6):850–861, 2008.

[72] S.-W. Chung, F. L. Miles, R. A. Sikes, C. R. Cooper, M. C. Farach-Carson, and B. A. Ogunnaike. Quantitative Modeling and Analysis of the Transforming Growth Factor beta Signaling Pathway. *Biophysical Journal*, 96(5):1733–1750, 2009.

[73] D. C. Clarke, M. D. Betterton, and X. Liu. Systems theory of Smad signalling. *Syst Biol*, 153(6):412–24, 2006.

[74] D. C. Clarke, M. L. Brown, R. A. Erickson, Y. Shi, and X. Liu. Transforming Growth Factor beta Depletion Is the Primary Determinant of Smad Signaling Kinetics. *Molecular and Cellular Biology*, 29(9):2443–2455, 2009.

[75] D. C. Clarke and X. Liu. Decoding the quantitative nature of TGF-β/Smad signaling. *Trends in Cell Biology*, 18(9):430–442, 2008.

[76] R. Cleary. Towing icebergs, falling dominoes and other adventures in applied mathematics. *Journal of the American Statistical Association*, 96(454):779–779, 2001.

[77] M. Cobo, P. Anderson, K. Benabdellah, M. G. Toscano, P. Muñoz, A. García-Pérez, I. Gutierrez, M. Delgado, and F. Martin. Mesenchymal stem cells expressing vasoactive intestinal peptide ameliorate symptoms in a model of chronic multiple sclerosis. *Cell transplantation*, 22(5):839–854, 2013.

[78] P. Coffer, C. Lutticken, A. Van Puijenbroek, M. Klop-de Jonge, F. Horn, and W. Kruijer. Transcriptional regulation of the junB promoter: analysis of STAT-mediated signal transduction. *Oncogene*, 10(5):985, 1995.

[79] N. J. Coorey, W. Shen, L. Zhu, and M. C. Gillies. Differential Expression of IL-6/gp130 Cytokines, Jak-STAT Signaling and Neuroprotection After Müller Cell Ablation in a Transgenic Mouse ModelRole of Müller Cells in IL-6/gp130 and Jak-STAT Activity. *Investigative ophthalmology & visual science*, 56(4):2151–2161, 2015.

[80] M. Coskun, A. K. Olsen, M. Bzorek, S. Holck, U. H. Engel, O. H. Nielsen, and J. T. Troelsen. Involvement of CDX2 in the crosstalk between TNF-α and Wnt signaling pathway in the colon cancer cell line Caco-2. *Carcinogenesis*, bgu037, 2014. doi: 10.1093/carcin/bgu037.

[81] E. Cousins and J. Nicholas. Role of human herpesvirus 8 interleukin-6-activated gp130 signal transducer in primary effusion lymphoma cell growth and viability. *Journal of virology*, 87(19):10816–10827, 2013.

[82] L. M. Coussens, L. Zitvogel, and A. K. Palucka. Neutralizing tumor-promoting chronic inflammation: a magic bullet? *Science*, 339(6117):286–291, 2013.

[83] B. A. Croker, D. L. Krebs, J.-G. Zhang, S. Wormald, T. A. Willson, E. G. Stanley, L. Robb, C. J. Greenhalgh, I. Förster, B. E. Clausen, et al. SOCS3 negatively regulates IL-6 signaling in vivo. *Nature immunology*, 4(6):540–545, 2003.

[84] M. Csete and J. Doyle. Bow ties, metabolism and disease. *Trends in Biotechnology*, 22(9):446–450, 2004.

[85] L. A. D'Alessandro, R. Samaga, T. Maiwald, S.-H. Rho, S. Bonefas, A. Raue, N. Iwamoto, A. Kienast, K. Waldow, R. Meyer, et al. Disentangling the Complexity of HGF Signaling by Combining Qualitative and Quantitative Modeling. *PLoS Computational Biology*, 11(4), 2015. doi:10.1371/journal.pcbi.1004192.

[86] L. Davey, S. A. Halperin, and S. F. Lee. Immunoblotting conditions for small peptides from streptococci. *Journal of microbiological methods*, 114:40–42, 2015.

[87] M. Davies, M. Robinson, E. Smith, S. Huntley, S. Prime, and I. Paterson. Induction of an epithelial to mesenchymal transition in human immortal and malignant keratinocytes by TGF-β1 involves MAPK, Smad and AP-1 signalling pathways. *Journal of cellular biochemistry*, 95(5):918–931, 2005.

[88] J. E. De Larco and G. J. Todaro. Growth factors from murine sarcoma virus-transformed cells. *Proceedings of the National Academy of Sciences*, 75(8):4001–4005, 1978.

[89] E. Deacu, Y. Mori, F. Sato, J. Yin, A. Olaru, A. Sterian, Y. Xu, S. Wang, K. Schulmann, A. Berki, et al. Activin type II receptor restoration in ACVR2-deficient colon cancer cells induces transforming growth factor-β response pathway genes. *Cancer research*, 64(21):7690–7696, 2004.

[90] J. E. Dennis Jr and R. B. Schnabel. *Numerical methods for unconstrained optimization and nonlinear equations*, volume 16. Siam, 1996. ISBN: 9780898713640 , Chapter 2.

[91] S. Dennler, S. Itoh, D. Vivien, P. ten Dijke, S. Huet, and J.-M. Gauthier. Direct binding of Smad3 and Smad4 to critical TGFβ-inducible elements in the promoter of human plasminogen activator inhibitor-type 1 gene. *The EMBO journal*, 17(11):3091–3100, 1998.

[92] D. Dhar, E. Seki, and M. Karin. NCOA5, IL-6, Type 2 Diabetes, and HCC: The deadly quartet. *Cell metabolism*, 19(1):6–7, 2014.

[93] G. M. Di Guglielmo, C. Le Roy, A. F. Goodfellow, and J. L. Wrana. Distinct endocytic pathways regulate TGF-β receptor signalling and turnover. *Nat Cell Biol*, 5(5):410–421, 2003.

[94] E. Dittrich, S. Rose-John, C. Gerhartz, J. Müllberg, T. Stoyan, K. Yasukawa, P. C. Heinrich, and L. Graeve. Identification of a region within the cytoplasmic domain of the interleukin-6 (IL-6) signal transducer gp130 important for ligand-induced endocytosis of the IL-6 receptor. *Journal of Biological Chemistry*, 269(29):19014–19020, 1994.

[95] S. Dominitzki, M. C. Fantini, C. Neufert, A. Nikolaev, P. R. Galle, J. Scheller, G. Monteleone, S. Rose-John, M. F. Neurath, and C. Becker. Cutting edge: trans-signaling via the soluble IL-6R abrogates the induction of FoxP3 in naive CD4+CD25 T cells. *J Immunol*, 179(4):2041–5, 2007.

[96] A. Dubrovska and S. Souchelnytskyi. Low-density microarray analysis of TGFβ1-dependent cell cycle regulation in human breast adenocarcinoma MCF7 cell line. *Biopolymers and Cell*, 30(2):107–117, 2014.

[97] I. Duffy, P. Varacallo, H. Klerk, and J. Hawker. Endothelial and Cancer Cells Have Differing Amounts of TGF Beta Receptors Involved in Angiogenesis. *The FASEB Journal*, 29(1 Supplement):554–4, 2015.

[98] C.-C. Duo, F.-Y. Gong, X.-Y. He, Y.-M. Li, J. Wang, J.-P. Zhang, and X.-M. Gao. Soluble calreticulin induces tumor necrosis factor-α (TNF-α) and interleukin (IL)-6 production by macrophages through Mitogen-Activated Protein Kinase (MAPK) and NFκB signaling pathways. *International journal of molecular sciences*, 15(2):2916–2928, 2014.

[99] E. Dursun, D. Gezen-Ak, H. Hanağası, B. Bilgiç, E. Lohmann, S. Ertan, İ. L. Atasoy, M. Alaylıoğlu, Ö. S. Araz, B. Önal, et al. The interleukin 1 alpha, interleukin 1 beta, interleukin 6 and alpha-2-macroglobulin serum levels in patients with early or late onset Alzheimer's disease, mild cognitive impairment or Parkinson's disease. *Journal of Neuroimmunology*, 283:50–57, 2015.

[100] T. Ebisawa, M. Fukuchi, G. Murakami, T. Chiba, K. Tanaka, T. Imamura, and K. Miyazono. Smurf1 Interacts with Transforming Growth Factor-β Type I Receptor through Smad7 and Induces Receptor Degradation. *Journal of Biological Chemistry*, 276(16):12477–12480, 2001.

[101] T. Ebisawa, M. Fukuchi, G. Murakami, T. Chiba, K. Tanaka, T. Imamura, and K. Miyazono. Smurf1 interacts with transforming growth factor-β type I receptor through Smad7 and induces receptor degradation. *Journal of Biological Chemistry*, 276(16):12477–12480, 2001.

[102] R. Ebner, R.-H. Chen, L. Shum, S. Lawler, T. F. Zioncheck, A. Lee, A. R. Lopez, and R. Derynck. Cloning of a type I TGF-β receptor and its effect on TGF-β binding to the type II receptor. *Science*, 260(5112):1344–1348, 1993.

[103] C. Ehlting, D. Haussinger, and J. BODE. Sp3 is involved in the regulation of SOCS3 gene expression. *Biochem. J*, 387:737–745, 2005.

[104] P. J. Eichhorn, L. Rodón, A. Gonzàlez-Juncà, A. Dirac, M. Gili, E. Martínez-Sáez, C. Aura, I. Barba, V. Peg, A. Prat, et al. USP15 stabilizes TGF-β receptor I and promotes oncogenesis through the activation of TGF-β signaling in glioblastoma. *Nature medicine*, 18(3):429–435, 2012.

[105] D. El Husseini, M.-C. Boulanger, A. Mahmut, R. Bouchareb, M.-H. Laflamme, D. Fournier, P. Pibarot, Y. Bossé, and P. Mathieu. P2Y2 receptor represses IL-6 expression by valve interstitial cells through Akt: Implication for calcific aortic valve disease. *Journal of molecular and cellular cardiology*, 72:146–156, 2014.

[106] A. Eldar, R. Dorfman, D. Weiss, H. Ashe, B. Shilo, and N. Barkai. Robustness of the BMP morphogen gradient in Drosophila embryonic patterning. *Nature*, 419(6904):304–308, 2002.

[107] J. Ellermeier, J. Wei, P. Duewell, S. Hoves, M. R. Stieg, T. Adunka, D. Noerenberg, H.-J. Anders, D. Mayr, H. Poeck, et al. Therapeutic efficacy of bifunctional siRNA combining TGF-β1 silencing with RIG-I activation in pancreatic cancer. *Cancer research*, 73(6):1709–1720, 2013.

[108] T. A. Endo, M. Masuhara, M. Yokouchi, R. Suzuki, H. Sakamoto, K. Mitsui, A. Matsumoto, S. Tanimura, M. Ohtsubo, H. Misawa, et al. A new protein containing an SH2 domain that inhibits JAK kinases. *Nature*, 387(6636):921–924, 1997.

[109] M. Ernst, M. Najdovska, D. Grail, T. Lundgren-May, M. Buchert, H. Tye, V. B. Matthews, J. Armes, P. S. Bhathal, N. R. Hughes, et al. STAT3 and STAT1 mediate IL-11–dependent and inflammation-associated gastric tumorigenesis in gp130 receptor mutant mice. *The Journal of clinical investigation*, 118(5):1727, 2008.

[110] M. Ernst and T. L. Putoczki. Molecular pathways: Il11 as a tumor-promoting cytokine—translational implications for cancers. *Clinical Cancer Research*, 20(22):5579–5588, 2014.

[111] W. B. Ershler and E. T. Keller. Age-associated increased interleukin-6 gene expression, late-life diseases, and frailty. *Annual review of medicine*, 51(1):245–270, 2000.

[112] I. Fabregat, J. Fernando, J. Mainez, and P. Sancho. TGF-β signaling in cancer treatment. *Current pharmaceutical design*, 20(17):2934–2947, 2014.

[113] A. Fahmi, N. Smart, A. Punn, R. Jabr, M. Marber, and R. Heads. p42/p44-MAPK and PI3K are sufficient for IL-6 family cytokines/gp130 to signal to hypertrophy and survival in cardiomyocytes in the absence of JAK/STAT activation. *Cellular signalling*, 25(4):898–909, 2013.

[114] W. FAIRLIE, D. De Souza, N. NICOLA, and M. Baca. Negative regulation of gp130 signalling mediated through tyrosine-757 is not dependent on the recruitment of SHP2. *Biochem. J*, 372:495–502, 2003.

[115] C. P. Fall. *Computational Cell Biology (Interdisciplinary Applied Mathematics; V. 20)*. Springer-Verlag New York, 2002. ISBN:0387953698.

[116] J. Fang, H. Xu, C. Yang, S. Kayarthodi, R. Matthews, V. N. Rao, and E. S. P. Reddy. Molecular mechanism of activation of transforming growth factor beta/smads signaling pathway in ets related genepositive prostate cancers. *J. Pharm. Sci. Pharmacol*, 1:82–85, 2014.

[117] G.-S. Feng, C. Hui, and T. Pawson. SH2-containing phosphotyrosine phosphatase as a target of protein-tyrosine kinases. *Science*, 259(5101):1607–1611, 1993.

[118] X. H. Feng and R. Derynck. Specificity and versatility in TGF-β signaling through Smads. *Annu Rev Cell Dev Biol*, 21:659–93, 2005.

[119] S. S. Ferguson. Evolving concepts in g protein-coupled receptor endocytosis: the role in receptor desensitization and signaling. *Pharmacological reviews*, 53(1):1–24, 2001.

[120] J. E. Ferrell and S. H. Ha. Ultrasensitivity part I: Michaelian responses and zero-order ultrasensitivity. *Trends in biochemical sciences*, 39(10):496–503, 2014.

[121] J. E. Ferrell, S. H. Ha, et al. Ultrasensitivity part II: multisite phosphorylation, stoichiometric inhibitors, and positive feedback. *Trends in biochemical sciences*, 39(11):556–569, 2014.

[122] J. Ferrell Jr. Self-perpetuating states in signal transduction: positive feedback, double-negative feedback and bistability. *Current opinion in cell biology*, 14(2):140–148, 2002.

[123] H. P. Fischer. Mathematical modeling of complex biological systems: from parts lists to understanding systems behavior. *Alcohol Research & Health*, 31(1):49, 2008.

[124] N. I. Fleming, R. N. Jorissen, D. Mouradov, M. Christie, A. Sakthianandeswaren, M. Palmieri, F. Day, S. Li, C. Tsui, L. Lipton, et al. SMAD2, SMAD3 and SMAD4 mutations in colorectal cancer. *Cancer research*, 73(2):725–735, 2013.

[125] A. Force, W. A. Cresko, F. B. Pickett, S. R. Proulx, C. Amemiya, and M. Lynch. The origin of subfunctions and modular gene regulation. *Genetics*, 170(1):433–446, 2005.

[126] F. A. Ford. *Modeling the environment: an introduction to system dynamics models of environmental systems*. Island Press, 1999. ISBN:1559636017.

[127] M. Freeman. Feedback control of intercellular signalling in development. *Nature*, 408(6810):313–319, 2000.

[128] T. Friedlander, A. E. Mayo, T. Tlusty, and U. Alon. Mutation rules and the evolution of Sparseness and Modularity in Biological Systems. *PloS one*, 8(8):e70444, 2013.

[129] Y. Fujio, K. Kunisada, H. Hirota, K. Yamauchi-Takihara, and T. Kishimoto. Signals through gp130 upregulate bcl-x gene expression via STAT1-binding cis-element in cardiac myocytes. *Journal of Clinical Investigation*, 99(12):2898, 1997.

[130] M. Funaba and L. S. Mathews. Identification and characterization of constitutively active Smad2 mutants: evaluation of formation of Smad complex and subcellular distribution. *Mol Endocrinol*, 14(10):1583–91, 2000.

[131] M. Funaba, C. M. Zimmerman, and L. S. Mathews. Modulation of Smad2-mediated signaling by extracellular signal-regulated kinase. *J Biol Chem*, 277(44):41361–8, 2002.

[132] A. Funahashi, Y. Matsuoka, A. Jouraku, H. Kitano, and N. Kikuchi. CellDesigner: a modeling tool for biochemical networks. In *Proceedings of the 38th conference on Winter simulation*, pages 1707–1712. Winter Simulation Conference, 2006.

[133] T. Gaarenstroom and C. S. Hill. TGF-β signaling to chromatin: how Smads regulate transcription during self-renewal and differentiation. *Elsevier*, 32:107–118, 2014. doi:10.1016/j.semcdb.2014.01.009.

[134] C. Gabay et al. Interleukin-6 and chronic inflammation. *Arthritis research and therapy*, 8(2):S3, 2006.

[135] A. Gal, T. Sjoblom, L. Fedorova, S. Imreh, H. Beug, and A. Moustakas. Sustained TGF[beta] exposure suppresses Smad and non-Smad signalling in mammary epithelial cells, leading to EMT and inhibition of growth arrest and apoptosis. *Oncogene*, 27(9):1218–1230, 2007.

[136] K. Gammon. Mathematical modelling: Forecasting cancer. *Nature*, 491(7425):S66–S67, 2012.

[137] S. P. Gao, K. G. Mark, K. Leslie, W. Pao, N. Motoi, W. L. Gerald, W. D. Travis, W. Bornmann, D. Veach, B. Clarkson, et al. Mutations in the EGFR kinase domain mediate STAT3 activation via IL-6 production in human lung adenocarcinomas. *The Journal of clinical investigation*, 117(12):3846, 2007.

[138] C. Garbers, S. Aparicio-Siegmund, and S. Rose-John. The IL-6/gp130/STAT3 signaling axis: recent advances towards specific inhibition. *Current opinion in immunology*, 34:75–82, 2015.

[139] V. García-Hernández, C. Flores-Maldonado, R. Rincon-Heredia, O. Verdejo-Torres, J. Bonilla-Delgado, I. Meneses-Morales, P. Gariglio, and R. G. Contreras. EGF Regulates Claudin-2 and-4 Expression Through Src and STAT3 in MDCK Cells. *Journal of cellular physiology*, 230(1):105–115, 2015.

[140] M. Gassmann, B. Grenacher, B. Rohde, and J. Vogel. Quantifying Western blots: pitfalls of densitometry. *Electrophoresis*, 30(11):1845–1855, 2009.

[141] L. A. Gavrilov and N. S. Gavrilova. The reliability theory of aging and longevity. *Journal of theoretical Biology*, 213(4):527–545, 2001.

[142] K. J. Geißler, M. J. Jung, L. B. Riecken, T. Sperka, Y. Cui, S. Schacke, U. Merkel, R. Markwart, I. Rubio, M. E. Than, et al. Regulation of Son of sevenless by the membrane-actin linker protein ezrin. *Proceedings of the National Academy of Sciences*, 110(51):20587–20592, 2013.

[143] GeneCards. http://www.genecards.org/ (accessed 30/06/2015).

[144] C. Gerhartz, B. Heesel, J. Sasse, U. Hemmann, C. Landgraf, J. Schneider-Mergener, F. Horn, P. C. Heinrich, and L. Graeve. Differential activation of acute phase response factor/STAT3 and STAT1 via the cytoplasmic domain of the interleukin 6 signal transducer gp130 I. Definition of a novel phosphotyrosine motif mediating STAT1 activation. *Journal of Biological Chemistry*, 271(22):12991–12998, 1996.

[145] F. G. Giancotti. Deregulation of cell signaling in cancer. *FEBS letters*, 588(16):2558–2570, 2014.

[146] D. Gilbert, H. Fuß, X. Gu, R. Orton, S. Robinson, V. Vyshemirsky, M. J. Kurth, C. S. Downes, and W. Dubitzky. Computational methodologies for modelling, analysis and simulation of signalling networks. *Briefings in Bioinformatics*, 7(4):339–353, 2006.

[147] Y. Gluzman. SV40-transformed simian cells support the replication of early SV40 mutants. *Cell*, 23(1):175–182, 1981.

[148] J. F. Goetschy, O. Letourneur, N. Cerletti, and M. A. Horisberger. The unglycosylated extracellular domain of type-II receptor for transforming growth factor-β. A novel assay for characterizing ligand affinity and specificity. *Eur J Biochem*, 241(2):355–62, 1996.

[149] C. Gong, S. Qu, B. Liu, S. Pan, Y. Jiao, Y. Nie, F. Su, Q. Liu, and E. Song. MiR-106b expression determines the proliferation paradox of TGF-β in breast cancer cells. *Oncogene*, 34(1):84–93, 2015.

[150] O. B. Goodman Jr, J. G. Krupnick, R. B. Penn, A. W. Gagnon, J. H. Keen, and J. L. Benovic. G-protein-coupled receptor endocytosis. *Catecholamines: Bridging Basic Science with Clinical Medicine: Bridging Basic Science with Clinical Medicine*, 42:429, 1997.

[151] M.-J. Goumans, G. Valdimarsdottir, S. Itoh, A. Rosendahl, P. Sideras, and P. ten Dijke. Balancing the activation state of the endothelium via two distinct TGF-β type I receptors. *EMBO J*, 21(7):1743–1753, 2002.

[152] A. Greenlund, M. Farrar, B. Viviano, and R. Schreiber. Ligand-induced IFN gamma receptor tyrosine phosphorylation couples the receptor to its signal transduction system (p91). *The EMBO journal*, 13(7):1591, 1994.

[153] A. M. Gressner, R. Weiskirchen, K. Breitkopf, and S. Dooley. Roles of TGF-β in hepatic fibrosis. *Front Biosci*, 7(1):d793–807, 2002.

[154] R. Grima and S. Schnell. Modelling reaction kinetics inside cells. *Essays Biochem*, 45:41–56, 2008.

[155] E. Gronroos, U. Hellman, C. H. Heldin, and J. Ericsson. Control of Smad7 stability by competition between acetylation and ubiquitination. *Mol Cell*, 10(3):483–93, 2002.

[156] J. Groppe, C. S. Hinck, P. Samavarchi-Tehrani, C. Zubieta, J. P. Schuermann, A. B. Taylor, P. M. Schwarz, J. L. Wrana, and A. P. Hinck. Cooperative assembly of TGF-β superfamily signaling complexes is mediated by two disparate mechanisms and distinct modes of receptor binding. *Molecular cell*, 29(2):157–168, 2008.

[157] L. Guan-de. MATLAB Curve Fitting Toolbox in Disposing of Experiment Data [J]. *Tractor & Farm Transporter*, 4:040, 2006.

[158] J. Gunawardena. A linear framework for time-scale separation in nonlinear biochemical systems. *PLoS One*, 7(5):e36321, 2012.

[159] X. Guo and X.-F. Wang. Signaling cross-talk between TGF-β/BMP and other pathways. *Cell research*, 19(1):71–88, 2009.

[160] S. Gusenbauer, E. Zanucco, P. Knyazev, and A. Ullrich. Erk2 but not Erk1 regulates crosstalk between Met and EGFR in squamous cell carcinoma cell lines. *Molecular cancer*, 14(1):54, 2015.

[161] S. K. Halder, Y. J. Cho, A. Datta, G. Anumanthan, A. J. Ham, D. P. Carbone, and P. K. Datta. Elucidating the mechanism of regulation of transforming growth factor beta Type II receptor expression in human lung cancer cell lines. *Neoplasia*, 13(10):912–22, 2011.

[162] J. Han, L. Zhang, X. Chen, B. Yang, N. Guo, and Y. Fan. Effects of all-trans retinoic acid on signal pathway of cyclooxygenase-2 and Smad3&7 in transforming growth factor-β-stimulated glomerular mesangial cells. *Experimental Biology and Medicine*, 2014. doi:10.1177/1535370213519216.

[163] D. Hanahan and L. M. Coussens. Accessories to the crime: functions of cells recruited to the tumor microenvironment. *Cancer cell*, 21(3):309–322, 2012.

[164] B. Hannon and M. Ruth. *Modeling dynamic biological systems*. Springer International Publishing, 2014. ISBN:9783319056142.

[165] G. K. Hansson and P. Libby. The immune response in atherosclerosis: a double-edged sword. *Nature Reviews Immunology*, 6(7):508–519, 2006.

[166] A. Hanyu, Y. Ishidou, T. Ebisawa, T. Shimanuki, T. Imamura, and K. Miyazono. The N domain of Smad7 is essential for specific inhibition of transforming growth factor-β signaling. *J Cell Biol*, 155(6):1017–27, 2001.

[167] S. Harroch, M. Revel, and J. Chebath. Induction by interleukin-6 of interferon regulatory factor 1 (IRF-1) gene expression through the palindromic interferon response element pIRE and cell type-dependent control of IRF-1 binding to DNA. *The EMBO journal*, 13(8):1942, 1994.

[168] L. Hawinkels, M. Paauwe, H. Verspaget, E. Wiercinska, J. Van Der Zon, K. Van Der Ploeg, P. Koelink, J. Lindeman, W. Mesker, P. Ten Dijke, et al. Interaction with colon cancer cells hyperactivates TGF-β signaling in cancer-associated fibroblasts. *Oncogene*, 33(1):97–107, 2014.

[169] S. Hayes, A. Chawla, and S. Corvera. TGFβ receptor internalization into EEA1-enriched early endosomes role in signaling to Smad2. *The Journal of cell biology*, 158(7):1239–1249, 2002.

[170] G. He, D. Dhar, H. Nakagawa, J. Font-Burgada, H. Ogata, Y. Jiang, S. Shalapour, E. Seki, S. E. Yost, K. Jepsen, et al. Identification of liver cancer progenitors whose malignant progression depends on autocrine IL-6 signaling. *Cell*, 155(2):384–396, 2013.

[171] G. He and M. Karin. NF-κB and STAT3–key players in liver inflammation and cancer. *Cell research*, 21(1):159–168, 2011.

[172] J.-H. He. Some asymptotic methods for strongly nonlinear equations. *International Journal of Modern Physics B*, 20(10):1141–1199, 2006.

[173] W. He, D. C. Dorn, H. Erdjument-Bromage, P. Tempst, M. A. Moore, and J. Massagué. Hematopoiesis controlled by distinct TIF1gamma and Smad4 branches of the TGFbeta pathway. *Cell*, 125(5):929–41, 2006.

[174] M. Heiner and D. Gilbert. Biomodel engineering for multiscale systems biology. *Progress in biophysics and molecular biology*, 111(2):119–128, 2013.

[175] P. Heinrich, I. Behrmann, S. Haan, H. Hermanns, G. Muller-Newen, and F. Schaper. Principles of interleukin (IL)-6-type cytokine signalling and its regulation. *Biochem. J*, 374:1–20, 2003.

[176] P. Heinrich, I. Behrmann, G. Muller-Newen, F. Schaper, and L. Graeve. Interleukin-6-type cytokine signalling through the gp130/Jak/STAT pathway1. *Biochem. J*, 334:297–314, 1998.

[177] R. Heinrich and S. Schuster. *The regulation of cellular systems*. Springer US, 1996. ISBN:9781461284925.

[178] C.-H. Heldin, K. Miyazono, and P. Ten Dijke. TGF-β signalling from cell membrane to nucleus through SMAD proteins. *Nature*, 390(6659):465–471, 1997.

[179] C.-H. Heldin and A. Moustakas. Role of Smads in TGFbeta signaling. *Cell and Tissue Research*, 347(1):21–36, 2012.

[180] H. M. Hermanns, S. Radtke, F. Schaper, P. C. Heinrich, and I. Behrmann. Non-redundant Signal Transduction of Interleukin-6-type Cytokines THE ADAPTER PROTEIN Shc IS SPECIFICALLY RECRUITED TO THE ONCOSTATIN M RECEPTOR. *Journal of Biological Chemistry*, 275(52):40742–40748, 2000.

[181] M. Hibi, M. Murakami, M. Saito, T. Hirano, T. Taga, and T. Kishimoto. Molecular cloning and expression of an IL-6 signal transducer, gp130. *Cell*, 63(6):1149–1157, 1990.

[182] S. E. Hiemer, A. D. Szymaniak, and X. Varelas. The transcriptional regulators TAZ and YAP direct transforming growth factor β-induced tumorigenic phenotypes in breast cancer cells. *Journal of Biological Chemistry*, 289(19):13461–13474, 2014.

[183] D. M. Hilbert, M. Kopf, B. A. Mock, G. Köhler, and S. Rudikoff. Interleukin 6 is essential for in vivo development of B lineage neoplasms. *The Journal of experimental medicine*, 182(1):243–248, 1995.

[184] C. S. Hill and R. Treisman. Transcriptional regulation by extracellular signals: mechanisms and specificity. *Cell*, 80(2):199–211, 1995.

[185] T. Hirano, K. Nakajima, and M. Hibi. Signaling mechanisms through gp130: a model of the cytokine system. *Cytokine & growth factor reviews*, 8(4):241–252, 1997.

[186] T. Hirano, K. Yasukawa, H. Harada, T. Taga, Y. Watanabe, T. Matsuda, S.-i. Kashiwamura, K. Nakajima, K. Koyama, A. Iwamatsu, et al. Complementary DNA for a novel human interleukin (BSF-2) that induces B lymphocytes to produce immunoglobulin. *Nature*, 324:73–76, 1986.

[187] M. Höfener, F. Pachl, B. Kuster, and N. Sewald. Inhibitor-based affinity probes for the investigation of JAK signaling pathways. *Proteomics*, 2015. doi:10.1002/pmic.201400324.

[188] J. J. Hornberg, F. J. Bruggeman, H. V. Westerhoff, and J. Lankelma. Cancer: a systems biology disease. *Biosystems*, 83(2):81–90, 2006.

[189] U. Horsten, G. Müller-Newen, C. Gerhartz, A. Wollmer, J. Wijdenes, P. C. Heinrich, and J. Grötzinger. Molecular modeling-guided mutagenesis of the extracellular part of gp130 leads to the identification of contact sites in the interleukin-6 (IL-6)· IL-6 receptor· gp130 complex. *Journal of Biological Chemistry*, 272(38):23748–23757, 1997.

[190] Y.-C. Hsiao, Y.-J. Chen, C.-H. Tang, and W.-C. Huang. Lapatinib induces IL-6 expression via MAPK pathway in triple-negative breast cancer cells. *Cancer Research*, 74(19 Supplement):157–157, 2014.

[191] M.-P. Hsu, R. Frausto, S. Rose-John, and I. L. Campbell. Analysis of IL-6/gp130 family receptor expression reveals that in contrast to astroglia, microglia lack the oncostatin M receptor and functional responses to oncostatin M. *Glia*, 63(1):132–141, 2015.

[192] J. J. Hughey, T. K. Lee, and M. W. Covert. Computational modeling of mammalian signaling networks. *Wiley Interdisciplinary Reviews: Systems Biology and Medicine*, 2(2):194–209, 2010.

[193] C.-H. Hung, H.-H. Yeh, H.-C. Wang, C.-C. Lin, T.-L. Tsai, W.-L. Huang, C.-F. Chang, and W.-C. Su. N-glycosylation on lung cancer cell-secreted IL-6 prolongs its activation on JAK/STAT pathway. *Cancer Research*, 74(19 Supplement):3452–3452, 2014.

[194] C. Hwangbo, N. Tae, S. Lee, O. Kim, O. Park, J. Kim, S. Kwon, and J. Lee. Syntenin regulates TGF-β1-induced Smad activation and the epithelial-to-mesenchymal transition by inhibiting caveolin-mediated TGF-β type I receptor internalization. *Oncogene*, 2015. doi:10.1038/onc.2015.100.

[195] J. N. Ihle. STATs: signal transducers and activators of transcription. *Cell*, 84(3):331–334, 1996.

[196] J. N. Ihle and I. M. Kerr. Jaks and Stats in signaling by the cytokine receptor superfamily. *Trends in Genetics*, 11(2):69–74, 1995.

[197] H. Ijichi, T. Ikenoue, N. Kato, Y. Mitsuno, G. Togo, J. Kato, F. Kanai, Y. Shiratori, and M. Omata. Systematic Analysis of the TGF-β-Smad Signaling Pathway in Gastrointestinal Cancer Cells. *Biochemical and Biophysical Research Communications*, 289(2):350–357, 2001.

[198] H. Ikushima and K. Miyazono. Biology of transforming growth factor-β signaling. *Curr Pharm Biotechnol*, 12(12):2099–107, 2011.

[199] G. J. Inman, F. J. Nicolás, and C. S. Hill. Nucleocytoplasmic shuttling of Smads 2, 3, and 4 permits sensing of TGF-β receptor activity. *Molecular cell*, 10(2):283–294, 2002.

[200] G. J. Inman, F. J. Nicolás, and C. S. Hill. Nucleocytoplasmic Shuttling of Smads 2, 3, and 4 Permits Sensing of TGF-β Receptor Activity. *Molecular Cell*, 10(2):283–294, 2002.

[201] M. I. Irandoust, L. H. Aarts, O. Roovers, J. Gits, S. J. Erkeland, and I. P. Touw. Suppressor of cytokine signaling 3 controls lysosomal routing of G-CSF receptor. *The EMBO journal*, 26(7):1782–1793, 2007.

[202] K. Ishihara and T. Hirano. IL-6 in autoimmune disease and chronic inflammatory proliferative disease. *Cytokine & growth factor reviews*, 13(4):357–368, 2002.

[203] H. Ishikawa, T. Maeda, H. Hikita, and K. Miyatake. The computerized derivation of rate equations for enzyme reactions on the basis of the pseudo-steady-state assumption and the rapid-equilibrium assumption. *Biochem. J*, 251:175–181, 1988.

[204] D. Javelaud and A. Mauviel. Crosstalk mechanisms between the mitogen-activated protein kinase pathways and Smad signaling downstream of TGF-β: implications for carcinogenesis. *Oncogene*, 24(37):5742–5750, 2005.

[205] L. Jayaraman and J. Massagué. Distinct oligomeric states of SMAD proteins in the transforming growth factor-β pathway. *J Biol Chem*, 275(52):40710–7, 2000.

[206] B. J. Jenkins, D. Grail, T. Nheu, M. Najdovska, B. Wang, P. Waring, M. Inglese, R. M. McLoughlin, S. A. Jones, N. Topley, H. Baumann, L. M. Judd, A. S. Giraud, A. Boussioutas, H. J. Zhu, and M. Ernst. Hyperactivation of Stat3 in gp130 mutant mice promotes gastric hyperproliferation and desensitizes TGF-β signaling. *Nat Med*, 11(8):845–52, 2005.

[207] B. J. Jenkins, D. Grail, T. Nheu, M. Najdovska, B. Wang, P. Waring, M. Inglese, R. M. McLoughlin, S. A. Jones, N. Topley, et al. Hyperactivation of Stat3 in gp130 mutant mice promotes gastric hyperproliferation and desensitizes TGF-β signaling. *Nature medicine*, 11(8):845–852, 2005.

[208] G. Jenkins. The role of proteases in transforming growth factor-β activation. *The international journal of biochemistry & cell biology*, 40(6):1068–1078, 2008.

[209] S. A. Jones, J. Scheller, and S. Rose-John. Therapeutic strategies for the clinical blockade of IL-6/gp130 signaling. *The Journal of clinical investigation*, 121(9):3375, 2011.

[210] J. E. F. Jr. Feedback loops and reciprocal regulation: recurring motifs in the systems biology of the cell cycle . *Current Opinion in Cell Biology*, 25(6):676 – 686, 2013.

[211] J. Jullien, V. Guili, L. F. Reichardt, and B. B. Rudkin. Molecular kinetics of nerve growth factor receptor trafficking and activation. *Journal of Biological Chemistry*, 277(41):38700–38708, 2002.

[212] C. Kahana. Regulation of cellular polyamine levels and cellular proliferation by antizyme and antizyme inhibitor. *Essays Biochem*, 46:47–62, 2009.

[213] D. Kamimura, Y. Arima, T. Hirano, H. Ogura, and M. Murakami. *IL-6 and Inflammatory Diseases*, pages 53–78. Springer Japan, 2014. ISBN:9784431544418, Book title: Cytokine Frontiers, editor: Takayuki Yoshimoto, Tomohiro Yoshimoto.

[214] D. Kamimura, K. Ishihara, and T. Hirano. *IL-6 signal transduction and its physiological roles: the signal orchestration model*, pages 1–38. Springer Berlin Heidelberg, 2004. ISBN:9783540202134 Book title: Reviews of physiology, biochemistry and pharmacology.

[215] B. Kaminska, A. Wesolowska, and M. Danilkiewicz. TGF beta signalling and its role in tumour pathogenesis. *Acta Biochim Pol*, 52(2):329–37, 2005.

[216] Y. Kamiya, K. Miyazono, and K. Miyazawa. Smad7 inhibits transforming growth factor-β family type i receptors through two distinct modes of interaction. *J Biol Chem*, 285(40):30804–13, 2010.

[217] T. Kamura, K. Maenaka, S. Kotoshiba, M. Matsumoto, D. Kohda, R. C. Conaway, J. W. Conaway, and K. I. Nakayama. VHL-box and SOCS-box domains determine binding specificity for Cul2-Rbx1 and Cul5-Rbx2 modules of ubiquitin ligases. *Genes & development*, 18(24):3055–3065, 2004.

[218] T. Kamura, S. Sato, D. Haque, L. Liu, W. G. Kaelin, R. C. Conaway, and J. W. Conaway. The Elongin BC complex interacts with the conserved SOCS-box motif present in members of the SOCS, ras, WD-40 repeat, and ankyrin repeat families. *Genes & development*, 12(24):3872–3881, 1998.

[219] J. S. Kang, C. Liu, and R. Derynck. New regulatory mechanisms of TGF-β receptor function. *Trends in cell biology*, 19(8):385–394, 2009.

[220] Y. Kang, C.-R. Chen, and J. Massagué. A self-enabling TGFβ response coupled to stress signaling: Smad engages stress response factor ATF3 for Id1 repression in epithelial cells. *Molecular cell*, 11(4):915–926, 2003.

[221] J.-T. Kao, C.-L. Feng, C.-J. Yu, S.-M. Tsai, P.-N. Hsu, Y.-L. Chen, and Y.-Y. Wu. IL-6, through p-STAT3 rather than p-STAT1, activates hepatocarcinogenesis and affects survival of hepatocellular carcinoma patients: a cohort study. *BMC gastroenterology*, 15(1):50, 2015.

[222] S.-c. Kao, R. K. Jaiswal, W. Kolch, and G. E. Landreth. Identification of the mechanisms regulating the differential activation of the mapk cascade by epidermal growth factor and nerve growth factor in PC12 cells. *Journal of Biological Chemistry*, 276(21):18169–18177, 2001.

[223] M. Kasprzycka, M. Marzec, X. Liu, Q. Zhang, and M. A. Wasik. Nucleophosmin/anaplastic lymphoma kinase (NPM/ALK) oncoprotein induces the T regulatory cell phenotype by activating STAT3. *Proceedings of the National Academy of Sciences*, 103(26):9964–9969, 2006.

[224] Y. Katsuno, S. Lamouille, and R. Derynck. TGF-β signaling and epithelial–mesenchymal transition in cancer progression. *Current opinion in oncology*, 25(1):76–84, 2013.

[225] P. Kavsak, R. K. Rasmussen, C. G. Causing, S. Bonni, H. Zhu, G. H. Thomsen, and J. L. Wrana. Smad7 Binds to Smurf2 to Form an E3 Ubiquitin Ligase that Targets the TGFbeta Receptor for Degradation. *Molecular Cell*, 6(6):1365–1375, 2000.

[226] P. Kavsak, R. K. Rasmussen, C. G. Causing, S. Bonni, H. Zhu, G. H. Thomsen, and J. L. Wrana. Smad7 binds to Smurf2 to form an E3 ubiquitin ligase that targets the TGFβ receptor for degradation. *Molecular cell*, 6(6):1365–1375, 2000.

[227] M. Kawabata, H. Inoue, A. Hanyu, T. Imamura, and K. Miyazono. Smad proteins exist as monomers in vivo and undergo homo- and hetero-oligomerization upon activation by serine/threonine kinase receptors. *EMBO J*, 17(14):4056–65, 1998.

[228] M. Kawano, T. Hirano, T. Matsuda, T. Taga, Y. Horii, K. Iwato, H. Asaoku, B. Tang, O. Tanabe, H. Tanaka, et al. Autocrine generation and requirement of BSF-2/IL-6 for human multiple myelomas. 1988.

[229] Y. Keshet and R. Seger. *The MAP kinase signaling cascades: a system of hundreds of components regulates a diverse array of physiological functions*, pages 3–38. Springer, 2010. ISBN:9781607617945, Book title: MAP Kinase Signaling Protocols, editor: Rony Seger.

[230] F. M. Khan, U. Schmitz, S. Nikolov, D. Engelmann, B. M. Pützer, O. Wolkenhauer, and J. Vera. Hybrid modeling of the crosstalk between signaling and transcriptional networks using ordinary differential equations and multi-valued logic. *Biochimica et Biophysica Acta (BBA)-Proteins and Proteomics*, 1844(1):289–298, 2014.

[231] R. Khokha, A. Murthy, and A. Weiss. Metalloproteinases and their natural inhibitors in inflammation and immunity. *Nature Reviews Immunology*, 13(9):649–665, 2013.

[232] D. J. Kim, M. L. Tremblay, and J. DiGiovanni. Protein tyrosine phosphatases, TC-PTP, SHP1, and SHP2, cooperate in rapid dephosphorylation of Stat3 in keratinocytes following UVB irradiation. *PLoS One*, 5(4):e10290, 2010.

[233] H. K. Kim. Role of ERK/MAPK signalling pathway in anti-inflammatory effects of Ecklonia cava in activated human mast cell line-1 cells. *Asian Pacific journal of tropical medicine*, 7(9):703–708, 2014.

[234] S. S. Kim, K. Shetty, V. Katuri, K. Kitisin, H. J. Baek, Y. Tang, B. Marshall, L. Johnson, B. Mishra, and L. Mishra. TGF-β signaling pathway inactivation and cell cycle deregulation in the development of gastric cancer: role of the beta-spectrin, ELF. *Biochem Biophys Res Commun*, 344(4):1216–23, 2006.

[235] A. Kimchi, X. F. Wang, R. A. Weinberg, S. Cheifetz, and J. Massagué. Absence of TGF-β receptors and growth inhibitory responses in retinoblastoma cells. *Science*, 240(4849):196–199, 1988.

[236] A. King, J. Billingham, and S. Otto. *Differential Equations: Linear, Nonlinear, Ordinary, Partial*. Cambridge University Press, 2003. ISBN:9780521016872.

[237] D. M. Kingsley. The TGF-β superfamily: new members, new receptors, and new genetic tests of function in different organisms. *Genes & development*, 8(2):133–146, 1994.

[238] I. Kinjyo, H. Inoue, S. Hamano, S. Fukuyama, T. Yoshimura, K. Koga, H. Takaki, K. Himeno, G. Takaesu, T. Kobayashi, et al. Loss of SOCS3 in T helper cells resulted in reduced immune responses and hyperproduction of interleukin 10 and transforming growth factor–β1. *The Journal of experimental medicine*, 203(4):1021–1031, 2006.

[239] T. Kishimoto, T. Taga, and S. Akira. Cytokine signal transduction. *Cell*, 76(2):253–262, 1994.

[240] H. Kitano. Computational systems biology. *Nature*, 420(6912):206–210, 2002.

[241] H. Kitano. Systems Biology: A Brief Overview. *Science*, 295(5560):1662–1664, 2002.

[242] H. Kitano. Cancer robustness: tumour tactics. *Nature*, 426(6963):125, 2003.

[243] H. Kitano. Biological robustness. *Nature Reviews Genetics*, 5(11):826–837, 2004.

[244] H. Kitano. Cancer as a robust system: implications for anticancer therapy. *Nature Reviews Cancer*, 4(3):227–235, 2004.

[245] H. Kitano. *Scientific Challenges in Systems Biology*, pages 3–13. Humana Press, 2007. ISBN:9781588297068 ,Book title : Introduction to systems biology, editor : S. Choi.

[246] H. Kitano. *The theory of biological robustness and its implication in cancer*, pages 69–88. Springer, 2007. ISBN:9783540313380, Book title: Systems Biology, editor: P. Bringmann, E. C. Butcher, G. Parry, B. Weiss.

[247] H. Kitano and K. Oda. Robustness trade-offs and host–microbial symbiosis in the immune system. *Molecular systems biology*, 2(1), 2006.

[248] J. Kleeff, T. Ishiwata, H. Maruyama, H. Friess, P. Truong, M. Büchler, D. Falb, and M. Korc. The TGF-β signaling inhibitor Smad7 enhances tumorigenicity in pancreatic cancer. *Oncogene*, 18(39):5363–5372, 1999.

[249] E. Klipp and W. Liebermeister. Mathematical modeling of intracellular signaling pathways. *BMC neuroscience*, 7(Suppl 1):S10, 2006.

[250] E. Klipp, W. Liebermeister, C. Wierling, A. Kowald, H. Lehrach, and R. Herwig. *Systems biology*. John Wiley & Sons, 2013. ISBN:9783527318742.

[251] H. Knüpfer and R. Preiß. Significance of interleukin-6 (IL-6) in breast cancer (review). *Breast cancer research and treatment*, 102(2):129–135, 2007.

[252] C.-Y. Ko, L.-H. Chang, Y.-C. Lee, E. Sterneck, C.-P. Cheng, S.-H. Chen, A.-M. Huang, J. T. Tseng, and J.-M. Wang. CCAAT/enhancer binding protein delta (CEBPD) elevating PTX3 expression inhibits macrophage-mediated phagocytosis of dying neuron cells. *Neurobiology of aging*, 33(2):422–e11, 2012.

[253] H. Koldsø and M. S. Sansom. Signal Transduction by a Cytokine Receptor: Multi-Scale Computational Studies of the Membrane Associated Gp130 Receptor Complex. *Biophysical Journal*, 104(2):608a, 2013.

[254] M. Kondo, K. Yamaoka, K. Sakata, K. Sonomoto, L. Lin, K. Nakano, and Y. Tanaka. Contribution of the Interleukin-6/STAT-3 Signaling Pathway to Chondrogenic Differentiation of Human Mesenchymal Stem Cells. *Arthritis & Rheumatology*, 67(5):1250–1260, 2015.

[255] M. Kopf, H. Baumann, G. Freer, M. Freudenberg, M. Lamers, T. Kishimoto, R. Zinkernagel, H. Bluethmann, and G. Köhler. Impaired immune and acute-phase responses in interleukin-6-deficient mice. *Nature*, 368(6469):339–342, 1994.

[256] T. Kordula, R. E. Rydel, E. F. Brigham, F. Horn, P. C. Heinrich, and J. Travis. Oncostatin M and the interleukin-6 and soluble interleukin-6 receptor complex regulate α1-antichymotrypsin expression in human cortical astrocytes. *Journal of Biological Chemistry*, 273(7):4112–4118, 1998.

[257] E. Korzus, H. Nagase, R. Rydell, and J. Travis. The mitogen-activated protein kinase and JAK-STAT signaling pathways are required for an oncostatin M-responsive element-mediated activation of matrix metalloproteinase 1 gene expression. *Journal of Biological Chemistry*, 272(2):1188–1196, 1997.

[258] H. Kouhara, Y. Hadari, T. Spivak-Kroizman, J. Schilling, D. Bar-Sagi, I. Lax, and J. Schlessinger. A lipid-anchored Grb2-binding protein that links FGF-receptor activation to the Ras/MAPK signaling pathway. *Cell*, 89(5):693–702, 1997.

[259] P. K. Kreeger and D. A. Lauffenburger. Cancer systems biology: a network modeling perspective. *Carcinogenesis*, 31(1):2–8, 2010.

[260] M. Kretzschmar, J. Doody, I. Timokhina, and J. Massagué. A mechanism of repression of TGFbeta/ Smad signaling by oncogenic Ras. *Genes Dev*, 13(7):804–16, 1999.

[261] S. Kume, M. Haneda, K. Kanasaki, T. Sugimoto, S. Araki, K. Isshiki, M. Isono, T. Uzu, L. Guarente, A. Kashiwagi, and D. Koya. SIRT1 inhibits transforming growth factor beta-induced apoptosis in glomerular mesangial cells via Smad7 deacetylation. *J Biol Chem*, 282(1):151–8, 2007.

[262] A. Kurisaki, S. Kose, Y. Yoneda, C. H. Heldin, and A. Moustakas. Transforming growth factor-β induces nuclear import of Smad3 in an importin-β1 and Ran-dependent manner. *Mol Biol Cell*, 12(4):1079–91, 2001.

[263] J. M. Kyriakis and J. Avruch. Mammalian MAPK signal transduction pathways activated by stress and inflammation: a 10-year update. *Physiological reviews*, 92(2):689–737, 2012.

[264] M. Laiho, M. Weis, and J. Massagué. Concomitant loss of transforming growth factor (TGF)-β receptor types I and II in TGF-β-resistant cell mutants implicates both receptor types in signal transduction. *Journal of Biological Chemistry*, 265(30):18518–18524, 1990.

[265] J. L. Leight, M. A. Wozniak, S. Chen, M. L. Lynch, and C. S. Chen. Matrix rigidity regulates a switch between TGF-β1-induced apoptosis and epithelial-mesenchymal transition. *Mol Biol Cell*, 23(5):781–91, 2012.

[266] L. Levy and C. S. Hill. Smad4 dependency defines two classes of transforming growth factor β (TGF-β) target genes and distinguishes TGF-β-induced epithelial-mesenchymal transition from its antiproliferative and migratory responses. *Molecular and cellular biology*, 25(18):8108–8125, 2005.

[267] L. Levy and C. S. Hill. Alterations in components of the TGF-β superfamily signaling pathways in human cancer. *Cytokine Growth Factor Rev*, 17(1-2):41–58, 2006.

[268] H. Li, S. Bergeron, M. G. Annis, P. M. Siegel, and D. Juncker. Serial analysis of 38 proteins during the progression of human breast tumor in mice using an antibody colocalization microarray. *Molecular & Cellular Proteomics*, 14(4):1024–1037, 2015.

[269] R. Li, A. C. Chung, Y. Dong, W. Yang, X. Zhong, and H. Y. Lan. The microRNA miR-433 promotes renal fibrosis by amplifying the TGF-β/Smad3-Azin1 pathway. *Kidney international*, 84(6):1129–1144, 2013.

[270] Y. Li, C. de Haar, M. Chen, J. Deuring, M. M. Gerrits, R. Smits, B. Xia, E. J. Kuipers, and C. J. van der Woude. Disease-related expression of the IL6/STAT3/SOCS3 signalling pathway in ulcerative colitis and ulcerative colitis-related carcinogenesis. *Gut*, 59(2):227–235, 2010.

[271] B. F. Lillemeier, M. Köster, and I. M. Kerr. Stat1 from the cell membrane to the dna. *The EMBO journal*, 20(10):2508–2517, 2001.

[272] C. Lin and L. Segel. *Mathematics Applied to Deterministic Problems in the Natural Sciences*. Society for Industrial and Applied Mathematics, 1988. ISBN:9780898712292, pp 302-320.

[273] C. Lin and L. Segel. *Mathematics Applied to Deterministic Problems in the Natural Sciences*. Society for Industrial and Applied Mathematics, 1988. ISBN:9780898712292, pp 185-224.

[274] X. Lin, X. Duan, Y.-Y. Liang, Y. Su, K. H. Wrighton, J. Long, M. Hu, C. M. Davis, J. Wang, F. C. Brunicardi, Y. Shi, Y.-G. Chen, A. Meng, and X.-H. Feng. PPM1A Functions as a Smad Phosphatase to Terminate TGFbeta Signaling. *Cell*, 125(5):915–928, 2006.

[275] P. B. Liton, G. Li, C. Luna, P. Gonzalez, and D. L. Epstein. Cross-talk between TGF-β1 and IL-6 in human trabecular meshwork cells. *Molecular vision*, 15:326, 2009.

[276] J. Little, D. Shepley, and D. Wert. Robustness of a gene regulatory circuit. *The EMBO Journal*, 18(15):4299–4307, 1999.

[277] L. Liu, R. Santora, J. N. Rao, X. Guo, T. Zou, H. M. Zhang, D. J. Turner, and J.-Y. Wang. Activation of TGF-β-Smad signaling pathway following polyamine depletion in intestinal epithelial cells. *American Journal of Physiology-Gastrointestinal and Liver Physiology*, 285(5):G1056–G1067, 2003.

[278] S. Liu, C. Ginestier, S. J. Ou, S. G. Clouthier, S. H. Patel, F. Monville, H. Korkaya, A. Heath, J. Dutcher, C. G. Kleer, et al. Breast cancer stem cells are regulated by mesenchymal stem cells through cytokine networks. *Cancer research*, 71(2):614–624, 2011.

[279] R. S. Lo and J. Massagué. Ubiquitin-dependent degradation of TGF-β-activated smad2. *Nat Cell Biol*, 1(8):472–8, 1999.

[280] D. J. Lockhart, H. Dong, M. C. Byrne, M. T. Follettie, M. V. Gallo, M. S. Chee, M. Mittmann, C. Wang, M. Kobayashi, H. Horton, and E. L. Brown. Expression monitoring by hybridization to high-density oligonucleotide arrays. *Nat Biotechnol*, 14(13):1675–80, 1996.

[281] D. J. Lockhart and E. A. Winzeler. Genomics, gene expression and DNA arrays. *Nature*, 405(6788):827–36, 2000.

[282] J. Logan. *A First Course in Differential Equations*. Springer Science+Business Media, LLC, 2010. ISBN:9781441975928.

[283] M. Lucas, L. Laplaze, and M. J. Bennett. Plant systems biology: network matters. *Plant, cell & environment*, 34(4):535–553, 2011.

[284] K. Luo and H. Lodish. Signaling by chimeric erythropoietin-TGF-β receptors: homodimerization of the cytoplasmic domain of the type I TGF-β receptor and heterodimerization with the type II receptor are both required for intracellular signal transduction. *The EMBO journal*, 15(17):4485, 1996.

[285] P. J. Lupardus, G. Skiniotis, A. J. Rice, C. Thomas, S. Fischer, T. Walz, and K. C. Garcia. Structural snapshots of full-length Jak1, a transmembrane gp130/IL-6/IL-6Rα cytokine receptor complex, and the receptor-Jak1 holocomplex. *Structure*, 19(1):45–55, 2011.

[286] C. Lutticken, U. M. Wegenka, J. Yuan, J. Buschmann, C. Schindler, A. Ziemiecki, A. G. Harpur, A. F. Wilks, K. Yasukawa, T. Taga, et al. Association of transcription factor APRF and protein kinase Jak1 with the interleukin-6 signal transducer gp130. *Science*, 263(5143):89–92, 1994.

[287] R. Luwor, B. Baradaran, L. Taylor, J. Iaria, T. Nheu, N. Amiry, C. Hovens, B. Wang, A. Kaye, and H. Zhu. Targeting Stat3 and Smad7 to restore TGF-β cytostatic regulation of tumor cells in vitro and in vivo. *Oncogene*, 32(19):2433–2441, 2012.

[288] H.-W. Ma and A.-P. Zeng. The connectivity structure, giant strong component and centrality of metabolic networks. *Bioinformatics*, 19(11):1423–1430, 2003.

[289] D. Machado, R. S. Costa, M. Rocha, E. C. Ferreira, B. Tidor, and I. Rocha. Modeling formalisms in systems biology. *AMB express*, 1(1):1–14, 2011.

[290] M. J. Macias, P. Martin-Malpartida, and J. Massagué. Structural determinants of Smad function in TGF-β signaling. *Trends in biochemical sciences*, 40(6):296–308, 2015.

[291] M. MacLeod and N. J. Nersessian. Strategies for coordinating experimentation and modeling in integrative systems biology. *Journal of Experimental Zoology Part B: Molecular and Developmental Evolution*, 322(4):230–239, 2014.

[292] A. MacNamara, C. Terfve, D. Henriques, B. P. Bernabé, and J. Saez-Rodriguez. State–time spectrum of signal transduction logic models. *Physical biology*, 9(4):045003, 2012.

[293] A. Mahdavi, R. E. Davey, P. Bhola, T. Yin, and P. W. Zandstra. Sensitivity analysis of intracellular signaling pathway kinetics predicts targets for stem cell fate control. *PLoS computational biology*, 3(7):e130, 2007.

[294] A. Mantovani, P. Allavena, A. Sica, and F. Balkwill. Cancer-related inflammation. *Nature*, 454(7203):436–444, 2008.

[295] A. Masoudi-Nejad, G. Bidkhori, S. H. Ashtiani, A. Najafi, J. H. Bozorgmehr, and E. Wang. Cancer systems biology and modeling: Microscopic scale and multiscale approaches. 30:60–69, 2015.

[296] J. Massagué. The transforming growth factor-β family. *Annu Rev Cell Biol*, 6:597–641, 1990.

[297] J. Massagué. TGF-β SIGNAL TRANSDUCTION. *Annual Review of Biochemistry*, 67(1):753–791, 1998.

[298] J. Massagué, L. Attisano, and J. L. Wrana. The TGF-β family and its composite receptors. *Trends in cell biology*, 4(5):172–178, 1994.

[299] J. Massagué, S. W. Blain, and R. S. Lo. TGF-β signaling in growth control, cancer, and heritable disorders. *Cell*, 103(2):295–309, 2000.

[300] J. Massagué, J. Seoane, and D. Wotton. Smad transcription factors. *Genes Dev*, 19(23):2783–810, 2005.

[301] J. Massagué and B. Kelly. Internalization of transforming growth factor-β and its receptor in BALB/c 3T3 fibroblasts. *Journal of cellular physiology*, 128(2):216–222, 1986.

[302] Y. Matsuoka, A. Funahashi, S. Ghosh, and H. Kitano. *Modeling and simulation using CellDesigner*, pages 121–145. Springer, 2014. ISBN: 9781493908042, Book title: Transcription Factor Regulatory Networks, editor: Etsuko Miyamoto-Sato, Hiroyuki Ohashi, Hirotaka Sasaki, Jun-ichi Nishikawa, Hiroshi Yanagawa.

[303] K. Matsushita, S. Itoh, S. Ikeda, Y. Yamamoto, Y. Yamauchi, and M. Hayashi. LIF/STAT3/SOCS3 Signaling Pathway in Murine Bone Marrow Stromal Cells Suppresses Osteoblast Differentiation. *Journal of cellular biochemistry*, 115(7):1262–1268, 2014.

[304] H. H. McAdams and A. Arkin. Simulation of prokaryotic genetic circuits. *Annual review of biophysics and biomolecular structure*, 27(1):199–224, 1998.

[305] H. H. McAdams and A. Arkin. It'sa noisy business! genetic regulation at the nanomolar scale. *Trends in genetics*, 15(2):65–69, 1999.

[306] E. Meir, G. Von Dassow, E. Munro, and G. Odell. Robustness, flexibility, and the role of lateral inhibition in the neurogenic network. *Current Biology*, 12(10):778–786, 2002.

[307] K. Melén, R. Fagerlund, J. Franke, M. Köhler, L. Kinnunen, and I. Julkunen. Importin α nuclear localization signal binding sites for STAT1, STAT2, and influenza A virus nucleoprotein. *Journal of Biological Chemistry*, 278(30):28193–28200, 2003.

[308] P. Melke, H. Jönsson, E. Pardali, P. ten Dijke, and C. Peterson. A Rate Equation Approach to Elucidate the Kinetics and Robustness of the TGF-β Pathway. *Biophysical Journal*, 91(12):4368–4380, 2006.

[309] M. Mihara, M. Hashizume, H. Yoshida, M. Suzuki, and M. Shiina. IL-6/IL-6 receptor system and its role in physiological and pathological conditions. *Clinical Science*, 122(4):143–159, 2012.

[310] H.-K. Min, F. Mirshahi, A. Verdianelli, T. Pacana, V. Patel, C.-G. Park, A. Choi, J.-H. Lee, C.-B. Park, S. Ren, et al. Activation of the GP130-STAT3 axis and its potential implications in nonalcoholic fatty liver disease. *American Journal of Physiology-Gastrointestinal and Liver Physiology*, 308(9):G794–G803, 2015.

[311] S. Mishra, J. Deng, P. Gowda, M. Rao, C. Lin, C. Chen, T. Huang, and L. Sun. Androgen receptor and microRNA-21 axis downregulates transforming growth factor beta receptor II (TGFBR2) expression in prostate cancer. *Oncogene*, 33(31):4097–4106, 2014.

[312] S. Mishra and L. Sun. Role of TGF-β superfamily ligand and mechanism of osteoblastic tumorigenesis of prostate cancer cells. *Cancer Research*, 72(8 Supplement):5317–5317, 2012.

[313] H. Mitchell, A. Choudhury, R. E. Pagano, and E. B. Leof. Ligand-dependent and -independent transforming growth factor-β receptor recycling regulated by clathrin-mediated endocytosis and Rab11. *Mol Biol Cell*, 15(9):4166–78, 2004.

[314] S. Mitchell, R. Tsui, and A. Hoffmann. *Studying NF-κB Signaling with Mathematical Models*, pages 647–661. Springer, 2015. ISBN:9781493924219, Book title: NF-kappa B: Methods and Protocols, editor: Michael J. May.

[315] T. Miyake, N. S. Alli, and J. C. McDermott. Nuclear function of Smad7 promotes myogenesis. *Mol Cell Biol*, 30(3):722–35, 2010.

[316] E. L. Molnár, H. Hegyesi, S. Tóth, Z. Darvas, V. László, C. Szalai, and A. Falus. Biosynthesis of interleukin-6, an autocrine growth factor for melanoma, is regulated by melanoma-derived histamine. 10(1):25–28, 2000.

[317] I. Moraga, G. Wernig, S. Wilmes, V. Gryshkova, C. P. Richter, W.-J. Hong, R. Sinha, F. Guo, H. Fabionar, T. S. Wehrman, et al. Tuning Cytokine Receptor Signaling by Re-orienting Dimer Geometry with Surrogate Ligands. *Cell*, 160(6):1196–1208, 2015.

[318] M. Morikawa, D. Koinuma, K. Miyazono, and C.-H. Heldin. Genome-wide mechanisms of Smad binding. *Oncogene*, 32(13):1609–1615, 2013.

[319] M. Morikawa, D. Koinuma, S. Tsutsumi, E. Vasilaki, Y. Kanki, C.-H. Heldin, H. Aburatani, and K. Miyazono. ChIP-seq reveals cell type-specific binding patterns of BMP-specific Smads and a novel binding motif. *Nucleic acids research*, 2011. doi: 10.1093/nar/gkr572.

[320] C. Moya, Z. Huang, P. Cheng, A. Jayaraman, and J. Hahn. Investigation of IL-6 and IL-10 signalling via mathematical modelling. *Systems Biology, IET*, 5(1):15–26, 2011.

[321] P. J. Murray. The JAK-STAT signaling pathway: input and output integration. *The Journal of Immunology*, 178(5):2623–2629, 2007.

[322] T. Naka, M. Narazaki, M. Hirata, T. Matsumoto, S. Minamoto, A. Aono, N. Nishimoto, T. Kajita, T. Taga, K. Yoshizaki, et al. STAT-induced STAT inhibitor. *Nature*, 387:925, 1997.

[323] A. Nakao, T. Imamura, S. Souchelnytskyi, M. Kawabata, A. Ishisaki, E. Oeda, K. Tamaki, J. Hanai, C. H. Heldin, K. Miyazono, and P. ten Dijke. TGF-β receptor-mediated signalling through Smad2, Smad3 and Smad4. *EMBO J*, 16(17):5353–62, 1997.

[324] A. Nakao, K. Okumura, and H. Ogawa. Smad7: a new key player in TGF-β-associated disease. *Trends in molecular medicine*, 8(8):361–363, 2002.

[325] T. Nakayama, L. K. Berg, and J. L. Christian. Dissection of inhibitory Smad proteins: both N- and C-terminal domains are necessary for full activities of Xenopus Smad6 and Smad7. *Mech Dev*, 100(2):251–62, 2001.

[326] M. Narazaki, B. A. Witthuhn, K. Yoshida, O. Silvennoinen, K. Yasukawa, J. N. Ihle, T. Kishimoto, and T. Taga. Activation of JAK2 kinase mediated by the interleukin 6 signal transducer gp130. *Proceedings of the National Academy of Sciences*, 91(6):2285–2289, 1994.

[327] M. F. Neurath and S. Finotto. IL-6 signaling in autoimmunity, chronic inflammation and inflammation-associated cancer. *Cytokine & growth factor reviews*, 22(2):83–89, 2011.

[328] S. E. Nicholson, D. De Souza, L. J. Fabri, J. Corbin, T. A. Willson, J.-G. Zhang, A. Silva, M. Asimakis, A. Farley, A. D. Nash, et al. Suppressor of cytokine signaling-3 preferentially binds to the SHP-2-binding site on the shared cytokine receptor subunit gp130. *Proceedings of the National Academy of Sciences*, 97(12):6493–6498, 2000.

[329] F. J. Nicolás, K. De Bosscher, B. Schmierer, and C. S. Hill. Analysis of Smad nucleocytoplasmic shuttling in living cells. *Journal of cell science*, 117(18):4113–4125, 2004.

[330] F. J. Nicolás and C. S. Hill. Attenuation of the TGF-β-Smad signaling pathway in pancreatic tumor cells confers resistance to TGF-β-induced growth arrest. *Oncogene*, 22(24):3698–3711, 2003.

[331] C. Niemand, A. Nimmesgern, S. Haan, P. Fischer, F. Schaper, R. Rossaint, P. C. Heinrich, and G. Müller-Newen. Activation of STAT3 by IL-6 and IL-10 in primary human macrophages is differentially modulated by suppressor of cytokine signaling 3. *The Journal of Immunology*, 170(6):3263–3272, 2003.

[332] U. Novak, A. Mui, A. Miyajima, and L. Paradiso. Formation of STAT5-containing DNA binding complexes in response to colony-stimulating factor-1 and platelet-derived growth factor. *Journal of Biological Chemistry*, 271(31):18350–18354, 1996.

[333] S. O'Barr and N. R. Cooper. The C5a complement activation peptide increases IL-1β and IL-6 release from amyloid-β primed human monocytes: implications for Alzheimer's disease. *Journal of neuroimmunology*, 109(2):87–94, 2000.

[334] C. A. O'Brien and S. C. Manolagas. Isolation and characterization of the human gp130 promoter Regulation by STATS. *Journal of Biological Chemistry*, 272(23):15003–15010, 1997.

[335] K. Oda and H. Kitano. A comprehensive map of the toll-like receptor signaling network. *Molecular systems biology*, 2(1), 2006.

[336] K. Oda, Y. Matsuoka, A. Funahashi, and H. Kitano. A comprehensive pathway map of epidermal growth factor receptor signaling. *Molecular systems biology*, 1(1), 2005.

[337] A. Ogata, D. Chauhan, G. Teoh, S. P. Treon, M. Urashima, R. L. Schlossman, and K. C. Anderson. IL-6 triggers cell growth via the Ras-dependent mitogen-activated protein kinase cascade. *The Journal of Immunology*, 159(5):2212–2221, 1997.

[338] B. Ortiz, A. W. Fabius, W. H. Wu, A. Pedraza, C. W. Brennan, N. Schultz, K. L. Pitter, J. F. Bromberg, J. T. Huse, E. C. Holland, et al. Loss of the tyrosine phosphatase PTPRD leads to aberrant STAT3 activation and promotes gliomagenesis. *Proceedings of the National Academy of Sciences*, 111(22):8149–8154, 2014.

[339] S. Padrissa-Altés, M. Bachofner, R. L. Bogorad, L. Pohlmeier, T. Rossolini, F. Böhm, G. Liebisch, C. Hellerbrand, V. Koteliansky, T. Speicher, et al.

Control of hepatocyte proliferation and survival by Fgf receptors is essential for liver regeneration in mice. *Gut*, 2014. doi:10.1136/gutjnl-2014-307874.

[340] J. A. Papin and B. O. Palsson. The jak-stat signaling network in the human b-cell: an extreme signaling pathway analysis. *Biophysical journal*, 87(1):37–46, 2004.

[341] J. H. Park, D. G. Watt, C. S. Roxburgh, P. G. Horgan, and D. C. McMillan. Colorectal Cancer, Systemic Inflammation, and Outcome. *cancer*, 7:10, 2015. doi:10.1097/SLA.0000000000001122.

[342] O. K. Park, T. S. Schaefer, and D. Nathans. In vitro activation of Stat3 by epidermal growth factor receptor kinase. *Proceedings of the National Academy of Sciences*, 93(24):13704–13708, 1996.

[343] S. H. Park. Fine tuning and cross-talking of TGF-β signal by inhibitory Smads. *J Biochem Mol Biol*, 38(1):9–16, 2005.

[344] B. Pasche. Role of transforming growth factor beta in cancer. *Journal of Cellular Physiology*, 186(2):153–168, 2001.

[345] A. R. Patel, J. Li, B. L. Bass, and J.-Y. Wang. Expression of the transforming growth factor-β gene during growth inhibition following polyamine depletion. *American Journal of Physiology-Cell Physiology*, 275(2):C590–C598, 1998.

[346] S. Pellegrini and I. Dusanter-Fourt. The structure, regulation and function of the Janus kinases (JAKs) and the signal transducers and activators of transcription (STATs). *European Journal of Biochemistry*, 248(3):615–633, 1997.

[347] S. B. Peng, L. Yan, X. Xia, S. A. Watkins, H. B. Brooks, D. Beight, D. K. Herron, M. L. Jones, J. W. Lampe, W. T. McMillen, N. Mort, J. S. Sawyer, and J. M. Yingling. Kinetic characterization of novel pyrazole TGF-β receptor I kinase inhibitors and their blockade of the epithelial-mesenchymal transition. *Biochemistry*, 44(7):2293–304, 2005.

[348] S. G. Penheiter, H. Mitchell, N. Garamszegi, M. Edens, J. J. Doré Jr, and E. B. Leof. Internalization-dependent and-independent requirements for transforming growth factor β receptor signaling via the Smad pathway. *Molecular and cellular biology*, 22(13):4750–4759, 2002.

[349] J. Penn, A. O Grobbelaar, and K. J Rolfe. Skin Regeneration: The Possibilities. *Recent Patents on Regenerative Medicine*, 1(2):164–172, 2011.

[350] M. Pickup, S. Novitskiy, and H. L. Moses. The roles of TGF [beta] in the tumour microenvironment. *Nature Reviews Cancer*, 13(11):788–799, 2013.

[351] C. E. Pierreux, F. J. Nicolás, and C. S. Hill. Transforming growth factor beta-independent shuttling of Smad4 between the cytoplasm and nucleus. *Mol Cell Biol*, 20(23):9041–54, 2000.

[352] M. P. Pinto. Microsoft excel 2010. *Edições Centro Atlântico*, 2011.

[353] M. C. Poffenberger, N. Straka, N. El Warry, D. Fang, I. Shanina, and M. S. Horwitz. Lack of IL-6 during coxsackievirus infection heightens the early immune response resulting in increased severity of chronic autoimmune myocarditis. *PLoS One*, 4(7):e6207, 2009.

[354] E. E. Powell, C. J. Edwards-Smith, J. L. Hay, A. D. Clouston, D. H. Crawford, C. Shorthouse, D. M. Purdie, and J. R. Jonsson. Host genetic factors influence disease progression in chronic hepatitis C. *Hepatology*, 31(4):828–833, 2000.

[355] C. Pozrikidis. *Numerical computation in science and engineering*, volume 307. Oxford university press New York, 1998. ISBN:978-0-19-537611-1.

[356] A. D. Pradhan, J. E. Manson, N. Rifai, J. E. Buring, and P. M. Ridker. C-reactive protein, interleukin 6, and risk of developing type 2 diabetes mellitus. *Jama*, 286(3):327–334, 2001.

[357] D. R. Principe, J. A. Doll, J. Bauer, B. Jung, H. G. Munshi, L. Bartholin, B. Pasche, C. Lee, and P. J. Grippo. TGF-β: duality of function between tumor prevention and carcinogenesis. *Journal of the National Cancer Institute*, 106(2):djt369, 2014.

[358] L. Pulaski, M. Landstrom, C. H. Heldin, and S. Souchelnytskyi. Phosphorylation of Smad7 at Ser-249 does not interfere with its inhibitory role in transforming growth factor-β-dependent signaling but affects Smad7-dependent transcriptional activation. *J Biol Chem*, 276(17):14344–9, 2001.

[359] T. Putoczki and M. Ernst. More than a sidekick: the IL-6 family cytokine IL-11 links inflammation to cancer. *Journal of leukocyte biology*, 88(6):1109–1117, 2010.

[360] X. Qu, X. Li, Y. Zheng, Y. Ren, V. G. Puelles, G. Caruana, D. J. Nikolic-Paterson, and J. Li. Regulation of Renal Fibrosis by Smad3 Thr388 Phosphorylation. *The American journal of pathology*, 184(4):944–952, 2014.

[361] C. Queitsch, T. Sangster, and S. Lindquist. Hsp90 as a capacitor of phenotypic variation. *Nature*, 417(6889):618–624, 2002.

[362] L. Rahib, B. D. Smith, R. Aizenberg, A. B. Rosenzweig, J. M. Fleshman, and L. M. Matrisian. Projecting cancer incidence and deaths to 2030: the unexpected burden of thyroid, liver, and pancreas cancers in the United States. *Cancer research*, 74(11):2913–2921, 2014.

[363] P. B. Rainey and T. F. Cooper. Evolution of bacterial diversity and the origins of modularity. *Research in microbiology*, 155(5):370–375, 2004.

[364] A. J. Ramsay, A. J. Husband, I. A. Ramshaw, S. Bao, K. I. Matthaei, G. Koehler, and M. Kopf. The role of interleukin-6 in mucosal IgA antibody responses in vivo. *Science*, 264(5158):561–563, 1994.

[365] J. N. Rao, L. Li, B. L. Bass, and J.-Y. Wang. Expression of the TGF-β receptor gene and sensitivity to growth inhibition following polyamine depletion. *American Journal of Physiology-Cell Physiology*, 279(4):C1034–C1044, 2000.

[366] D. W. Ray, S.-G. Ren, and S. Melmed. Leukemia inhibitory factor (LIF) stimulates proopiomelanocortin (POMC) expression in a corticotroph cell line. Role of STAT pathway. *Journal of Clinical Investigation*, 97(8):1852, 1996.

[367] A. J. Rivett. Regulation of intracellular protein turnover: covalent modification as a mechanism of marking proteins for degradation. *Current topics in cellular regulation*, 28:291–337, 1985.

[368] D. Roder, N. Creighton, D. Baker, R. Walton, S. Aranda, and D. Currow. Changing roles of population-based cancer registries in Australia. *Australian Health Review*, 2015. doi:10.1071/AH14250.

[369] M. Rokavec, M. G. Öner, H. Li, R. Jackstadt, L. Jiang, D. Lodygin, M. Kaller, D. Horst, P. K. Ziegler, S. Schwitalla, et al. IL-6R/STAT3/miR-34a feedback loop promotes EMT-mediated colorectal cancer invasion and metastasis. *The Journal of clinical investigation*, 124(4):1853, 2014.

[370] M. Rokavec, M. G. Öner, H. Li, R. Jackstadt, L. Jiang, D. Lodygin, M. Kaller, D. Horst, P. K. Ziegler, S. Schwitalla, et al. IL-6R/STAT3/miR-34a feedback loop promotes EMT-mediated colorectal cancer invasion and metastasis. *The Journal of clinical investigation*, 125(3):1362, 2015.

[371] C. Roxburgh and D. McMillan. Cancer and systemic inflammation: treat the tumour and treat the host. *British journal of cancer*, 110(6):1409–1412, 2014.

[372] S. Rutherford. Between genotype and phenotype: protein chaperones and evolvability. *Nature Reviews Genetics*, 4(4):263–274, 2003.

[373] S. Rutherford and S. Lindquist. Hsp90 as a capacitor for morphological evolution. *Nature*, 396(6709):336–342, 1998.

[374] Y. Sako and M. Ueda. *Cell signaling reactions: single-molecular kinetic analysis*. Springer Science & Business Media, 2010. ISBN: 9789048198634, Chapter 1.

[375] S. Sakon, X. Xue, M. Takekawa, T. Sasazuki, T. Okazaki, Y. Kojima, J.-H. Piao, H. Yagita, K. Okumura, H. Nakano, et al. NF-κB inhibits TNF-induced accumulation of ROS that mediate prolonged MAPK activation and necrotic cell death. *The EMBO journal*, 22(15):3898–3909, 2003.

[376] D. Salomon. Transforming Growth Factor β in Cancer: Janus, the Two-Faced God. *Journal of the National Cancer Institute*, 106(2):djt441, 2014.

[377] A. N. Samraj, O. M. Pearce, H. Läubli, A. N. Crittenden, A. K. Bergfeld, K. Banda, C. J. Gregg, A. E. Bingman, P. Secrest, S. L. Diaz, et al. A red meat-derived glycan promotes inflammation and cancer progression. *Proceedings of the National Academy of Sciences*, 112(2):542–547, 2015.

[378] J. F. Santibanez, M. Quintanilla, and C. Bernabeu. TGF-β/TGF-β receptor system and its role in physiological and pathological conditions. *Clinical science*, 121(6):233–251, 2011.

[379] A. Sasaki, H. Yasukawa, A. Suzuki, S. Kamizono, T. Syoda, I. Kinjyo, M. Sasaki, J. A. Johnston, and A. Yoshimura. Cytokine-inducible SH2 protein-3 (CIS3/SOCS3) inhibits Janus tyrosine kinase by binding through the N-terminal kinase inhibitory region as well as SH2 domain. *Genes to Cells*, 4(6):339–351, 1999.

[380] P. M. Sato, K. Yoganathan, J. H. Jung, and S. G. Peisajovich. The robustness of a signaling complex to domain rearrangements facilitates network evolution. *PLoS biology*, 12(12):e1002012, 2014.

[381] F. Schaper, C. Gendo, M. Eck, J. Schmitz, C. Grimm, D. Anhuf, I. Kerr, and P. Heinrich. Activation of the protein tyrosine phosphatase SHP2 via the interleukin-6 signal transducing receptor protein gp130 requires tyrosine kinase Jak1 and limits acute-phase protein expression. *Biochem. J*, 335:557–565, 1998.

[382] C. Schindler and J. Darnell Jr. Transcriptional responses to polypeptide ligands: the JAK-STAT pathway. *Annual review of biochemistry*, 64(1):621–652, 1995.

[383] C. Schlichting and M. Pigliucci. *Phenotypic evolution: a reaction norm perspective*, pages xii + 387. Sinauer Associates Incorporated, 1998. ISBN: 0-87893-799-4.

[384] B. Schmierer and C. S. Hill. Kinetic analysis of Smad nucleocytoplasmic shuttling reveals a mechanism for transforming growth factor beta-dependent nuclear accumulation of Smads. *Mol Cell Biol*, 25(22):9845–58, 2005.

[385] B. Schmierer and C. S. Hill. TGF[beta]-SMAD signal transduction: molecular specificity and functional flexibility. *Nat Rev Mol Cell Biol*, 8(12):970–982, 2007.

[386] B. Schmierer, A. L. Tournier, P. A. Bates, and C. S. Hill. Mathematical modeling identifies Smad nucleocytoplasmic shuttling as a dynamic signal-interpreting system. *Proceedings of the National Academy of Sciences*, 105(18):6608–6613, 2008.

[387] R. Schumann, C. Kirschning, A. Unbehaun, H. Aberle, H. Knope, N. Lamping, R. Ulevitch, and F. Herrmann. The lipopolysaccharide-binding protein is a secretory class 1 acute-phase protein whose gene is transcriptionally activated by APRF/STAT/3 and other cytokine-inducible nuclear proteins. *Molecular and cellular biology*, 16(7):3490–3503, 1996.

[388] P. R. Segarini, D. M. Rosen, and S. M. Seyedin. Binding of Transforming Growth Factor-β to Cell Surface Proteins Varies with Cell Type. *Molecular Endocrinology*, 3(2):261–272, 1989.

[389] P. B. Sehgal, G. Grieninger, and G. Tosato. *Regulation of the acute phase and immune responses: interleukin-6*. New York Academy of Sciences, 1989. ISBN: 0-89766-532-5.

[390] T. Sekimoto, N. Imamoto, K. Nakajima, T. Hirano, and Y. Yoneda. Extracellular signal-dependent nuclear import of Stat1 is mediated by nuclear pore-targeting complex formation with NPI-1, but not Rch1. *The EMBO journal*, 16(23):7067–7077, 1997.

[391] K. S. Sfanos, H. A. Hempel, and A. M. De Marzo. *The role of inflammation in prostate cancer*, pages 153–181. Springer Basel, 2014. ISBN:9783034808361, Book title: Inflammation and Cancer editor: Bharat B. Aggarwal, Bokyung Sung, Subash Chandra Gupta.

[392] A. E. Sgro, D. J. Schwab, J. Noorbakhsh, T. Mestler, P. Mehta, and T. Gregor. From intracellular signaling to population oscillations: bridging size- and time-scales in collective behavior. *Molecular Systems Biology*, 11(1), 2015.

[393] F. Shi, P. Zhou, and R. Wang. Coupled positive feedback loops regulate the biological behavior. pages 169–173, 2012.

[394] Q. Shi, L. Qin, W. Wei, F. Geng, R. Fan, Y. S. Shin, D. Guo, L. Hood, P. S. Mischel, and J. R. Heath. Single-cell proteomic chip for profiling intracellular signaling pathways in single tumor cells. *Proceedings of the National Academy of Sciences*, 109(2):419–424, 2012.

[395] W. Shi, C. Sun, B. He, W. Xiong, X. Shi, D. Yao, and X. Cao. GADD34-PP1c recruited by Smad7 dephosphorylates TGFbeta type I receptor. *J Cell Biol*, 164(2):291–300, 2004.

[396] Y. Shi and J. Massagué. Mechanisms of TGF-β signaling from cell membrane to the nucleus. *Cell*, 113(6):685–700, 2003.

[397] Y. Shi, Y. F. Wang, L. Jayaraman, H. Yang, J. Massagué, and N. P. Pavletich. Crystal structure of a Smad MH1 domain bound to DNA: insights on DNA binding in TGF-β signaling. *Cell*, 94(5):585–94, 1998.

[398] K. Shuai, C. M. Horvath, L. H. T. Huang, S. A. Qureshi, D. Cowburn, and J. E. Darnell. Interferon activation of the transcription factor Stat91 involves dimerization through SH2-phosphotyrosyl peptide interactions. *Cell*, 76(5):821–828, 1994.

[399] R. L. Siegel, K. D. Miller, and A. Jemal. Cancer statistics, 2015. *CA: a cancer journal for clinicians*, 65(1):5–29, 2015.

[400] M. Simonsson, C. H. Heldin, J. Ericsson, and E. Gronroos. The balance between acetylation and deacetylation controls Smad7 stability. *J Biol Chem*, 280(23):21797–803, 2005.

[401] J. K. Sinfield, A. Das, D. J. O'Regan, S. G. Ball, K. E. Porter, and N. A. Turner. p38 MAPK alpha mediates cytokine-induced IL-6 and MMP-3 expression in human cardiac fibroblasts. *Biochemical and biophysical research communications*, 430(1):419–424, 2013.

[402] A. Singh, A. Jayaraman, and J. Hahn. Modeling regulatory mechanisms in IL-6 signal transduction in hepatocytes. *Biotechnology and bioengineering*, 95(5):850–862, 2006.

[403] A. M. Singh, D. Reynolds, T. Cliff, S. Ohtsuka, A. L. Mattheyses, Y. Sun, L. Menendez, M. Kulik, and S. Dalton. Signaling network crosstalk in human pluripotent cells: a Smad2/3-regulated switch that controls the balance between self-renewal and differentiation. *Cell stem cell*, 10(3):312–326, 2012.

[404] G. Skiniotis, M. J. Boulanger, K. C. Garcia, and T. Walz. Signaling conformations of the tall cytokine receptor gp130 when in complex with IL-6 and IL-6 receptor. *Nature structural & molecular biology*, 12(6):545–551, 2005.

[405] G. Skiniotis, P. J. Lupardus, M. Martick, T. Walz, and K. C. Garcia. Structural organization of a full-length gp130/LIF-R cytokine receptor transmembrane complex. *Molecular cell*, 31(5):737–748, 2008.

[406] T. Slater. Recent advances in modeling languages for pathway maps and computable biological networks. *Drug discovery today*, 19(2):193–198, 2014.

[407] P. C. Smith, A. Hobisch, D.-L. Lin, Z. Culig, and E. T. Keller. Interleukin-6 and prostate cancer progression. *Cytokine & growth factor reviews*, 12(1):33–40, 2001.

[408] P. D. Smolen, D. A. Baxter, and J. H. Byrne. Mathematical modeling and analysis of intracellular signaling pathways. *From Molecules to Networks-An Introduction to Cellular and Molecular Neuroscience*, pages 391–429, 2004.

[409] P. D. Smolen, D. A. Baxter, and J. H. Byrne. *Modelling and Analysis of Intracellular Signalling Pathways*, chapter 6, pages 176–201. Academic Press, 3rd edition, 2014. ISBN:9780123971791, Book title:From molecules to networks: an introduction to cellular and molecular neuroscience.

[410] R. V. Solé and S. Valverde. Spontaneous emergence of modularity in cellular networks. *Journal of The Royal Society Interface*, 5(18):129–133, 2008.

[411] W. Somers, M. Stahl, and J. S. Seehra. 1.9 Å crystal structure of interleukin 6: implications for a novel mode of receptor dimerization and signaling. *The EMBO journal*, 16(5):989–997, 1997.

[412] D. J. Son, J. E. Hong, J. O. Ban, J. H. Park, H. L. Lee, S. M. Gu, J. Y. Hwang, M. H. Jung, D. W. Lee, S.-B. Han, et al. Synergistic Inhibitory Effects of Cetuximab and Cisplatin on Human Colon Cancer Cell Growth via Inhibition of the ERK-Dependent EGF Receptor Signaling Pathway. *BioMed Research International*, 2015, 2015. Article ID: 397563.

[413] S. Souchelnytskyi, K. Tamaki, U. Engström, C. Wernstedt, P. ten Dijke, and C.-H. Heldin. Phosphorylation of Ser465 and Ser467 in the C terminus of Smad2 mediates interaction with Smad4 and is required for transforming growth factor-β signaling. *Journal of Biological Chemistry*, 272(44):28107–28115, 1997.

[414] M. B. Spom and A. B. Roberts. Role of retinoids in differentiation and carcinogenesis. *Cancer Research*, 43(7):3034–3040, 1983.

[415] N. Stahl, T. G. Boulton, T. Farruggella, N. Y. Ip, S. Davis, B. A. Witthuhn, F. W. Quelle, O. Silvennoinen, G. Barbieri, S. Pellegrini, et al. Association and activation of Jak-Tyk kinases by CNTF-LIF-OSM-IL-6 beta receptor components. *Science*, 263(5143):92–95, 1994.

[416] N. Stahl, T. J. Farruggella, T. G. Boulton, Z. Zhong, J. Darnell, and G. D. Yancopoulos. Choice of STATs and other substrates specified by modular tyrosine-based motifs in cytokine receptors. *Science*, 267(5202):1349–1353, 1995.

[417] R. Starr, T. A. Willson, E. M. Viney, L. Murray, J. R. Rayner, B. J. Jenkins, T. J. Gonda, W. S. Alexander, D. Metcalf, N. A. Nicola, et al. A family of cytokine-inducible inhibitors of signalling. *Nature*, 387(6636):917–921, 1997.

[418] F. Steinhagen, A. P. McFarland, L. G. Rodriguez, P. Tewary, A. Jarret, R. Savan, and D. M. Klinman. IRF-5 and NF-κB p50 co-regulate IFN-β and IL-6 expression in TLR9-stimulated human plasmacytoid dendritic cells. *European journal of immunology*, 43(7):1896–1906, 2013.

[419] A. Stephanou, D. Isenberg, S. Akira, T. Kishimoto, and D. Latchman. The nuclear factor interleukin-6 (NF-IL6) and signal transducer and activator of transcription-3 (STAT-3) signalling pathways co-operate to mediate the activation of the hsp90β gene by interleukin-6 but have opposite effects on its inducibility by heat shock. *Biochem. J*, 330:189–195, 1998.

[420] D. W. Strand, Y.-Y. Liang, F. Yang, D. A. Barron, S. J. Ressler, I. G. Schauer, X.-H. Feng, and D. R. Rowley. TGF-β induction of FGF-2 expression in stromal cells requires integrated Smad3 and MAPK pathways. *American journal of clinical and experimental urology*, 2(3):239, 2014.

[421] L. Su, X. Wu, Q. Zhou, C. Wang, and B. Liu. Cancer-associated fibroblast promotes gastric cancer invasion and epithelial-mesenchymal transition via the IL-6/JAK/STAT3 signaling pathway. *Cancer Research*, 74(19 Supplement):4803–4803, 2014.

[422] I. Surovtsova, N. Simus, T. Lorenz, A. König, S. Sahle, and U. Kummer. Accessible methods for the dynamic time-scale decomposition of biochemical systems. *Bioinformatics*, 25(21):2816–2823, 2009.

[423] C. Suzuki, G. Murakami, M. Fukuchi, T. Shimanuki, Y. Shikauchi, T. Imamura, and K. Miyazono. Smurf1 regulates the inhibitory activity of Smad7 by targeting Smad7 to the plasma membrane. *J Biol Chem*, 277(42):39919–25, 2002.

[424] A. Symes, T. Gearan, J. Eby, and J. S. Fink. Integration of Jak-Stat and AP-1 signaling pathways at the vasoactive intestinal peptide cytokine response element regulates ciliary neurotrophic factor-dependent transcription. *Journal of Biological Chemistry*, 272(15):9648–9654, 1997.

[425] T. Taga. Gp130, a shared signal transducing receptor component for hematopoietic and neuropoietic cytokines. *Journal of neurochemistry*, 67(1):1–10, 1996.

[426] T. Taga and T. Kishimoto. Gp130 and the interleukin-6 family of cytokines. *Annual review of immunology*, 15(1):797–819, 1997.

[427] Y. Tajima, K. Goto, M. Yoshida, K. Shinomiya, T. Sekimoto, Y. Yoneda, K. Miyazono, and T. Imamura. Chromosomal region maintenance 1

(CRM1)-dependent nuclear export of Smad ubiquitin regulatory factor 1 (Smurf1) is essential for negative regulation of transforming growth factor-β signaling by Smad7. *J Biol Chem*, 278(12):10716–21, 2003.

[428] M. Takahashi-Tezuka, Y. Yoshida, T. Fukada, T. Ohtani, Y. Yamanaka, K. Nishida, K. Nakajima, M. Hibi, and T. Hirano. Gab1 acts as an adapter molecule linking the cytokine receptor gp130 to ERK mitogen-activated protein kinase. *Molecular and cellular biology*, 18(7):4109–4117, 1998.

[429] H. Y. Tan and T. W. Ng. Accurate step wedge calibration for densitometry of electrophoresis gels. *Optics Communications*, 281(10):3013–3017, 2008.

[430] Y. Tang, K. Kitisin, W. Jogunoori, C. Li, C. X. Deng, S. C. Mueller, H. W. Ressom, A. Rashid, A. R. He, J. S. Mendelson, J. M. Jessup, K. Shetty, M. Zasloff, B. Mishra, E. P. Reddy, L. Johnson, and L. Mishra. Progenitor/stem cells give rise to liver cancer due to aberrant TGF-β and IL-6 signaling. *Proc Natl Acad Sci U S A*, 105(7):2445–50, 2008.

[431] K. Taniguchi and M. Karin. IL-6 and related cytokines as the critical lynchpins between inflammation and cancer. 26(1):54–74, 2014.

[432] K. Taniguchi, L.-W. Wu, S. I. Grivennikov, P. R. de Jong, I. Lian, F.-X. Yu, K. Wang, S. B. Ho, B. S. Boland, J. T. Chang, et al. A gp130-Src-YAP module links inflammation to epithelial regeneration. *Nature*, 519(7541):57–62, 2015.

[433] P. ten Dijke, K. Miyazono, and C. H. Heldin. Signaling inputs converge on nuclear effectors in TGF-β signaling. *Trends Biochem Sci*, 25(2):64–70, 2000.

[434] S. Thiolloy, J. R. Edwards, B. Fingleton, D. B. Rifkin, L. M. Matrisian, and C. C. Lynch. An osteoblast-derived proteinase controls tumor cell survival via TGF-β activation in the bone microenvironment. *PLoS ONE*, 7(1), 2012.

[435] S. Thomas, B. A. Quinn, S. K. Das, R. Dash, L. Emdad, S. Dasgupta, X.-Y. Wang, P. Dent, J. C. Reed, M. Pellecchia, et al. Targeting the Bcl-2 family for cancer therapy. *Expert opinion on therapeutic targets*, 17(1):61–75, 2013.

[436] P. V. Tran, S. A. Lachke, and R. W. Stottmann. Toward a systems-level understanding of the Hedgehog signaling pathway: defining the complex, robust, and fragile. *Wiley Interdisciplinary Reviews: Systems Biology and Medicine*, 5(1):83–100, 2013.

[437] M. Turner, D. Chantry, and M. Feldmann. Transforming growth factor β induces the production of interleukin 6 by human peripheral blood mononuclear cells. *Cytokine*, 2(3):211–216, 1990.

[438] A. K. Tyagi. *MATLAB and SIMULINK for Engineers*. Oxford University Press, 2012. ISBN:0198072449.

[439] J. Tyson, K. Chen, and B. Novak. Network dynamics and cell physiology. *Nature Reviews Molecular Cell Biology*, 2(12):908–916, 2001.

[440] T. S. Udayakumar, M. S. Stratton, R. B. Nagle, and G. T. Bowden. Fibroblast growth factor-1 induced promatrilysin expression through the activation of extracellular-regulated kinases and STAT3. *Neoplasia*, 4(1):60–67, 2002.

[441] U. Valcourt, M. Kowanetz, H. Niimi, C.-H. Heldin, and A. Moustakas. TGF-β and the Smad signaling pathway support transcriptomic reprogramming during epithelial-mesenchymal cell transition. *Molecular biology of the cell*, 16(4):1987–2002, 2005.

[442] K. E. van der Vos and P. J. Coffer. The extending network of FOXO transcriptional target genes. *Antioxidants & redox signaling*, 14(4):579–592, 2011.

[443] J. Van Helden, A. Naim, R. Mancuso, M. Eldridge, L. Wernisch, D. Gilbert, and S. J. Wodak. Representing and analysing molecular and cellular function in the computer. *Biological chemistry*, 381(9-10):921–935, 2000.

[444] J. Van Snick. Interleukin-6: an overview. *Annual review of immunology*, 8(1):253–278, 1990.

[445] X. Varelas, R. Sakuma, P. Samavarchi-Tehrani, R. Peerani, B. M. Rao, J. Dembowy, M. B. Yaffe, P. W. Zandstra, and J. L. Wrana. TAZ controls Smad nucleocytoplasmic shuttling and regulates human embryonic stem-cell self-renewal. *Nat Cell Biol*, 10(7):837–48, 2008.

[446] E. A. Variano, J. H. McCoy, and H. Lipson. Networks, dynamics, and modularity. *Physical review letters*, 92(18):188701, 2004.

[447] F. Ventura, J. Doody, F. Liu, J. L. Wrana, and J. Massagué. Reconstitution and transphosphorylation of TGF-β receptor complexes. *Embo J*, 13(23):5581–9, 1994.

[448] C. Vermes, J. J. Jacobs, J. Zhang, G. Firneisz, K. A. Roebuck, and T. T. Glant. Shedding of the interleukin-6 (IL-6) receptor (gp80) determines the ability of IL-6 to induce gp130 phosphorylation in human osteoblasts. *Journal of Biological Chemistry*, 277(19):16879–16887, 2002.

[449] J. M. G. Vilar, R. Jansen, and C. Sander. Signal Processing in the TGF-β Superfamily Ligand-Receptor Network. *PLoS Comput Biol*, 2(1):e3, 2006.

[450] A. F. Villaverde, D. Henriques, K. Smallbone, S. Bongard, J. Schmid, D. Cicin-Sain, A. Crombach, J. Saez-Rodriguez, K. Mauch, E. Balsa-Canto, et al. BioPreDyn-bench: a suite of benchmark problems for dynamic modelling in systems biology. *BMC systems biology*, 9(1):8, 2015.

[451] T. Vincent, E. P. Neve, J. R. Johnson, A. Kukalev, F. Rojo, J. Albanell, K. Pietras, I. Virtanen, L. Philipson, P. L. Leopold, et al. A SNAIL1–SMAD3/4 transcriptional repressor complex promotes TGF-β mediated epithelial–mesenchymal transition. *Nature cell biology*, 11(8):943–950, 2009.

[452] J. Visser, J. Hermisson, G. Wagner, L. Meyers, H. Bagheri-Chaichian, J. Blanchard, L. Chao, J. Cheverud, S. Elena, and W. Fontana. Perspective: evolution and detection of genetic robustness. *Evolution*, 57(9):1959–1972, 2003.

[453] W. Vogel, R. Lammers, J. Huang, and A. Ullrich. Activation of a phosphotyrosine phosphatase by tyrosine phosphorylation. *Science*, 259(5101):1611–1614, 1993.

[454] G. Volpin, M. Cohen, M. Assaf, T. Meir, R. Katz, and S. Pollack. Cytokine Levels (IL-4, IL-6, IL-8 and TGFβ) as Potential Biomarkers of Systemic Inflammatory Response in Trauma Patients. *International orthopaedics*, 38(6):1303–1309, 2014.

[455] L. Von Bertalanffy. *General system theory: Foundations, development, applications*. George Braziller New York, 1968. ISBN: 0807604534.

[456] G. von Dassow, E. Meir, E. M. Munro, and G. M. Odell. The segment polarity network is a robust developmental module. *Nature*, 406(6792):188–192, 2000.

[457] A. Wagner. *Robustness and evolvability in living systems*. Princeton University Press, 2013. ISBN: 0-691-12240-7.

[458] G. Wagner and L. Altenberg. Perspective: Complex adaptations and the evolution of evolvability. *Evolution*, pages 967–976, 1996.

[459] J. Wagner and J. Keizer. Effects of rapid buffers on Ca2+ diffusion and Ca2+ oscillations. *Biophysical Journal*, 67(1):447, 1994.

[460] J. Wagner, L. Ma, J. Rice, W. Hu, A. Levine, and G. Stolovitzky. p53–Mdm2 loop controlled by a balance of its feedback strength and effective dampening using ATM and delayed feedback. *IEE Proceedings-Systems Biology*, 152(3):109–118, 2005.

[461] J. Wagner and G. Stolovitzky. Stability and Time-Delay Modeling of Negative Feedback Loops. *Proceedings of the IEEE*, 96(8):1398–1410, Aug 2008.

[462] L. M. Wakefield, D. M. Smith, T. Masui, C. C. Harris, and M. B. Sporn. Distribution and modulation of the cellular receptor for transforming growth factor-β. *The Journal of Cell Biology*, 105(2):965–975, 1987.

[463] M. Wan, X. Cao, Y. Wu, S. Bai, L. Wu, X. Shi, and N. Wang. Jab1 antagonizes TGF-β signaling by inducing Smad4 degradation. *EMBO Rep*, 3(2):171–6, 2002.

[464] M. Wang, M. Weiss, M. Simonovic, G. Haertinger, S. P. Schrimpf, M. O. Hengartner, and C. von Mering. PaxDb, a database of protein abundance averages across all three domains of life. *Molecular & cellular proteomics*, 11(8):492–500, 2012.

[465] M. Watanabe, N. Masuyama, M. Fukuda, and E. Nishida. Regulation of intracellular dynamics of Smad4 by its leucine-rich nuclear export signal. *EMBO Rep*, 1(2):176–82, 2000.

[466] U. M. Wegenka, J. Buschmann, C. Lütticken, P. C. Heinrich, and F. Horn. Acute-phase response factor, a nuclear factor binding to acute-phase response elements, is rapidly activated by interleukin-6 at the posttranslational level. *Molecular and cellular biology*, 13(1):276–288, 1993.

[467] H. Wen, J. Ma, M. Zhang, and G. Ma. The comparison research of nonlinear curve fitting in Matlab and LabVIEW. *IEEE*, pages 74–77, 2012.

[468] Z. Wen, Z. Zhong, and J. E. Darnell. Maximal activation of transcription by Statl and Stat3 requires both tyrosine and serine phosphorylation. *Cell*, 82(2):241–250, 1995.

[469] T. E. Wheldon. *Mathematical models in cancer research*. Taylor & Francis, 1988. ISBN: 0852742916.

[470] N. Wiener. Cybernetics; or control and communication in the animal and the machine. 1948. ISBN: 978-0-262-73009-9.

[471] R. Wieser, J. Wrana, and J. Massagué. GS domain mutations that constitutively activate T beta RI, the downstream signaling component in the TGF-β receptor complex. *The EMBO journal*, 14(10):2199, 1995.

[472] M. Wilhelm, J. Schlegl, H. Hahne, A. M. Gholami, M. Lieberenz, M. M. Savitski, E. Ziegler, L. Butzmann, S. Gessulat, H. Marx, et al. Mass-spectrometry-based draft of the human proteome. *Nature*, 509(7502):582–587, 2014.

[473] E. H. Wilkes, P. Casado, and P. R. Cutillas. Approaches for measuring signalling plasticity in the context of resistance to targeted cancer therapies. *Biochemical Society transactions*, 42(4):791–797, 2014.

[474] A. F. Wilks and A. G. Harpur. Cytokine signal transduction and the JAK family of protein tyrosine kinases. *Bioessays*, 16(5):313–320, 1994.

[475] W. C. Wimsatt. *Robustness, Reliability, and Overdetermination (1981)*, pages 61–87. Springer, 2012. ISBN:9789400727588 Book title:Characterizing the Robustness of Science Editors:Léna Soler, Emiliano Trizio, Thomas Nickles, William Wimsatt.

[476] J. Wolf, S. Rose-John, and C. Garbers. Interleukin-6 and its receptors: a highly regulated and dynamic system. *Cytokine*, 70(1):11–20, 2014.

[477] S. Wormald and D. J. Hilton. Inhibitors of cytokine signal transduction. *Journal of Biological Chemistry*, 279(2):821–824, 2004.

[478] S. Wormald and D. J. Hilton. The negative regulatory roles of suppressor of cytokine signaling proteins in myeloid signaling pathways. *Current opinion in hematology*, 14(1):9–15, 2007.

[479] S. Wormald, J.-G. Zhang, D. L. Krebs, L. A. Mielke, J. Silver, W. S. Alexander, T. P. Speed, N. A. Nicola, and D. J. Hilton. The comparative roles of suppressor of cytokine signaling-1 and-3 in the inhibition and desensitization of cytokine signaling. *Journal of Biological Chemistry*, 281(16):11135–11143, 2006.

[480] C. Wu, Y. Gong, J. Yuan, W. Zhang, G. Zhao, H. Li, A. Sun, Y. Zou, J. Ge, et al. microRNA-181a represses ox-LDL-stimulated inflammatory response in dendritic cell by targeting c-Fos. *Journal of lipid research*, 53(11):2355–2363, 2012.

[481] J. W. Wu, M. Hu, J. Chai, J. Seoane, M. Huse, C. Li, D. J. Rigotti, S. Kyin, T. W. Muir, R. Fairman, J. Massagué, and Y. Shi. Crystal structure of a phosphorylated Smad2. Recognition of phosphoserine by the MH2

domain and insights on Smad function in TGF-β signaling. *Mol Cell*, 8(6):1277–89, 2001.

[482] Z. Xiao, R. Latek, and H. F. Lodish. An extended bipartite nuclear localization signal in Smad4 is required for its nuclear import and transcriptional activity. *Oncogene*, 22(7):1057–69, 2003.

[483] Z. Xiao, X. Liu, Y. I. Henis, and H. F. Lodish. A distinct nuclear localization signal in the N terminus of Smad 3 determines its ligand-induced nuclear translocation. *Proceedings of the National Academy of Sciences*, 97(14):7853–7858, 2000.

[484] L. Xie, B. K. Law, M. E. Aakre, M. Edgerton, Y. Shyr, N. A. Bhowmick, and H. L. Moses. Transforming growth factor beta-regulated gene expression in a mouse mammary gland epithelial cell line. *Breast Cancer Res*, 5(6):R187–98, 2003.

[485] J. Xu and R. Derynck. Does Smad6 methylation control BMP signaling in cancer? *Cell Cycle*, 13(8):1209–1210, 2014.

[486] L. Xu, Y. G. Chen, and J. Massagué. The nuclear import function of Smad2 is masked by SARA and unmasked by TGFbeta-dependent phosphorylation. *Nat Cell Biol*, 2(8):559–62, 2000.

[487] L. Xu, Y. Kang, S. Çöl, and J. Massagué. Smad2 Nucleocytoplasmic Shuttling by Nucleoporins CAN/Nup214 and Nup153 Feeds TGFbeta Signaling Complexes in the Cytoplasm and Nucleus. *Molecular Cell*, 10(2):271–282, 2002.

[488] X. Xu, Y.-L. Sun, and T. Hoey. Cooperative DNA binding and sequence-selective recognition conferred by the STAT amino-terminal domain. *Science*, 273(5276):794–797, 1996.

[489] T. Yamada, K. Tobita, S. Osada, T. Nishihara, and M. Imagawa. CCAAT/enhancer-binding protein δ gene expression is mediated by APRF/STAT3. *Journal of biochemistry*, 121(4):731–738, 1997.

[490] T. Yamamoto, Y. Sekine, K. Kashima, A. Kubota, N. Sato, N. Aoki, and T. Matsuda. The nuclear isoform of protein-tyrosine phosphatase TC-PTP regulates interleukin-6-mediated signaling pathway through STAT3 dephosphorylation. *Biochemical and biophysical research communications*, 297(4):811–817, 2002.

[491] T. Yamazaki. Differential Expression of gp130 on Human CD8+ T Cell Subsets and the Role Of STAT3 in CD8+ T Cell Development. 2012.

[492] X. Yan and Y. G. Chen. Smad7: not only a regulator, but also a cross-talk mediator of TGF-β signalling. *Biochem J*, 434(1):1–10, 2011.

[493] M. Yanagisawa, K. Nakashima, T. Takizawa, W. Ochiai, H. Arakawa, and T. Taga. Signaling crosstalk underlying synergistic induction of astrocyte differentiation by BMPs and IL-6 family of cytokines. *FEBS letters*, 489(2):139–143, 2001.

[494] C. Yang, C. Li, M. Li, X. Tong, X. Hu, X. Yang, X. Yan, L. He, and C. Wan. CYP2S1 depletion enhances colorectal cell proliferation is associated with PGE2-mediated activation of β-catenin signaling. *Experimental cell research*, 331(2):377–386, 2015.

[495] Z. Yao, S. Fenoglio, D. C. Gao, M. Camiolo, B. Stiles, T. Lindsted, M. Schlederer, C. Johns, N. Altorki, V. Mittal, et al. TGF-β IL-6 axis mediates selective and adaptive mechanisms of resistance to molecular targeted therapy in lung cancer. *Proceedings of the National Academy of Sciences*, 107(35):15535–15540, 2010.

[496] T. Yi, Y. Huang, M. Simon, and J. Doyle. Robust perfect adaptation in bacterial chemotaxis through integral feedback control. *Proceedings of the National Academy of Sciences*, 97(9):4649–4653, 2000.

[497] K. Yoshida, T. Taga, M. Saito, S. Suematsu, A. Kumanogoh, T. Tanaka, H. Fujiwara, M. Hirata, T. Yamagami, T. Nakahata, et al. Targeted disruption of gp130, a common signal transducer for the interleukin 6 family of cytokines, leads to myocardial and hematological disorders. *Proceedings of the National Academy of Sciences*, 93(1):407–411, 1996.

[498] M. Yu, P. Trobridge, Y. Wang, S. Kanngurn, S. Morris, S. Knoblaugh, and W. Grady. Inactivation of TGF-β signaling and loss of PTEN cooperate to induce colon cancer in vivo. *Oncogene*, 33(12):1538–1547, 2014.

[499] J. Zavadil, M. Bitzer, D. Liang, Y.-C. Yang, A. Massimi, S. Kneitz, E. Piek, and E. P. Böttinger. Genetic programs of epithelial cell plasticity directed by transforming growth factor-β. *Proceedings of the National Academy of Sciences*, 98(12):6686–6691, 2001.

[500] D. Zhang, M. Sun, D. Samols, and I. Kushner. STAT3 participates in transcriptional activation of the C-reactive protein gene by interleukin-6. *Journal of Biological Chemistry*, 271(16):9503–9509, 1996.

[501] J. Zhang, H. Tsoi, X. Li, H. Wang, J. Gao, K. Wang, M. Y. Go, S. C. Ng, F. K. Chan, J. J. Sung, et al. Carbonic anhydrase IV inhibits colon cancer development by inhibiting the Wnt signalling pathway through targeting the WTAP–WT1–TBL1 axis. *Gut*, 2015. doi:10.1136/gutjnl-2014-308614.

[502] J.-G. Zhang, D. Metcalf, S. Rakar, M. Asimakis, C. J. Greenhalgh, T. A. Willson, R. Starr, S. E. Nicholson, W. Carter, W. S. Alexander, et al. The SOCS box of suppressor of cytokine signaling-1 is important for inhibition of cytokine action in vivo. *Proceedings of the National Academy of Sciences*, 98(23):13261–13265, 2001.

[503] Q. Zhang, N. Yu, and C. Lee. Mysteries of TGF-β paradox in benign and malignant cells. *Frontiers in oncology*, 4, 2014. doi:10.3389/fonc.2014.00094.

[504] S. Zhang, T. Fei, L. Zhang, R. Zhang, F. Chen, Y. Ning, Y. Han, X. H. Feng, A. Meng, and Y. G. Chen. Smad7 antagonizes transforming growth factor beta signaling in the nucleus by interfering with functional Smad-DNA complex formation. *Mol Cell Biol*, 27(12):4488–99, 2007.

[505] T. Zhang, J. Ma, and X. Cao. Grb2 regulates Stat3 activation negatively in epidermal growth factor signalling. *Biochem. J*, 376:457–464, 2003.

[506] Y. Zhang and R. Derynck. Regulation of Smad signalling by protein associations and signalling crosstalk. *Trends Cell Biol*, 9(7):274–9, 1999.

[507] Y. Zhang, X.-H. Feng, and R. Derynck. Smad3 and Smad4 cooperate with c-Jun/c-Fos to mediate TGF-β-induced transcription. *Nature*, 394(6696):909–913, 1998.

[508] Y.-Y. Zhang, Y.-C. Fan, M. Wang, D. Wang, and X.-H. Li. Atorvastatin attenuates the production of IL-1β, IL-6, and TNF-α in the hippocampus of an amyloid β1-42-induced rat model of Alzheimer's disease. *Clinical interventions in aging*, 8:103, 2013.

[509] Z. Zhong, Z. Wen, and J. Darnell. Stat3: a STAT family member activated by tyrosine phosphorylation in response to epidermal growth factor and interleukin-6. *Science*, 264(5155):95–98, 1994.

[510] H. Zhu, P. Kavsak, S. Abdollah, J. L. Wrana, and G. H. Thomsen. A SMAD ubiquitin ligase targets the BMP pathway and affects embryonic pattern formation. *Nature*, 400(6745):687–93, 1999.

[511] Z. Zi, Z. Feng, D. A. Chapnick, M. Dahl, D. Deng, E. Klipp, A. Moustakas, and X. Liu. Quantitative analysis of transient and sustained transforming growth factor-β signaling dynamics. *Mol Syst Biol*, 7, 2011.

[512] Z. Zi and E. Klipp. SBML-PET: a Systems Biology Markup Language-based parameter estimation tool. *Bioinformatics*, 22(21):2704–2705, 2006.

[513] Z. Zi and E. Klipp. Constraint-Based Modeling and Kinetic Analysis of the Smad Dependent TGF-β Signaling Pathway. *PLoS ONE*, 2(9):e936, 2007.

[514] A. Zilberstein, R. Ruggieri, J. Korn, and M. Revel. Structure and expression of cDNA and genes for human interferon-β-2, a distinct species inducible by growth-stimulatory cytokines. *The EMBO journal*, 5(10):2529, 1986.

[515] G. Zubay. In vitro synthesis of protein in microbial systems. *Annual review of genetics*, 7(1):267–287, 1973.